
Doctoral Dissertations


Student Theses and Dissertations

Fall 2017

Theoretical calculations for electron impact ionization of atoms and molecules

Sadek Mohamed Fituri Amami

Follow this and additional works at: https://scholarsmine.mst.edu/doctoral_dissertations

 Part of the [Atomic, Molecular and Optical Physics Commons](#)

Department: Physics

Recommended Citation

Amami, Sadek Mohamed Fituri, "Theoretical calculations for electron impact ionization of atoms and molecules" (2017). *Doctoral Dissertations*. 2617.

https://scholarsmine.mst.edu/doctoral_dissertations/2617

This thesis is brought to you by Scholars' Mine, a service of the Missouri S&T Library and Learning Resources. This work is protected by U. S. Copyright Law. Unauthorized use including reproduction for redistribution requires the permission of the copyright holder. For more information, please contact scholarsmine@mst.edu.

THEORETICAL CALCULATIONS FOR ELECTRON IMPACT IONIZATION OF
ATOMS AND MOLECULES

by

SADEK MOHAMED FITURI AMAMI

A DISSERTATION

Presented to the Graduate Faculty of the

MISSOURI UNIVERSITY OF SCIENCE AND TECHNOLOGY

In Partial Fulfillment of the Requirements for the Degree

DOCTOR OF PHILOSOPHY

in

PHYSICS

2017

Approved by

Don H. Madison, Advisor

Jerry L. Peacher

Michael Schulz

Daniel Fischer

Gregory Gelles

Copyright 2017

SADEK MOHAMED FITURI AMAMI

All Rights Reserved

PUBLICATION DISSERTATION OPTION

This dissertation consists of the following ten articles which have been published as follows:

Paper I: Pages 31-54 have been published by Phys Rev A.91.032707 (March 2015).

Paper II: Pages 55-78 have been published by Phys Rev A.90.012704 (July 2014).

Paper III: Pages 79-93 have been published by J. Phys. B: At. Mol. Opt. Phys. 49 185202 (September 2016).

Paper IV: Pages 94-118 have been published by Phys Rev A.93.062704 (June 2016).

Paper V: Pages 119-143 have been published by Phys Rev A.90.062707 (December 2014).

Paper VI: Pages 144-148 have been published by PhysRevA.91.069906 (June 2015).

Paper VII: Pages 149-165 have been published by PhysRevA.92 032706 (September 2015).

Paper VIII: Pages 166-184 have been published by J. Phys. B: At. Mol. Opt. Phys (January 2009).

Paper IX: Pages 185-205 have been published by PhysRevA.95.022701 (February 2017).

Paper X.: Pages 206-224 have been published by THE JOURNAL OF CHEMICAL PHYSICS 136, 094302 (March 2012).

Paper XI. Pages 225-244 have been submitted to J. Phys. B: At. Mol. Opt. Phys (September 2017)

ABSTRACT

In the last twenty years, significant progress has been made for the theoretical treatment of electron impact ionization ($e,2e$) of atoms and molecules and, for some cases, very nice agreement between experiment and theory has been achieved. In particular, excellent agreement between theory and experiment and theory has been achieved for ionization of hydrogen and helium. However, agreement between experiment and theory is not nearly as good for ionization of larger atoms and molecules. In the first part of this dissertation, different theoretical approaches will be employed to study the triply differential cross section (TDCS) for low and intermediate energy electron-impact ionization of Neon and Argon for different orbital states. There is a very recent interest in studying ionization of Laser aligned atoms in order to get a better understanding about electron impact ionization of molecules. In the next part of this dissertation, results will be presented for electron-impact ionization of three laser aligned atoms, *Mg*, *Ca*, and *Na*. The comparison between the theory and experiment showed that our three body distorted wave (3DW) model gave excellent agreement with experiment in the scattering plane but very poor agreement perpendicular to the scattering plane. An explanation for this poor agreement out of the scattering plane has been provided by comparing our theoretical results with those of the time depended close coupling (TDCC) model and this explanation is also provided in this dissertation.

Recently, significant attention has been directed towards obtaining a better understanding of electron-impact ionization of molecules which are significantly more challenging than atoms. In the last part of this dissertation, results will be presented for electron-impact ionization of three different molecules (N_2 , H_2O , and CH_4) which have been studied comprehensively using different theoretical approximations for different types of geometries. The published papers in section two contain a detailed analysis and discussion for each of these topics.

ACKNOWLEDGMENTS

The first appreciation goes to my family, especially my father and mother for the remarkable and valuable support since I was little kid until this moment. My father was always behind my success during all my educational stages. He always believed that I will get whatever I was seeking and pursuing. At the same level, I got all the emotional support and love from my mother as well. She was and still is the spring of love, kindness, and tenderness. Also, I am really thankful to my wife who stood beside me, supported me, and worked very hard to provide me an appropriate study environment. Utmost appreciation and gratitude goes to my advisors, Dr. Madison and Dr. Peacher, for their support and guidance throughout my graduate study. Special thanks goes to my advisor, Dr. Madison, for his help, patience, and guidance as I completed my PhD. An extended appreciation goes to my advisory committee, Dr. Michael Schulz, Dr. Daniel Fischer and Dr. Gregory Gelles, for their remarkable questions and patience. Also, my thanks go to all my professors who taught me the graduate courses. To all faculty and staff members, my colleagues, my friends in the physics department, and friends in our community who stood beside me with support and love when my house burned, today I say thank you all. Special thanks go to the Police and fire departments, ICRM and Red Cross for their valuable support. My deepest appreciation goes to my friend, Yousef Elmehdwi, and his family, for his hospitality, open arms, warm heart during that event and after, and all his help. Last but not the least, I am thankful to everyone in the physics department, international affairs, and graduate office for making our university campus a very good environment for students with full support. Thanks to the Ministry of Higher Education in Libya and Tripoli University Scholarship, as well as the physics department and the NSF for financial supports.

TABLE OF CONTENTS

	Page
PUBLICATION DISSERTATION OPTION	iii
ABSTRACT	iv
ACKNOWLEDGMENTS	v
LIST OF ILLUSTRATIONS	xiii
 SECTION	
1. GENERAL INTRODUCTION	1
2. GEOMETRIES AND KINEMATICS OF THE STUDY	8
3. THEORETICAL MODELS AND APPROXIMATIONS	12
3.1. THEORY OF ELECTRON IMPACT IONIZATION	12
3.2. DIFFERENTIAL CROSS SECTIONS FOR ATOMS AND MOLECULES .	13
3.2.1. Scattering Theory	14
3.2.2. The Lippmann-Schwinger Equation	16
3.2.3. Born Approximations and its First Order	18
3.3. DISTORTED WAVE BORN APPROXIMATION	22
3.4. THREE-BODY DISTORTED WAVE APPROXIMATION (3DW)	25
3.5. WARD AND MACEK APPROXIMATION	29

PAPER

I. KINEMATICALLY COMPLETE STUDY OF LOW-ENERGY ELECTRON-IMPACT IONIZATION OF NEON: INTERNORMALIZED CROSS SECTIONS IN 3D KINEMATICS	31
ABSTRACT	31
1. INTRODUCTION	32
2. EXPERIMENT	34
3. THEORETICAL MODELS	35
3.1. DWB2-RM	35
3.2. BSR	36
3.3. The Three-Body Distorted-Wave Approximation	37
3.3.1. 3DW	37
3.3.2. DWBA-WM	39
4. RESULTS AND DISCUSSION	41
5. CONCLUSIONS	49
ACKNOWLEDGMENTS	50
REFERENCES	50
II. THEORETICAL AND EXPERIMENTAL INVESTIGATION OF (e,2e) IONIZATION OF ARGON (3p) IN ASYMMETRIC KINEMATICS AT INTERMEDIATE ENERGY	55
ABSTRACT	55
1. INTRODUCTION	56
2. EXPERIMENTAL APPARATUS	59
3. THEORY	60
3.1. 3DW	60
3.2. DWB2-RM	62
3.3. BSR	62

4. RESULTS	65
5. CONCLUSION	68
ACKNOWLEDGMENTS	70
REFERENCES	70
III. EXPERIMENTAL AND THEORETICAL TRIPLE DIFFERENTIAL CROSS SECTIONS FOR ELECTRON IMPACT IONIZATION OF A_r (3p) FOR EQUAL ENERGY FINAL STATE ELECTRONS	79
ABSTRACT	79
1. INTRODUCTION	80
2. EXPERIMENTAL PROCEDURE	81
3. THEORETICAL FRAMEWORK	82
3.1. 3DW Approximation	83
3.2. DWBA Approximation	85
3.3. WM Approximation	85
4. RESULTS AND DISCUSSION	86
5. CONCLUSIONS	90
ACKNOWLEDGMENTS	91
REFERENCES	91
IV. KINEMATICALLY COMPLETE STUDY OF LOW-ENERGY ELECTRON-IMPACT IONIZATION OF ARGON: INTERNORMALIZED CROSS SECTIONS IN 3D KINEMATICS	94
ABSTRACT	94
1. INTRODUCTION	95
2. EXPERIMENT	97
3. THEORETICAL MODELS	100
3.1. BSR	100
3.2. The 3DW Approximation	104

4.	RESULTS AND DISCUSSION	106
5.	CONCLUSIONS	112
	ACKNOWLEDGMENTS	114
	REFERENCES	114
V.	THEORETICAL AND EXPERIMENTAL (e,2e) STUDY OF ELECTRON- IMPACT IONIZATION OF LASER-ALIGNED Mg ATOMS	119
	ABSTRACT	119
1.	INTRODUCTION	120
2.	THEORETICAL FRAMEWORK	121
2.1.	TDCC	121
2.2.	3DW	121
3.	RESULTS AND DISCUSSION	127
4.	ANALYSIS OF THE EXPERIMENTAL DATA	133
4.1.	Effects of Depolarization on the Experimental Data	133
4.2.	In-Plane Excited-State Population Estimates due to Radiation Trapping	136
4.3.	In-Plane Excited-State Population due to Residual Ellipticity of the Laser Beam Polarization	137
5.	CONCLUSION	139
	ACKNOWLEDGMENTS	140
	REFERENCES	140
VI.	THEORETICAL AND EXPERIMENTAL (e,2e) STUDY OF ELECTRON- IMPACT IONIZATION OF LASER-ALIGNED Mg ATOMS	144
	ABSTRACT	144
VII.	EVIDENCE FOR UNNATURAL PARITY CONTRIBUTIONS TO ELECTRON- IMPACT IONIZATION OF LASER-ALIGNED ATOMS	149
	ABSTRACT	150

1. INTRODUCTION	150
2. THEORY	151
3. RESULTS	155
4. CONCLUSION	162
ACKNOWLEDGMENTS	162
REFERENCES	163
VIII. IONIZATION DIFFERENTIAL CROSS SECTION MEASUREMENTS FOR N_2 AT LOW INCIDENT ENERGY IN COPLANAR AND NON-COPLANAR GEOMETRIES	166
ABSTRACT	166
1. INTRODUCTION	167
2. EXPERIMENTAL PROCEDURES	169
3. THEORY	172
3.1. The M3DW Approximation	173
3.2. The DWBA Approximation	174
3.3. DWBA	174
4. COMPARISON OF THEORY TO EXPERIMENT.....	175
5. DISCUSSION AND CONCLUSIONS	182
ACKNOWLEDGMENTS	182
REFERENCES	183
IX. ELECTRON-IMPACT IONIZATION OF H_2O AT LOW PROJECTILE EN- ERGY: INTERNORMALIZED TRIPLE-DIFFERENTIAL CROSS SECTIONS IN THREE-DIMENSIONAL KINEMATICS	185
ABSTRACT	185
1. INTRODUCTION	186
2. EXPERIMENTAL METHOD	188
3. THEORETICAL MODELS	190

4.	RESULTS AND DISCUSSION	191
5.	CONCLUSIONS	198
	ACKNOWLEDGMENTS	199
	REFERENCES	200
X.	LOW ENERGY (e,2e) MEASUREMENTS OF CH_4 AND NEON IN THE PERPENDICULAR PLANE	206
	ABSTRACT	206
1.	INTRODUCTION	207
2.	EXPERIMENTAL APPARATUS	209
3.	THEORETICAL FRAMEWORK	211
4.	RESULTS	212
4.1.	Predicted Scattering Signatures using a Classical Mode	212
4.2.	2p Orbital of Neon	213
4.3.	1t ₂ State of Methane	216
4.4.	Comparison Between the Iso-Electronic Species.....	219
5.	CONCLUSIONS	219
	ACKNOWLEDGMENTS	221
	REFERENCES	221
XI.	DIFFERENTIAL CROSS SECTION MEASUREMENTS FOR IONIZATION OF N_2 IN COPLANAR GEOMETRY	225
	ABSTRACT	225
1.	INTRODUCTION	225
2.	THE EXPERIMENTAL APPARATUS	230
3.	THEORY	232
4.	COPLANAR DOUBLY-SYMMETRIC EXPERIMENTS 100 EV ABOVE THE $3\sigma_g$ IP	233
5.	COPLANAR MEASUREMENTS WITH FIXED ANGLES.....	236

5.1. Results for Outgoing Electron Energies of 10 eV	236
5.2. Results for Outgoing Electron Energies of 20 eV.....	239
6. DISCUSSION AND CONCLUSIONS	241
ACKNOWLEDGMENTS	242
REFERENCES	242
SECTION	
4. SUMMARY AND CONCLUSIONS	245
REFERENCES	252
VITA.....	256

LIST OF ILLUSTRATIONS

Figure	Page
SECTION	
2.1. The x - z Plane shows the Scattering Plane for Heidelberg group (Coplanar).	8
2.2. The y - z Plane shows the Half-Perpendicular Plane for Heidelberg group	8
2.3. The x - y Plane shows the Full-Perpendicular Plane for Heidelberg group.	9
2.4. The x - z Plane shows the Scattering Plane or detecting Plane (Coplanar) when $\Psi = 0^\circ$, while the Perpendicular Plane determined by $\Psi = 90^\circ$ for Manchester group.	11
3.1. Illustrates the single ionization process.	12
PAPER I	
1. Experimental and theoretical TDCS for ionization of Ne ($2p$) by incident electrons with energy $E_0 = 65$ eV, presented as 3D images.	41
2. TDCS for the ionization of Ne ($2p$) presented as a function of the ejected electron (e_2) emission angle at different scattering angles θ_1 ($-8.5^\circ \pm 1.5^\circ$, $-12.5^\circ \pm 2.5^\circ$, $-20^\circ \pm 5^\circ$) and ejected-electron energies E_2 (2.0 eV \pm 1.0 eV, 4.5 eV \pm 1.5 eV, 8.0 eV \pm 2.0 eV).	44
3. Same as Figure 2, except that the theoretical calculations are the 3DW (thick black lines) and DWBA-WM (thin red lines).	45
4. Same as Figure 2, except that the theoretical calculations are the BSR (thick black lines) and 3DW (thin red lines).	46
PAPER II	
1. Schematic diagram of the coincidence electronics used to accumulating a coincidence timing spectrum at each kinematics.	59
2. Experimental and theoretical TDCS for 200 eV electron-impact ionization of argon.	63
3. Experimental and theoretical TDCS for 200 eV electron-impact ionization of argon.	64
4. Same as Figure 3 except that absolute values of the theories are shown in atomic units.	68

PAPER III

1. Schematic view of experimental setup and coincidence electronics. 83
2. TDCS in atomic units for electron-impact ionization of the argon 3p orbital using the coplanar symmetric geometry—both final state electrons have the same energy and are detected at the same angle on opposite sides of the incident beam direction. 87
3. TDCS in atomic units for electron-impact ionization of the argon 3p orbital using the coplanar symmetric geometry—both final state electrons have the same energy and are detected at the same angle on opposite sides of the incident beam direction. 88
4. TDCS in atomic units for electron-impact ionization of the argon 3p orbital for 200 eV incident electrons and equal energy sharing for final state electrons with $E_1 = E_2 = 92.12$ eV. 90

PAPER IV

1. Schematic view of the employed reaction microscope for electron-scattering experiments. 98
2. Experimental and theoretical FDCS for ionization of Ar(3p) by incident electrons with energy $E_0 = 66$ eV, presented as 3D images. 106
3. FDCS for the ionization of Ar(3p) presented as a function of the ejected electron (e_2) emission angle at scattering angles $\theta_1 = -10^\circ$ (top row), $\theta_1 = -15^\circ$ (center row), and $\theta_1 = -20^\circ$ (bottom row) for ejected-electron energies $E_2 = 3$ eV (left column), $E_2 = 5$ eV (center column), and $E_2 = 10$ eV (right column). 107
4. Same as Fig. 2 for the “half-perpendicular” plane, i.e., the yz -plane of Fig. 1(a). 108
5. Same as Figure 2 for the “full-perpendicular” plane, i.e., the xy -plane of Figure 1(a). 109

PAPER V

1. Experimental and theoretical TDCS for electron-impact ionization of the 3s state of Mg. 128
2. Experimental and theoretical TDCS for electron-impact ionization of the 3s state of Mg for symmetric coplanar geometry. 129
3. Experimental and theoretical TDCS for electron-impact ionization of the laser-aligned 3p state of Mg. 130

4.	Experimental and theoretical TDCS for electron-impact ionization of the laser-aligned $3p$ state of Mg	131
5.	Same as in Figure 4	132
6.	Variation of the measured fluorescence signal as a function of the polarization angle of the laser beam.	136
7.	Examples of the angular shape of the pure P-state charge cloud excited by elliptically polarized laser radiation that produces different values of the fluorescence polarization.	138

PAPER VI

1.	Experimental and theoretical TDCS for electron-impact ionization of the laser-aligned $3p$ state of Mg	146
2.	Experimental and theoretical TDCS for electron-impact ionization of the laser-aligned $3p$ state of Mg	147
3.	Same as Figure 2 except for larger beta angles.	148

PAPER VII

1.	Geometry of the scattering experiments performed on Mg [17] and for the new Ca experiments reported here.	152
2.	Triple differential cross sections for the electron-impact ionization of excited-state Mg for equal energy-sharing between the outgoing electrons of $E_1 = E_2 = 20$ eV.	156
3.	Same as Figure 2, except now we show only the $\theta_1 = 30^\circ$ TDCC calculation.	158
4.	Triple differential cross sections for the electron-impact ionization of excited-state Na for equal energy-sharing between the outgoing electrons of $E_1 = E_2 = 20$ eV.	159
5.	Triple differential cross sections for the electron-impact ionization of excited-state Ca for equal energy-sharing between the outgoing electrons of $E_1 = E_2 = 30$ eV.	161

PAPER VIII

1.	The experimental geometry adopted in this work.	168
2.	Binding energy spectra for outgoing electron energies of $4.6\text{~eV} \pm 0.5$ eV taken with the electrons detected at a forward angle of 45° to the z -axis.	171

3.	Normalised TDCS data for outgoing electron energies of $4.6 \text{ eV} \pm 0.5 \text{ eV}$ in (a) a coplanar geometry, (b) for the incident electron at 45° to the detection plane, and (c) for the perpendicular geometry.	177
4.	Normalised TDCS data for outgoing electron energies of $9.7 \text{ eV} \pm 0.5 \text{ eV}$ taken in (a) a coplanar geometry, (b) for the incident electron at 45° to the detection plane, and (c) for a perpendicular geometry.....	178
5.	Normalised TDCS data for outgoing electron energies of $4.6 \text{ eV} \pm 0.5 \text{ eV}$ and $14.5 \text{ eV} \pm 0.5 \text{ eV}$ taken in (a) a coplanar geometry, (b) for the incident electron at 45° to the detection plane, and (c) for the perpendicular geometry.	179
6.	Normalised TDCS data for equal outgoing electron energies of $20 \text{ eV} \sim 0.5 \text{ eV}$ taken in (a) a coplanar geometry, (b) for the incident electron at 45° to the detection plane, and (c) for the perpendicular geometry.....	181

PAPER IX

1.	Summed TDCS for experiment (top panel) and OAMO theory (bottom panel) presented as 3D images for electron-impact ($E_0 = 81 \text{ eV}$) ionization of $1b_1$ and $3a_1$ orbitals of H_2O	192
2.	Experimental and theoretical triple-differential cross sections (TDCS) for electron-impact ($E_0 = 81 \text{ eV}$) ionization of $1b_1$ and $3a_1$ orbitals of H_2O presented as a function of the ejected electron (e_2) emission angle at scattering angles $\theta_1 = -6^\circ$ and $\theta_1 = -10^\circ$ for ejected-electron energies $E_2 = 5 \text{ eV}$ (left column) and $E_2 = 10 \text{ eV}$ (right column).	195
3.	Same as Figure 2 for the “half-perpendicular” plane, i.e., the yz -plane of Fig. 1(a).196	
4.	Same as Figure 2 for the “full-perpendicular” plane, i.e., the xy -plane of Fig. 1(a).197	

PAPER X

1.	Diagram of the geometry used in this study. A perpendicular geometry ($\psi = 90^\circ$) is defined when the momentum of the incident electron is perpendicular to that of the outgoing electrons, i.e., the detection plane.	209
2.	Experimental and theoretical TDCS for the $2p$ orbital of neon.	214
3.	Experimental and theoretical DWBA TDCS for the $1t_2$ HOMO state of CH_4 . ..	216
4.	Experimental and theoretical (M3DW) TDCS for the $1t_2$ HOMO state of CH_4 . .	218

PAPER XI

1.	The coplanar geometries in the experiments. (a) and (d) show the geometry when the fixed angle was 45° , (b) and (e) show where the fixed angle was 90° and (c) and (f) show the geometry for a fixed angle of 125°	228
----	---	-----

2. Measurements with incident electron energy 100 eV above the IP for the $3\sigma_g$ state, in both (a) a coplanar doubly-symmetric geometry and (b) for the incident electron beam direction k_0 at an angle of 45° to the detection plane spanned by k_1 and k_2 234
3. Example of a binding energy spectrum, taken for outgoing electron energies of 10 eV at scattering angles of 45° 237
4. Results for outgoing energies of 10 eV, for the $3\sigma_g$ state (a-c) and the $1\pi_u$ state (d-f). 238
5. Results with outgoing electron energies of 20 eV for the $3\sigma_g$ and $1\pi_u$ states. ... 240

SECTION

1. GENERAL INTRODUCTION

In atomic, molecular, and optical science, the central importance is the atomic collisions phenomena, which plays an important role in many different fields such as, plasma physics, Laser physics, astrophysics, chemical physics and several other fields. In essence, such a phenomena includes collisions between an elementary particles (charged particles: electron, protons and etc.) and an atomic system (atoms, molecules, and ions). Understanding these collisions is very important for understanding the behavior and the changes in the internal structures of atoms and molecules. The behavior of these particles during the collision processes with an atomic system could be different from one particle to another. More specifically in other words, the projectile can experience any kind of collision as an ionization, excitation, or elastic collision. A collision can be defined as an elastic collision if the projectile (electron, proton, etc.) and the target (atom or molecule) scatter without losing a part of its kinetic energy or the internal energy (potential energy) during the collision, i.e., the internal structure before and after the collision process should remain unchanged for both the projectile and the target. In contrast, if part of the kinetic energy has been lost during a same event, then it is called an Inelastic collision. In this kind of collision, there are many possibilities that could happen which make the study of the field more complicated, and requires lots of efforts to understand the physics beyond all these types such as ionization, excitation, photoionization, and several other kinds of collisions. Likewise, when the projectile gains energy from the target, thereby changing its final kinetic energy, this collision is known as a Superelastic collision [1].

The study of atomic and molecular collisions is often called the few body problem and these problems have been studied for long time by Physicists. Schrödinger solved the most important equation in quantum mechanics for the two body problem (Hydrogen Atom). However, the Schrödinger equation is analytically unsolvable for atoms have more than two interacting particles without approximations [2].

In atomic and molecular physics, one of the most important collision processes is electron impact ionization due to many applications in Lasers, astrophysics, plasma, and fluorescence lights. Therefore, understanding the mechanism and the properties of all objects involved in the collision are very important. Moreover, in order to get a complete understanding of the process, the momenta and energies of all those particles that participated in the collision event must be determined.

The topic of this dissertation is electron impact ionization processes, which is also called the $(e, 2e)$ process, where the projectile is an electron, while the target could be an atom or molecule. So, the projectile (the incident electron) collides with the target (atom/molecule) and ionizes it by ejecting an electron from any of the shells of the atom or the molecule, and then the projectile scatters with a certain angle away from the ejected electron. As a result, the two continuum electrons will be detected experimentally in the final channel. The information about the $(e, 2e)$ ionization process can be obtained by measuring the triply differential cross section (TDCS) that is proportional to the probability that the two outgoing electrons will have certain energies and move in certain directions with respect to the z -axis.

The problem of getting the TDCS is not a new problem, but it has long history of interest since the remarkable work done by Eharhadt *et al.* in 1970s [3][4][5]. In fact, the triple differential cross section is essential to understanding the mechanism of the ionization dynamics which provides a sensitive test of the theoretical models as well as playing a major role as a powerful tool to comprehensively examine different theoretical

methods. Therefore, experimental and theoretical groups have paid a lot of attention to electron impact ionization in the past three and half decades, which makes the $(e, 2e)$ collision process very important to ionization process investigation.

As a result of the unsolvable Schrödinger equation for more than two particles, there have been several different approximation methods proposed to solve this problem. However, in this dissertation we are only going to focus on the models and the approximations that we have used in our study, and give a brief review about the comparisons with other models that will be shown in the papers section.

To begin, the study in this dissertation has compared different theoretical models with several experimental work for atoms and molecules for different geometries and kinematics of low and intermediate energies (see the geometries section for more details). The comparisons and the results can be found at the papers section.

The first theoretical model we have used is Three Body Distorted Wave-function model (3DW & M3DW) for atoms and molecules. This model has three different approximations which a brief definition will be given in this section. First of all is the Three Body Distorted Wave (3DW or M3DW), where the exact Coulomb interaction between the two outgoing electrons has been used in the final state of the T-matrix. Next is the Three Body Distorted Wave-Ward-Macek approximation (3DW-WM), which sometimes we called just (WM). In this approximation, the Post Coulomb Interaction (PCI) replaces by the Ward-Macek approximation in the final state of the collision [2]. The second version of the 3DW model that has been used in this dissertation is the Distorted Wave Born Approximation (DWBA). In this model, the Coulomb interaction factor between the two outgoing electrons is not included in the final state of the T-matrix, i.e., the Post Collision Interaction (PCI) is completely neglected in this case. All these approximations will be demonstrated in details later in the theory section.

In fact, these two models, the 3DW and DWBA for atoms and molecules, have evolved over the past two decades with the computer development and other experimental techniques as well as the other theoretical approaches to calculate heavier atoms and molecules. Other theoretical models that have been used are the Convergent Close-coupling (CCC) model which was the first successful non-perturbative calculation (we will not discuss it in this dissertation since we did not compare our results with it), the Time Depend close-coupling (TDCC) method, the Second-Order hybrid Distorted-Wave R-matrix (DWB2-RM), and the B-spline R-matrix (BSR) which recently seems to be the most promising approach for atoms due to the very good agreement with some recent experimental work [6].

The TDCC method is one of the successful approaches since 1990s which is a non-perturbative calculation. It has been introduced for the first time by Colgan *et al.* [7] and used to calculate the triple differential cross section (TDCS) for the hydrogen atom. TDCC is based on generating a wave function for the two outgoing electrons (scattered and ejected electrons). Also in this method, the direct and the exchange potential contains the interaction of the remaining electrons and the two-electron wave function (for more details, please see [8]). In other words, this approach uses the expansion of the wave functions in terms of partial waves and then solves the time-dependent Schrödinger equation numerically. Later on, the method has been modified and generalized to calculate the TDCS for Molecular hydrogen (H_2) as well, and a very good agreement with experiment has been obtained, Colgan et al.[9][10]. Even though the TDCS for an aligned hydrogen molecule (H_2) at low projectile energies can be obtained by using the TDCC method, the challenge of getting TDCS for high incident energies still remains because of the limitation in computing power due to the large number of partial waves required to solve the time dependent Schrödinger equation (more details about the TDCC can be found in the *Mg, Ca, Na* paper).

The Second-Order hybrid Distorted-Wave R-matrix (DWB2-RM) is another successful approach that was originally extended from the R-matrix method by Bartschat and Burke and used for the electron impact ionization processes [11]. In fact, the model has been

described fully by Bartschat *et al.* in [11][13][14]. But briefly, the basic idea of this method can be illustrated in order to understand the differences between this method and the others. Basically, this method is connected two well-known approaches, the DWBA and R-matrix (or close-coupling extension), to calculate the TDCS for electron impact ionization. The DWBA is employed for the initial state before the collision by describing the wave function of the incident (fast) electron by a distorted wave function, and ignoring the correlation of the target with this electron. In addition, a modification of the integration over the slow (ejected) electron energy has been done to approximate the exchange effects between the outgoing electrons in the final state. Furthermore, the feature that the R-matrix approach which allows for the solution covering a wide range of energies of the ejected electron is using a single diagonalization of the Hamiltonian matrix instead of the close-coupling method [15]. Even though, the Second-Order hybrid Distorted-Wave R-matrix (DWBA2-RM) approach was formulated for small energy losses with respect to the projectile energy, and highly asymmetric kinematics as well as the DWB1-RM (First-Order hybrid Distorted-Wave R-matrix) approach, fairly good agreement was found with experiment even for lower incident energy ($< 100 \text{ eV}$) [16][17][18][19]. Although the main deficit of the method comes from neglecting both PCI and the exchange between the outgoing electrons in the final state, surprisingly good agreement with the experimental data, especially in the shape of the magnitude, was found even better than the BSR (*B – spline R – matrix*) approach (discussed below), see [19]. As a matter of fact, this model still may be considered as a standard and useful approximation for calculating the TDCS for low energies (few hundreds eV) of the ($e, 2e$) process.

Last but not the least; the non-perturbative BSR (*B – spline R – matrix*) approach is also one of the most recent successful models employed to calculate TDCS for electron impact ionization ($e, 2e$) for atoms. The BSR model is introduced first by Zatsarinny and Bartschat [21][22][23][24]. The model is different from all the previous approaches. In this model, the estimation of the effect of the high-lying Rydberg states depends on a

huge number of pseudo-states, beside the inclusion of the ionization continuum in the ab initio solution of the close-coupling equations [25][26]. Although the BSR is a complex calculation, it has two significant innovations that may stand behind its success. The first is that BSR can use different sets of non-orthogonal orbitals to represent both the bound and continuum one-electron orbitals. The second innovation is that the R-matrix basis functions are represented by a set of *B*-splines [26][28][29][30]. The BSR approach has been examined for many (*e*, *2e*) calculations for relatively simple atoms, such as quasi-one electron (*H-like*) or quasi-two electron (*He-like*) [31]. Most recently, the BSR was found to be a convenient model even for some complex atoms like *Ne* and *Ar*, which recently makes this model seem to be the most promising development [32].

We have compared all the above models for several different kinematics and geometries. More details can be found in the publications section.

Moreover, we have studied electron impact ionization for align Magnesium atoms (*Mg-3p*), beside an extended study for Sodium (*Na*) and Calcium (*Ca*) compared with (*Mg-3p*) results (see [33] our Mg-paper by comparing the 3DW model for atoms with the TDCC model. Reasonable agreement was found between the two models and the experimental data, with the exception of a big discrepancy between the 3DW and TDCC and the experimental data in one case. Overall, we found good agreement in the scattering plane and very bad agreement for alignment perpendicular to the scattering plane (See *Mg*-paper for details [33][34]).

For Molecular calculations, we have compared two different theoretical approximations for the M3DW model with experimental work. The first approximation is called OAMO (Orientation Averaged Molecular Orbital) approximation, while the second one is called PA (Proper Average) (see papers section for more information). We have performed these two approximations for some molecules (such as N_2 , and H_2O) so far. For the diatomic molecule N_2 , we have performed M3DW, DWBA, and WM calculations to compare with the experimental data. Three states, $3\sigma_g$, 1ν and $2\sigma_g$, have been studied for a range

of geometries (coplanar ($\Psi = 0^\circ$) to perpendicular plane ($\Psi = 90^\circ$) see Figure 2.4) and symmetric sharing energies for the outgoing electrons. Although the low energy of the incident electron (~ 10 and ~ 20 eV above the ionization potential of the $3\sigma_g$, $1\pi_u$ and $2\sigma_g$ states) was very challenging to most theoretical models, the M3DW was more accurate than WM in some cases, while the WM approximation was better in other cases (more discussion and details can be found in the N2 publication). For the water molecule (H_2O), we have made a comprehensive study for the incident electron energy of 81 eV, and compared two different approximations (OAMO & PA) with the experimental data that was performed by Dorn and his co-workers in Heidelberg Germany. Over all, the PA approximation showed much better agreement with the experimental data than the OAMO approximation for both Coplanar and full-perpendicular planes. However, both PA and OAMO showed remarkable similarity with each other while having discrepancies with the experimental data for the half-perpendicular plane (more details can be found in the publication).

This section is divided into three parts. Following this introduction, the geometries and kinematics used to calculate the TDCS and compare with the experimental data are described. A description of our theoretical model for atoms and molecules, and its approximations that are used to calculate the cross sections is then presented.

2. GEOMETRIES AND KINEMATICS OF THE STUDY

In general, there are three common geometries have been used to measure and calculate the triple differential cross-section (TDCS) for the collisions. We will describe these geometries for two different experimental groups. Also, we will clarify the main differences between them.

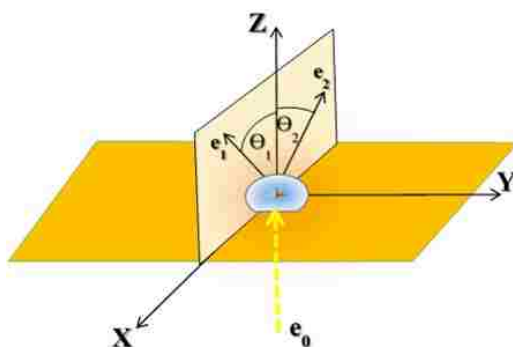


Figure 2.1. The x - z Plane shows the Scattering Plane for Heidelberg group (Coplanar). The incident, scattered and ejected electrons energies are e_0 , e_1 and e_2 respectively, and θ_1 and θ_2 are the scattered and ejected angles respectively.

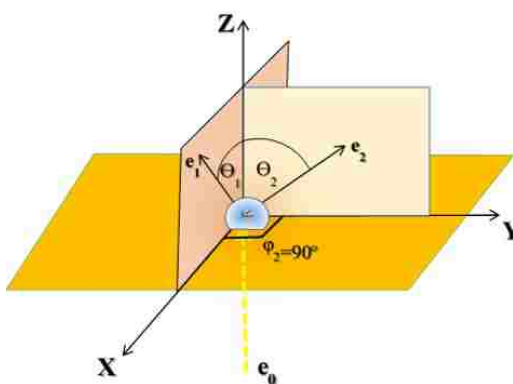


Figure 2.2. The y - z Plane shows the Half-Perpendicular Plane for Heidelberg group. Same parameters as 2.1, and φ_2 is the ejected electron azimuthal angle.

The first geometries are those used by the Heidelberg laboratory. These geometries are called Coplanar (scattering plane), Half-Perpendicular plane, and Full Perpendicular Plane (see Figures 2.1, 2.2, and 2.3 respectively). However, we have also calculated TDCS

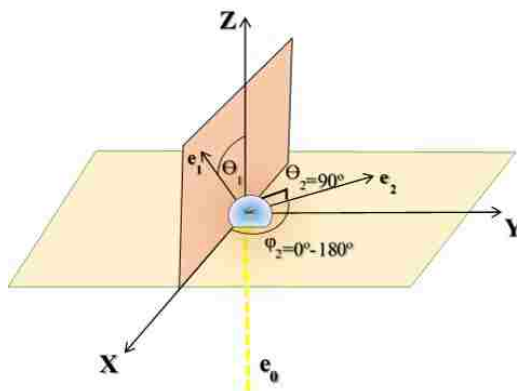


Figure 2.3. The x - y Plane shows the Full-Perpendicular Plane for Heidelberg group. Same parameters as in Figures 2.1 and 2.2, and φ_2 is the ejected electron azimuthal angle, and is detected and calculated from 0° to 180° .

for two different geometries used by the Manchester laboratory denoted as Coplanar and Perpendicular plane (see Figure 2.4). The differences between the Manchester and Heidelberg geometries are the name of the x - z plane and how they measure the cross-section for those different geometries. The Manchester group have the ability to move the electron gun between their two main planes, x - z and y - z , by rotating through a particular angle ($\Psi = 0^\circ$ and $\Psi = 90^\circ$). So, if the projectile gun angle ($\Psi = 0^\circ$), this is called Coplanar geometry, but if $\Psi = 90^\circ$, the geometry is called the Perpendicular plane, which is exactly the same as Heidelberg full perpendicular plane. However, the detectors here are fixed on the scattering plane (detection plane), and the cross section measurements are taken on the scattering plane itself. For the Heidelberg group, the projectile is always parallel to the z -direction, which comes from the negative side to the positive side of the z -axis, and then collides with the target sitting in the origin, see Figure 2.1. In this case, the detectors of the outgoing electrons move from plane to plane as needed in order to detect the scattered and ejected electrons. As mentioned above, these are basically the three main geometries that have been used in this dissertation (see papers section). However, we have performed calculations for the first experiment measured by Kate Nixon and Andrew Murray for Mg(3p) atom aligned

by laser [35], which put more challenges into theoretical models due to the big discrepancy between theoretical calculation and experimental data for one of the cases. (more details can be found in the publication section: [36][37]).

The coplanar geometry or scattering plane (x - z plane), which considered in all our calculations, is defined by the momentum vectors of the incoming and outgoing electrons, which are always in the scattering plane. The incoming electron collides with the bound electron (on the target) in the interaction region, and scatters with a scattering angle (θ_1), and the collision ionizes the target. During the moment of the collision, the bound electron will be ejected to a certain angle called the ejected electron angle (θ_2). Both the scattered and ejected electron will be detected in the scattering plane, which is perpendicular to both the Full-perpendicular plane (x - y) and the Half-perpendicular plane (y - z) see Figure 2.1. The second plane is the Half-perpendicular plane (HP). In this plane, the scattered electron is still detected on the scattering plane, while the ejected electron is detected in the (z - y) plane (half-perpendicular plane), see Figure 2.2. In the third plane, the scattered electron is also remaining in the scattering plane, while, the ejected electron is detected in the (x - y) plane as in Figure 2.3.

The features that can be seen from the coplanar TDCS measurements or calculations are two main peaks, one is called “*binary peak*” and the other is called “*recoil peak*”. In fact, the binary peak and the recoil peak represent the outgoing electrons angular distribution. The binary peak can be found on the opposite side of the z -axis than the projectile electron and this is due to the repulsion between the two continuum electrons in the scattering plane (0° - 180°), while the recoil peak can be seen or observed in the backward direction of the binary peak in the other half of the scattering plane (180° - 360°), which occurs when the ejected electron is back scattered by the nuclei. Moreover, the binary peak usually happens at an angle a little bit larger than the momentum transfer angle (\mathbf{q}), and the recoil peak usually smaller than ($-\mathbf{q}$) in most cases, especially when the scattered electron (e_1) is faster than the ejected electron (e_2). Furthermore, the binary and recoil peaks also may split

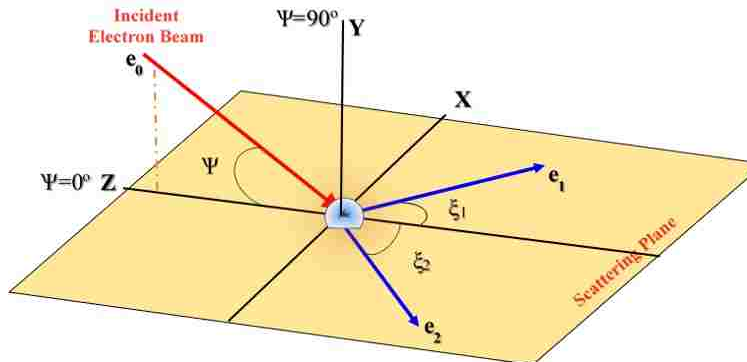


Figure 2.4. The x - z Plane shows the Scattering Plane or detecting Plane (Coplanar) when $\Psi = 0^\circ$, while the Perpendicular Plane determined by $\Psi = 90^\circ$ for Manchester group.

into two peaks in some cases at high incident electron energy and small scattered electron angle, i.e., instead of seeing two peaks in the scattering plane, one can see four peaks for the angular distribution. For instant, a $(e, 2e)$ study by Yong-Ki Kim[38] for Li^+ , Na^+ , and K^+ ions showed that both the binary and recoil peaks for the case of p -state ionization split into two peaks at an incident electron energy (~ 0.5 KeV) and an angle of 10° for the scattered electron[39]. Also, we have seen that for Ar (3p) atom at even at a lower energy of 66eV, and three different angles ($10^\circ, 15^\circ$, and 20°) [37].

It is also important to explain another distinguishing feature between the measurements of both experimental groups and that is the two different types of the kinematics used. These kinematical conditions are called *symmetric* and *asymmetric*. For the Heidelberg group, the symmetric geometry means that both the ejected and scattered electrons have different angles ($\theta_1 \neq \theta_2$) and equal outgoing electron energies ($E_1 = E_2$), see Figures 2.1-2.3. While for Manchester group, it means that the electrons have equal energy ($E_1 = E_2$), and equal detection angles, see Figure 2.4 for more details. The second kinematical measurement is the asymmetric, which can be seen for Heidelberg group and Manchester group as in Figures 2.1-2.4, where the outgoing electron energies are not equal ($E_1 \neq E_2$), and the scattered electron angle (θ_1 or ξ_1) is fixed at a certain angle, while the ejected electron angle (θ_2 or ξ_2) is detected at angles ranging between (θ_2 or $\xi_2 = 0^\circ$ - 180°).

3. THEORETICAL MODELS AND APPROXIMATIONS

3.1. THEORY OF ELECTRON IMPACT IONIZATION

In this dissertation, the main process of interest is the electron impact ionization of atoms and molecules, where a collision event occurs between an electron and a target (atom or molecule). In an inelastic collision changes and this is ionization for all the papers presented in the next chapter. To visualize the ionization process that this dissertation deals with, please see Figure 3.1. Figure 3.1 shows in general that an incident electron with energy (E_0) collides with a target (atom or molecule/ in any state), and after short time of the collision, a removal of one or more electrons from the target will have occurred. If one electron is ejected from the atom or molecule after the collision by the incident electron, the process then is known as a single ionization, which is what this dissertation is focusing on, and it is also known as the ($e,2e$) process.

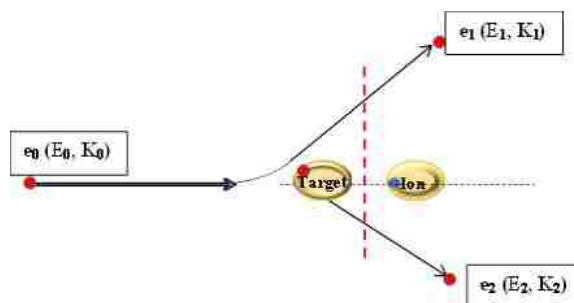


Figure 3.1. Illustrates the single ionization process. Left of the dashed red line shows the process before the collision and right is after the collision.

However, the incident electron could release two or more electrons from the target depending on its energy, and then the process is called multiple ionization. Moreover, there is another type of ionization which is called autoionization. In this type of ionization, the outer shell of the target loses two electrons that excited by the incoming electron while the target will be ionized at a lower energy state after emitting another electron.

For additional illustration, assume Z is a target in the ground state interacting with an incident electron e_0 which has kinetic energy E_0 and momenta k_0 . An expression for direct single ionization can be written as:

$$e_0^-(E_0, \vec{k}_0) + Z \rightarrow Z^+ + e_1^-(E_1, \vec{k}_1) + e_2^-(E_2, \vec{k}_2) \quad (1)$$

where Z^+ represents the ion that produced after the collision between the incident electron and the target, while e_1 and e_2 denotes the scattered (fast) electron and the ejected (slow) electron with kinetic energy and momenta E_1, k_1 and E_2, k_2 respectively.

Due to conservation of the total energy for the system, the incident energy and momenta can be written respectively in the following equations as:

$$E_{\text{int}} = \varepsilon_i + E_1 + E_2 \quad (2)$$

and

$$\vec{k}_{\text{int}} = \vec{k}_1 + \vec{k}_2 + \vec{P} \quad (3)$$

So,

$$\vec{P} = \vec{k}_{\text{int}} - \vec{k}_1 - \vec{k}_2 \quad (4)$$

where ε_i refers to the ionization potential, while P represents the residual ion momentum.

The momentum transferred to the target can be written as

$$\vec{q} = \vec{k}_{\text{in}} - \vec{k}_a \quad (5)$$

3.2. DIFFERENTIAL CROSS SECTIONS FOR ATOMS AND MOLECULES

In general, there are a few different types of cross sections for electron impact ionization such as the singly ($d\sigma/d\Omega$), doubly ($d^2\sigma/d\Omega_1 dE_1$) and fully (or triply) differential cross sections. In this dissertation, the triply differential cross section will be taken into

consideration. The triply differential cross section (TDCS) can be expressed for atoms and molecules as

$$\frac{d^3\sigma}{d\Omega_1 d\Omega_2 dE_1} \text{ (For atom), and } \frac{d^5\sigma}{d\Omega_1 d\Omega_2 dE_1} \text{ (for molecule)} \quad (6)$$

where E_1 and E_2 in expression 6 are the outgoing electrons energies, while $d\Omega_1$ and $d\Omega_2$ are the solid angles of both outgoing electrons respectively after the collision. The differential cross section can be expressed in terms of the momenta of the incident, scattered, and ejected electrons and the transition matrix (T-matrix) as will be seen later in the next sections.

3.2.1. Scattering Theory. In general, the quantum mechanics should be used to treat the electron collisions instead of the classical mechanics treatment. Consequently, in quantum mechanics physics, the Hamiltonian (H) for the projectile motion, which is considered an observable of the system, can be express as:

$$H = K + V \quad (7)$$

the kinetic energy operator is denoted by K , where $K = \frac{-1}{2}V^2$, and the potential energy is referred by V or P.E, which represents the reaction between the target and the electron before the collision.

Now we need to solve the Schrödinger equation and we will use $\Psi(r)$ for the wavefunction associated with any free particle moving in the space and its eigenstates are the solutions of the Schrödinger equation as in Equation 8 below. The eigenstate of K can be obtained from Equation 9 by using the wavefunction Φ .

$$(E_T - H) |\Psi\rangle = 0 \quad (8)$$

$$(E_T - K) |\Phi\rangle = 0 \quad (9)$$

Now the Schrödinger equation for the system can be written as:

$$\left[\frac{-1}{2} \nabla^2 + V(r) \right] \psi(r) = E_T \psi(r) \quad (10)$$

where the first part is the kinetic energy K and the second $V(r)$, is the scattering potential and E_T is the energy of the electron which is given in atomic units by:

$$E_T = \frac{k^2}{2} \quad (11)$$

where k^2 is the momentum of the electron. Now if we define a new potential energy for the system by multiplying both sides of Equation 10 by -2 , and write $2V(r) = U(r)$, then we get:

$$[\nabla^2 + k^2 - U(r)] \psi(r) = 0 \quad (12)$$

The Equation 6 can then be solved numerically if $V(r)$ considered to be goes to zero faster than $\frac{1}{r}$ as $r \rightarrow \infty$. This leads to an asymptotic form of the desired solution for Equation 12 [41] which is given by:

$$\psi(r)_{r \rightarrow \infty} \rightarrow C(e^{i\mathbf{k} \cdot \mathbf{r}} + f(k, \theta, \phi) \frac{e^{+ikr}}{r}) \quad (13)$$

where $\Psi(r)$ is the wavefunction for the steady state which contains a departing spherical wave for the scattered (fast) electron and a plane-wave for the incident electron (projectile). Here C is a normalization constant that does not depend on any of the spherical coordinates (r , θ and ϕ), and the function $f(k, \theta, \phi)$ is represent the scattering amplitude which is related to the differential cross section by

$$\frac{d\sigma}{d\Omega} = |f(k, \Omega)|^2 \quad (14)$$

where Ω is the scattering angle denoted by θ and ϕ , and $d\Omega = \sin\theta d\theta d\phi$. So, $f(k, \Omega)$, the scattering amplitude depends on the energy of the projectile and the scattering angles. The triply (sometimes called fully) differential cross section can be measured/ calculated if the two outgoing electrons are detected, and theoretically it is given by:

$$\frac{d^3\sigma}{d\Omega_1 d\Omega_2 dE_1} = \frac{k_1 k_2}{k_{\text{inc}}} |f(k, \Omega)|^2 \quad (15)$$

As mentioned above the Schrödinger equation is solvable only for two particles, however, approximations must be made to obtain the scattering amplitude $f(k, \Omega)$ for more than two-particles. Therefore, we will first study and illustrate some of these approximations such as the Lippmann-Schwinger equation, Born approximation, and first-order Born approximation.

3.2.2. The Lippmann-Schwinger Equation. If we start from Equation 12, we can write it again as

$$[\nabla^2 + k^2]\psi_k(r) = U(r)\psi_k(r) \quad (16)$$

So, by using the Lippmann-Schwinger equation and taking the boundary conditions into account, the general solution of the wavefunction $\Psi_k(r)$ can be found as:

$$\Psi_k^\pm(r) = \Phi_k(r) + \int G_0^\pm(r, r') U(r') \Psi_k^\pm(r') dr' \quad (17)$$

and the homogeneous equation is

$$[\nabla^2 + k^2]\Phi_k(r) = 0 \quad (18)$$

where $\Psi_k(r)$ is just a plane-wave given by:

$$\Phi_k(r) = (2\pi)^{-3/2} \exp(ik \cdot r) \quad (19)$$

$G_0^\pm(r, r')$ in Equation 17 is called the Green's function. The (-) sign denotes an incoming wave, while the (+) represents an outgoing wave. Equation 17 for outgoing wave can be written in the symbolic form as:

$$\Psi_k^+ = \Phi_k + G_0^+ U \Psi_k^+ \quad (20)$$

where G_0^+ is the Green's function of the free particle, which satisfies the following equation:

$$[\nabla^2 + k^2]G_0^+(r, r') = \delta(r - r') \quad (21)$$

and the solution of it is:

$$G_0^+(r, r') = -\frac{1}{4\pi} \frac{e^{ik|r-r'|}}{|r - r'|} \quad (22)$$

also, it can be written in an integral form as

$$G_0^+(r, r') = -\frac{1}{(2\pi)^3} \lim_{\varepsilon \rightarrow 0^+} \int \frac{e^{ik'(r-r')}}{k'^2 - k^2 - i\varepsilon} dk' \quad (23)$$

which for large r becomes:

$$G_0^+(r, r') \simeq \lim_{r \rightarrow \infty} -\frac{1}{4\pi} \frac{e^{ik\hat{r} \cdot r'}}{r} e^{ikr} \quad (24)$$

where k_i and k_f are the initial and final momentum vector respectively, and k_f is equal to $k\hat{r}$, where \hat{r} is a unit vector in the direction of the scattered particle, where $r = |r - r'|$.

Now if we substitute $G_0^+(r, r')$ in Equation 24 into in 17, we get:

$$\Psi_k^+(r) \lim_{r \rightarrow \infty} \Phi_{k_i}(r) - \frac{e^{ikr}}{4\pi r} \int e^{-ik_f \cdot r'} U(r') \Psi_k^+(r') dr' \quad (25)$$

By comparing between Equation 25 and Equation 13, the scattering amplitude can be written as:

$$f(\theta, \phi) = -2\pi^2 \langle \Phi_{k_f} | U | \Psi_{k_i}^+ \rangle \quad (26)$$

The transition matrix is related to the scattering amplitude where

$$T_{fi} = \langle \Phi_{k_f} | U | \Psi_{k_i}^+ \rangle \quad (27)$$

3.2.3. Born Approximations and its First Order. As shown in Equation 20, the wave function for the outgoing electron can be written in a symbolic form as: $\Psi_k^+ = \Phi_k + G_0^+ U \Psi_k^+$

Consequently, in order to obtain the inhomogeneous (distorted) part of the wavefunction, Equation 20 has to be solved by iteration. So, the distorted part is

$$\Psi_d(r) = G_0^+ U \Psi_k^+ = \int G_0^+(r, r') U(r') \Psi_k^+(r') dr' \quad (29)$$

By replacing $\Psi_k^+(r')$ in Equation 29 by $\Phi_k(r)$, which is the initial wavefunction in a zero-order approximation, and solving by iteration, we can generate a sequence of higher order approximations. The first order approximation would be

$$\Psi_k^{(1)}(r) = \int G_0^+(r, r') U(r') \Phi_k(r') dr' \quad (30)$$

and the second-order approximation would be

$$\Psi_k^{(2)}(r) = \int G_0^+(r, r') U(r') \Psi_k^{(1)}(r') dr' \quad (31)$$

Substituting Equation 30 in Equation 31, we get an expanded form of the second order

$$\Psi_k^{(2)}(r) = \int \int G_0^+(r, r') U(r') G_0^+(r', r'') U(r'') \Phi_k(r'') dr' dr'' \quad (32)$$

so, Equation 32 can be written simply in symbolic form as:

$$\Psi_k^{(2)}(r) = G_0^+ U G_0^+ U \Psi_0 = (G_0^+ U)^2 \Phi_k \quad (33)$$

Now, the wavefunction can be generalized to n-order as:

$$\Psi_k^{(m)} = (G_0^+ U)^m \Psi_0 = G_0^+ U \Psi_k^{(m-1)} \quad (34)$$

where Ψ_k^m represents the immediate previous order approximation for the wavefunction in the sequence, and n is an integer positive number ($m = 1, 2, \dots, \infty$). We can also write Equation 34 as a summation form

$$\Psi_k^+ = \sum_{m=1}^{\infty} (G_0^+ U)^{m-1} \Phi_k \quad (35)$$

Also, it can be expressed in a symbolic form which is known as the Born series [42] as:

$$\Psi_k^+ = \Phi_k + G^+ U \Phi_k \quad (36)$$

here the full Green's function G^+ is given by

$$G^+ = G_0^+ + G_0^+ U G_0^+ + G_0^+ U G_0^+ U G_0^+ + \dots \quad (37)$$

Now the insertion of the Born series into the scattering amplitude (26) gives :

$$f(k, \Omega) = -2\pi^2 \left\langle \Phi_{k_f} \left| U \left| \sum_{m=1}^{\infty} (G_0^+ U)^{m-1} \Phi_{k_i} \right. \right. \right\rangle \quad (38)$$

and this can be written in a general form as

$$f(k, \Omega) = f_{B1} + f_{B2} + f_{B3} + \dots + f_{Bm} + \dots \quad (39)$$

So, the sum of the first m -terms for the Born scattering amplitude is

$$f_{Bm} = \sum_{n=1}^m f_{Bn} \quad (40)$$

and

$$f_{Bn} = -2\pi^2 \langle \Phi_{k_f} | U | (G_0^+ U)^{n-1} \Phi_{k_i} \rangle \quad (41)$$

where f_{Bn} is the n^{th} Born term

Now if use Equation 38 for $m = 1$, we get

$$f(k, \Omega) = -2\pi^2 \langle \Phi_{k_f} | U | (G_0^+ U)^0 \Phi_{k_i} \rangle \quad (42)$$

where $(G_0^+ U)^0 = 1$, so we get

$$f_{B1} = -2\pi^2 \langle \Phi_{k_f} | U | \Phi_{k_i} \rangle \quad (43)$$

where f_{B1} is the first order Born approximation, which is the most common approach in collision theory. Here U represents the potential energy, and Φ_{k_f} (Φ_{k_i}) is the final (initial) wavefunction. Since the plane wave has been used for both the final and the initial particles, we can rewrite Equation 42 as the following:

$$\begin{aligned} f_{B1} &= N \int e^{ik_i r} U(r) e^{-ik_f r} dr \\ &= N \int e^{i(k_i - k_f)r} U(r) dr \\ &= N \int e^{iqr} U(r) dr \end{aligned} \quad (44)$$

where N is the normalization factor, and $k_i - k_f$ is equal to q . Where k_i (k_f) are the initial (final) momentum for the incoming (outgoing particles), and q is the momentum transferred between them.

Now as we saw previously in Equation 15 that $|f(k, \Omega)|^2$ is proportional to the differential cross section, i.e. $\frac{d^3\sigma}{d\Omega_1 d\Omega_2 dE_1} \propto |f(k, \Omega)|^2$. So here the triple differential cross section (TDCS) for the First order Born Approximation (FBA) is

$$\frac{d^3\sigma}{d\Omega_1 d\Omega_2 dE_1} = \frac{k_1 k_2}{k_{\text{int}}} |f_{B1}|^2 \quad (45)$$

In summary the First-order Born Approximation treats the incident and the scattered particle (electron in our case) as a plane wave, while the ejected particle is treated as a coulomb wave. Although all the interactions between the particles are not included in the potential energy $U(r)$, this approximation (FBA) still works well for atoms and molecules for high energy. As an example, a $(e, 2e)$ study for H_2O was carried out by Champion et al, in 2001 [43] and they found that the FBA gave good agreement between the theoretical calculations and experimental data. In addition, good agreement was found with the experimental data for the TDCS for electron impact ionization of helium atoms for high incident electron energy [44].

Actually this approximation has been improved by including higher terms in the amplitude, which increased the chance of getting better agreements with the experimental data at intermediate and low energies. This inclusion of higher order terms, however, increases the time of computer usage and the TDCS calculations. In addition to that, the Born series will may diverge for lower than intermediate because of the potential if supported any bound state.

For all these disadvantages mentioned above, it was necessary to improve this approximation [41] and think about other method in order to get better agreement with experimental work. Therefore, one way to fix this problem is using the distorted wave for the initial and final wave function. For that reason, in this work our concern will be about the low and intermediate energies using the distorted wave function of Born approximation which will be the next major discussion.

3.3. DISTORTED WAVE BORN APPROXIMATION

In fact, this Approximation came to be as an alternative for the weakness that appeared as divergence of the Born series that mentioned above for low and intermediate energies. Basically, the distorted wave Born Approximation (DWBA) depends on an essential idea that is breaking down the interaction potential into two parts, an exact treatment and a perturbed treatment, i.e., the first part is solved exactly while the second one is solved by using the perturbation theory. To show that, we can start with Equation 45 to represent the exact T-matrix for the $(e, 2e)$ process as the following equation:

$$T = \langle \Phi_f | H - H_0 | \Phi_i \rangle \quad (45)$$

where

$$H | \Phi_f \rangle = E | \Phi_f \rangle \quad (46)$$

and

$$H_0 | \Phi_i \rangle = E | \Phi_i \rangle \quad (47)$$

where H and H_0 are represent the full Hamiltonian for the system and an approximate initial-state Hamiltonian respectively, while the initial and final eigenfunctions for both Hamiltonians denoted by Φ_i and Φ_f respectively. Now, to introduce one of the most successful approximations for the electron impact ionization calculations, which the first order DWBA, we first define H_0 and H and all the T-matrix elements. Therefore, we start define the initial-state Hamiltonian in the standard DWBA as:

$$H_0 = H_{\text{targ}} + T_{K.E} + U_{\text{int}} \quad (48)$$

where H_0 in Equation 47 represents the Hamiltonian for the target and is the kinetic energy for the projectile, while U_{int} indicates the initial-state spherically symmetric potential for the interaction between the projectile and the target. So, the eigenfunction of the Hamiltonian

(H_{target}) of the target must satisfy the following equation:

$$H_{target} |\psi_{target}\rangle = E_{target} |\psi_{target}\rangle \quad (49)$$

where Ψ_{target} is the eigenfunction and E_{target} is the eigenenergy of the Hamiltonian. Now the Hamiltonian H_{target} can be written as

$$H_{target} = (-1/2) \sum_{i=1}^n \nabla_i^2 - \sum_{i=1}^n \frac{Z}{r_i} + \sum_{i=1}^{n-1} \sum_{j=i+1}^n \frac{1}{|\vec{r}_i - \vec{r}_j|} \quad (50)$$

In Equation 49, the kinetic energy operator for the target is denoted by the first term, while the second term represents the potential energy of the interaction between the electrons and the nucleus, and the third term is the potential energy of the inter-electronic repulsion.

Now, we can write the extended expression for U_{int} (the initial distorted potential that composed of a spherically symmetric approximation for the reaction between the target and the incident electrons which can be obtained from the charge density of the target (atom or molecule)).

$$U_{int}(r) = U_{ele}(r) + U_{nuc}(r) \quad (51)$$

The wavefunctions in Equation 45 also can be written in an extended expression for atom as the following:

$$|\Phi_i\rangle = |\psi_{HF}(\vec{r}_2) \chi_i(\vec{r}_1)\rangle \quad (52)$$

and

$$\langle \Phi_f | = \langle \chi_1(\vec{r}_1) \chi_2(\vec{r}_2) \psi_{ion} | \quad (53)$$

The Equation 51 shows that Φ_i (the initial state) is consisted of the product of $\chi_i(\vec{r}_1)$ the projectile wavefunction (an incident electron in our case) and $\Psi_{HF}(\vec{r}_2)$ the Hartree-Fock wavefunction for the target (atom or molecule). The final state wavefunction Φ_f is consists

of the product of $\chi_1(\vec{r}_1)$ and $\chi_2(\vec{r}_2)$, which are the final states distorted waves of the scattered and ejected electron respectively that can be obtained from U_{ion} , the final state distorted potential. The initial state distorted wave represented by $\chi_i(\vec{r}_1)$, which can be obtained from the initial state distorted potential U_{int} (the spherically symmetric for V_{int} which is the initial state interaction between the target and the projectile. So,

$$(T_{K.E} + U_{int}) \chi_i = \varepsilon_{int} \chi_i \quad (54)$$

and

$$(T_{K.E} + U_{ion}) \chi_{1(2)} = \varepsilon_{1(2)} \chi_{1(2)} \quad (55)$$

where ε_{int} is the energy of the projectile (electron), and $\varepsilon_{1(2)}$ is the energy of both outgoing electrons (the scattered and ejected). The sample U_{ion} represents the final state distorting potential which is composed of the spherically symmetric approximation of the bound electrons in the ion which are interacted with the outgoing electron and the contribution of the nucleus. Likewise, the full exact Hamiltonian for the system can be defined as:

$$H = H_{targ} + T_{K.E} + V_{int} \quad (56)$$

where V_{int} is the initial-state interaction between the target and the projectile.

Now from Equations 55 and 47 we get

$$H - H_0 = V_{int} - U_{int} \quad (57)$$

That led to the final form of DWBA, which can be obtained by substituting Equations 51,52 and 56 in Equation 45, so we get

$$T_{dir}^{DWBA} = \langle \chi_1(\vec{r}_1) \chi_2(\vec{r}_2) \psi_{ion} | V_{int} - U_{int} | \psi_{HF}(\vec{r}_2) \chi_i(\vec{r}_1) \rangle \quad (58)$$

Equation 58 is called the direct T-matrix of the Distorted Wave Born Approximation (DWBA) for atoms. However, this approximation is also valid for molecules. But the difference is in the initial state wavefunction. In molecules calculations, we use Dyson wave function for the initial state of the bound electron Ψ_{dy} (see details [45]), and accept that is the same physics that mentioned for atoms. Consequently, the T-matrix in Equation 58 becomes for molecules as the following:

$$T_{dir}^{MDWBA} = \langle \chi_1(\vec{r}_1) \chi_2(\vec{r}_2) \psi_{ion} | V_{int} - U_{int} | \psi_{Dy}(\vec{r}_2) \chi_i(\vec{r}_1) \rangle \quad (59)$$

In summary, it has been shown in many studies that the DWBA approach was actually one of the most successful methods that calculating triply differential cross section for electron impact ionization ($e,2e$) see [2] and [45][46][47]. The strength of this approach is that the inclusion of the short-range effects between the atom or ion and the two outgoing electrons. However, the main fail came from the fact that the correlation of the final state electron-electron was only taken into account of the first order [48]. Although the distorted wave Born approximation (DWBA) has been succeeded in providing good agreement with experimental data for atoms heavier than H and He in projectile (electron) energies higher than 100 eV [2], and the short time consumer that needed for the calculation (few seconds), there was urgent need that made a constellation of researchers thinking of other methods that has ability to cover a range of energies lower than $\sim 100\text{eV}$, as will be seen in the next section.

3.4. THREE-BODY DISTORTED WAVE APPROXIMATION (3DW)

The three body distorted wave approximation came after several attempts that tried to solve the weakness of the DWBA approach and other approaches in getting good agreements for low energies [49]. One of these efforts is BBK approach, which referred to Brauner, Briggs, and Klar, the first researcher group as we believe, who used the final state

wavefunction which fulfilled the exact asymptotic solution for the three body Schrödinger equation [48]. In brief, BBK showed that the inclusion of the post collision interaction (PCI), the Coulomb interaction between the two electrons, is useful in reducing the discrepancy between the theoretical calculation and experimental data for atoms for low incident electron energy. In addition, for hydrogen atom, BBK proved that better agreement was possible to obtain for low incident electron energy. The approximation of the exact final state wavefunction that has been used in BBK approach for hydrogen calculation can be described as [49]:

$$\Psi_f \approx CW_1 CW_2 C_{12} \quad (60)$$

where C_{12} (the Coulomb distortion factor) represents the final-state Coulomb interaction effects between the projectile and the ejected electron (PCI), and $CW_{1(2)}$ is a Coulomb wave for the projectile (ejected electron) in the field of a proton. For heavier atoms and molecules, however, this approach failed due the consideration that has been taken into account to treat heavy ions as a point charge. Therefore, a generalization of Equation 60, which is also call 3C approach, to the distorted wave approximation is crucially needed for improving the agreements for atoms heavier than hydrogen.

Now the starting point in this case is the DWBA (see 53). So here the comparable final state Φ_f of the developed DWBA would be

$$\langle \Phi_f | \approx \langle \chi_1(\vec{r}_1) \chi_2(\vec{r}_2) \psi_{ion} C_{12}(r_{12}, K_{12}) | \quad (61)$$

We used the exact post collision Coulomb interaction (PCI) between the two outgoing electrons which represented in 61 by $C_{12}(r_{12}, K_{12})$, where r_{12} and K_{12} are the relative distance between the two outgoing electron and relative momenta respectively. The final wavefunction shown above is normally called three-body distorted wave (3DW) for atom which is contributed to develop the three body distorted wave approximation. Actually, the theoretical foundation for 3DW has been demonstrated by Prideaux and Madison [49].

Here the post-collision interaction (PCI) between the two final state electron can be written as

$$C_{e-e}(\mathbf{k}_{12}, \mathbf{r}_{12}) = e^{\frac{-\pi\gamma}{2}} \Gamma(1 - i\gamma) {}_1F_1(i\gamma, 1, -i(k_{12}r_{12} + \mathbf{k}_{12} \bullet \mathbf{r}_{12})) \quad (62)$$

where $\Gamma(1 - i\gamma)$ is the gamma function, γ is the Sommerfeld parameter $\gamma = \frac{1}{v_{12}}$ which is a measure of the strength of the coulomb interaction between the two electrons, F_1 is a confluent Hypergeometric function, $k_{12} = \mu v_{12}$, $\mu = \frac{1}{2}$ is the reduced mass for two electrons, and v_{12} is the relative velocity between the two electrons.

The direct t -matrix of the 3DW in Equation 58 for atoms becomes

$$T_{dir}^{3DW} = \langle \chi_1(\vec{r}_1) \chi_2(\vec{r}_2) C_{12}(r_{12}, K_{12}) \psi_{ion} | V_{int} - U_{int} | \psi_{HF}(\vec{r}_2) \chi_i(\vec{r}_1) \rangle \quad (63)$$

Later on, the approximation has been generalized by Gao et al. to be used for molecule calculations [27],[32]. Similarly, the direct t -matrix for molecules would be the modification of the Equation 59

$$T_{dir}^{M3DW} = \langle \chi_1(\vec{r}_1) \chi_2(\vec{r}_2) C_{12}(r_{12}, K_{12}) \psi_{ion} | V_{int} - U_{int} | \psi_{Dy}(\vec{r}_2) \chi_i(\vec{r}_1) \rangle \quad (64)$$

In fact, one of the attractive advantages of the wavefunction shown in Equation 61 lies on the fact that it is an exact asymptotic solution of the three body problem. Moreover, the physics beyond the features of the 3DW approach is that the final state Coulomb interaction: between the two continuum electrons (e_1 and e_2), between the screened nuclear charge and the scattered electron (e_1), and between the screened nuclear charge and the ejected electron (e_2) are included in all the perturbation's terms, i.e. to all orders in the perturbation theory [50]. Also, the perturbation theory contained the coulomb interactions between both initial states for the projectile (electron) and a screened nuclear charge for a neutral

atom. However, the only interaction contained to first order in the 3DW approach is the initial-state non-spherical projectile-active-electron interaction which will be described as the following:

In the 3DW approach, the initial-state distorting potential can be expressed as

$$U_{int} = U_a + U_{ion} \quad (65)$$

while the initial-state interaction (the full potential) is given by

$$V_i = \sum_{j=1}^N \frac{z_p(-1)}{r_{1j}} + U_{ion} \quad (66)$$

where N is the number of electrons in the target, z_p is the projectile (electron in our case) charge, and U_{ion} represents the interaction between the rest of the remaining electrons in the target including the nuclei and the incident electron. So, if we have only one active electron then V_{int} can be approximated as

$$V_{int} = U_{ion} - \frac{1}{r_{12}} \quad (67)$$

Here U_a in Equation 65 is the spherically symmetric interaction potential between the active electron (e_2) and the incident electron (e_1) and $(\frac{-1}{r_{12}})$ denotes the interaction between the projectile electron and the active target electron.

Now subtracting Equation 64 from Equation 65, we get

$$V_{int} - U_{int} = -\frac{1}{r_{12}} - U_a \quad (68)$$

Substituting Equations 66 in Equation 62, we get

$$T_{dir}^{3DW} = \langle \chi_1(\vec{r}_1) \chi_2(\vec{r}_2) C_{12}(r_{12}, K_{12}) \psi_{ion} | -\frac{1}{r_{12}} - U_a | \psi_{HF}(\vec{r}_2) \chi_i(\vec{r}_1) \rangle \quad (69)$$

Similarly for molecules,

$$T_{dir}^{M3DW} = \langle \chi_1(\vec{r}_1) \chi_2(\vec{r}_2) C_{12}(r_{12}, K_{12}) \psi_{ion} | -\frac{1}{r_{12}} - U_a | \psi_{Dy}(\vec{r}_2) \chi_i(\vec{r}_1) \rangle \quad (70)$$

3.5. WARD AND MACEK APPROXIMATION

The Ward-Macek approximation [51], the WM as denoted wherever in our papers, is one of the most powerful approximations in treating the low energy electron impact ionization. Obviously, using the full Coulomb interaction that has been used in the 3DW (in Equation 62 is likely to overestimate the influence of the PCI. In fact, this approximation has been examined for most of our atoms work, and we found that for lower energies it is often gives very good agreement with experimental work. In this approximation, the actual final state electron-electron separation r_{12} has been replaced by an average value directed parallel to k_{12} . So, the full final state Coulomb interaction in Equation 62 becomes as

$$C_{e-e} = e^{-\frac{\pi\gamma}{2}} \Gamma(1 - i\gamma) {}_1F_1(i\gamma, 1, -ik_{12}r_{12} - ik_{12}r_{12}^{ave}) \quad (71)$$

where r_{12}^{ave} is the average separation between the two outgoing electrons, and it is given by

$$r_{12}^{ave} = \frac{\pi^2}{16 \varepsilon_t} \left(1 + \frac{0.627}{\pi} \sqrt{\varepsilon_t} \ln \varepsilon_t \right)^2 \quad (72)$$

where ε_t is the total energy of the two outgoing electrons (scattered and ejected electrons).

Now, the C_{e-e} factor becomes independent on r_{12} and k_{12} , and can be removed outside the T-matrix integral, which reduces the calculation difficulty and save time consumer of the calculation from the few days to few seconds. The squared absolute value of the Coulomb factor can be written as

$$|C_{e-e}|^2 = \left| e^{-\frac{\pi\gamma}{2}} \Gamma(1 - i\gamma) {}_1F_1(i\gamma, 1, -2ik_{12}r_{12}^{ave}) \right|^2 \quad (73)$$

Where the squared absolute value of $(e^{-\frac{\pi\gamma}{2}}\Gamma(1-i\gamma))$ is called Gamow factor (N_{ee}), which can be expressed as

$$N_{ee} = \left| e^{-\frac{\pi\gamma}{2}} \Gamma(1-i\gamma) \right|^2 = \frac{(\pi/k_{12})}{(e^{\pi/k_{12}} - 1)} \quad (74)$$

So, the Equation 73 becomes

$$|C_{e-e}|^2 = N_{ee} \left| {}_1F_1(i\gamma, 1, -2ik_{12}r_{12}^{ave}) \right|^2 \quad (75)$$

With

$$v_{12} = \frac{-1}{|k_1 - k_2|} \text{ and } k_{12} = |k_1 - k_2| \quad (76)$$

where $|C_{e-e}|^2$, which is introduced by Ward and Macek, is called also M_{ee}

So, in this case the WM t -matrix of the stranded DWBA can be re-expressed by using the approximation of the Coulomb interaction

$$T_{dir}^{WM} = C_{e-e} \langle \chi_1(\vec{r}_1) \chi_2(\vec{r}_2) \psi_{ion} | V_{int} - U_{int} | \psi_{t \text{ arg}}(\vec{r}_2) \chi_i(\vec{r}_1) \rangle \quad (77)$$

where $\Psi_{t \text{ arg}}$ is either the Hartree- Fock wavefunction for an atom or the Dyson wavefunction for a molecule.

Because the cross section is proportional to the square of the T-matrix, in the Ward-Macek approximation the triply differential cross-section (TDCS) would be the multiplication of the standard DWBA amplitude and Mee factor.

$$\frac{d^3\sigma^{WM}}{d\Omega_1 d\Omega_2 dE_2} = M_{ee} \frac{d^3\sigma^{DWBA}}{d\Omega_1 d\Omega_2 dE_2} \quad (78)$$

PAPER**I. KINEMATICALLY COMPLETE STUDY OF LOW-ENERGY
ELECTRON-IMPACT IONIZATION OF NEON: INTERNORMALIZED CROSS
SECTIONS IN 3D KINEMATICS**

Xueguang Ren,^{1,2}Sadek Amami,³Oleg Zatsarinny,⁴Thomas Pflüger,^{1,2}Marvin Weyland,^{1,2}
Woon Yong Baek,¹Hans Rabus,¹Klaus Bartschat,⁴Don Madison,³and Alexander Dorn²

¹Physikalisch-Technische Bundesanstalt,

38116, Braunschweig, Germany

²Max-Planck-Institut für Kernphysik,

69117, Heidelberg, Germany

³Physics Department,

Missouri University of Science and Technology,

Rolla, Missouri 65409, USA

⁴Department of Physics and Astronomy,

Drake University,

Des Moines, Iowa 50311, USA

ABSTRACT

Low-energy ($E_0 = 65$ eV) electron-impact single ionization of Ne ($2p$) has been investigated to thoroughly test state-of-the-art theoretical approaches. The experimental data were measured using a reaction microscope, which can cover nearly the entire 4π solid angle for the secondary electron emission energies ranging from 2 eV to 8 eV, and projectile scattering angles ranging from 8.5° to 20.0° . The experimental triple-differential cross sections are internormalized across all measured scattering angles and ejected energies.

The experimental data are compared to predictions from a hybrid second-order distorted-wave Born plus R -matrix approach, the distorted-wave Born approximation with inclusion of post-collision interaction (PCI), a three-body distorted-wave approach (3DW), and a B -spline R -matrix (BSR) with pseudostates approach. Excellent agreement is found between experiment and predictions from the 3DW and BSR models, for both the angular dependence and the relative magnitude of the cross sections in the full three-dimensional parameter space. The importance of PCI effects is clearly visible in this low-energy electron-impact ionization process.

1. INTRODUCTION

Electron-impact ionization of atoms and molecules is of fundamental importance in a wide variety of sciences and modeling applications, including the physics and chemistry of planetary atmospheres, reactive plasmas, and more recently [1, 2, 3] even radiation tumor therapy, in which the secondary low-energy electrons produced by primary ionizing radiation can effectively induce substantial strand breaks in deoxyribonucleic acid (DNA) and their subunits. Precise experimental data are hence important to aid in the development of theoretical models and to understand the mechanism of the ionization dynamics.

The full information about the ionization dynamics can be obtained in kinematically complete experiments, or so-called $(e, 2e)$ studies [4, 5], which determine the momentum vectors of all free particles. Such experiments serve as a powerful tool to comprehensively test theoretical models that account for the quantum mechanical few-body interactions. In recent years, theory has made tremendous progress in describing the electron-impact ionization dynamics, which is now considered to be well understood for the simplest systems such as atomic hydrogen and helium [6, 7, 8].

Much more challenging, however, is the treatment of more complex targets, e.g., the neon ($2p$) and argon ($3p$) ionization dynamics. Theoretical models, which have been frequently used to describe ionization processes in heavy complex targets, are a hybrid

distorted-wave Born approximation (DWBA) plus R -matrix (close-coupling) approach [9, 10, 11, 12], the DWBA with inclusion of the post-collision interaction (PCI) by the Gamow factor calculated with the Ward-Macek method [13], the three-body distorted-wave (3DW) approach (see e.g. [14, 15, 16, 17, 18, 19, 20]), and most recently the B -spline R -matrix (BSR) approach [21, 22]. Except for BSR, which includes a large number of pseudostates to estimate the effect of the high-lying Rydberg states and the ionization continuum in the *ab initio* solution of the close-coupling equations, the approaches treat at least some part of the process perturbatively to first or second order. The theoretical models have been tested by experiments over a wide range of impact energies, collision dynamics, and targets. Reasonable agreement between theoretical predictions and experimental findings has been found for high and sometimes also intermediate and low impact energies. (See, for example, [14, 15, 16, 17, 18, 19, 21, 22, 23, 24, 25, 26, 27, 28, 29].)

Recent studies for the electron-impact ionization of Ne ($2p$) at an incident energy $E_0 = 100$ eV showed an unprecedented agreement between experiment and BSR predictions regarding both the shape (i.e., the angular dependence) and the relative magnitude of the triple-differential cross sections (TDCS) [22]. The experiment was performed by measuring internormalized TDCS in the full three-dimensional (3D) parameter space, i.e., not limited to the most popular co-planar or other specialized geometries. These “3D-TDCS” presentations provide a thorough test ground for theory [22]. Since the physical effects of PCI as well as electron exchange and charge-cloud polarization in the projectile-target interaction are expected to become even more pronounced with decreasing projectile energy, the present study extends the previous work on electron-impact ionization of Ne ($2p$) to the even lower impact energy of $E_0 = 65$ eV to further test the different theories.

The TDCSs were measured by covering a large part of the full solid angle for the emitted electron. Since the experimental data are internormalized for different kinematical situations, a *single common scaling factor is sufficient* to fix the relative magnitude of the experimental and theoretical data for all cases. After deciding on that factor, the angular

dependence and the relative magnitude of the measured TDCS can be compared with the theoretical predictions. The measurements reported here cover a range of ejected-electron energies ($E_2 = 2.0$ eV, 4.5 eV and 8.0 eV) and projectile scattering angles ($\theta_2 = 8.5^\circ$, 12.5° , and 20.0°). The experimental data are compared with theoretical predictions from several calculations based on the hybrid second-order DWBA plus R -matrix approach (DWB2-RM), the DWBA with inclusion of PCI using the Ward-Macek method (DWBA-WM) [13], 3DW, and BSR.

This paper is organized as follows. After a brief description of the experimental apparatus in Section 2, we summarize the essential points of the four theoretical models in Section 3. The results are presented and discussed in Section 4, before we finish with the conclusions. Unless specified otherwise, atomic units (a.u.) are used throughout.

2. EXPERIMENT

The experiment was performed with an advanced reaction microscope, which was especially built for the electron-impact experiment [30]. It was recently updated by using a newly developed pulsed photoemission electron gun and a pulsed electric field for fragmentation detection [31]. Since details of the experimental setup can be found in [31, 32], only a brief outline will be given here. A well-focused (≈ 1 mm diameter), pulsed electron beam crosses a supersonic neon gas jet, which is produced by supersonic gas expansion through a $30 \mu\text{m}$ nozzle and two-stage differential pumping. The pulsed electron beam is generated by a photoemission electron gun, in which a pulsed ultraviolet laser (266 nm) illuminates a tantalum photocathode ($\Delta T \approx 0.5$ ns and $\Delta E_0 \approx 0.5$ eV).

Using uniform electric and magnetic fields, the fragments in the final state are projected onto two position- and time-sensitive multi-hit detectors equipped with fast delay-line readout. For single ionization, triple coincidences of both outgoing electrons (e_1 and e_2) and the recoil ion are recorded. From the positions of the hits and the times of flight (TOF), the vector momenta of the detected particles can be determined. Note that the

projectile beam axis (defining the z -direction) is adjusted exactly parallel to the electric and magnetic extraction fields. Therefore, after passing the target gas jet, the beam arrives at the center of the electron detector, where a central bore in the multichannel plates allows for the undeflected electrons to pass without inducing a hit. The detection solid angle for electrons is close to 4π , apart from the acceptance holes at small forward and backward angles where the electrons end up in the detector bore.

3. THEORETICAL MODELS

We have used four different theoretical models to describe the present electron-impact ionization process. Their essential ingredients will be summarized below. More information can be found in the references given.

3.1. DWB2-RM. The hybrid approach is originally based on the work of Bartschat and Burke [9]. The key idea is the assumption that a “fast” projectile acts as a perturbation on the initial target, ultimately resulting in an ejected electron scattering from the residual ion. In this respect, it is a generalization of the photoelectron process, except that the Coulomb interaction between the projectile and the target leads to a number of terms in the multipole expansion, compared to a single term in the electric dipole approximation. Also, the projectile (described by a distorted wave) can interact with the target multiple times. In our model, we include second-order interactions, thereby labeling the first part of the model “DWB2”. More details can be found in [10, 11, 12].

The second part of the model requires a description of the initial state and the scattering of the ejected electron from the residual ion. For this part, we employ the R -matrix (RM) method to solve the resulting close-coupling equations. Since the computer code is limited to the use of a single set of orthogonal one-electron orbitals, we employ the multi-configuration expansions developed by Burke and Taylor [33] for the $(2s^22p^5)^2P$ and $(2s2p^6)^2S$ states of Ne^+ included in this part of the problem.

Until the development of the fully nonperturbative BSR with pseudostates approach described in the next subsection, DWB2-RM was the standard method to account at least partially for channel-coupling effects in electron-impact ionization of complex targets, i.e., beyond quasi-one and quasi-two electron systems. The major shortfalls of the method are the asymmetric treatment of the two electrons (one by a distorted wave, one by a close-coupling expansion) and the neglect of both exchange and PCI effects. Hence, we generally expect the method to be appropriate for incident energies of several hundred eV, highly asymmetry energy sharing, and small scattering angles of the (fast) projectile. However, even in situations like those investigated in the present work, we find that comparing with results from a well-tested model such as DWB2-RM remains useful, in light of the very complex BSR calculations. Such a comparison may also be helpful to check possible normalization issues that have been noticed to affect results obtained, for example, in models that use the correct asymptotic form of the three-body Coulomb problem but may not be sufficiently accurate for describing the actual ionization process near the nucleus. Given its ability to employ accurate representations of the initial bound state as well as the final ionic states and to account for the most important channel-coupling effects, DWB2-RM should be fairly reliable to predict the probability for the actual ionization process, although it may not predict the bending of the binary and recoil lobes (see below) according to PCI effects.

3.2. BSR. The details of the BSR calculations carried out for this work were described in [21, 22]. Briefly, we employ a 679-state nonrelativistic BSR (close-coupling) model, with 55 states representing the bound spectrum and the remaining 624 the target continuum. All singlet and triplet target states with total electronic angular momentum $L = 0 - 4$ were included. The continuum pseudostates in the present calculations cover the energy region up to 85 eV.

The R -matrix radius was set to $30 a_0$, where $a_0 = 0.529 \times 10^{-10}$ m is the Bohr radius. We employed 70 B -splines to span this radial range using a semi-exponential knot grid. The scattering model contained up to 2,280 scattering channels, leading to generalized

eigenvalue problems with matrix dimensions up to 150,000 in the B -spline basis that is used for the expansion of the outer target orbitals (including the pseudoorbitals) as well as the projectile wave function inside the R -matrix box. Partial waves for total orbital angular momenta $L \leq 25$ were obtained numerically, followed by a top-up procedure to estimate the contributions from even higher L values.

The ionization amplitudes were determined by a two-step process, in which the scattering amplitudes for excitation of the pseudostates are mapped to true continuum states of the ejected-electron–residual-ion system through overlap factors between the pseudostates and these continuum states. This projection method (details can be found in [34, 35]) corresponds to an effective interpolation scheme [36] that becomes increasingly accurate with increasing density of the pseudospectrum. To obtain numerically stable results, it is important to use the same close-coupling expansion (here just a two-state model with the $(2s^22p^5)^2P$ and $(2s2p^6)^2S$ states of Ne^+) to generate both the pseudostates in a bound-state close-coupling model and the physical electron-ion scattering states used for the projection. Since the BSR approach, in contrast to the DWB2-RM model described above, employs individually optimized, and hence nonorthogonal, orbital sets, the two ionic states can be represented sufficiently well without relying on additional pseudoorbitals.

3.3. The Three-Body Distorted-Wave Approximation. The three-body distorted-wave (3DW) approach has been previously discussed in [19, 20, 27]. Here we present a brief overview with the key features of the theory necessary for the present discussion. In the present paper, two different approximations will be presented.

3.3.1. 3DW. In the 3DW model, the direct T -matrix is given by

$$T_{dir}^{3DW} = \langle \Psi_f | W | \Psi_i \rangle, \quad (1)$$

where, for ionization of an atom, the initial-state wave function Ψ_i is described as a product of the initial Hartree-Fock bound-state wave function ψ_{HF} for the target and a distorted-wave function χ_i for the incoming electron (the projectile):

$$\Psi_i = \psi_{\text{HF}} \chi_i. \quad (2)$$

The perturbation (W) is given by

$$W = V_i - U_i. \quad (3)$$

Here V_i is the interaction between the incident electron and the atom, and U_i is the initial-state spherically symmetric static approximation for U_i , which is asymptotically equal to zero. The final-state wave function is described as a product of two final-state continuum electron distorted waves (χ_1 for the scattered and χ_2 for the ejected electron, respectively), and the Coulomb interaction between the outgoing electrons (C_{12}), normally called the PCI:

$$\Psi_f = \chi_1 \chi_2 C_{12}. \quad (4)$$

In the 3DW model, we use the exact electron-electron Coulomb interaction between the two electrons for C_{12} , which requires the evaluation of a six-dimensional (6D) numerical integral. This factor is a product of a gamma factor and a hypergeometric function:

$$C_{12}(r_{12}, k_{12}) = e^{-\frac{\pi\gamma}{2}} \Gamma(1 - i\gamma) {}_1F_1(i\gamma, 1, -i[k_{12}r_{12} + k_{12} \cdot r_{12}]) \quad (5)$$

Here r_{12} is the relative distance between the two electrons, k_{12} is the relative momentum, $k_{12} = \mu v_{12}$, $\mu = \frac{1}{2}$ in atomic units is the reduced mass for the two continuum electrons, and v_{12} is the relative velocity between the two electrons. The factor ${}_1F_1$ is a confluent

hypergeometric function, $\Gamma(1 - i\gamma)$ is the gamma function, and $\gamma = \frac{1}{v_{12}}$ is the Sommerfeld parameter, which is a measure of the strength of the Coulomb interaction between the two electrons.

Finally, the direct 3DW T -matrix becomes

$$T_{dir}^{3DW} = \langle \chi_1 \chi_2 C_{12} | V_i - U_i | \psi_{HF} \chi_i \rangle, \quad (6)$$

The exchange T -matrix T_{exc}^{3DW} is identical to Eq. (6), except that the scattered and ejected electrons are exchanged in the final-state wave function Ψ_f .

3.3.2. DWBA-WM. The second approximation we will present is the DWBA-WM (Distorted Wave Born Approximation with Ward-Macek method) to calculate the TDCS for ionization of Ne ($2p$) [13]. In this model, the term $k_{12} \cdot r_{12}$ is replaced by $k_{12} r_{12}^{ave}$, where the average value r_{12}^{ave} of the electron-electron separation is defined by

$$r_{12}^{ave} = \frac{\pi^2}{16\varepsilon_t} \left(1 + \frac{0.627}{\pi} \sqrt{\varepsilon_t} \ln \varepsilon_t \right)^2, \quad (7)$$

with ε_t denoting the total energy of the two electrons. Since the Ward-Macek approximation for the Coulomb repulsion factor C_{12}^{WM} does not explicitly depend on the electronic coordinates, it can be removed from the T -matrix integral. This reduces the computational difficulty and required time substantially.

We can write the square of the Coulomb factor as

$$|C_{12}^{WM}|^2 = N_{ee} |{}_1F_1(i\gamma, 1, -2ik_{12}r_{12}^{ave})|^2, \quad (8)$$

where N_{ee} , the so-called Gamov factor [13], is defined as

$$N_{ee} = |e^{-\frac{\pi\gamma}{2}} \Gamma(1 - i\gamma)|^2 = \frac{\pi/k_{12}}{(e^{\pi/k_{12}} - 1)}. \quad (9)$$

With these approximations, the direct DWBA-WM T -matrix becomes

$$T_{dir}^{DWBA-WM} = C_{12}^{WM} [\langle \chi_1 \chi_2 | V_i - U_i | \psi_{HF} \chi_i \rangle], \quad (10)$$

or

$$T_{dir}^{DWBA-WM} = C_{12}^{WM} T_{dir}^{DWBA}, \quad (11)$$

Finally, with the T -matrix given in atomic units, the TDCS in both theories can be expressed as

$$TDCS = \frac{1}{(2\pi)^5} \frac{k_1 k_2}{k_i} (|T_{dir}|^2 + |T_{exc}|^2 + |T_{dir} - T_{exc}|^2), \quad (12)$$

where k_i , k_1 , and k_2 are the magnitudes of the momenta of the initial, scattered, and ejected electrons, respectively.

Calculations are typically classified in terms of orders of perturbation theory. However, this classification can become ambiguous since any physics contained in the approximate wave function is contained to all orders of perturbation theory, while the physics contained in the perturbation will be contained to the order of the calculation. For the 3DW model, the electron-electron interaction is contained in the approximate final-state wave function; hence, this physics is contained to all orders of perturbation theory. The non-perturbative BSR calculation also accounts for PCI to all orders of perturbation theory, but only within the R -matrix box. This is the reason, why in the BSR calculations for ionization the box size is generally chosen larger than required by the typical rule that exchange between the projectile electron and the target electrons is negligible. The DWBA-WM model contains an estimate for the electron-electron interaction in the approximate system wave function, i.e., it contains an approximation for PCI to all orders. The DWB2-RM model, finally, contains the electron-electron interaction in the perturbation, but only inside

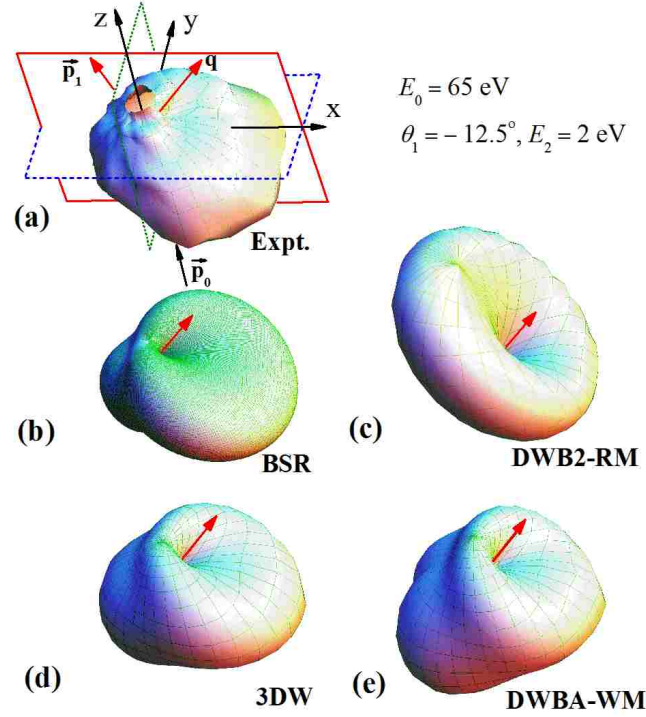


Figure 1. Experimental and theoretical TDCS for ionization of Ne ($2p$) by incident electrons with energy $E_0 = 65 \text{ eV}$, presented as 3D images. The scattering angle is $\theta_1 = -12.5^\circ \pm 2.5^\circ$, and the ejected electron energy is $E_2 = 2.0 \text{ eV} \pm 1.0 \text{ eV}$. Panel (a) shows the experimental 3D TDCS, while panels (b)–(e) represent the predictions from the BSR, DWB2-RM, 3DW, and DWBA-WM models, respectively.

the reaction region, i.e., a standard (small) R -matrix box of about $12 a_0$ in the present case. Within this box, PCI would be accounted for to second order, but this is not the region where it is most important. Hence, DWB2-RM neglects almost all PCI effects.

4. RESULTS AND DISCUSSION

Figure 1 exhibits the experimental and theoretical TDCSs for ionization of Ne ($2p$) by 65 eV electron-impact as three-dimensional (3D) polar plots for a projectile scattering angle of $\theta_1 = -12.5^\circ$ as a function of the emission direction of a slow ejected electron with $E_2 = 2.0 \text{ eV}$ energy. Panel 1 (a) corresponds to the experimental data, while panels 1 (b)–(e) show the calculated results from the BSR, DWB2-RM, 3DW and DWBA-WM

models, respectively. The projectile enters from the bottom and is scattered to the left (hence the minus in the notation for the angle). These two vectors define the scattering (xz) plane as indicated by the solid frame in panel (a). The momentum transfer to the target is indicated by the arrow labeled q .

In these 3D-plots, the TDCS for a particular direction is given as the distance from the origin of the plot to the point on the surface, which is intersected by the ionized electron's emission direction. [Below we follow the common notation of referring to the slower of the two outgoing electrons as "ionized", "emitted", or "ejected", and to the faster one as "scattered".] The kinematics chosen displays exemplarily the principal features of the emission pattern: it is governed by the well-known binary and recoil lobes. The binary lobe is oriented roughly along the direction of the momentum transfer q , thus corresponding to electrons emitted after a single binary collision with the projectile. In the opposite direction the recoil lobe is found, where the outgoing slow electron additionally backscatters in the ionic potential. For ionization of p -states, the binary peak often exhibits a minimum along the momentum transfer direction. This is the result of the characteristic momentum profile of a p -orbital that has a node for vanishing momentum. Additionally, the emitted electron is repelled by the scattered projectile due to the long-range nature of the Coulomb force. These PCI effects tilt the binary and recoil lobes away from the scattered projectile direction. Further, the binary lobe exhibits a much flatter shape in comparison with 3D emission patterns for high and intermediate energies.

Comparing the experimental results to the various theoretical predictions, we see that the BSR and 3DW calculations generally show good agreement with the data. The DWBA-WM calculation yields reasonable agreement with the experimental data in the binary region, but significant discrepancies appear in the recoil region, particularly for the cross sections outside the scattering plane. The DWB2-RM calculations often also reproduces the relative shape of the experimental 3D cross sections, except that major discrepancies are observed near the direction of the scattered projectile. This problem is

due to the fact that PCI effects are effectively neglected in the DWB2-RM model while they are accounted for to all orders in the 3DW, to all orders in the BSR (up to $30 a_0$ away from the center), and approximately (everywhere) to all orders in DWBA-WM.

For a more quantitative comparison between experiment and theory, cross section cuts through the 3D TDCS image along the three orthogonal planes as indicated in Figures 1 (a) are presented in Figures 2–4. Those are the xz -plane or scattering plane (solid line in Figure 1(a)), the yz -plane or perpendicular plane (dotted line), and the xy -plane or full-perpendicular plane (dashed line), in Figures. 2–4 these planes are shown in the left, middle, and right columns of the figures, respectively. In Figures 2, 3 and 4 the same experimental data are compared to the BSR and DWB2-RM results (Figure 2), the 3DW and DWBA-WM results (Figure 3) and the BSR and 3DW calculations (Figure 4), respectively. The studied kinematical conditions correspond to projectile scattering angles from $\theta_1 = -8.5^\circ$ to -20° and ejected electron energies from $E_2 = 2.0$ eV to 8.0 eV. The global scaling factor used to normalize the experimental data to the theories was found by achieving the best visual fit of experiment and the BSR and 3DW calculations for the TDCS in the scattering plane at $\theta_1 = -12.5^\circ$ and $E_2 = 2.0$ eV, as shown in Figures 2 (d) and 3 (d). It was subsequently applied to all other kinematics and planes.

In Figures 2–4 the experimental cross sections are presented as a function of the ejected electron emission angles. The data are integrated over an out-of-plane angular range of $\pm 10^\circ$. This should have only minor implications for the scattering plane, where the cross section varies slowly for small out-of-plane angles. The scattering plane cuts through the binary and the recoil peaks, and it contains the momentum transfer vector indicated in the diagrams by an arrow. In the scattering plane, we observe the well-known binary and recoil patterns. The characteristic dip along the q direction or splitting of the binary peak mentioned above is indicated in the experimental data in particular for the larger scattering angle case $\theta_1 = -20^\circ$. Here, one smaller peak close to the projectile scattering (i.e., near-forward) direction and one larger peak at larger angles with respect to q are observed.

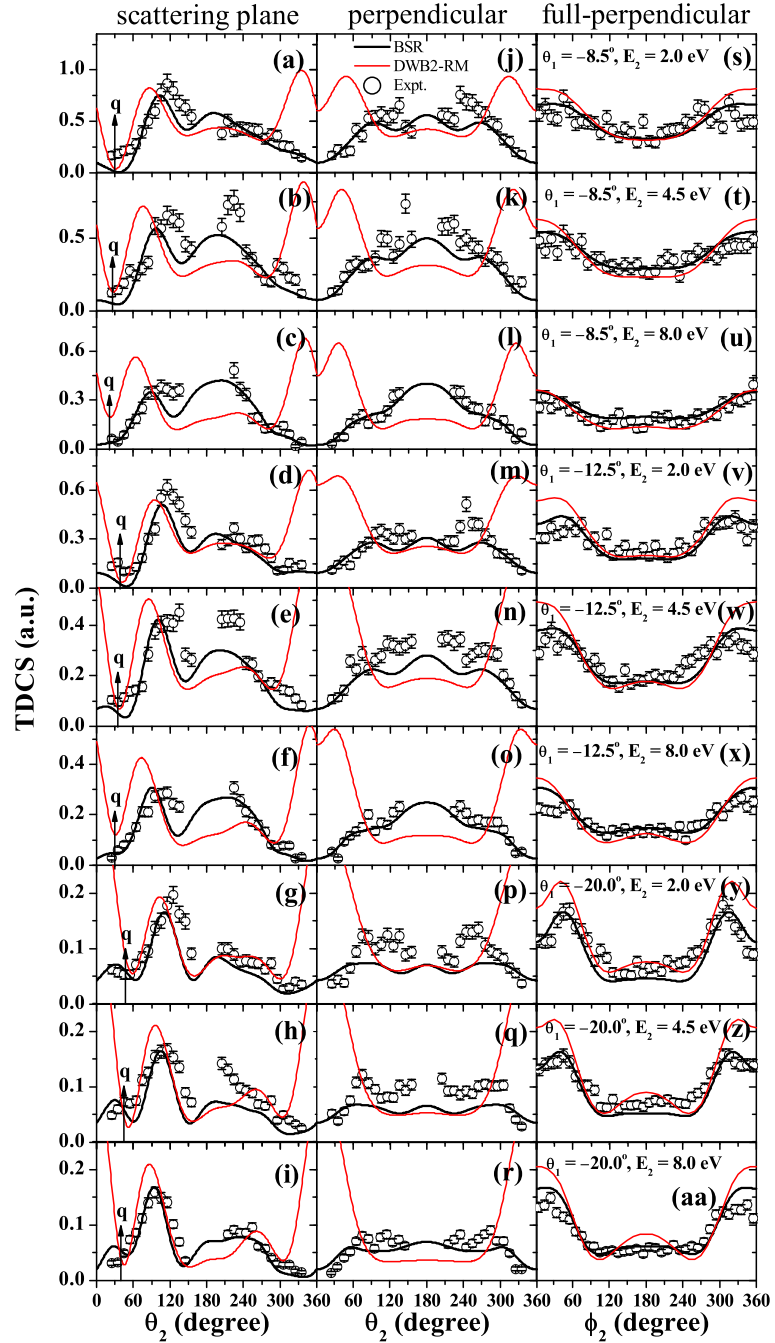


Figure 2. TDCS for the ionization of Ne (2p) presented as a function of the ejected electron (e_2) emission angle at different scattering angles θ_1 ($-8.5^\circ \pm 1.5^\circ$, $-12.5^\circ \pm 2.5^\circ$, $-20^\circ \pm 5^\circ$) and ejected-electron energies E_2 (2.0 eV ± 1.0 eV, 4.5 eV ± 1.5 eV, 8.0 eV ± 2.0 eV). Left column: TDCS in the xz -plane (scattering plane). Central column: TDCS in the yz -plane (perpendicular plane). Right column: TDCS in the xy -plane (full-perpendicular plane). The various collision kinematics (θ_1 , E_2) are labeled in the panels of the right column. Thick black lines: BSR model, thin red lines: DWB2-RM model. The open circles (\circ) with error bars represent the experimental data.

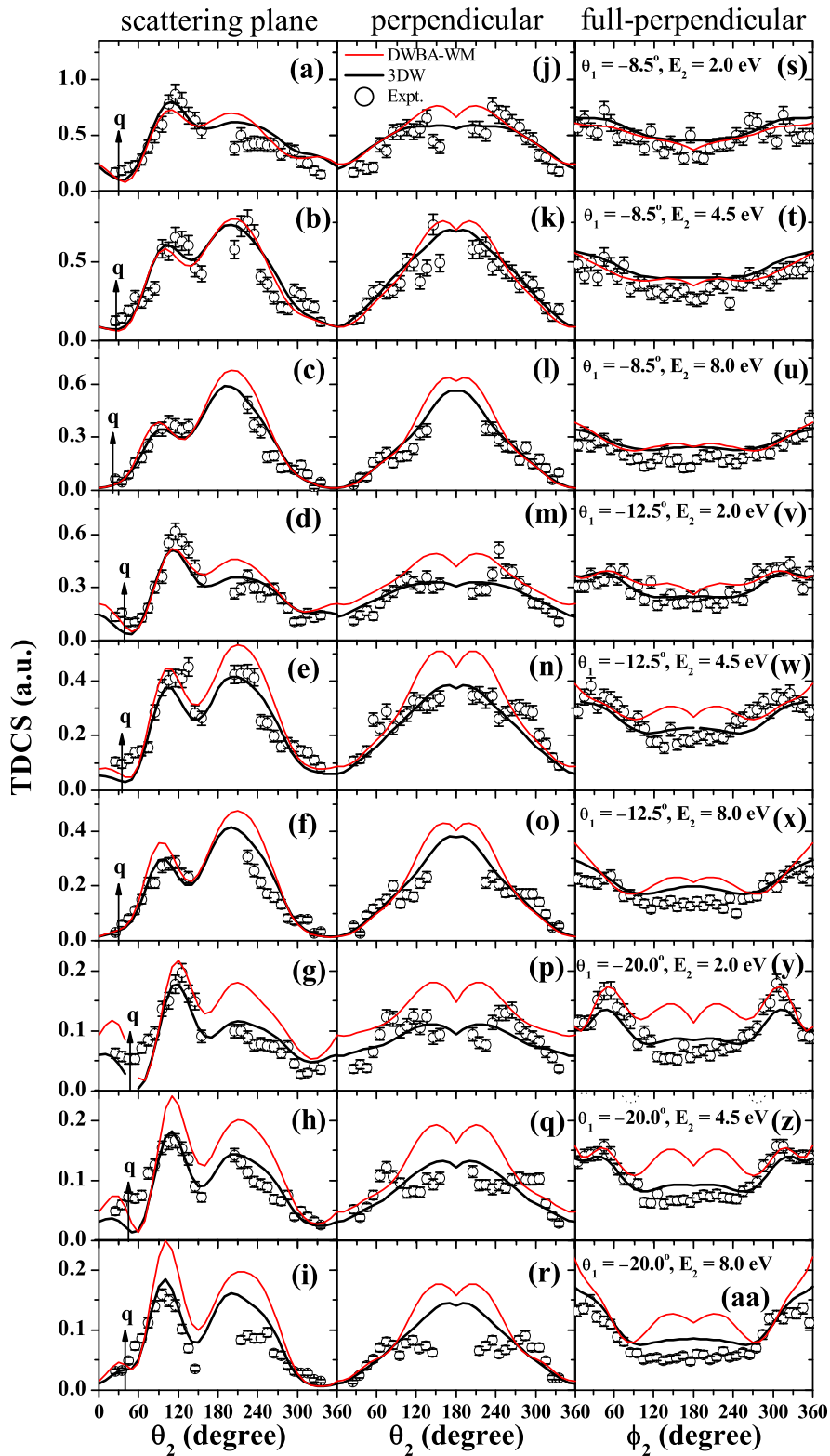


Figure 3. Same as Figure 2, except that the theoretical calculations are the 3DW (thick black lines) and DWBA-WM (thin red lines).

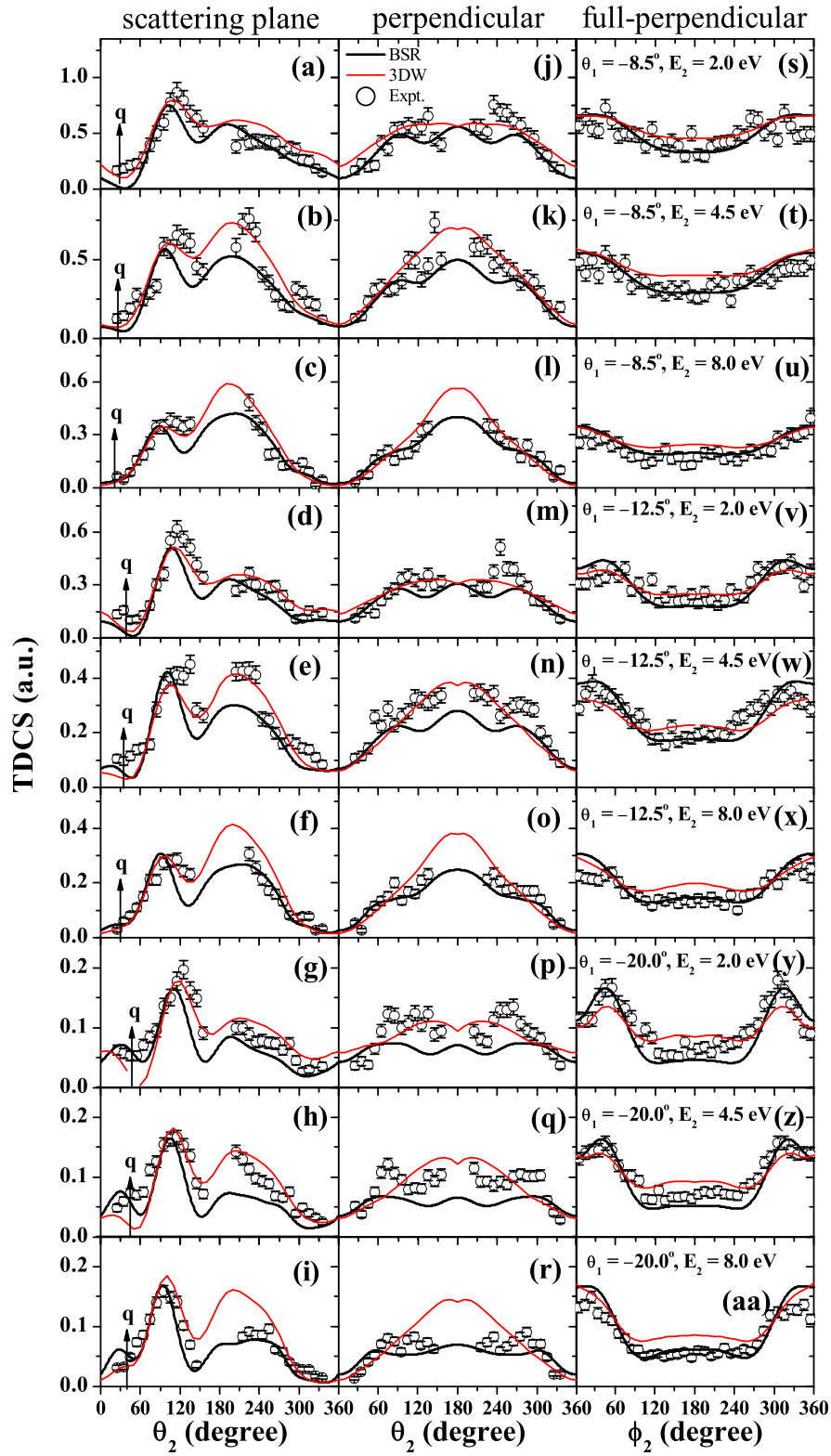


Figure 4. Same as Figure 2, except that the theoretical calculations are the BSR (thick black lines) and 3DW (thin red lines).

This is another signature of the enhanced PCI effect in the low-energy regime, where the binary peak is significantly suppressed near the forward direction. In the perpendicular plane, there is an indication of a three-lobe structure, particularly for the larger projectile scattering angles. This plane cuts through the double-lobe binary peak, thereby resulting in two symmetric maxima in the ranges $\theta_2 = 60^\circ - 90^\circ$ and $\theta_2 = 270^\circ - 300^\circ$, respectively. In addition the recoil lobe gives rise to the central maximum at $\theta_2 = 180^\circ$. In this plane PCI acts strongest for emission angles near 0° and 360° .

In the full-perpendicular plane, which is perpendicular to the incident-projectile direction, the ejected electron's polar angle is fixed to $\theta_2 = 90^\circ$ and the azimuthal angle ϕ_2 is varied. The observed structures for emission at azimuthal angles near 0° and 360° and also for some cases near $\phi_2 = 60^\circ$ and 300° are caused by the binary peak. The recoil peak most likely influences the cross sections near $\phi_2 = 180^\circ$. In this plane the influence of PCI appears to be small over the entire angular range.

In Figure 2 the experimental data are compared to predictions from the BSR and DWB2-RM models. Overall, excellent agreement between BSR and the experimental data is noticed regarding both the angular dependence of the cross sections and the relative magnitude over the entire range of angle and energy conditions analyzed. The general features observed in the three planar cuts, including the strong PCI effect near the forward direction, are well reproduced by the BSR theory, except that for some cases the experimental cross section exhibits enhanced intensity for the recoil peaks in the scattering plane, as seen in panels (b), (e), and (h) of Figure 2. In the perpendicular plane, the BSR theory is able to reproduce the observed three-lobe structure, while slight deviations in the magnitude of the three-lobe structure are visible for the case of $\theta_1 = -20^\circ$ (c.f. panels (p)–(r) in Figure 2). The best agreement between BSR and the experimental data is found for the full-perpendicular plane.

Regarding the DWB2-RM theory, significant discrepancies between its predictions and the experimental data are observed near the projectile forward direction, as can be seen in the left (scattering plane) and central columns (perpendicular plane) of Figure 2. This problem is again due to the very weak PCI effect in this model. Outside the forward direction ($\theta_2 = 60^\circ - 300^\circ$) the DWB2-RM calculations often yield reasonable agreement with the experimental data and the BSR theory. In the full-perpendicular plane, good agreement is found between the DWB2-RM calculations and the measurements.

In Figure 3 the experimental data are compared to predictions from the 3DW and DWBA-WM models. The DWBA-WM results are generally in good agreement with the experimental data, especially for the smallest projectile scattering angle of $\theta_1 = -8.5^\circ$. For the larger scattering angles of $\theta_1 = -12.5^\circ$ and -20° , DWBA-WM overestimates the magnitude of the recoil-peak contributions in all three planes. The DWBA-WM model provides a clear improvement over the DWB2-RM calculations in that its predictions become reasonable in the angular range of θ_2 close to 0° and 360° . This indicates that the PCI effect plays a very important role in the low-energy ionization processes studied here.

There is overall excellent agreement between the 3DW predictions and the experimental data concerning both the angular dependence of the cross sections and the relative magnitude over the entire range of angle and energy conditions analyzed. This is particularly true in the scattering plane (left column of Figure 3) and the full-perpendicular plane (right column of Figure 3). The only noticeable systematic differences occur in the perpendicular plane (central column of Figure 3), where the 3DW predicts less structure than is indicated in the data.

Overall, both the 3DW and BSR theories exhibit excellent agreement with the experimental data. A direct comparison between the experimental data and these two apparently best calculations is presented in Figure 4. Noticeable deviations include some results for the scattering plane, where the BSR calculations slightly underestimate the magnitude of the recoil peaks for the ejected energy of $E_2 = 4.5$ eV compared to the

experimental data and the 3DW calculations, and the case of $\theta_1 = -20.0^\circ$ and $E_2 = 8.0$ eV, where the 3DW model overestimates the magnitude of the recoil peak. In the perpendicular plane, the BSR calculation predicts the structure seen in the data better than the 3DW. The best overall agreement between theory and the experiment is found for the cross sections in the full-perpendicular plane.

5. CONCLUSIONS

We have reported a comprehensive study of the electron-impact ionization dynamics of Ne ($2p$) at a low incident projectile energy of 65 eV. The three-dimensional representations of the triple-differential cross sections obtained experimentally were internormalized across all scattering angles of θ_1 from -8.5° to -20.0° and ejected electron energies of E_2 from 2.0 eV to 8.0 eV, thus providing a thorough test for the theoretical models. The experimental data were compared to predictions from the DWB2-RM, DWBA-WM, 3DW, and BSR models. The DWB2-RM model provides reasonable cross sections for ionization geometries of θ_2 from 60° to 300° , where PCI effects do not play a significant role. The predictions from the DWBA-WM model, where PCI is accounted for via the Ward-Macek approximation, improves the results for θ_2 close to 0° and 360° . This clearly indicates that PCI effects play a very important role in the present low-energy ionization processes.

The experimental data and the BSR and 3DW results, on the other hand, reveal an unprecedented degree of agreement not only in the angular dependence but also in the relative magnitude of the triple-differential cross section over a range of scattering angles and ejection energies in the entire 3D parameter space.

ACKNOWLEDGMENTS

This work was supported, in part, by the United States National Science Foundation under grants No. PHY-1068237 (SA and DM), No. PHY-1212450 and No. PHY-1430245 (OZ and KB), and the XSEDE allocations No. PHY-090031 (OZ and KB) and TG-MCA075029 (SA and DM). SA would also like to thank the Libyan Ministry of Higher Education's Scholarship for funding.

REFERENCES

- [1] B. Boudaïffa, P. Cloutier, D. Hunting, M.A. Huels, and L. Sanche. Resonant formation of dna strand breaks by low-energy (3 to 20 ev) electrons. *Science*, 287:1658, 2000.
- [2] G. Hanel, B. Gstir, S. Denifl, P. Scheier, M. Probst, B. Farizon, M. Farizon, E. Illenberger, and T. D. Märk. Electron attachment to uracil: Effective destruction at subexcitation energies. *Phys. Rev. Lett.*, 90:188104, 2003.
- [3] S. Tonzani and C. H. Greene. Radiation damage to dna: Electron scattering from the backbone subunits. *J. Chem. Phys.*, 125:094504, 2006.
- [4] H. Ehrhardt, M. Schulz, T. Tekaatt, and K. Willmann. Ionization of helium: Angular correlation of the scattered and ejected electrons. *Phys. Rev. Lett.*, 22:89, 1969.
- [5] U. Amaldi, A. Egidi, R. Marconero, and G. Pizzella. Use of a two channeltron coincidence in a new line of research in atomic physics. *Rev. Sci. Instrum.*, 40:1001, 1969.
- [6] T. N. Resigno, M. Baertschy, W.A. Isaacs, and C.W. McCurdy. Collisional breakup in a quantum system of three charged particles. *Science*, 286:2474, 1999.

- [7] X. Ren, I. Bray, D. V. Fursa, J. Colgan, M. S. Pindzola, T. Pflüger, A. Senftleben, S. Xu, A. Dorn, and J. Ullrich. Electron-impact ionization of helium: A comprehensive experiment benchmarks theory. *Phys. Rev. A*, 83:052711, 2011.
- [8] O. Zatsarinny and K. Bartschat. Nonperturbative treatment of ionization with excitation of helium by electron impact. *Phys. Rev. Lett.*, 107:023203, 2011.
- [9] K Bartschat and P G Burke. The r-matrix method for electron impact ionisation. *J. Phys. B*, 20(13):3191, 1987.
- [10] R H G Reid, K Bartschat, and A Raeker. Initial-state, final-state and higher-order effects in electron impact ionization of helium atoms. *J. Phys. B*, 31(3):563, 1998.
- [11] Yanghua Fang and Klaus Bartschat. Convergent second-order calculations for simultaneous electron-impact ionization-excitation of helium. *J. Phys. B*, 34(2):L19, 2001.
- [12] Klaus Bartschat and Oleg Vorov. Channel-coupling, target-structure, and second-order effects in electron-impact ionization of Ar($3p$) and Ar($3s$). *Phys. Rev. A*, 72:022728, Aug 2005.
- [13] S. J. Ward and J. H. Macek. Wave functions for continuum states of charged fragments. *Phys. Rev. A*, 49:1049, 1994.
- [14] A. Naja, E. M. Staicu Casagrande, A. Lahmam-Bennani, M. Stevenson, B. Lohmann, C. Dal Cappello, K. Bartschat, A. Kheifets, I. Bray, and D. V. Fursa. (e, 2e) triple differential cross-sections for ionization beyond helium: the neon case at large energy transfer. *J. Phys. B*, 41:085205, 2008.
- [15] L. R. Hargreaves, M. Stevenson, and B. Lohmann. Absolute triple-differential cross sections for intermediate energy electron impact ionization of neon and argon. *J. Phys. B*, 43:205202, 2010.

- [16] M. A. Stevenson, L. R. Hargreaves, B. Lohmann, I. Bray, D. V. Fursa, K. Bartschat, and A. Kheifets. Fully differential cross-section measurements for electron-impact ionization of neon and xenon. *Phys. Rev. A*, 79:012709, 2009.
- [17] X. Ren, A. Senftleben, T. Pflüger, A. Dorn, K. Bartschat, and J. Ullrich. Benchmark experiment for electron-impact ionization of argon: Absolute triple-differential cross sections via three-dimensional electron emission images. *Phys. Rev. A*, 83:052714, 2011.
- [18] X. Ren, A. Senftleben, T. Pflüger, J. Ullrich, K. Bartschat, and A. Dorn. Erratum: Benchmark experiment for electron-impact ionization of argon: Absolute triple-differential cross sections via three-dimensional electron emission images [phys. rev. a **83** , 052714 (2011)]. *Phys. Rev. A*, 89:029904(E), 2014.
- [19] S. Amami, M. Ulu, Z. Nur Ozer, M. Yavuz, S. Kazgoz, M. Dogan, O. Zatsarinny, K. Bartschat, and D. Madison. Theoretical and experimental investigation of $(e, 2e)$ ionization of argon $3p$ in asymmetric kinematics at intermediate energy. *Phys. Rev. A*, 90:012704, 2014.
- [20] Sadek Amami, Andrew Murray, Al Stauffer, Kate Nixon, Gregory Armstrong, James Colgan, and Don Madison. Theoretical and experimental $(e, 2e)$ study of electron-impact ionization of laser-aligned mg atoms. *Phys. Rev. A*, 90:062707, Dec 2014.
- [21] O. Zatsarinny and K. Bartschat. Nonperturbative treatment of electron-impact ionization of ar($3p$). *Phys. Rev. A*, 85:032708, 2012.
- [22] T. Pflüger, O. Zatsarinny, K. Bartschat, A. Senftleben, X. Ren, J. Ullrich, and A. Dorn. Electron-impact ionization of neon at low projectile energy: An internormalized experiment and theory for a complex target. *Phys. Rev. Lett.*, 110:153202, 2013.

- [23] Hari Chaluvadi, C. G. Ning, and Don Madison. Theoretical triple-differential cross sections of a methane molecule by a proper-average method. *Phys. Rev. A*, 89:062712, Jun 2014.
- [24] Ola Al-Hagan, Christian Kaiser, Andrew James Murray, and Don Madison. Atomic and molecular signatures for charged-particle ionization. *Nat Phys*, 5:59–63, Jan 2009.
- [25] Ola Al-Hagan, A. J. Murray, C. Kaiser, J. Colgan, and D. H. Madison. Electron-impact-ionization cross sections of h_2 for low outgoing electron energies from 1 to 10 eV. *Phys. Rev. A*, 81:030701, Mar 2010.
- [26] S. Bellm, J. Lower, R. P. McEachran, E. Weigold, C. Ryan-Anderson, and D. H. Madison. Spin- and fine-structure-resolved ionization of krypton. *Phys. Rev. A*, 78:062707, Dec 2008.
- [27] Don H. Madison and Ola Al-Hagan. The distorted-wave born approach for calculating electron-impact ionization of molecules. *Journal of Atomic, Molecular, and Optical Physics*, 2010:24, 2010.
- [28] Arne Senftleben, Ola Al-Hagan, Thomas Pflüger, Xueguang Ren, Don Madison, Alexander Dorn, and Joachim Ullrich. Fivefold differential cross sections for ground-state ionization of aligned h_2 by electron impact. *The Journal of Chemical Physics*, 133(4):–, 2010.
- [29] Kate L. Nixon, Andrew James Murray, Hari Chaluvadi, Sadek Amami, Don H. Madison, and Chuangang Ning. Low energy (e,2e) measurements of ch_4 and neon in the perpendicular plane. *The Journal of Chemical Physics*, 136(9):–, 2012.
- [30] X. Ren, A. Senftleben, T. Pflüger, A. Dorn, K. Bartschat, and J. Ullrich. Signatures of projectile–nucleus scattering in three-dimensional (e,2e) cross sections for argon. *J. Phys. B*, 43:035202, 2010.

- [31] Xueguang Ren, Thomas Pflüger, Marvin Weyland, Woon Yoon Baek, Hans Rabus, Joachim Ullrich, and Alexander Dorn. An $(e, 2e + \text{ion})$ study of low-energy electron-impact ionization and fragmentation of tetrahydrofuran with high mass and energy resolutions. *J. Chem. Phys.*, 141:134314, 2014.
- [32] J. Ullrich, R. Moshhammer, A. Dorn, R. Dörner, L.Ph.H. Schmidt, and H. Schmidt-Böcking. Recoil-ion and electron momentum spectroscopy: reaction-microscopes. *Rep. Prog. Phys.*, 66:1463, 2003.
- [33] P G Burke and K T Taylor. R-matrix theory of photoionization. application to neon and argon. *J. Phys. B*, 8(16):2620, 1975.
- [34] Oleg Zatsarinny and Klaus Bartschat. Nonperturbative b-spline r-matrix-with-pseudostates calculations for electron-impact ionization of helium. *Phys. Rev. A*, 85:062709, Jun 2012.
- [35] Oleg Zatsarinny and Klaus Bartschat. The b-spline r-matrix method for atomic processes: application to atomic structure, electron collisions and photoionization. *J. Phys. B*, 46(11):112001, 2013.
- [36] I. Bray, C. J. Guilfoile, A. S. Kadyrov, D. V. Fursa, and A. T. Stelbovics. Ionization amplitudes in electron-hydrogen collisions. *Phys. Rev. A*, 90:022710, Aug 2014.

II. THEORETICAL AND EXPERIMENTAL INVESTIGATION OF (e,2e) IONIZATION OF ARGON (3p) IN ASYMMETRIC KINEMATICS AT INTERMEDIATE ENERGY

Sadek Amami¹, Melike Ulu², Zehra Nur Ozer², Murat Yavuz², Suay Kazgoz²,
Mevlut Dogan², Oleg Zatsarinny³, Klaus Bartschat³, and Don Madison¹

¹Physics Department, Missouri,
University of Science and Technology,
Rolla, MO 65409, USA.

²Department of Physics,
e-COL Laboratory, Afyon Kocatepe University,
03200, Afyon, Turkey

³Department of Physics and Astronomy,
Drake University,
Des Moines, IA 50311, USA

ABSTRACT

The field of electron-impact ionization of atoms, or (e,2e), has provided significant detailed information about the physics of collisions. For ionization of hydrogen and helium, essentially exact numerical methods have been developed which can correctly predict what will happen. For larger atoms, we do not have theories of comparable accuracy. Considerable attention has been given to ionization of inert gases and, of the inert gases, argon seems to be the most difficult target for theory. There has been several studies comparing experiment and perturbative theoretical approaches over the last few decades, and generally qualitative but not quantitative agreement is found for intermediate energy incident electrons. Recently a new non-perturbative method, the B-spline R-matrix (BSR), was

introduced which appears to be very promising for ionization of heavier atoms. We have recently performed an experimental and theoretical investigation for ionization of argon, and we found that, although the BSR gave reasonably good agreement with experiment, there were also some cases of significant disagreement. The previous study was performed for 200 eV incident electrons and ejected electron energies of 15 eV and 20 eV. The purpose of the present work is to extend this study to a much larger range of ejected electron energies (15 eV – 50 eV) to see if theory gets better with increasing energy as would be expected for a perturbative calculation. The experimental results are compared with both the BSR and two different perturbative calculations.

1. INTRODUCTION

There has been a long history of interest in the problem of obtaining triple-differential cross sections (TDCS) for electron-impact ionization of atoms [called an (e,2e) process] since the pioneering work of Ehrhardt and his collaborators [1, 2, 3]. One of the important reasons that measurements of TDCS have remained of interest for so many years lies in the fact that these experiments represent the most sensitive test of theoretical models since all kinematic parameters are determined (except for the spin). Consequently, accurate experimental measurements remain in demand for testing new theoretical developments.

In the early days of this work, the theoretical calculations were primarily first- or second- order distorted-wave (DWB1 or DWB2) [4, 5, 6, 7, 8, 9, 10, 11, 12] or first- or second-order R-matrix (DWB1-RM or DWB2-RM) calculations [13, 14]. By the 1990's, computers became powerful enough to be able to perform non-perturbative calculations. Starting at that time the convergent close-coupling (CCC) approach [15, 16, 17, 18], the exterior complex-scaling (ECS) approach [19, 20, 21, 22, 23], and the time-dependent close-coupling (TDCC) method [24, 25, 26, 27] were applied to electron-impact ionization of hydrogen and helium. Excellent agreement was found between experiment and theory, so these two problems can be regarded as 'solved'. However, the development of similarly

'exact' non-perturbative methods for heavier atoms has proven to be very difficult. The most promising recent development seems to be the B-spline R-matrix (BSR) approach introduced by Zatsarinny and Bartschat [28, 29, 30, 31, 32]. Very good agreement between experiment and the BSR results was found for ionization of helium [29, 30], and neon [28]. The agreement was not as good for ionization of Ar [32], although the principal problem lay with the original experimental data, which were recently corrected [33] for 200 eV incident energy. Nevertheless, even after the correction (the same experimental problem occurred for the 71 eV data [32]), agreement between experiment and theory will be far from perfect.

Argon has been studied from the discharge point of view for more than 100 years, and there have been several (e,2e) measurements made for argon over the past few decades. Groups in Australia and Orsay, France have studied ejection of the 2p electrons for incident electron energies greater than 1 keV [34, 35, 36]. Lahmam-Bennani et al. [37] have presented measurements of absolute TDCS for ionization of the 3p electrons and Avaldi et al. [38] have shown that distorted-wave impulsive approximations satisfactorily described the TDCS at the Bethe ridge conditions. The Orsay group proposed a high incident energy (720 eV) experiment, in which the incident electron energy loss is large and momentum transfer is small. Under this condition, the two outgoing electrons strongly interact with each other [36, 37, 38, 39].

There are a few (e,2e) experimental studies for argon in asymmetric geometry for intermediate energies. In this geometry, the post-collision interaction (PCI) and exchange effects can be very important, especially for slow ejected electrons. The first experimental study of argon at 100 eV and 250 eV incident energies was performed by Ehrhardt et al. [40] at asymmetric kinematics. The Australian group has presented a series of experimental studies on 3s and 3p ionization of argon at low to intermediate energies [41, 42, 43, 44]. They have focused generally on an incident energy of 113.5 eV and low electron ejection energies and they have compared the experimental data with the DWBA. Using the same kinematic conditions, a comparative study was made by Stevenson and Lohmann over an

extended angular range using a magnetic angle changer [45]. Recently, both experimental and theoretical investigations have concentrated on ionization of the outer 3p orbital of argon at an intermediate incident energy (200 eV) for asymmetric kinematics. These kinematics were chosen due to the anticipation that multiple competing interactions (such as PCI and exchange effects) will be important. Stevenson et al. [46] compared their measurements with the DWBA, the DWB1-RM and DWB2-RM predictions, and they found good agreement with experiment for the high ejection energies, and large discrepancies for lower ejection energies. More recently, Ren et al. [32, 33, 47] reported measurements for incident energies of 195 eV and 70.8 eV. They found good agreement with the RM calculations even for lower incident energy of 70.8 eV. Finally, Hargreaves et al. [48] examined argon (3p) ionization, and they also found significant discrepancies between experiment and theory.

Last year, we reported an experimental and theoretical study of the ionization of the Argon 3p orbital at 200 eV incident energy for asymmetric coplanar geometry, ejected electron energies of 15 and 20 eV, and three fixed scattered electron angles of 10° , 15° and 20° [40]. DWB1-RM, DWB2-RM, and non-perturbative B-spline R-matrix (BSR) results were compared with experiment. Surprisingly, good agreement between the BSR calculation and experiment was found only for the smallest scattering angle (10°) with very significant differences for 20° . In fact, the DWB2-RM results gave better shape agreement with experiment than the BSR for the larger scattering angles. This is surprising since one would expect a perturbative approach to become less accurate with increasing angles (decreasing cross section) while a non-perturbative approach should not have this problem.

The purpose of the present paper is to further investigate this situation. The previous work represented an angular scan for two fixed ejected electron energies. Here we report an energy scan for two fixed scattering angles. Comparing results from perturbative and non-perturbative calculations, one would expect a perturbative calculation to get better with increasing energy while a non-perturbative calculation should not be affected by energy (as long as it is converged). The highest energy considered in the previous work was 20 eV and

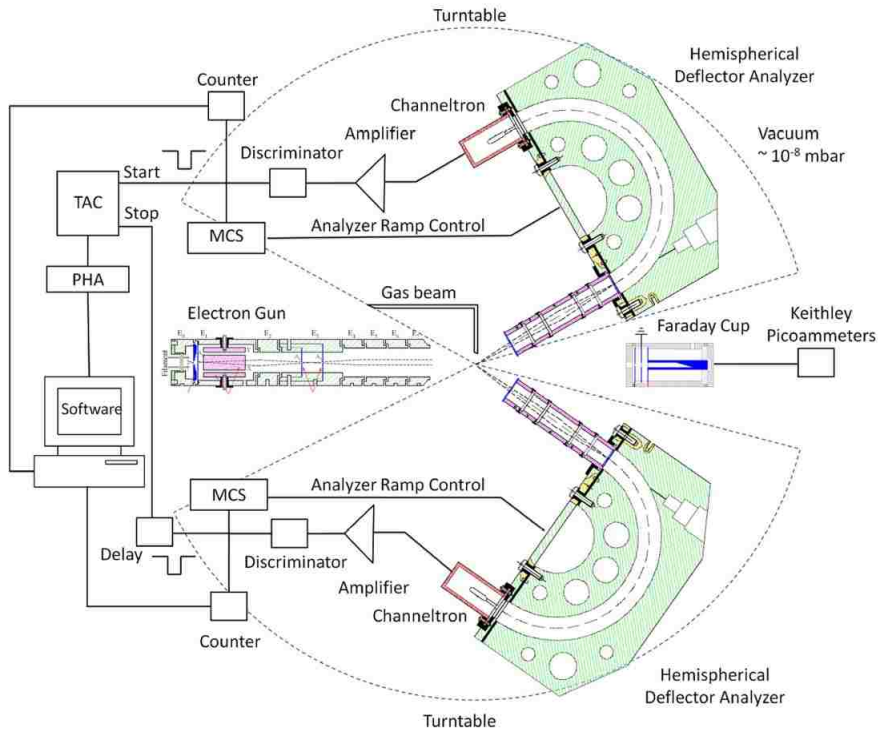


Figure 1. Schematic diagram of the coincidence electronics used to accumulating a coincidence timing spectrum at each kinematics.

here we examine energies ranging from 15 eV to 50 eV for scattering angles of 10° and 15° . As mentioned above, it is expected that PCI and exchange effects are probably important for these energies. Consequently, in addition to the DWBA-RM and BSR calculations, we also compare with a 3-body distorted-wave (3DW) calculation that includes PCI to all orders of perturbation theory.

2. EXPERIMENTAL APPARATUS

The experiments described here were performed using an electron spectrometer especially designed for electron-electron coincidence experiments in the e-COL laboratory, Afyon. A detailed description of the apparatus and its applications to ionization of He [49, 50], Ar [51], and H_2 [52, 53] targets is given in references. As described previously [54], the electron spectrometer is comprised of an electron gun, two hemispherical electron

analyzers, and a Faraday cup. A schematic diagram of the electron spectrometer and electron pulse handling system is shown in Figure 1. The spectrometer is contained in a cylindrical stainless steel vacuum chamber. The pressure in the chamber was maintained at $\sim 5.0 \times 10^{-6}$ mbar during data handling. This spectrometer operated at an electron current of $\sim 1 \mu\text{A}$ with a resolution of $\sim 0.6 \text{ eV}$. The (e,2e) technique is used to detect two outgoing electrons in coincidence after ionization of the target atom. The two electrons produced by single ionization of an atom are energy analyzed by hemispherical electron energy analyzers and detected by Channel Electron Multipliers (CEM), which are mounted on the hemispherical electron energy analyzers. This technique has an advantage for obtaining single ionization events for which the outgoing electrons have originated from the same ionization event. To do this, time correlation between the detected electrons is taken into account. The time delay between the electrons is converted to a signal that is recorded by computer, and a narrow coincidence peak in the timing spectrum is observed.

3. THEORY

We have used three different numerical methods to describe the process of interest. Each of them has been described previously. Hence we will only summarize them briefly to the extent necessary for the present discussion, but provide references where interested readers can find more information.

3.1. 3DW. The three-body distorted wave (3DW) approach has been described in previous works, so we will just present the aspects of the theory necessary for the present discussion [55]. The T-matrix can be written as

$$T_{fi}^{3DW} = \langle \Phi_f | W | \Phi_i \rangle \quad (1)$$

where Φ_i and Φ_f are the initial- and final-state wave functions respectively, and W is the perturbation. In the 3DW approximation, the initial-state wavefunction Φ_i is approximated as a product of the initial bound state of the atom (ψ_A) times a distorted wave function χ_i for the incoming electron (the projectile)

$$\Phi_i = \Psi_A \chi_i \quad (2)$$

For atoms, we use Hartree-Fock bound state wave function (ψ_{HF}) for the target. The perturbation (W) is given by

$$W = V - U_i \quad (3)$$

Here V is the interaction between the incident electron and the atom, and U_i is the initial state spherically symmetric static approximation for V , which is asymptotically equal to zero.

The final-state wave function Φ_f is approximated as a product of two final-state continuum electrons distorted waves (χ_{scat} and χ_{eject}), and the Coulomb interaction between the outgoing electrons ($C_{ele-ele}$), normally called the post-collision interaction (PCI),

$$\Phi_f = \chi_{scat} \chi_{eject} C_{ele-ele} \quad (4)$$

We use the exact post-collision Coulomb interaction between the two electrons ($C_{ele-ele}$), which is equal to a Gamov Factor times a hypergeometric function,

$$C_{ele-ele}(\mathbf{r}_{12}, \mathbf{k}_{12}) = \Gamma\left(1 - \frac{i}{k_{12}}\right) e^{-\frac{2\pi}{k_{12}}} {}_1F_1(\mathbf{r}_{12}, \mathbf{k}_{12}) \quad (5)$$

Here \mathbf{r}_{12} is the relative distance between the two electrons and \mathbf{k}_{12} is the relative momenta. With these approximations, the 3DW T -matrix becomes

$$T_{fi}^{3DW} = \langle \chi_{scat} \chi_{eject} C_{ele-ele} | V - U_i | \Psi_A \chi_i \rangle \quad (6)$$

Finally, the triple differential cross section (TDCS) can be written in atomic units as

$$\frac{d^3\sigma}{d\Omega_f d\Omega_e dE_e} = \frac{1}{(2\pi)^5} \frac{k_f k_e}{k_i} (|T|^2) \quad (7)$$

3.2. DWB2-RM. As mentioned above, a partially successful theory for electron-impact ionization has been a hybrid approach, in which the interaction of a “fast” projectile electron with the target is described by a first-order or second-order distorted-wave approach, while the initial bound state and the scattering of a “slow” ejected electron from the residual ion is treated by an R-matrix (RM) approach. These DWB1-RM [56] and DWB2-RM [57] models were formulated for highly asymmetric kinematics and small energy losses compared to the incident energy. Details of the hybrid approach can be found in many previous publications, e.g. [14, 33, 56]. Given that emission of the 3p electron is generally the dominant ionization process in the kinematical regime considered here, it is not surprising that using either a first-order or an approximate second-order treatment of the projectile produced very similar results. Also, coupling only the two final ionic states $(3s^2 3p^5)^2P^o$ and $(3s 3p^6)^2S$, rather than employing a much larger RMPS expansion for the ejected-electron–residual-ion problem, is generally sufficient. A key issue, on the other hand, is the description of the initial bound state and the final ionic states included in the close-coupling expansion for the electron scattering from the residual ion. In the hybrid method, we use the multi-configuration expansions developed by Burke and Taylor [58] for the corresponding photoionization problem.

3.3. BSR. The BSR method is based on two steps: 1) the treatment of electron collisions with neutral argon using an extensive close-coupling expansion that contains both physical and pseudo-states, with the latter being used to approximate the effect of high-lying discrete Rydberg states as well as the coupling to various (depending on the final ionic states) ionization continua; and 2) the construction of the *ionization* amplitude by combining the scattering amplitudes for *excitation* of the pseudo-states using coefficients obtained by

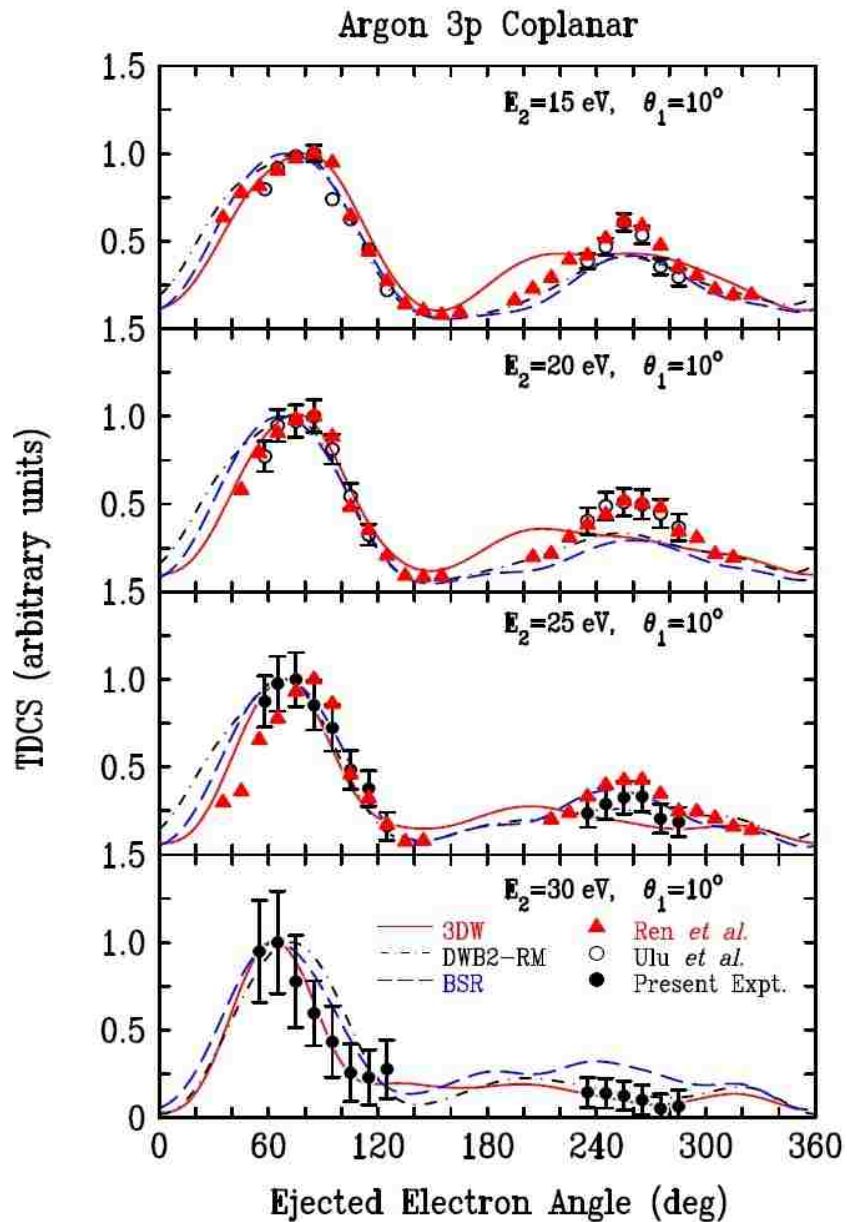


Figure 2. Experimental and theoretical TDCS for 200 eV electron-impact ionization of argon. The projectile scattering angle is 10° and the ejected electron energies are noted in each sub section of the figure. The theoretical calculations are: 3DW – solid line; dash-dot – DWB2-RM; and dashed – BSR. The experimental data are: triangles – Ren *et al.* [47]; open circles – Ulu *et al.* [51]; and solid circles – present results. All theories and experiment were normalized to 1.0 at the maximum of the binary peak (see text).

direct projection of the wavefunction to the various scattering channels associated with a particular final ionic state. For the case at hand, we performed a non-relativistic RMPS

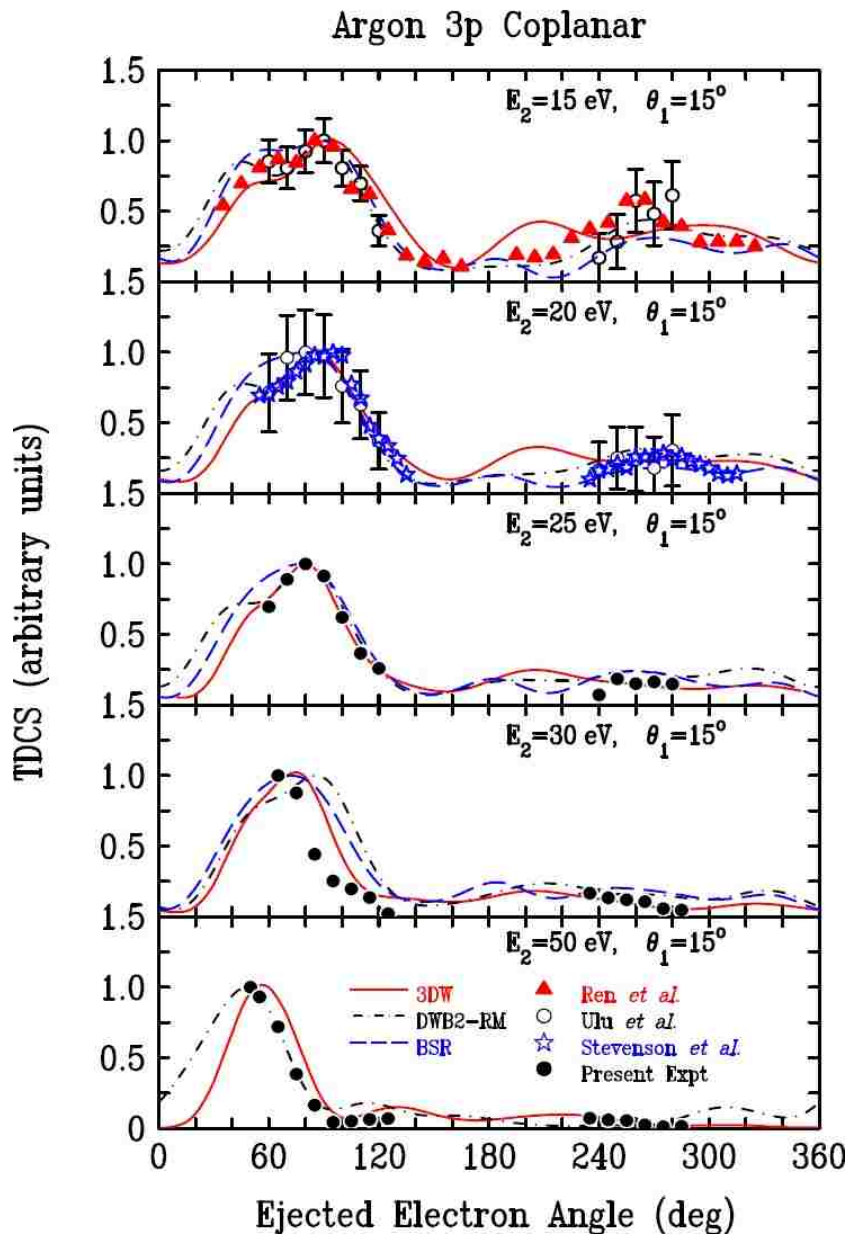


Figure 3. Experimental and theoretical TDCS for 200 eV electron-impact ionization of argon. The projectile scattering angle is 15° and the ejected electron energies are noted in each sub section of the figure. The theoretical calculations are: 3DW – solid line; dash-dot – DWB2-RM; and dashed – BSR. The experimental data are: triangles – Ren *et al.*[47]; open circles – Ulu *et al.* [51]; stars – Stevenson *et al.* [46] and solid circles – present results.

calculation for e-Ar collisions with a total of 482 states in the close-coupling expansion. The atomic wave functions for neutral Ar were obtained by the B-spline box-based close-coupling method [59]. Altogether, we generated 482 physical and pseudo target states with

coupled orbital angular momenta $L = 0 - 5$ and energies reaching up to 80 eV. In the first step, we obtained the scattering amplitudes for excitation of all pseudo-states using our suite of BSR codes [60] for electron collisions.

The last, and most crucial, step in the process is the generation of the ionization amplitudes. This is done by summing up the amplitudes for excitation of all energetically accessible pseudostates, with the weight factors given by the overlap of the pseudostates and the true continuum functions [28]. At this stage in the calculation, consistency between the models for the bound states (physical and pseudo) and the physical continuum scattering channels is critical. We ensure this consistency by employing the same expansions coupling the three ionic states $(3s^23p^5)^2P^o$, $(3s^3p^6)^2S$, and $(3s^23p^43d)^2S$ states. More details can be found in [28,32,33].

4. RESULTS

The TDCS for electron-impact ionization of Ar(3p) as a function of the ejected electron angle are presented in Figures 2 and 3 for two different scattering angles ($\theta_1 = 10^0$ and 15^0) (Looking at the scattering plane from above, the ejected electron observation angles are measured clockwise and the projectile scattering angles are measured counter-clockwise.) Results are presented for ejected-electron energies ranging between 15 eV and 50 eV. The present experimental data are compared with our earlier measurements [51] as well as the measurements of Stevenson et al. [46] and Ren et al. [47]. The experimental data are also compared with 3DW (three-body distorted-wave) model, the DWB2-RM (second-order distorted-wave Born R -matrix) model, as well as the non-perturbative BSR (B -spline R -matrix) approach. Since the measurements are not absolute, all experimental data and theoretical calculations have been normalized to unity at their peak, thereby allowing for a shape comparison. The primary difference between the two perturbative calculations (3DW and DWB2-RM) is the fact that the 3DW model contains one ‘collision’ between the projectile and target and PCI is included to all orders of perturbation theory

while DWB2-RM accounts for up to two ‘collisions’ between the projectile and target with PCI contained to second order within the R-matrix box. In addition, DWB2-RM contains exchange between the ejected electron and target to numerical accuracy while the 3DW uses the Furness-McCarthy approximation [61] for this exchange effect. From Figures 2 and 3, it is seen that overall there is excellent agreement between four different sets of measurements taken at different times and in different laboratories. The only noticeable difference occurs for 25 eV and 10° where it appears that there is a small shift in the location of the binary peak between the present measurements and those of Ren et al. [47]. The overall good agreement between the various measurements indicates the accuracy of the present measurements of the TDCS.

Looking in detail first at Figure 2, it is seen that the BSR and DWB2-RM results are in reasonably good agreement with experiment for all four of the measured energies. For the binary peak, all three theories are in very good agreement with each other and experiment. For 25 eV, all three theories predict the same binary peak angle, in excellent agreement with the present data. For 30 eV, the DWB2-RM binary peak is slightly shifted to higher angles as compared to the other two theories and experiment. Overall, the 3DW calculation appears to give the best prediction for the width of the binary peak. On the other hand, the 3DW provides the worst agreement with experiment for the recoil peak, except for the highest energy where the 3DW is in excellent agreement with data. The BSR calculation, which one would expect should give the best agreement with experiment, is in excellent agreement with the data for 25 eV, and very good for the other energies, except for the height of the recoil peak (too small for low energies and too high for large, energies). The DWB2-RM results are very similar to the BSR.

It is interesting to note that both perturbative calculations exhibit improved agreement with experiment with increasing ejected electron energy as one would expect. The fact that the 3DW results agree better with the binary peak than the DWB2-RM for 30 eV indicates that PCI is more important than higher-order interactions between the projectile

and target. For the recoil peak, the second interaction with the target is clearly much more important than PCI. The fact that the agreement between experiment and theory for the BSR does not exhibit any noticeable energy dependence would also be expected for a converged non-perturbative calculation.

Figure 3 presents a similar comparison for a larger projectile scattering angle. There are no BSR results shown for 50 eV, due to excessive computer demands that would have been required to achieve convergence for this energy. Again the BSR model yields overall reasonably good agreement with the data. However, for the smaller electron ejection energies, the experimental binary peak has a noticeable small-angle shoulder that is predicted very nicely by both perturbative calculations. The BSR results exhibit a small shoulder for the lowest energy but not for the higher ones. The largest discrepancy between experiment and theory for the binary peak was found for the 30 eV case. For the recoil peak, there is relatively good agreement between experiment and all three theories for all the measured cases, except for the smallest energy where the 3DW exhibits some unobserved structure. Surprisingly, overall the perturbative approaches appear to yield a little better agreement with experiment than the BSR for this case. Probably the DWB2-RM yields the best overall agreement with experiment. This indicates that, for larger scattering angles, multiple interactions with the target are more important than PCI.

Since the experimental data were not determined on an absolute scale, we have normalized experiment and theory to unity for the binary peak. It is, however, also of significant interest to look at the relative absolute values predicted by the theories. Figure 4 shows the same theoretical cross sections presented in Figure 3, but now on an absolute scale. In general, the 3DW results tend to predict the smallest binary peak and the DWB2-RM results the largest, with the difference being nearly a factor of 2. Obviously absolute, or at least cross-normalized measurements, would be highly desirable.

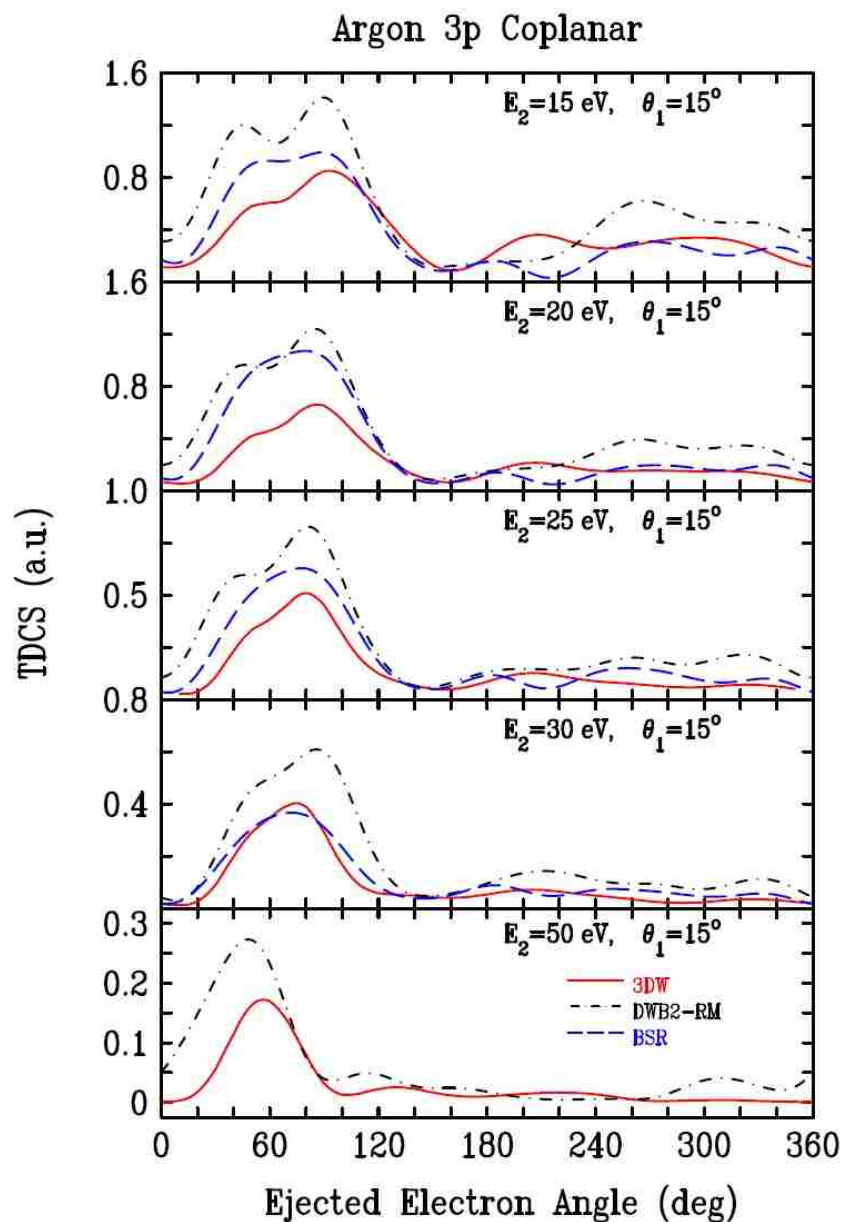


Figure 4. Same as Figure 3 except that absolute values of the theories are shown in atomic units.

5. CONCLUSION

While there are very accurate non-perturbative numerical calculations available for electron-impact ionization of hydrogen and helium, no comparable accurate calculation has been reported for ionization of heavier atoms such as the inert gases. Recently, Zat-

sarinny and Bartschat introduced the non-perturbative *B*-spline *R*-matrix (BSR) approach for ionization of inert gases, which had some significant success but without resolving all remaining discrepancies between experiment and theory. There have been several previous studies comparing experiment with perturbative theoretical calculations for electron-impact ionization of argon, and significant discrepancies have been found. We recently compared experiment and theory for 200 eV electron impact ionization of Ar for three projectile scattering angles and ejected electron energies of 15 eV and 20 eV. The current study revealed a qualitative agreement between experiment and both the perturbative and non-perturbative calculations but there were still significant differences.

The purpose of the present work was to extend this comparison to a much larger energy range (10 eV to 50 eV) to see if any general trends could be found. The study was limited to two projectile scattering angles -10° and 15° . Overall the BSR results were in reasonably good agreement with experiment – but not as good as has been found for hydrogen and helium. For 10° , the BSR width of the binary peak was broader than experiment for the higher energies, and the magnitude of the recoil peak was too small for small energies and too large for the highest energy. The width of the binary peak predicted by the 3DW was closest to experiment, and the agreement between experiment and the 3DW improved dramatically with increasing ejection energy and excellent agreement was found for the highest energy measured. For 15° , again the BSR results were in reasonably good agreement with experiment particularly for the recoil peak. For the binary peak, the BSR predicted a wider peak than found by experiment and the detailed shape of a low angle shoulder was better predicted by both the perturbative calculations. Again the 3DW results for the recoil peak gave better agreement with experiment with increasing energy with excellent agreement being achieved already by 20 eV. In summary, the BSR was reasonably good for all measured cases but did not predict all the detailed structure that the perturbative approaches did predict. All calculations showed some good points and some weak points, and hence it would be difficult to pick the ‘best’ one.

ACKNOWLEDGMENTS

This work was supported, in part, by the United States National Science Foundation under grants No. PHY-1068237 (SA and DM), PHY-1068140 (KB) and PHY-1212450 (OZ and KB), and by the XSEDE allocations TG-MCA07S029 (SA and DM) and PHY-090031 (OZ and KB). The Experimental part of this work was supported by the Scientific and Technological Research Council of Turkey (TUBITAK) through grant 109T738 and by BAPK through grant 12.FENED.05.

REFERENCES

- [1] H. Ehrhardt, K.H. Hesselbacher, K. Jung, and K. Willmann. Collisional ionization of helium by slow electrons. *Journal of Physics B: Atomic and Molecular Physics*, 5(8):1559–1571, 1972. cited By 50.
- [2] H. Ehrhardt, K.H. Hesselbacher, K. Jung, M. Schulz, and K. Willmann. Collisional ionization of helium by 250 ev electrons: Experiments with completely determined kinetics. *Journal of Physics B: Atomic and Molecular Physics*, 5(11):2107–2116, 1972. cited By 53.
- [3] H. Ehrhardt, K.H. Hesselbacher, K. Jung, E. Schubert, and K. Willmann. Electron impact ionization of argon: Measurements of triple differential cross sections. *Journal of Physics B: Atomic and Molecular Physics*, 7(1):69–78, 1974. cited By 44.
- [4] D.H. Madison, R.V. Calhoun, and W.N. Shelton. Triple-differential cross sections for electron-impact ionization of helium. *Physical Review A*, 16(2):552–562, 1977. cited By 120.
- [5] D.H. Madison. Full second-order distorted-wave calculation without approximations for atomic excitation by electron impact. *Physical Review Letters*, 53(1):42–45, 1984. cited By 21.

- [6] C.T. Whelan and H.R.J. Walters. A new version of the distorted-wave impulse approximation-application to coplanar symmetric ionization. *Journal of Physics B: Atomic, Molecular and Optical Physics*, 23(17):2989–2995, 1990. cited By 27.
- [7] X. Zhang, C.T. Whelan, and H.R.J. Walters. (e,2e) cross sections for ionization of helium in coplanar symmetric geometry. *Journal of Physics B: Atomic, Molecular and Optical Physics*, 23(17):L509–L516, 1990. cited By 36.
- [8] X. Zhang, C.T. Whelan, and H.R.J. Walters. Energy sharing (e,2e) collisions-ionisation of helium in the perpendicular plane. *Journal of Physics B: Atomic, Molecular and Optical Physics*, 23(10):L173–L178, 1990. cited By 45.
- [9] E.P. Curran, C.T. Whelan, and H.R.J. Walters. On the electron impact ionization of h(ls) in coplanar asymmetric geometry. *Journal of Physics B: Atomic, Molecular and Optical Physics*, 24(2):L19–L25, 1991. cited By 28.
- [10] X. Zhang, C.T. Whelan, and H.R.J. Walters. Electron impact ionization of the noble gases in coplanar symmetric geometry over the energy range 100 to 1000 ev. *Zeitschrift für Physik D Atoms, Molecules and Clusters*, 18(4):309–310, 1991. cited By 8.
- [11] X. Zhang, C.T. Whelan, and H.R.J. Walters. Distorted-wave born approximation calculations of (e, 2 e) reactions. *Zeitschrift für Physik D Atoms, Molecules and Clusters*, 23(4):301–308, 1992. cited By 14.
- [12] H.R.J. Walters, H. Ast, C.T. Whelan, R.M. Dreizler, H. Graf, C.D. Schröter, J. Bonfert, and W. Nakel. Relativistic (e, 2 e) collisions on atomic inner shells in symmetric geometry. *Zeitschrift für Physik D Atoms, Molecules and Clusters*, 23(4):353–357, 1992. cited By 38.
- [13] K. Bartschat and P.G. Burke. The r-matrix method for electron impact ionisation. *Journal of Physics B: Atomic and Molecular Physics*, 20(13):3191–3200, 1987. cited By 96.

- [14] K. Bartschat and O. Vorov. Channel-coupling, target-structure, and second-order effects in electron-impact ionization of ar(3p) and ar(3s). *Physical Review A - Atomic, Molecular, and Optical Physics*, 72(2), 2005. cited By 30.
- [15] I. Bray. Low-energy electron-impact ionization of atomic hydrogen with equal energy outgoing electrons. *Journal of Physics B: Atomic, Molecular and Optical Physics*, 33(3):581–595, 2000. cited By 64.
- [16] I. Bray. Close-coupling approach to coulomb three-body problems. *Physical Review Letters*, 89(27):2732011–2732014, 2002. cited By 144.
- [17] I. Bray, D.V. Fursa, A.S. Kheifets, and A.T. Stelbovics. Electrons and photons colliding with atoms: Development and application of the convergent close-coupling method. *Journal of Physics B: Atomic, Molecular and Optical Physics*, 35(15):R117–R146, 2002. cited By 178.
- [18] K. Bartschat and I. Bray. Electron-impact ionization of atomic hydrogen from the 1s and 2s states. *Journal of Physics B: Atomic, Molecular and Optical Physics*, 29(15):L577–L583, 1996. cited By 94.
- [19] T.N. Rescigno, M. Baertschy, W.A. Isaacs, and C.W. McCurdy. Collisional breakup in a quantum system of three charged particles. *Science*, 286(5449):2474–2479, 1999. cited By 390.
- [20] T.N. Rescigno and B.I. Schneider. Electron-impact excitation of the t and v states of ethylene: An ab initio study. *Physical Review A*, 45(5):2894–2902, 1992. cited By 77.
- [21] T.N. Rescigno, B.H. Lengsfeld, C.W. McCurdy, and S.D. Parker. Ab initio description of polarization in low-energy electron collisions with polar molecules: Application to electron-nh₃ scattering. *Physical Review A*, 45(11):7800–7809, 1992. cited By 42.

- [22] R. Celiberto and T.N. Rescigno. Dependence of electron-impact excitation cross sections on the initial vibrational quantum number in H_2 and D_2 molecules: $X^1g^+1b_u+1$ and g^+1c_u1 transitions. *Physical Review A*, 47(3):1939–1945, 1993. cited By 52.
- [23] T.J. Gil, C.W. McCurdy, T.N. Rescigno, and B.H. Lengsfeld III. Polarization and correlation effects in elastic electron- Li_2 scattering. *Physical Review A*, 47(1):255–263, 1993. cited By 7.
- [24] J. Colgan, M.S. Pindzola, F. Robicheaux, C. Kaiser, A.J. Murray, and D.H. Madison. Differential cross sections for the ionization of oriented H_2 molecules by electron impact. *Physical Review Letters*, 101(23), 2008. cited By 44.
- [25] J. Colgan, O. Al-Hagan, D.H. Madison, C. Kaiser, A.J. Murray, and M.S. Pindzola. Triple differential cross sections for the electron-impact ionization of H_2 molecules for equal and unequal outgoing electron energies. *Physical Review A - Atomic, Molecular, and Optical Physics*, 79(5), 2009. cited By 26.
- [26] J. Colgan, O. Al-Hagan, D.H. Madison, A.J. Murray, and M.S. Pindzola. Deep interference minima in non-coplanar triple differential cross sections for the electron-impact ionization of small atoms and molecules. *Journal of Physics B: Atomic, Molecular and Optical Physics*, 42(17), 2009. cited By 20.
- [27] J. Colgan and M.S. Pindzola. Double- and triple-differential cross sections for the low-energy electron-impact ionization of hydrogen. *Physical Review A - Atomic, Molecular, and Optical Physics*, 74(1), 2006. cited By 42.
- [28] O. Zatsarinny and K. Bartschat. Nonperturbative treatment of ionization with excitation of helium by electron impact. *Physical Review Letters*, 107(2), 2011. cited By 45.

- [29] O. Zatsarinny and K. Bartschat. Nonperturbative b-spline r-matrix-with-pseudostates calculations for electron-impact ionization of helium. *Physical Review A - Atomic, Molecular, and Optical Physics*, 85(6), 2012. cited By 21.
- [30] O. Zatsarinny and K. Bartschat. Nonperturbative treatment of electron-impact ionization of ar(3p). *Physical Review A - Atomic, Molecular, and Optical Physics*, 85(3), 2012. cited By 14.
- [31] O. Zatsarinny and K. Bartschat. The b-spline r-matrix method for atomic processes: Application to atomic structure, electron collisions and photoionization. *Journal of Physics B: Atomic, Molecular and Optical Physics*, 46(11), 2013. cited By 41.
- [32] X. Ren, T. Pflüger, J. Ullrich, O. Zatsarinny, K. Bartschat, D.H. Madison, and A. Dorn. Low-energy electron-impact ionization of argon: Three-dimensional cross section. *Physical Review A - Atomic, Molecular, and Optical Physics*, 85(3), 2012. cited By 12.
- [33] X. Ren, A. Senftleben, T. Pflüger, A. Dorn, K. Bartschat, and J. Ullrich. Benchmark experiment for electron-impact ionization of argon: Absolute triple-differential cross sections via three-dimensional electron emission images. *Physical Review A - Atomic, Molecular, and Optical Physics*, 83(5), 2011. cited By 15.
- [34] X. Ren, A. Senftleben, T. Pflüger, J. Ullrich, K. Bartschat, and A. Dorn. Erratum: Benchmark experiment for electron-impact ionization of argon: Absolute triple-differential cross sections via three-dimensional electron emission images [phys. rev. a 83, 052714 (2011)]. *Physical Review A - Atomic, Molecular, and Optical Physics*, 89(2), 2014. cited By 4.
- [35] Steven Cavanagh and Birgit Lohmann. (e, 2e) investigation of inner-shell ionization in argon. *Journal of Physics B: Atomic, Molecular and Optical Physics*, 30(6):L231–L236, 1997. cited By 22.

- [36] I. Taouil, A. Duguet, A. Lahmam-Bennani, B. Lohmann, J. Rasch, C.T. Whelan, and H.R.J. Walters. (e, 2e) ionization of the 2p orbital of argon. *Journal of Physics B: Atomic, Molecular and Optical Physics*, 32(1):L5–L11, 1999. cited By 23.
- [37] E.M.S. Casagrande, F. Catoire, A. Naja, X.G. Ren, A. Lahmam-Bennani, M. Nekkab, C. Dal Cappello, K. Bartschat, and C.T. Whelan. New coplanar (e,2e) experiments for the ionisation of he and ar atoms. *Journal of Electron Spectroscopy and Related Phenomena*, 161(1-3 SPEC. ISS.):27–30, 2007. cited By 4.
- [38] A. Lahmam-Bennani, H.F. Wellenstein, A. Duguet, and M. Rouault. Absolute triple differential cross sections for the 3p ionisation of argon by electron impact. *Journal of Physics B: Atomic and Molecular Physics*, 16(1):121–130, 1983. cited By 33.
- [39] L. Avaldi, I.E. McCarthy, and G. Stefani. Electron impact ionisation of argon at intermediate energy and momentum transfer: An (e,2e) investigation. *Journal of Physics B: Atomic, Molecular and Optical Physics*, 22(20):3305–3314, 1989. cited By 10.
- [40] F. Catoire, E.M. Staicu-Casagrande, M. Nekkab, C. Dal Cappello, K. Bartschat, and A. Lahmam-Bennani. Investigation of the (e, 2e) single ionization of he and ar at large energy loss close to minimum momentum transfer. *Journal of Physics B: Atomic, Molecular and Optical Physics*, 39(12):2827–2838, 2006. cited By 32.
- [41] M.A. Haynes and B. Lohmann. Coplanar symmetric (e, 2e) cross sections for argon 3s ionization. *Journal of Physics B: Atomic, Molecular and Optical Physics*, 34(5):L131–L136, 2001. cited By 23.
- [42] M.A. Haynes and B. Lohmann. Low-energy triple differential cross sections for argon 3s electron impact ionization. *Journal of Physics B: Atomic, Molecular and Optical Physics*, 33(21):4711–4721, 2000. cited By 34.

- [43] M.A. Haynes and B. Lohmann. Comparative study of argon 3p electron-impact ionization at low energies. *Physical Review A. Atomic, Molecular, and Optical Physics*, 64(4):447011–447014, 2001. cited By 31.
- [44] M.A. Stevenson and B. Lohmann. Triple-differential cross-section measurements of electron-impact ionization of argon 3s in the backward scattering direction. *Physical Review A - Atomic, Molecular, and Optical Physics*, 73(2), 2006. cited By 22.
- [45] M.A. Stevenson and B. Lohmann. Fully differential cross-section measurements for electron-impact ionization of argon over the complete in-plane angular range. *Physical Review A - Atomic, Molecular, and Optical Physics*, 77(3), 2008. cited By 17.
- [46] M. Stevenson, G.J. Leighton, A. Crowe, K. Bartschat, O.K. Vorov, and D.H. Madison. Experimental and theoretical (e, 2e) studies of argon (3p) ionization in asymmetric geometry. *Journal of Physics B: Atomic, Molecular and Optical Physics*, 38(4):433–440, 2005. cited By 25.
- [47] M. Stevenson, J. Leighton, A. Crowe, K. Bartschat, K. Vorov, and H. Madison. Erratum: Experimental and theoretical (e,2e) studies of argon (3p) ionization in asymmetric geometry (journal of physics b: Atomic, molecular and optical physics (2005) 38 (433-440)). *Journal of Physics B: Atomic, Molecular and Optical Physics*, 40(8):1639–1641, 2007. cited By 9.
- [48] X. Ren, A. Senftleben, T. Pflüger, A. Dorn, K. Bartschat, and J. Ullrich. Signatures of projectile-nucleus scattering in three-dimensional (e,2e) cross sections for argon. *Journal of Physics B: Atomic, Molecular and Optical Physics*, 43(3), 2010. cited By 31.

- [49] M. Ulu, Z.N. Ozer, M. Yavuz, O. Zatsarinny, K. Bartschat, M. Dogan, and A. Crowe. Experimental and theoretical investigation of $(e, 2e)$ ionization of $ar(3p)$ in asymmetric kinematics at 200 ev. *Journal of Physics B: Atomic, Molecular and Optical Physics*, 46(11), 2013. cited By 9.
- [50] O. Sise, M. Dogan, I. Okur, and A. Crowe. $(e, 2e)$ experiments on $(2s2)1s$, $(2p2) 1d$ and $(2s2p)1p$ autoionizing levels of helium in the direction of the binary lobe. *Journal of Physics B: Atomic, Molecular and Optical Physics*, 43(18), 2010. cited By 11.
- [51] L.R. Hargreaves, M.A. Stevenson, and B. Lohmann. Absolute triple-differential cross sections for intermediate energy electron impact ionization of neon and argon. *Journal of Physics B: Atomic, Molecular and Optical Physics*, 43(20), 2010. cited By 15.
- [52] O. Sise, M. Dogan, I. Okur, and A. Crowe. Electron-impact excitation of the $(2p2) 1d$ and $(2s2p) 1p$ autoionizing states of helium. *Physical Review A - Atomic, Molecular, and Optical Physics*, 84(2), 2011. cited By 15.
- [53] Z.N. Ozer, H. Chaluvadi, M. Ulu, M. Dogan, B. Aktas, and D. Madison. Young's double-slit interference for quantum particles. *Physical Review A - Atomic, Molecular, and Optical Physics*, 87(4), 2013. cited By 22.
- [54] Z.N. Ozer, M. Ulu, B. Aktas, and M. Dogan. Observing quantum level interference effects with electron spectrometer. *Acta Physica Polonica A*, 123(2):363–364, 2013. cited By 5.
- [55] M. Dogan, M. Ulu, Z.N. Ozer, M. Yavuz, and G. Bozkurt. *J. Spectr*, 2013, 2013. cited By 7.
- [56] D.H. Madison and O. Al-Hagan. *J. At. Mol. Opt. Phys.*, 2010, 2010. cited By 47.
- [57] K. Bartschat and P.G. Burke. Electron impact ionisation of argon. *Journal of Physics B: Atomic, Molecular and Optical Physics*, 21(17):2969–2975, 1988. cited By 28.

- [58] R.H.G. Reid, K. Bartschat, and A. Raeker. Initial-state, final-state and higher-order effects in electron impact ionization of helium atoms. *Journal of Physics B: Atomic, Molecular and Optical Physics*, 31(3):563–571, 1998. cited By 63.
- [59] R.H.G. Reid, K. Bartschat, and A. Raeker. *J. Phys. B*, 33(22), 2000. cited By 36.
- [60] P.G. Burke and K.T. Taylor. R-matrix theory of photoionization. application to neon and argon. *Journal of Physics B: Atomic and Molecular Physics*, 8(16):2620–2639, 1975. cited By 248.
- [61] O. Zatsarinny and C. Froese Fischer. Oscillator strengths for transitions to high-lying excited states of carbon. *Journal of Physics B: Atomic, Molecular and Optical Physics*, 35(22):4669–4683, 2002. cited By 47.

III. EXPERIMENTAL AND THEORETICAL TRIPLE DIFFERENTIAL CROSS SECTIONS FOR ELECTRON IMPACT IONIZATION OF A_r (3p) FOR EQUAL ENERGY FINAL STATE ELECTRONS

Sadek Amami¹, Zehra N Ozer², Mevlut Dogan², Murat Yavuz², Onur Varol² and
Don Madison¹

¹Department of Physics,

Missouri University of Science and Technology,

Rolla, Missouri, USA

²Department of Physics,

e-COL Laboratory, Afyon Kocatepe University,

03200, Afyon, Turkey

ABSTRACT

There have been several studies of electron-impact ionization of inert gases for asymmetric final state energy sharing and normally one electron has an energy significantly higher than the other. However, there have been relatively few studies examining equal energy final state electrons. Here we report experimental and theoretical triple differential cross sections for electron impact ionization of Ar (3p) for equal energy sharing of the outgoing electrons. Previous experimental results combined with some new measurements are compared with distorted wave born approximation (DWBA) results, DWBA results using the Ward–Macek (WM) approximation for the post collision interaction (PCI), and three-body distorted wave (3DW) which includes PCI without approximation. The results show that it is crucially important to include PCI in the calculation particularly for lower energies and that the WM approximation is valid only for high energies. The 3DW, on the other hand, is in reasonably good agreement with data down to fairly low energies.

1. INTRODUCTION

Detailed physical information related to collision studies can be obtained from triple differential cross section (TDCS) measurements for electron-impact ionization of targets using the so called (e, 2e) coincidence technique. In this technique, both final state electrons are detected in coincidence and the energy of the electrons is also measured. As a result, everything about the collision is determined except the spin of the electrons. This level of detail provides for very sensitive testing of theoretical models and different kinematical conditions can provide tests for different aspects of the theoretical model. In recent years, significant theoretical advances have been made for describing the electron-impact ionization dynamics of atomic hydrogen and helium and there is now essentially exact agreement between experiment and theory for these two atoms. The approaches that work for hydrogen and helium also typically work well for ionization of atoms which can be described as quasi-one and quasi-two electron targets with an inert core. Theoretical progress for treating more complex atoms such as inert gases has been much slower. However, it was recently demonstrated that a new non-perturbative B-spline R-matrix method with pseudostates (BSR) and the three-body distorted wave (3DW) approach provided excellent agreement for electron-impact ionization of neon for a fairly low impact energy of 61 eV [1]. The close coupling approaches had been getting better over the years and this work demonstrated that it was possible for close coupling methods to treat complex atoms. The surprise was that the non-perturbative 3DW did so well (as good as the BSR). The strength of the 3DW is that it contains the post collision interaction (PCI) in the final state wavefunction and this work indicated that PCI must be a very important interaction in the low energy ionization of neon. More recently, a similar study was completed for 66 eV ionization of argon and for this case, the BSR was in significantly better agreement with experiment than the 3DW [2]. Evidently PCI is not as important for argon as it was for neon or some new physical effects become more important for the larger atom. We have recently tested the accuracy of the BSR and 3DW for high incident energy (200 eV) electron impact ionization

of argon and a wide range of ejected electron energies (15–50 eV) and two different projectile scattering angles (10° and 15°) [3]. In that study, we found that both the BSR and 3DW gave very good agreement with the binary peak (peak near the direction of momentum transfer). However, for the recoil peak (peak near the direction of the negative momentum transfer), the BSR was in better agreement with experiment for the lower energies. For the 3DW, agreement with experiment improved with increasing ejected electron energy as would be expected and the agreement was quite good for the higher energies. For the asymmetric energies examined, the speeds of the two final state electrons were significantly different so one would expect that PCI might not be very important. On the other hand, one would also expect that as the speeds became closer together, PCI would be more important and most important for cases in which the speeds were equal. Over the years, there have been several experimental and theoretical studies performed for ionization of argon with asymmetric final state energies [3, 4, 5, 6, 7, 8, 9, 10, 11, 12, 13, 14, 15, 16, 17, 18, 19, 20, 21] but very few for symmetric final state energies [22, 23, 24]. Consequently, the purpose of this work is to test the validity of the theory for ionization of the 3p-state of argon for equal energy final state electrons with a broad range of final state energies ranging from 15 to 100 eV. The present implementation of the BSR pseudostate expansion for the ejected electron is not suitable for high energies so we will only compare with the 3DW and distorted wave born approximation (DWBA) theoretical approaches. We will compare theory and experiment with previously reported experiments by Haynes and Lohmann [22] and Nixon and Murray [23] for lower energy final state electrons and some new measurements for higher energy final state electrons.

2. EXPERIMENTAL PROCEDURE

The (e, 2e) coincidence technique has been used to measure TDCSs using an electron spectrometer designed to work in the low to intermediate energy regime in coplanar geometry. The spectrometer has a conventional design that consists of an energy selected

electron gun and two hemispherical electron energy analyzers with channel electron multipliers (CEMs) to detect outgoing electrons after the ionization event. The apparatus has been used previously for Ar studies and more detail may be found in [21, 25, 26]. As a brief description; an electron beam of about $1 \mu\text{A}$ produced by an electron gun collides with gas target perpendicularly. Two outgoing electrons that are extracted from reaction center are detected by two hemispherical electron energy analyzers in coincidence. The positions of the analyzers are mounted on two independent turntables and they can be varied from 30° to 140° with respect to the electron beam direction. Another turntable allows for the rotation of a Faraday cup around the interaction region. For the case of equal energy sharing measurements, the incident electron losses some of its energy to ionize the target and the rest of the energy is equally shared by the two outgoing electrons. The two outgoing electrons are detected in coincidence to separate the ionization events from other final reaction channels. The electrons were focused by an electrostatic lens system located at the entrance of a hemispherical analyzer and energy-analyzed. The energy selected electrons were detected by a CEM located at the exit of the hemispherical electron energy analyzers. The signals from the two CEMs were registered and analyzed by a multi-parameter listmode data acquisition system. The coincidence electronics and a schematic view of the experimental set up is shown in Figure 1. Control of the experiment is facilitated by using a computer to control and adjust the voltages on the analyzers and electron gun. In this way, the experiment can operate for several weeks with the same operating conditions which is required for data accumulation.

3. THEORETICAL FRAMEWORK

In this work, we have used the three different perturbation approximations (3DW, DWBA and DWBA using the Ward–Macek (WM) approximation for PCI) that were used in the previous study for asymmetric final state energies [3]. Each of these has been described

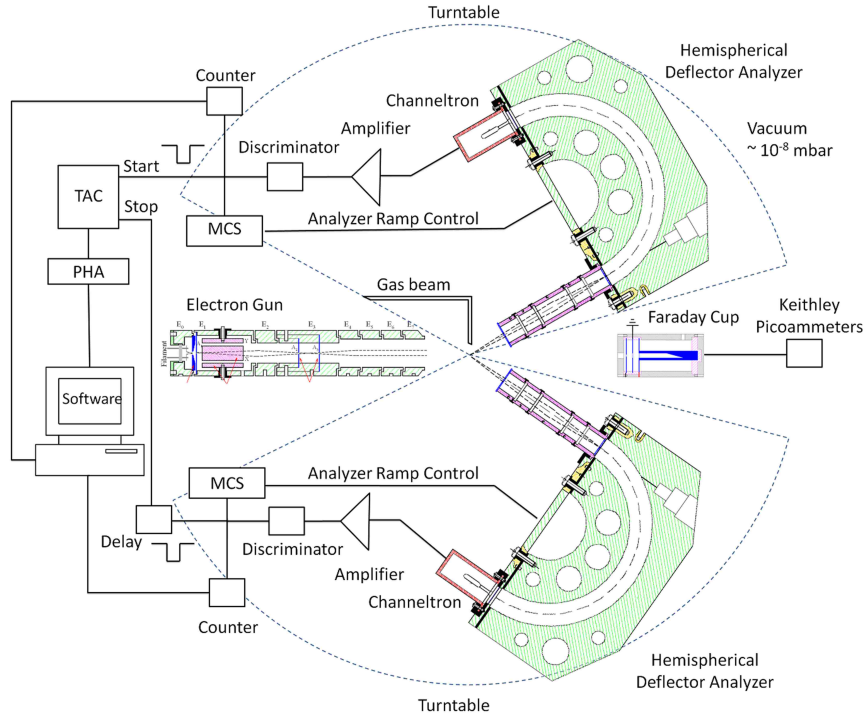


Figure 1. Schematic view of experimental setup and coincidence electronics.

in detail previously [3, 27, 28, 29] so here we will only give a brief summary of the models to show the differences and similarities. Since the DWBA is a special case of the more general 3DW approximation, we will discuss the 3DW first.

3.1. 3DW Approximation. The 3DW direct scattering T – *matrix* can be written as

$$T_{dir}^{3DW} = \langle \Psi_f | W | \Psi_i \rangle \quad (1)$$

Here Ψ_i and Ψ_f are the initial- and final-state wave functions for the system respectively, and W is the perturbation. The initial-state wavefunction Ψ_i is approximated as a product of a distorted wave function χ_i for the incoming electron (the projectile) times the initial Hartree–Fock bound state for the target 3p state (ψ_{HF})

$$\Psi_i = \psi_{HF}(\mathbf{r}_2) \chi_i(\mathbf{r}_1) \quad (2)$$

where r_1 is the coordinate for the projectile electron and r_2 is the coordinate for the initially bound electron. The final-state wave function Ψ_f for the two outgoing electrons, which we will call the scattered and ejected electron for convenience, is approximated as a product of two final-state continuum electron distorted waves (χ_1 and χ_2), and the Coulomb interaction between the outgoing electrons (C_{12}), which is normally called the post-collision interaction (PCI)

$$\Psi_f = C_{12}(\mathbf{k}_{12}, \mathbf{r}_{12}) \chi_1(\mathbf{r}_1) \chi_2(\mathbf{r}_2) \quad (3)$$

where K_{12} is the relative momentum between the two electrons and r_{12} is the relative distance between the two electrons. The Coulomb interaction is given by

$$C_{12}(\mathbf{k}_{12}, \mathbf{r}_{12}) = e^{-\frac{\pi\gamma}{2}} \Gamma(1 - i\gamma) {}_1F_1(i\gamma, 1, -i[k_{12}r_{12} + \mathbf{k}_{12} \cdot \mathbf{r}_{12}]) \quad (4)$$

Here $\Gamma(1 - i\gamma)$ is a gamma factor, ${}_1F_1$ is a confluent hypergeometric function, $k_{12} = \mu v_{12}$, $\mu = \frac{1}{2}$ is the reduced mass for the two electrons in atomic units, v_{12} is the relative velocity between the two continuum electrons, and $\gamma = \frac{1}{v_{12}}$ is the Sommerfeld parameter. The perturbation W is given by

$$W = V - U_i \quad (5)$$

where V is the exact initial state interaction between the atom and the incident electron and U_i is the initial state spherically symmetric static approximation for V which is asymptotically equal to zero. The approximations we make for $V - U_i$ are discussed in detail by Madison and Al-Hagan [28]. Briefly, we assume that the interaction between the incident electron and passive bound electrons contained in both V and U_i are the same. Consequently, the perturbation is approximated by

$$W = \frac{1}{r_{12}} - U_a(r_1) \quad (6)$$

where U_a is the spherically symmetric interaction potential between the incident projectile and the active electron. If one looks at previous DWBA publications, one finds that sometimes $W = \frac{1}{r_{12}}$ (see e.g. [4]) and sometimes Equation (6). If one assumes that the initial and final state wavefunctions for the initially bound electron are orthogonal, then the $U_a(r_1)$ term will vanish in the DWBA amplitude (see below). In the 3DW approximation, this orthogonality will not make the $U_a(r_1)$ term vanish so it is important to keep it. With these approximations, the direct 3DW T-matrix becomes

$$T_{dir}^{3DW} = \langle \chi_1(\mathbf{r}_1) \chi_2(\mathbf{r}_2) C_{12}(\mathbf{k}_{12}, \mathbf{r}_{12}) | \frac{1}{\mathbf{r}_{12}} - U_a(r_1) | \psi_{HF}(\mathbf{r}_2) \chi_i(\mathbf{r}_1) \rangle \quad (7)$$

3.2. DWBA Approximation. In the standard DWBA approximation, the interaction between the two continuum electrons in the final state wavefunction is ignored in the T-matrix. Thus the DWBA $T - matrix$ is

$$T_{dir}^{DWBA} = \langle \chi_1(\mathbf{r}_1) \chi_2(\mathbf{r}_2) | \frac{1}{\mathbf{r}_{12}} - U_a(r_1) | \psi_{HF}(\mathbf{r}_2) \chi_i(\mathbf{r}_1) \rangle \quad (8)$$

3.3. WM Approximation. In the third approximation, we use the WM approximation [30, 31] for the Coulomb interaction of Equation (4). In this model, the term $[k_{12}r_{12} + k_{12}.r_{12}]$ in the hypergeometric function is replaced by $2k_{12}r_{12}^{ave}$, where r_{12}^{ave} is the average value of the electron–electron separation. In this approximation, the direct WM $T - matrix$ becomes

$$T_{dir}^{WM} = C_{12}^{WM}(r_{ave}, k_{12}) \langle \chi_1(\mathbf{r}_1) \chi_2(\mathbf{r}_2) | \frac{1}{\mathbf{r}_{12}} - U_a(r_1) | \psi_{HF}(\mathbf{r}_2) \chi_i(\mathbf{r}_1) \rangle \quad (9)$$

or

$$T_{dir}^{WM} = C_{12}^{WM}(r_{ave}, k_{12}) T_{dir}^{DWBA} \quad (10)$$

where

$$C_{12}^{WM}(r_{ave}, k_{12}) = e^{\frac{-\pi\gamma}{2}} \Gamma(1 - i\gamma) {}_1F_1(i\gamma, 1, -2ik_{12}r_{ave}) \quad (11)$$

can be removed from the integral since it does not depend on the coordinates being integrated. Finally, the TDCS in all three approximations can be written as (atomic units)

$$TDCS = \frac{d^3\sigma}{d\Omega_f d\Omega_e dE_e} = \frac{1}{(2\pi)^5} \frac{k_1 k_2}{k_i} (|T_{dir}|^2 + |T_{exc}|^2 + |T_{dir} - T_{exc}|^2) \quad (12)$$

where k_1 , k_2 , and k_i , are the magnitudes of the momenta of the scattered, ejected and initial electrons, respectively, and T_{exc} is the exchange T - *matrix*, which is similar to T_{dir} the direct T - *matrix* except that the two final state electrons are interchanged in the final state wavefunction Ψ_f .

4. RESULTS AND DISCUSSION

We first compare with some previously published equal final state energy measurements of Haynes and Lohmann [22] and Nixon and Murray [23]. For this case, not only were the final state energies equal, the electrons were measured at equal angles on opposite sides of the beam direction in the scattering plane—the so called coplanar symmetric geometry. The DWBA, WM and 3DW results are compared with those data in Figures 2 and 3 for final state electron energies ranging from 15 to 100 eV. The Haynes and Lohmann data are the solid up triangles (red) and the Nixon and Murray data are the open down triangles. For each case, the experimental data have been normalized to a best visual fit to the 3DW results. The dashed– dotted (blue) curve are the results of the DWBA calculation, the dashed (green) curve are the results of the DWBA calculation using the WM approximation for PCI and solid (red) curve are the results of the 3DW calculation using full PCI.

It is seen that the DWBA, which has PCI only to first order, completely fails to predict even the shape of the data. The cross sections must be zero for 0° and 180° which is obviously not satisfied by the DWBA. In fact the DWBA predicts the largest cross section

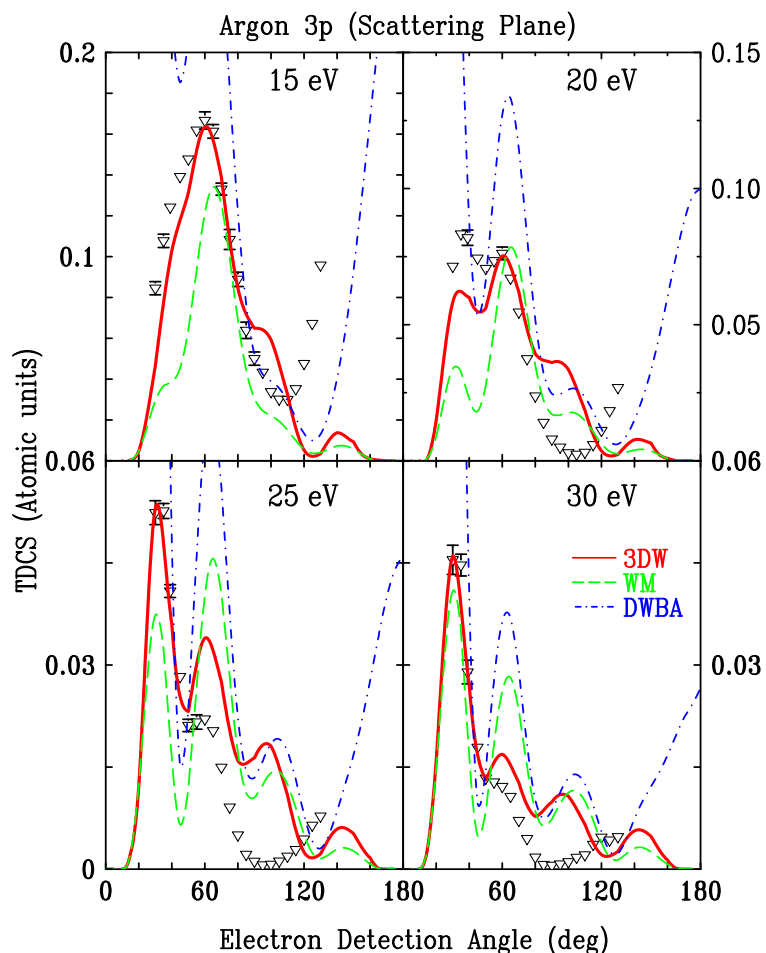


Figure 2. TDCS in atomic units for electron-impact ionization of the argon 3p orbital using the coplanar symmetric geometry—both final state electrons have the same energy and are detected at the same angle on opposite sides of the incident beam direction. The final state energies of the two electrons are noted in each panel. The open down pointing triangles are the experimental data of Nixon and Murray [23]. The experimental data have been normalized to a best visual fit to the 3DW results. The different theoretical curves are noted in the legend.

for 0° . With full PCI, the 3DW is in qualitative agreement with all the data except for an apparent large angle peak for the lowest energies. The 3DW does a reasonable good job of predicting the double peak seen at 20 eV and its evolution into a shoulder which is gone by 35 eV. For 40 eV and higher, the 3DW is in very good agreement with experiment. For 50 eV, the 3DW agrees better with the Haynes and Lohmann data than the Nixon and Murray data. Even the WM approximation is in remarkably better agreement with experiment than

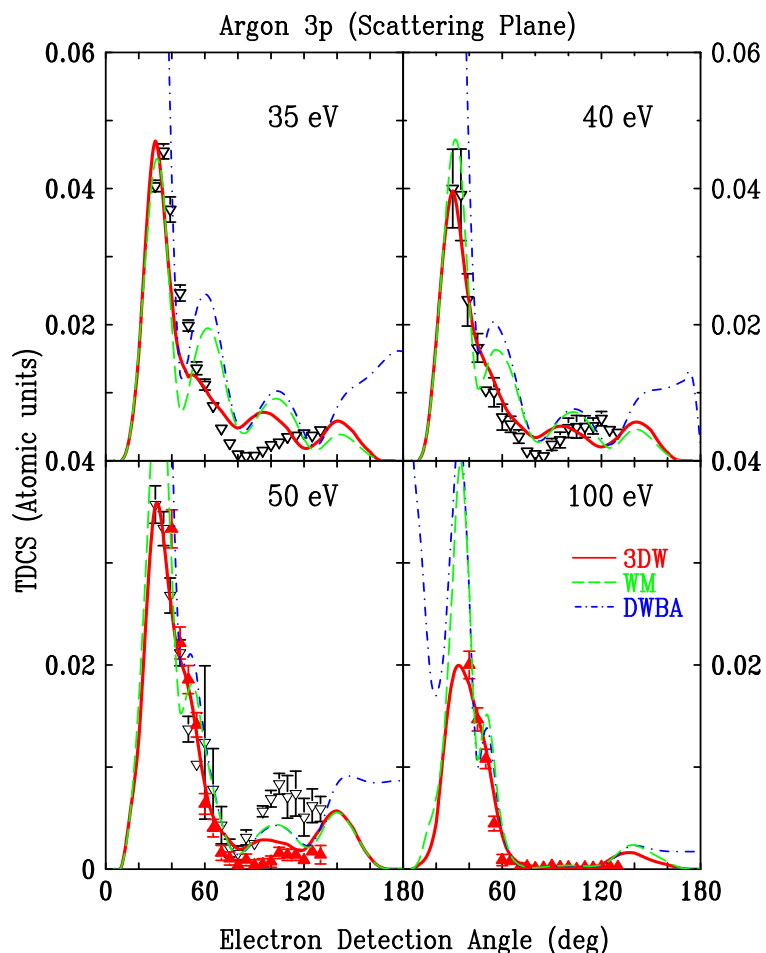


Figure 3. TDCS in atomic units for electron-impact ionization of the argon 3p orbital using the coplanar symmetric geometry—both final state electrons have the same energy and are detected at the same angle on opposite sides of the incident beam direction. The final state energies of the two electrons are noted in each panel. The open down pointing triangles are the experimental data of Nixon and Murray [23] and the solid (red) up point triangles are the experimental data of Haynes and Lohmann [22]. The experimental data have been normalized to a best visual fit to the 3DW results. The different theoretical curves are noted in the legend.

the DWBA although the agreement is not nearly as good as the 3DW. All of this shows the strong importance of PCI for this collision geometry. The electrons have the largest angular separation at 90° in this geometry. Comparing the difference between the DWBA and either the WM or 3DW at 90° shows that PCI is still very important even for the largest angular separation.

Figure 4 compares the present experimental results (solid circles) with the same three theoretical calculations. For Figures 2 and 3, both electron detectors are rotated in coincidence in opposite directions to keep the same angle between each electron and the beam direction. For the present measurements, one electron detector is kept fix at the θ_1 angle noted in each panel and the other detector is rotated 0° to 360° clockwise (in principle) starting on the opposite side of the incident beam direction. Obviously it is not physically possible to measure all these angles due to other equipment in the chamber. For this type of measurement, the cross sections must be zero when the ejected electron angle is $360^\circ - \theta_1$. Again, the experimental data have been normalized to a best visual fit to the 3DW results.

For angles $10^\circ - 30^\circ$, the 3DW and WM results have a three peak structure which is consistent with the experimental data and there is relatively good agreement between experiment and theory. There is less difference between the different theories for this case than was seen in Figures 3 and 4. For the closest case of 100 eV shown on Figure 3, WM had two peaks which appears to be non-physical whereas 3DW has one which is also consistent with measured data. For this case, WM is in qualitative agreement with the shape of the data for all cases except $\theta_1 = 40^\circ$. As a result, the WM approximation appears to be better for high energy and asymmetric angles than high energy and symmetric angles. It seems reasonable (to us) to assume that using the actual Coulomb interaction between the two final state electrons should be better than using an approximation for this interaction. However, we have previously found cases in which the WM results agree better with experiment than the 3DW. This could be fortuitous or it could indicate that the full Coulomb interaction is too strong for some cases.

The agreement between experiment and theory for the two larger projectile scattering angles is not as good as the smaller angles. For 40° , theory predicts two small angle peaks whereas experiment only has a single peak. Although both experiment and theory have a single small angle peak for 50° , the peak location significantly different. Interestingly, the agreement for the larger ejected electron angles is much better than the smaller angles.

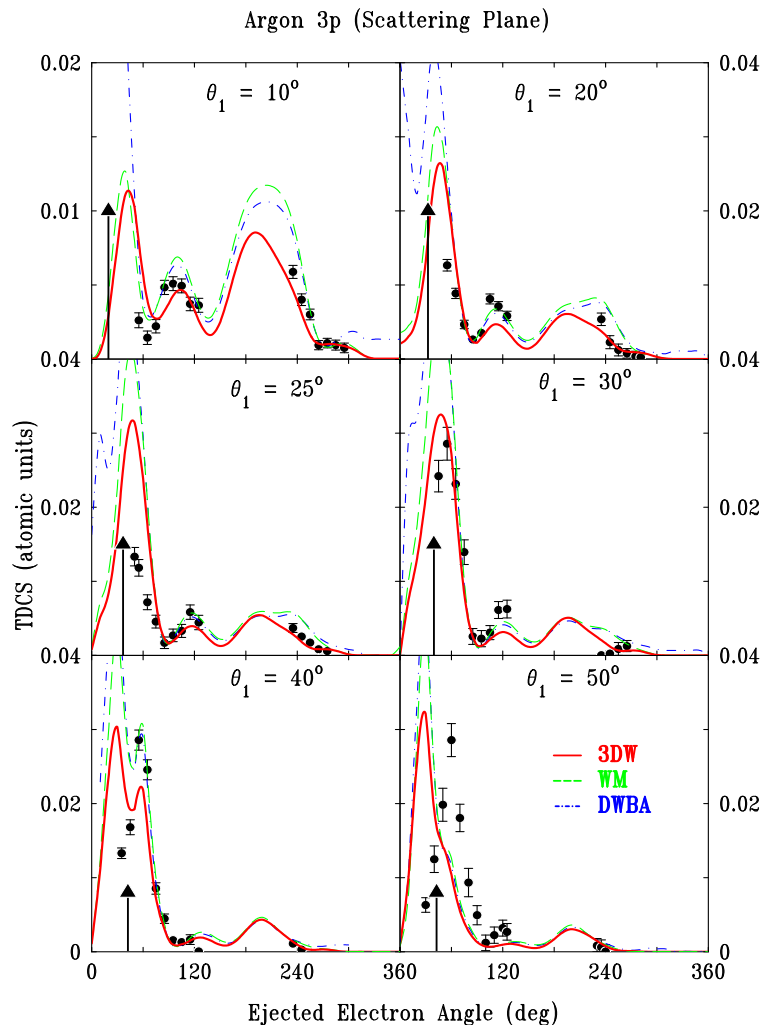


Figure 4. TDCS in atomic units for electron-impact ionization of the argon 3p orbital for 200 eV incident electrons and equal energy sharing for final state electrons with $E_1 = E_2 = 92.12$ eV. One electron detector is kept fix at the θ_1 angle noted in each panel and the other detector is rotated $0^\circ - 360^\circ$ (in principle) starting on the opposite side of the incident beam direction. The different theoretical curves are noted in the legend. The experimental data have been normalized to a best visual fit to the 3DW results.

5. CONCLUSIONS

We have examined the importance of PCI for electron-impact ionization of argon for the case of both final state electrons having equal energies where one might expect PCI to be important. We examined an equal energy range from 15 to 100 eV. For the case of equal ejection angles, including PCI was crucially important and theory predicts a completely

incorrect shape for the cross section without it. Although still important at 100 eV, its effect was significantly less. For the case of asymmetric scattering angles and 92.12 eV, PCI was not very important except for small projectile scattering and electron ejection angles. Evidently, even though the energies are the same, the electrons fly apart so fast that PCI is important only for a very short period of time. The WM approximation for PCI becomes better with increasing energy and is better for high energy and asymmetric angles than high energy and symmetric angles. In terms of agreement between experiment and theory, the 3DW was in qualitative agreement with the equal energy and equal angles experiments down to final state electrons of 15 eV and good quantitative agreement for electrons of 40 eV and higher. For the case of equal energies and asymmetric angles, very good agreement was found for projectile scattering angles of 30° and smaller.

ACKNOWLEDGMENTS

This work was supported by the Scientific and Technological Research Council of Turkey (TUBITAK) through Grant No. 109T738 and by BAPK through Grant No. 15.HIZ.DES.130. SA and DM would like to acknowledge the support of the US National Science Foundation under Grant. No. PHY- 1505819.

REFERENCES

- [1] Zatsarinny O Pflüger T Weyland M Baek W Y Rabus H Bartschat K Madison D Ren X, Amami S and Dorn A. *Phys. Rev. A*, 91:032707, 2015.
- [2] Zatsarinny O Pflüger T Weyland M Dorn A Madison D Ren X, Amami S and Bartschat K. *Phys. Rev. A*, 93:062704, 2016.
- [3] Ozer Z N Yavuz M Kazgoz S Dogan M Amami S, Ulu M and Madison D. *Phys. Rev. A*, 90, 2014.

- [4] Walters H R J Allan R J Bickert P Hink W Zhang X, Whelan C T and Schonberger S. *J. Phys. B: At. Mol. Opt. Phys.*, 25(20):4325, 1992.
- [5] Cavanagh S and Lohmann B. *J. Phys. B: At. Mol. Opt. Phys.*, 30(6):L231, 1997.
- [6] Haynes M A and Lohmann B. *Phys. Rev.A*, 64, 2001.
- [7] Crowe A Bartschat K Vorov O K Stevenson M, Leighton G J and Madison D H. *J. Phys. B: At. Mol. Opt. Phys.*, 38(4):433, 2005.
- [8] Bartschat K and Vorov O. *Phys. Rev.A*, 72:022728, 2005.
- [9] Stevenson M A and Lohmann B. *Phys. Rev.A*, 73, 2006.
- [10] Naja A Ren X G Lahman-Bennani A Nekkab M Dal Cappello C Bartschat K Staicu Casagrande E M, Catoire F and Whelan C T. *J. Electron Spectrosc. Relat. Phenom.*, 161:27, 2007.
- [11] Hu X Y Y and Zhou. *Phys. Lett. A*, 372:4809, 2008.
- [12] S. Otranto. Initial-state correlation in the electron-impact ionization of argon. *Phys. Rev. A*, 79:012705, Jan 2009.
- [13] Pflüger T Dorn A Bartschat K Ren X, Senftleben A and Ullrich J. *J. Phys. B: At. Mol. Opt. Phys.*, 43(3), 2010.
- [14] Olson R E de Lucio O G, Otranto S and DuBois R D. *Phys. Rev. Lett.*, 104, 2010.
- [15] Stevenson M A Hargreaves L R and Lohmann B. *J. Phys. B: At. Mol. Opt. Phys.*, 43(20), 2010.
- [16] Ren X et al. *J. Phys.: Conf. Ser.*, 212(1), 2010.
- [17] Zhang P Xu S Zhang S F Zhu X L Feng W T Yan S, Ma X and Liu H P. *J. Phys. B: At. Mol. Opt. Phys.*, 44(5), 2011.

- [18] Patidar V Purohit G and Sud K K. *Nucl. Instrum. Methods Phys. Res. B*, 269:745, 2011.
- [19] Ullrich J Zatsarinny O Bartschat K Madison D H Ren X, Pflüger T and Dorn A. *Phys. Rev. A*, 85, 2012.
- [20] Yan S Xu S Zhang S F Zhu X L Feng W T Zhang P, Ma X and Liu H P. *Phys. Rev. A*, 86, 2012.
- [21] Yavuz M Ulu M, Ozer Z N and Dogan M. *J. Phys. B: At. Mol. Opt. Phys.*, 46(11), 2013.
- [22] Haynes M B and Lohmann. *J. Phys. B: At. Mol. Opt. Phys.*, 34(5):L131, 2001.
- [23] Nixon K L J and Murray A. *Phys. Rev. A*, 87, 2013.
- [24] Xu S Li-Qing C Xing-Ju W, Xiang-Jun C and Ke-Zun. X. *Chin. Phys. Soc.*, 13(11):1857, 2004.
- [25] Ozer Z N Yavuz M Dogan M, Ulu M and Bozkurt G. *J. Spectrosc.*, 2013, 2013.
- [26] Varol O Yavuz M-Dogan M Ozer Z N, Amami S and Madison D. *J. Phys.: Conf. Ser.*, 635(5):1, 2015.
- [27] Madison D H Prideaux A and Bartschat K. *Phys. Rev. A*, 72, 2005.
- [28] Madison D H O and Al-Hagan. *At. Mol. Opt. Phys.*, 2010, 2010.
- [29] Stauffer A Nixon K Armstrong G Colgan J Amami S, Murray A and Madison D. *Phys. Rev. A*, 90, 2014.
- [30] Stauffer A Nixon K Armstrong G Colgan J Amami S, Murray A and Madison D. *Phys. Rev. A*, 91:069906(E), 2015.
- [31] Ward S J H and Macek J. *Phys. Rev.*, 49:1049, 1994.

IV. KINEMATICALLY COMPLETE STUDY OF LOW-ENERGY ELECTRON-IMPACT IONIZATION OF ARGON: INTERNORMALIZED CROSS SECTIONS IN 3D KINEMATICS

Xueguang Ren,¹ Sadek Amami,² Oleg Zatsarinny,³ Thomas Pflüger,¹ Marvin Weyland,^{1,4}
Alexander Dorn,¹ Don Madison,² and Klaus Bartschat³

¹Max-Planck-Institut für Kernphysik,
69117 Heidelberg, Germany

²Physics Department,
Missouri University of Science and Technology,
Rolla, Missouri 65409, USA

³Department of Physics and Astronomy,
Drake University,
Des Moines, Iowa 50311, USA

⁴Physikalisch-Technische Bundesanstalt,
38116 Braunschweig, Germany

ABSTRACT

As a further test of advanced theoretical methods to describe electron-impact single ionization processes in complex atomic targets, we extended our recent work on Ne($2p$) ionization (Ren *et al.*, Phys. Rev. A **91**, 032707 (2015)) to Ar($3p$) ionization at the relatively low incident energy of $E_0 = 66$ eV. The experimental data were obtained with a reaction microscope, which can cover nearly the entire 4π solid angle for the secondary electron emission. We present experimental data for detection angles of 10° , 15° , and 20° for the faster of the two outgoing electrons as function of the detection angle of the secondary electron with energies of 3 eV, 5 eV, and 10 eV, respectively. Comparison with theoretical

predictions from a B -spline R -matrix (BSR) with pseudostates approach and a three-body distorted-wave approach (3DW), for detection of the secondary electron in three orthogonal planes as well as the entire solid angle, shows overall satisfactory agreement between experiment and the BSR results, whereas the 3DW approach faces difficulties in predicting some of the details of the angular distributions. These findings are different from our earlier work on $\text{Ne}(2p)$, where both the BSR and 3DW yielded comparable levels of agreement with the experimental data.

1. INTRODUCTION

Electron-impact ionization of atoms and molecules is of fundamental importance in both basic science and a wide variety of applications, including but not limited to modeling the physics and chemistry of planetary atmospheres, the interpretation of astrophysical data, optimizing the energy transport in reactive plasmas, and understanding as well as ultimately utilizing the effect of ionizing radiation on biological tissue in medical applications.

The full information about the ionization dynamics can be obtained in kinematically complete experiments, or so-called $(e,2e)$ studies [1, 2], which determine the momentum vectors of all free particles. Moreover, in recent years experimental techniques were developed that allow to simultaneously access a large fraction of the entire solid angle and a large range of energies of the continuum electrons in the final state [3, 4]. Such experiments serve as a powerful tool to comprehensively test theoretical models that account for the quantum mechanical few-body interactions. In recent years, theory has made tremendous progress in describing the electron-impact ionization dynamics of atomic hydrogen and helium, as well as targets such as the light alkali and alkaline-earth elements. When it comes to ionization of the outermost valence electron, these systems can usually be well described as quasi-one and quasi-two electron targets with an inert core.

Much more challenging, however, is the treatment of more complex targets, such as the heavy noble gases Ne–Xe [5, 6, 7, 8, 9, 10, 11, 12, 13, 14, 15]. In recent years, we measured the ionization of Ne($2p$) [5, 6] and Ar($3p$) [7, 8]. For Ne($2p$), unprecedented agreement between experiment and predictions from a B -spline R -matrix (BSR) with pseudostates approach was obtained first for a projectile energy of 100 eV [5] and most recently also for the even lower energy of 65 eV [6]. While other theoretical models pretty much failed, a three-body distorted-wave (3DW) approach [9, 10, 11, 12] also did very well in comparison with experiment for the latter case. This suggested the importance of accounting for the post-collision interaction (PCI) at such low energies of both outgoing electrons.

Regarding Ar($3p$), the comparison between experiment and the BSR predictions improved dramatically after a cross-normalization error in the processing of the experimental raw data was discovered [16, 17]. For the higher incident projectile energy of 200 eV and asymmetric energy sharing between the two outgoing electrons, relatively good agreement was also achieved between experiment and a hybrid theory, which described the projectile by a distorted-wave and the initial bound state as well as the ejected-electron–residual-ion interaction by a close-coupling expansion [18, 19]. For 71 eV incident energy, however, the hybrid method was inappropriate. Furthermore, the normalization correction alone did not bring completely satisfactory agreement between experiment and the BSR predictions either.

The purpose of the present study, therefore, was twofold. First, after learning many lessons from the Ne($2p$) experiments, not only regarding the proper cross normalization but also the need for setting narrow energy and angular acceptance windows of the detectors, a new set of benchmark data for an even lower incident energy (66 eV) was to be generated. Experimentally, this was achieved with further improvements on the reaction microscope and the data processing procedure. Second, it seemed important to investigate whether the success of the 3DW approach for Ne($2p$) [6] would hold up also in the case of Ar($3p$). In

fact, in light of the remaining discrepancies between experiment and the BSR results for Ar($3p$) at 71 eV [17], it was hoped that a second successful theory might provide additional clues for mutual improvement.

Ar($3p$) ionization was also studied by the Lohmann group in the coplanar asymmetric geometry, in particular at $E_0 = 113.5$ eV [20, 21, 22] using a conventional (e,2e) spectrometer. In their more recent studies, a magnetic angle changer enabled the observation of the entire angular range for the slow ejected electron within the scattering plane. The same coplanar asymmetric geometry was studied by Amami *et al.* [23] at $E_0 = 200$ eV. Murray *et al.* [24, 25] observed collisions with equal energy sharing of both outgoing electrons from near-threshold to intermediate energies and from the coplanar to the perpendicular plane geometry.

This paper is organized as follows. After a brief description of the experimental apparatus in Section 2, we summarize the essential points of the two theoretical models in Section 3. The results are presented and discussed in Section 4, before we finish with the conclusions. Unless specified otherwise, atomic units (a.u.) are used throughout.

2. EXPERIMENT

Experiments were performed with an advanced reaction microscope [3] that was specially built for electron-impact ionization studies as drawn in Figure 1. It was recently updated with a newly designed pulsed photoemission electron gun and a pulsed electric ion-extraction field for better ion-detection efficiency [26, 27]. Since details of the experimental setup can be found in [3, 26, 27], only a brief outline will be given here. The well-focused (≈ 1 mm diameter), pulsed electron beam with an energy of $E_0 = 66$ eV is crossed with a continuous supersonic argon gas jet, which is produced using a $30\mu\text{m}$ nozzle and two-stage supersonic gas expansion. The electron beam is generated by illuminating a tantalum photocathode with a pulsed ultraviolet laser beam ($\lambda = 266$ nm, $\Delta t < 0.5$ ns). The energy and temporal width of the electron pulses are about 0.5 eV (ΔE_0) and 0.5 ns (Δt_0), respectively.

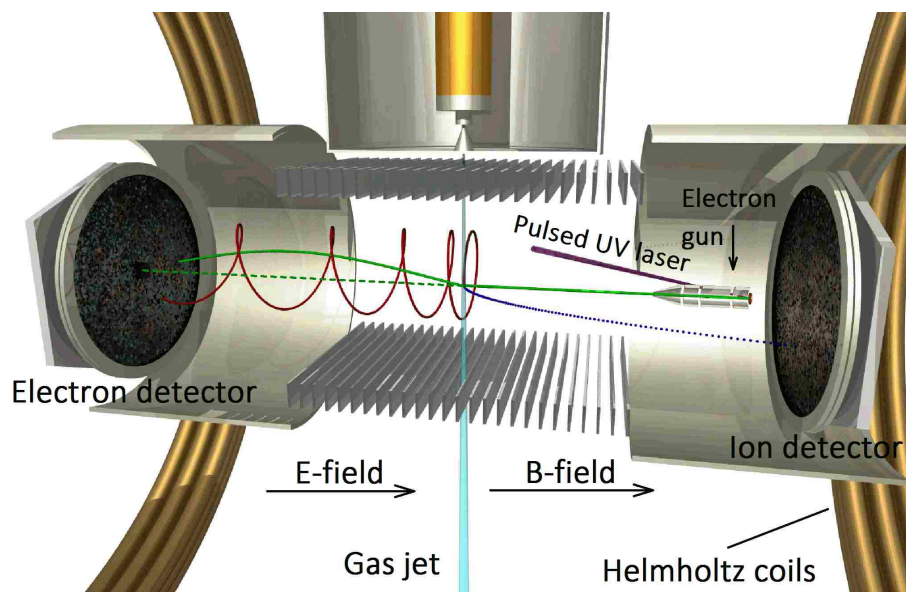


Figure 1. Schematic view of the employed reaction microscope for electron-scattering experiments.

Homogeneous magnetic and electric fields guide electrons (spiral lines in Figure 1) and ions (dotted line) from the reaction volume onto two position- and time-sensitive microchannel plate detectors that are equipped with fast multi-hit delay-line readout. By measuring the time-of-flight and the impact position for each particle their vector momenta after the collision are determined. The projectile beam axis (defining the longitudinal z -direction) is aligned parallel to the electric and magnetic extraction fields. Therefore, after crossing the target gas jet, the unscattered primary beam (dashed line) reaches the center of the electron detector, where a central bore in the multichannel plates allows it to pass without inducing a signal. The detection solid angle for recoil Ar^+ ions is 4π . The acceptance angle for detection of electrons up to an energy of 15 eV is also close to 4π , except for the acceptance holes at small forward and backward angles where the electrons end up in the detector bore.

Single ionization is recorded by triple-coincidence detection of two electrons (e_1 and e_2) and the recoil ion. Therefore, two electrons arriving within a short time interval have to be individually registered with the electron detector. Since we consider asymmetric

energy sharing and forward scattering for the faster electron in the present work, the times-of-flight of both electrons always differ by more than 20 ns. Consequently, detector and electronic dead-times do not affect our data acquisition.

In our experiment, data are recorded in a single run by the list mode (event-by-event) data acquisition. The three-dimensional momentum vectors and, consequently, kinetic energies and emission angles of final-state electrons and ions are determined from the individually measured time-of-flight and position in the offline data analysis. Since the complete experimentally accessible phase space is measured simultaneously, all relative data are cross-normalized and only a single global factor is required in comparison of theory and experiment [5, 6].

Compared to earlier experiments[8, 17], we significantly improved the electron momentum resolution of the spectrometer by increasing the homogeneity of the extraction fields and reducing the time-of-flight uncertainty due to the shorter projectile pulses. This improvement manifests itself in the resolution for the electron binding energy ($E_B = E_0 - E_1 - E_2$), for which we achieved $\Delta E_B \approx 2.0$ eV. This is about a factor of three better than before.

Consequently, as suggested in Ref. [28], the intervals of scattering angles $\Delta\theta_1$ and ejected electron energies ΔE_2 , over which the experimental data are integrated, were narrowed in the present work in order to reduce the resulting uncertainties in the cross-section values. The individual acceptance intervals employed in the experimental data analysis were $\theta_1 = -10^\circ \pm 1^\circ$, $-15^\circ \pm 1^\circ$ and $-20^\circ \pm 2^\circ$ for the detection angle θ_1 of the fast outgoing electron. For the slow outgoing electron, the windows for the energy resolution were set as $E_2 = 3 \text{ eV} \pm 1 \text{ eV}$, $5 \text{ eV} \pm 1 \text{ eV}$, and $10 \text{ eV} \pm 1 \text{ eV}$, while the angular resolution was $\Delta\theta_2 = \pm 3^\circ$ and $\Delta\phi_2 = \pm 3^\circ$. As a result, we see for some kinematical conditions that angular emission maxima and minima become better resolved in the experimental cross-section data compared to our earlier measurement [8, 17]. This will be further elucidated below.

3. THEORETICAL MODELS

We used two theoretical methods to describe the present electron-impact ionization process. Although they have been described previously, we summarize the essential ideas and the particular ingredients for the current cases of interest in order to make this paper self-contained. Even more detailed information can be found in the references given.

3.1. BSR. The BSR method (see [29] for a detailed summary and an overview of various applications) and the accompanying computer code [30] were originally developed as an alternative to the well-known R -matrix approach developed by Burke and collaborators in Belfast. An extensive description of the latter can be found in [31]. In order to allow for calculations of electron-impact ionization processes, the BSR method, like the Belfast implementation, was extended by introducing a large number of pseudostates. This became known as the R -matrix with pseudostates (RMPS) approach [32]. Regarding the basic idea, it is equivalent to the “convergent close-coupling” (CCC) approach developed by Bray and co-workers (see [33] for a recent review). Most importantly, the effect of the countable infinite number of high-lying Rydberg states and the uncountable infinite ionization continuum in the close-coupling expansion is approximated by a large (but finite) number of compact, and hence box-normalizable, pseudostates.

After the pseudostate close-coupling methods turned out to be extremely successful in the description of transitions between discrete physical bound states, without significant modifications needed to generate the results of interest for such transitions, the question became how to potentially extract results for the ionization process. While the total ionization cross section for a given initial state could be obtained in a straightforward way by just adding up the excitation cross sections for all transitions from this state to pseudostates with energies above the ionization threshold, the situation is much more complicated if cross sections that are differential in energy and/or angle are required.

Details and further references to the original papers can be found in the reviews mentioned above. Here we briefly repeat how the physical *ionization* cross sections are obtained from the *excitation* amplitudes for the pseudostates [34]. To begin with, we are interested in the ionization amplitude

$$f(L_0 M_0 S_0 M_{S_0}, k_0 \mu_0 \rightarrow L_f M_f S_f M_{S_f}, k_1 \mu_1, k_2 \mu_2) \quad (1)$$

for an initial target state with orbital angular momentum L_0 and spin S_0 (with projections M_0 and M_{S_0} , respectively) leading to a final ionic state with corresponding quantum numbers labeled by the subscript f , by an electron with initial linear momentum k_0 and spin projection μ_0 resulting in two outgoing electrons described by k_1, μ_1 and k_2, μ_2 . We obtain this *ionization* amplitude by projecting the *excitation* amplitudes for the pseudostates (superscript p),

$$\begin{aligned} f^p(L_0 M_0 S_0 M_{S_0}, k_0 \mu_0 \rightarrow L M S M_S, k_1 \mu_1) &= \sqrt{\frac{\pi}{k_0 k_1}} \sum_{l_0, l_1, L_T, S_T, \Pi_T, M_{L_T}, M_{S_T}} i^{(l_0 - l_1)} \sqrt{(2l_0 + 1)} \\ &\times (L_0 M_0, l_0 0 | L_T M_{L_T}) (L M, l_1 m_1 | L_T M_{L_T}) (S_0 M_{S_0}, \frac{1}{2} \mu_0 | S_T M_{S_T}) \\ &\times (S M_S, \frac{1}{2} \mu_1 | S_T M_{S_T}) T_{l_0 l_1}^{L_T S_T \Pi_T}(\alpha_0 L_0 S_0 \rightarrow \alpha L S) Y_{l_1 m_1}(\theta_1, \varphi_1), \end{aligned} \quad (2)$$

to the true continuum functions for electron scattering from the residual ion, $\Psi_{L_f M_f S_f M_{S_f}}^{k_2 \mu_2 (-)}$, and summing over all energetically accessible pseudostates using the ansatz

$$\begin{aligned} &f(L_0 M_0 S_0 M_{S_0}, k_0 \mu_0 \rightarrow L_f M_f S_f M_{S_f}, k_1 \mu_1, k_2 \mu_2) \\ &= \sum_p \langle \Psi_{L_f M_f S_f M_{S_f}}^{k_2 \mu_2 (-)} | \Phi^p(n l n' l', L S) \rangle f^p(L_0 M_0 S_0 M_{S_0}, k_0 \mu_0 \\ &\quad \rightarrow L M S M_S, k_1 \mu_1). \end{aligned} \quad (3)$$

In this multichannel generalization of Equation (15) proposed by Bray and Fursa [35], $T_{l_0 l_1}^{L_T S_T \Pi_T}$ ($\alpha_0 L_0 S_0 \rightarrow \alpha_1 L_1 S_1$) is an element of the T matrix for a given L_T , total spin S_T , and parity Π_T of the collision system. Choosing the z -axis along the direction of the incident beam simplifies the formula to $m_0 = 0$ for the orbital angular momentum projection of the incident electron.

As seen from Equation (3), the above procedure requires the overlap factors $\langle \Psi_{L_f M_f S_f M_{S_f}}^{f, k_2(-)} | \Phi^P(n l n' l', LS) \rangle$ between the true continuum states and the corresponding pseudostates. The continuum states, which describe electron scattering from the residual ion, are once again obtained using the R -matrix method, with the *same* close-coupling expansion that is employed for generating the bound pseudostates. This is a critical issue, since it allows for the preservation of the crucial channel information through the projection.

Finally, the fully differential cross section (FDCS) is given by

$$\frac{d\sigma}{d\Omega_1 dE_1 d\Omega_2 dE_2} = \frac{k_1 k_2}{k_0} \left| f(L_0 M_0 S_0 M_{S_0}, k_0 \mu_0 \rightarrow L_f M_f S_f M_{S_f}, k_1 \mu_1, k_2 \mu_2) \right|^2, \quad (4)$$

where E_i, Ω_i ($i = 1, 2$) denote the energy and the solid-angle element for detection of the two electrons.

For the present work, we started with multi-configurations expansions of the three ionic states $(3s^2 3p^5)^2 P^o$, $(3s 3p^6)^2 S$, and $(3s^2 3p^4 3d)^2 S$ of Ar^+ . These states were generated by the B -spline box-based close-coupling method [36] inside a box of radius $a = 28 a_0$, where $a_0 = 0.529 \times 10^{-10}$ m denotes the Bohr radius. The one-electron orbitals were expanded in a B -spline basis and then used as the core basis to construct 482 states of neutral argon by adding another electron. All one-electron orbitals that made up these states were forced to vanish at the box boundary.

The number of physical states that can be generated by this method depends on the radius of the R -matrix (B -spline) box. The physical states are those that fit into the box with a sufficiently well decreasing exponential tail, while the pseudostates are pushed up

in energy due to the forced number of nodes within the box. It is also worth noting that the one-electron orbitals with the same value of the angular momentum are not forced to be orthogonal to each other in the BSR implementation, nor to the continuum orbitals used for the expansion of the scattering wavefunction inside the R -matrix box in the subsequent collision calculation. This leads to additional complexities in setting up and diagonalizing the Hamiltonian matrix, but it also has many practical advantages [29]. In particular, releasing the orthogonality restriction provides high flexibility in the description of complex targets with strong term-dependence of the one-electron orbitals. In the present work, the 482 states had coupled orbital angular momenta $L \leq 5$ and energies reaching up to 80 eV.

We then performed a non-relativistic calculation for e-Ar collisions with all 482 states included in the close-coupling expansion. The resulting equations were solved with a parallelized version of the BSR suite of computer codes [30]. Contributions from target+projectile symmetries with coupled orbital angular momenta up to 25 were included in the partial-wave expansion. The model contained up to 1,445 scattering channels, leading to generalized eigenvalue problems with matrix dimensions up to 90,000 in the B -spline basis. This calculation yields scattering amplitudes for excitation of all physical and pseudo-states. The amplitudes for the latter are finally projected to the true e-Ar⁺ collision states for the ejected electron to obtain the ionization amplitudes. As mentioned above, in order to keep this projection consistent, it is crucial to employ the same close-coupling expansion, in our case involving the three states of Ar⁺ mentioned above, that was used to generate the target states in the first place.

As a final remark, RMPS methods in general contain the full correlations, including the post-collision interaction (PCI), between all electrons involved within the R -matrix box, similarly to the CCC implementation that also employs orbitals of finite range. Hence, the size of the R -matrix box is not solely determined by the range of the discrete target states for which transitions should be described, but also by the goal of accounting as much as possible for the long-range correlations between the two electrons that can get far away

from the target nucleus, i.e., the projectile and the “ejected” electron, even though the latter can actually not reach the detector in the original theoretical formulation. In principle, the dependence of the results on the box size could be tested, but in reality such tests are limited by the available computational resources. However, practitioners of the pseudostate close-coupling approach have gained much experience over the past two decades regarding the choice of appropriate parameters.

3.2. The 3DW Approximation. Since the details of the 3DW approximation have been outlined before [9, 10, 11, 12], only an overview will be given here. In the 3DW approximation, the direct T matrix is given by

$$T_{dir}^{3DW} = \langle \Psi_f | W | \Psi_i \rangle. \quad (5)$$

For ionization of an atom, the initial-state wave function Ψ_i is approximated as a product of the initial Hartree-Fock bound-state wave function ψ_{HF} for the target and a distorted-wave function χ_0 for the incoming electron (the projectile):

$$\Psi_i = \psi_{HF} \chi_0. \quad (6)$$

The perturbation (W) is given by

$$W = V_i - U_i. \quad (7)$$

Here V_i is the interaction between the incident electron and the atom, while U_i is the initial-state spherically symmetric static approximation for V_i , which asymptotically approaches zero. The final-state wave function is approximated as a product of two final-state continuum electron distorted waves (χ_1 for the scattered and χ_2 for the ejected electron, respectively),

and the Coulomb interaction between the outgoing electrons (C_{12}), normally called PCI:

$$\Psi_f = \chi_1 \chi_2 C_{12}. \quad (8)$$

In the 3DW approximation, we incorporate the exact electron-electron Coulomb interaction between the two electrons for C_{12} , which requires the evaluation of a six-dimensional (6D) numerical integral. This factor is a product of a Γ factor and a hypergeometric function [6]. Finally, the direct 3DW T matrix becomes

$$T_{dir}^{3DW} = \langle \chi_1 \chi_2 C_{12} | V_i - U_i | \psi_{HF} \chi_0 \rangle. \quad (9)$$

The exchange T matrix T_{exc}^{3DW} is identical to Eq. (5), except that the scattered and ejected electrons are exchanged in the final-state wave function Ψ_f .

Finally, the FDCS can be written for the T matrix in atomic units as

$$\text{FDCS} = \frac{1}{(2\pi)^5} \frac{k_1 k_2}{k_0} \left(|T_{dir}|^2 + |T_{exc}|^2 + |T_{dir} - T_{exc}|^2 \right). \quad (10)$$

where k_0 , k_1 , and k_2 are the magnitudes of the momenta of the initial, scattered, and ejected electrons, respectively.

Calculations are typically classified in terms of orders of perturbation theory. However, this classification can become ambiguous, since any physics contained in the approximate wave function is contained to all orders of perturbation theory, while the physics contained in the perturbation will be contained to the order of the calculation. For the 3DW approximation, the electron-electron interaction is contained in the approximate final-state wave function; hence, this physics is contained to all orders of perturbation theory. As mentioned above, the nonperturbative BSR calculation also accounts for PCI to all orders of

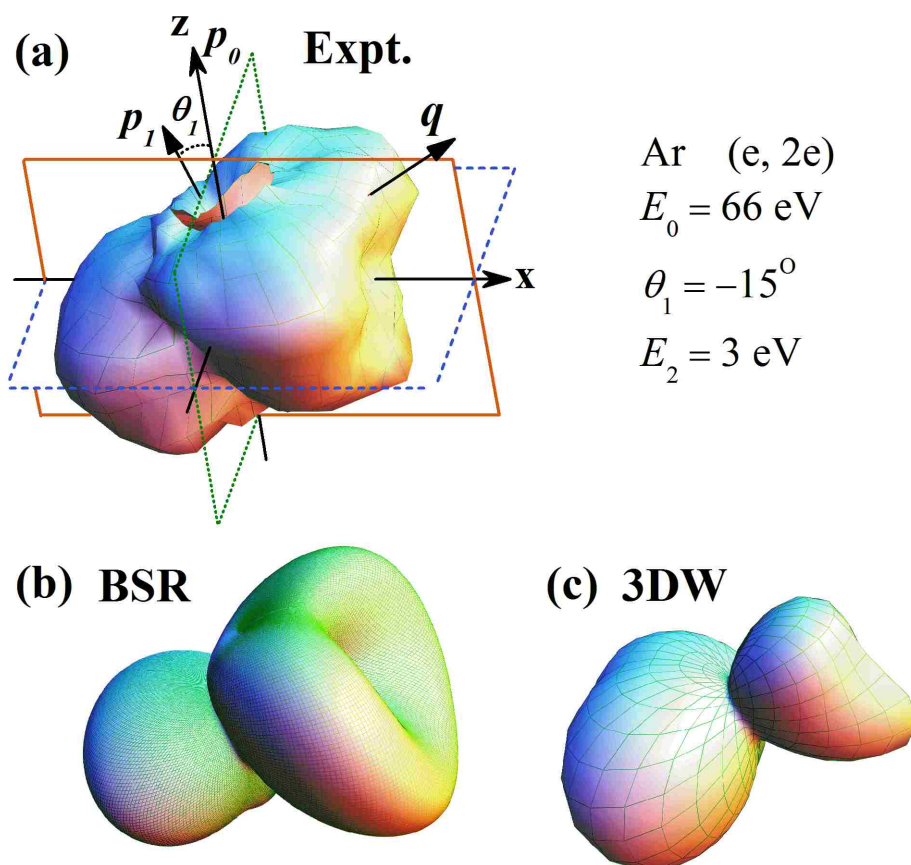


Figure 2. Experimental and theoretical FDCS for ionization of Ar($3p$) by incident electrons with energy $E_0 = 66 \text{ eV}$, presented as 3D images. The scattering angle is $\theta_1 = -15^\circ$, and the ejected electron energy is $E_2 = 3 \text{ eV}$. Panel (a) shows the experimental 3D FDCS, while panels (b) and (c) represent the predictions from the BSR and 3DW theories, respectively.

perturbation theory, but only within the R -matrix box. In BSR calculations for ionization, therefore, the box size is generally chosen larger than required by the typical rule [31] that exchange between the projectile electron and the target electrons is negligible.

4. RESULTS AND DISCUSSION

Figure 1 exhibits the experimental and theoretical FDCSs for ionization of Ar($3p$) by 66 eV electron impact as three-dimensional (3D) polar plots for a projectile scattering angle of $\theta_1 = -15^\circ$ as a function of the emission direction of a slow ejected electron with

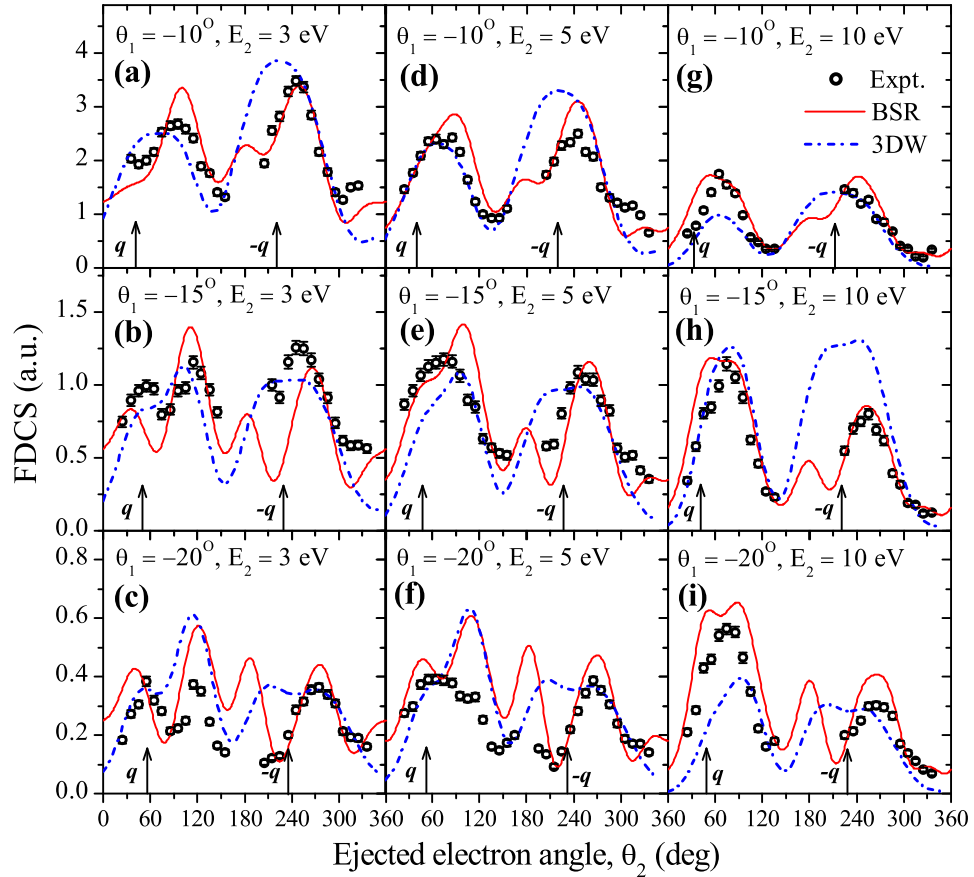


Figure 3. FDCS for the ionization of Ar(3p) presented as a function of the ejected electron (e_2) emission angle at scattering angles $\theta_1 = -10^\circ$ (top row), $\theta_1 = -15^\circ$ (center row), and $\theta_1 = -20^\circ$ (bottom row) for ejected-electron energies $E_2 = 3$ eV (left column), $E_2 = 5$ eV (center column), and $E_2 = 10$ eV (right column). The vertical arrows indicate the momentum transfer direction, q and its opposite, $-q$. The results are for the scattering plane, i.e., the xz -plane of Fig. 1(a).

$E_2 = 3$ eV energy. Panel (a) corresponds to the experimental data, while panels (b) and (c) show the calculated results from the BSR and 3DW theories, respectively. The projectile enters from the bottom and is scattered to the left (hence the minus in the notation for the angle). These two vectors define the scattering (xz) plane, as marked by the solid frame in panel (a). The momentum transfer to the target is indicated by the arrow labeled q .

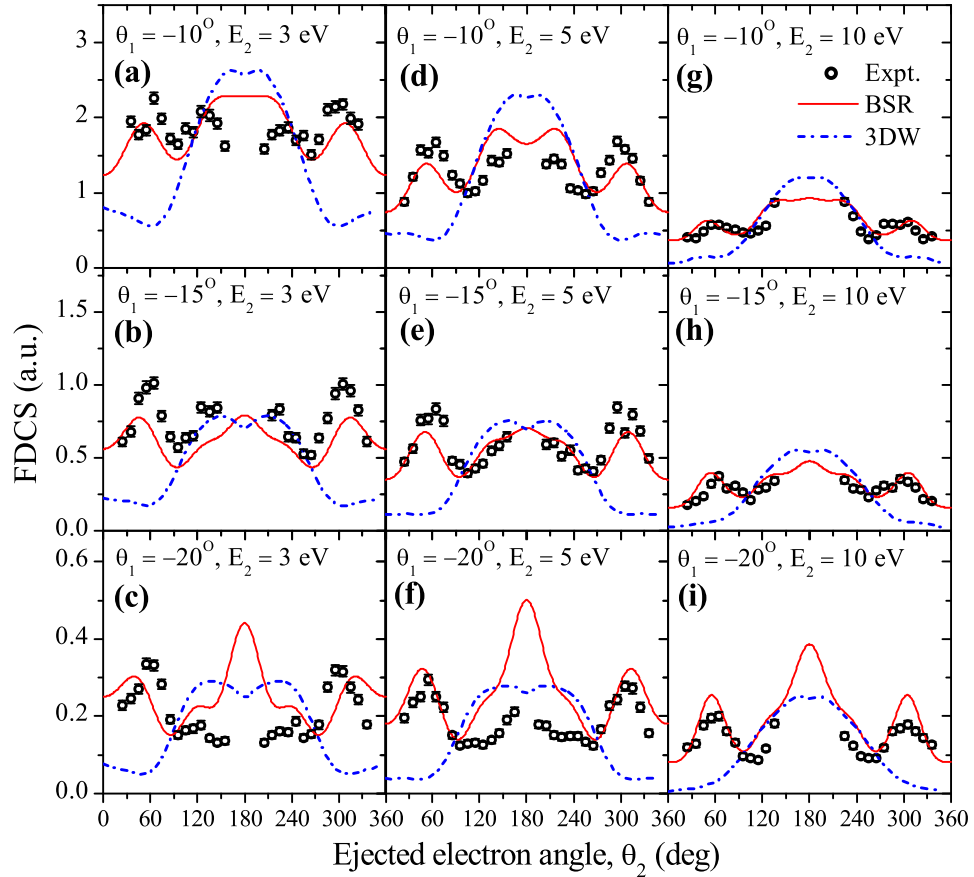


Figure 4. Same as Fig. 2 for the “half-perpendicular” plane, i.e., the yz -plane of Fig. 1(a).

In these 3D-plots, the FDCS for a particular direction is given as the distance from the origin of the plot to the point on the surface, which is intersected by the ejected electron’s emission direction. [Below we follow the common notation of referring to the slower of the two outgoing electrons as “ejected”, and to the faster one as “scattered”.] The kinematics chosen displays exemplarily the principal features of the emission pattern: it is governed by the well-known binary and recoil lobes. The binary lobe is oriented roughly along the direction of the momentum transfer q , thus corresponding to electrons emitted after a single binary collision with the projectile. In the opposite direction the recoil lobe is found, where the outgoing slow electron, initially moving in the binary direction, additionally backscatters in the ionic potential. For ionization from p -orbitals, the binary

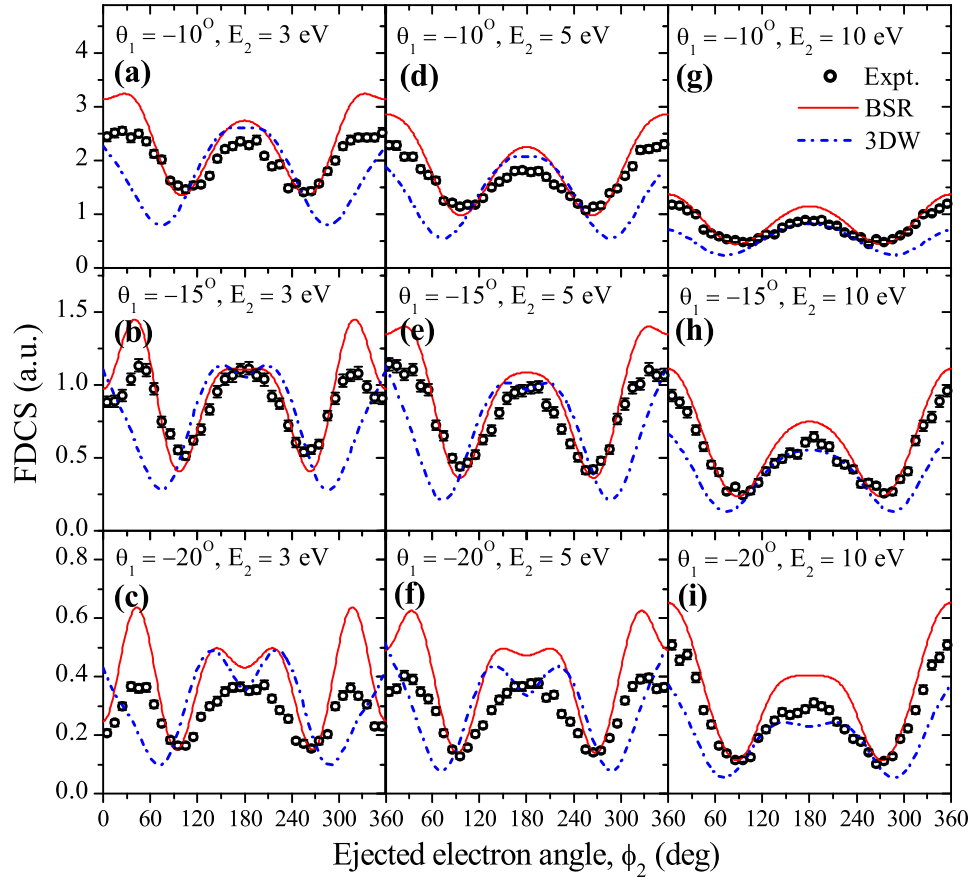


Figure 5. Same as Figure 2 for the “full-perpendicular” plane, i.e., the xy -plane of Figure 1(a).

peak often exhibits a minimum along the momentum transfer direction. This is the result of the characteristic momentum profile of a p -orbital that has a node for vanishing momentum. Additionally, the ejected electron is repelled by the scattered projectile due to the long-range nature of the Coulomb force. These PCI effects tilt the binary and recoil lobes away from the scattered projectile direction. Furthermore, at these relatively low energies the binary lobe exhibits a much flatter shape in comparison with 3D emission patterns for high and intermediate energies.

Comparing the experimental data to the two sets of theoretical results, we see that the BSR predictions are in overall good agreement with the data. In contrast to ionization of Ne($2p$) [6] for comparable kinematical parameters, the 3DW theory underestimates the out-of-scattering-plane size of the binary peak relative to the recoil peak for the case shown.

For a more quantitative comparison between experiment and theory, the cross sections in three orthogonal planes are presented in Figures 2–4. Those are the xz -plane or scattering plane, the yz -plane or half-perpendicular plane, and the xy -plane or full-perpendicular plane, which are cuts through the 3D FDCS image as indicated in Figure 1(a). The studied kinematical conditions correspond to projectile scattering angles of $\theta_1 = -10^\circ$, -15° , and -20° , and to ejected electron energies of $E_2 = 3$ eV, 5 eV, and 10 eV, respectively. The global scaling factor used to normalize the experimental data to the theories was found by achieving a good visual fit of experiment and the BSR calculations for the FDCS in the scattering plane at $\theta_1 = -10^\circ$ and $E_2 = 3$ eV (Figure 2(a)). This factor was subsequently applied to all other kinematics and planes, i.e., the experimental data are consistently cross-normalized to each other.

Figure 2 shows a comparison between experiment and theory for detection of the secondary electron in the scattering plane. As can already be seen in the 3D plots, the BSR is in better agreement with experiment than the 3DW. Although the 3DW is in reasonably good agreement with the data for the binary peak at the smaller projectile scattering angles, it tends to predict a broader and often also higher recoil peak. The BSR, on the other hand, is in reasonably good agreement with the data, particularly for the two smaller projectile scattering angles.

For the largest projectile scattering angle and low ejected electron energies, the two theories agree better with each other than with experiment for the binary peak. As mentioned earlier, p -orbital cross sections often exhibit a double binary peak with a minimum near the momentum transfer direction. This behavior can indeed be seen in a few cases, particularly for the larger projectile scattering angles and lower energies. The BSR predicts a double

recoil peak for all cases. The 3DW results exhibit a double peak only for $\theta_1 = -20^\circ$. For smaller θ_1 , it appears that these two peaks merge into a single peak. The peaks are more separated in the BSR results, with one of them being positioned near 180° . For this peak, intensity increases with increasing scattering angle. Unfortunately, the cross section close to 180° cannot be accessed experimentally. Only for $\theta_1 = -20^\circ$ and $E_2 = 5$ eV, the available data suggest a possible peak around 180° . Nevertheless, in this case as well as for $\theta_1 = -20^\circ$ and $E_2 = 3$ eV, the measured cross section in the vicinity of 180° lies significantly below the BSR predictions.

Figure 3 shows a comparison between experiment and theory for the yz -plane (half-perpendicular plane). For this plane, symmetry considerations require the cross sections to be symmetric about 180° , which can indeed be seen in both theory and experiment. Here, the BSR is in much better agreement with experiment than the 3DW. Problems for the BSR remain at $\theta_1 = -20^\circ$ for $E_2 = 3$ eV and 5 eV. In these cases, the predicted peak at $\theta_2 = 180^\circ$ is either not seen at all, or there is at best a very weak indication in the experimental data. This finding is similar to that noted above also for the scattering plane. The yz -plane also reveals the too-narrow binary peak of the 3DW calculation that is already visible in the 3D plot (see Fig. 1). The 3DW binary peak is not contributing significantly to the yz -plane cross section and, consequently, all panels show that the predicted cross section is significantly smaller than observed experimentally for $\theta_2 \leq 90^\circ$ and, by symmetry, for $\theta_2 \geq 270^\circ$. As a result, the 3DW shows no indication of a binary/recoil peak in the yz -plane.

Figure 4 shows the comparison between experiment and theory for the full-perpendicular plane (i.e., the xy -plane). Here, the experimental angular acceptance covers the entire $0^\circ - 360^\circ$ range, but the cross sections are again symmetric with respect to 180° . The binary and recoil peaks are observed in the vicinity of $\phi_2 = 0^\circ$ and 180° , respectively. Both 3DW and BSR are in rather good agreement with the experimental data, except that the binary peaks are again too narrow in the 3DW curves. Furthermore, the 3DW does not reproduce the apparent minimum that is seen in some cases for $\phi_2 = 0^\circ$.

It is worthwhile to note that our measurements for the scattering plane are qualitatively consistent with those of the Lohmann group [20, 21, 22], which were obtained at the higher projectile energy of $E_0 = 115.5$ eV. For the projectile scattering angle $\theta_1 = -15^\circ$, for instance, we observe that with increasing ejected electron energy E_2 the two maxima of the binary peak, which are clearly visible at $E_2 = 3$ eV, merge to a single maximum at $E_2 = 10$ eV. The same behavior was reported in Ref. [20] for the same scattering angle. Furthermore, Refs. [21, 22] provide some information regarding the pronounced peak at $\theta_2 = 180^\circ$ predicted by the BSR theory. For $\theta_1 = -15^\circ$, such a peak was indeed observed in the coplanar cross sections for $E_2 = 2$ eV, but it was strongly reduced and became almost invisible for $E_2 = 5$ eV. This trend is not seen in the BSR results at the present projectile energy.

We finish this section by commenting again on the improved momentum resolution of the current apparatus and the reduced angular and energy ranges that the data are summed over compared with our earlier measurement at $E_0 = 70.8$ eV [8]. Looking at the measured cross sections for corresponding kinematical cases in both experiments, it becomes clear that the overall patterns are consistent while the angular resolution is better for the present data. For the scattering plane, this can be seen by comparing Figure 2(c) with Figure 4(g) in [8], where the dip in the binary peak is clearly deeper in the present measurements. The same holds for the half-perpendicular plane, which was labeled “perpendicular plane” in [8]. In particular, we recommend comparing panels Figure 3(a,b,c) above with Figure 4(d,f,h) in [8], respectively.

5. CONCLUSIONS

We have reported a comprehensive study of the electron-impact ionization dynamics of Ar($3p$) at the relatively low incident projectile energy of 66 eV. The fully-differential cross sections obtained experimentally were internormalized across three scattering angles θ_1 from -10° to -20° and three ejected electron energies E_2 from 3 eV to 10 eV. The present

experimental data substantially enhance the still very limited set of data currently available to thoroughly test theoretical methods for describing this complex and highly correlated problem.

Overall, our experimental data and the BSR predictions agree at a similar level as in previous studies, in particular for the two smaller scattering angles $\theta_1 = -10^\circ$ and -15° , whereas the 3DW results reveal significant deviations from experiment in some cases. The latter findings are different from our recent work on Ne($2p$) ionization [6], where both BSR and 3DW yielded comparable levels of agreement with the experimental data. It is conceivable that the energies considered in this work are too low for the 3DW approach, which does not contain channel coupling. Another possibility for the difficulties could be the fact that the current implementation of the 3DW method uses single-configuration descriptions of the initial bound and the final ionic target states, rather than the multi-configuration expansions with term-dependent orbitals that can be employed in the BSR approach.

One of the primary strengths of the 3DW approach lies in the exact treatment of PCI. Accordingly, we find that the 3DW is in qualitative agreement with experiment concerning the angular positions of the peaks in the scattering plane, which are strongly influenced by PCI. On the other hand, the 3DW cross section in the binary regime is too small, particularly outside the scattering plane. This results in poor agreement with experiment and the BSR predictions in the half-perpendicular plane. Based on the present results, we conclude that the important physical effects determining the cross sections appear to be very different for Ne and Ar, since the 3DW was in good agreement for Ne for essentially the same kinematics.

ACKNOWLEDGMENTS

This work was supported, in part, by the United States National Science Foundation under grants No. PHY-1505819 (SA and DM), No. PHY-1430245 and No. PHY-1520970 (OZ and KB), and the XSEDE allocations TG-MCA075029 (SA and DM) and No. PHY-090031 (OZ and KB). SA would also like to thank the Libyan Ministry of Higher Education's Scholarship for financial support.

REFERENCES

- [1] H. Ehrhardt, M. Schulz, T. Tekaatt, and K. Willmann. *Phys. Rev. Lett.*, 22:89, 1969.
- [2] U. Amaldi, A. Egidi, R. Marconero, and G. Pizzella. *Rev. Sci. Instrum.*, 40:1001, 1969.
- [3] J. Ullrich, R. Moshhammer, A. Dorn, R. Dörner, L.Ph.H. Schmidt, and H. Schmidt-Böcking. *Rep. Prog. Phys.*, 66:1463, 2003.
- [4] M Dürr, C Dimopoulou, A Dorn, B Najjari, I Bray, D V Fursa, Zhangjin Chen, D H Madison, K Bartschat, and J Ullrich. Single ionization of helium by 102 ev electron impact: three-dimensional images for electron emission. *J. Phys. B*, 39(20):4097, 2006.
- [5] T. Pflüger, O. Zatsarinny, K. Bartschat, A. Senftleben, X. Ren, J. Ullrich, and A. Dorn. *Phys. Rev. Lett.*, 110:153202, 2013.
- [6] Xueguang Ren, Sadek Amami, Oleg Zatsarinny, Thomas Pflüger, Marvin Weyland, Woon Yong Baek, Hans Rabus, Klaus Bartschat, Don Madison, and Alexander Dorn. Kinematically complete study of low-energy electron-impact ionization of neon: Internormalized cross sections in three-dimensional kinematics. *Phys. Rev. A*, 91:032707, Mar 2015.

- [7] Xueguang Ren, Arne Senftleben, Thomas Pflüger, Alexander Dorn, Klaus Bartschat, and Joachim Ullrich. Benchmark experiment for electron-impact ionization of argon: Absolute triple-differential cross sections via three-dimensional electron emission images. *Phys. Rev. A*, 83:052714, May 2011.
- [8] X. Ren, T. Pflüger, J. Ullrich, O. Zatsarinny, K. Bartschat, D. H. Madison, and A. Dorn. Low-energy electron-impact ionization of argon: Three-dimensional cross section. *Phys. Rev. A*, 85:032702, Mar 2012.
- [9] A. Prideaux and D. H. Madison. Role of the postcollision interaction in electron-impact ionization of argon and krypton. *Phys. Rev. A*, 67:052710, May 2003.
- [10] Don H. Madison and Ola Al-Hagan. The distorted-wave born approach for calculating electron-impact ionization of molecules. *J. At. Mol. Opt. Phys.*, 2010:367180, 2010.
- [11] Sadek Amami, Andrew Murray, Al Stauffer, Kate Nixon, Gregory Armstrong, James Colgan, and Don Madison. Theoretical and experimental ($e, 2e$) study of electron-impact ionization of laser-aligned mg atoms. *Phys. Rev. A*, 90:062707, Dec 2014.
- [12] Sadek Amami, Andrew Murray, Al Stauffer, Kate Nixon, Gregory Armstrong, James Colgan, and Don Madison. Erratum: Theoretical and experimental ($e, 2e$) study of electron-impact ionization of laser-aligned mg atoms [phys. rev. a 90, 062707 (2014)]. *Phys. Rev. A*, 91:069906, Jun 2015.
- [13] X. Ren, A. Senftleben, T. Pflüger, A. Dorn, K. Bartschat, and J. Ullrich. *J. Phys. B*, 43:035202, 2010.
- [14] I. Taouil, Alain Duguet, Azzedine Lahmam-Bennani, Birgit Lohmann, Jens Rasch, Colm T Whelan, and H R James Walters. ($e, 2e$) ionization of the 2p orbital of argon. *J. Phys. B*, 32(1):L5, 1999.

- [15] F. K. Miller, H. R. J. Walters, and Colm T. Whelan. Energy-sharing ($e, 2e$) collisions: Ionization of the inert gases in the perpendicular plane. *Phys. Rev. A*, 91:012706, Jan 2015.
- [16] Xueguang Ren, Arne Senftleben, Thomas Pflüger, Joachim Ullrich, Klaus Bartschat, and Alexander Dorn. Erratum: Benchmark experiment for electron-impact ionization of argon: Absolute triple-differential cross sections via three-dimensional electron emission images [phys. rev. a **83**, 052714 (2011)]. *Phys. Rev. A*, 89:029904, Feb 2014.
- [17] X. Ren, T. Pflüger, J. Ullrich, O. Zatsarinny, K. Bartschat, D. H. Madison, and A. Dorn. Erratum: Low-energy electron-impact ionization of argon: Three-dimensional cross section [phys. rev. a 85, 032702 (2012)]. *Phys. Rev. A*, 92:019901, Jul 2015.
- [18] K Bartschat and P G Burke. The r-matrix method for electron impact ionisation. *J. Phys. B*, 20(13):3191, 1987.
- [19] Klaus Bartschat and Oleg Vorov. Channel-coupling, target-structure, and second-order effects in electron-impact ionization of Ar($3p$) and Ar($3s$). *Phys. Rev. A*, 72:022728, Aug 2005.
- [20] Matthew A. Haynes and Birgit Lohmann. Comparative study of argon $3p$ electron-impact ionization at low energies. *Phys. Rev. A*, 64:044701, Sep 2001.
- [21] M. A. Stevenson and B. Lohmann. Fully differential cross-section measurements for electron-impact ionization of argon over the complete in-plane angular range. *Phys. Rev. A*, 77:032708, Mar 2008.
- [22] L R Hargreaves, M A Stevenson, and B Lohmann. Absolute triple-differential cross sections for intermediate energy electron impact ionization of neon and argon. *J. Phys. B*, 43(20):205202, 2010.

- [23] Sadek Amami, Melike Ulu, Zehra Nur Ozer, Murat Yavuz, Suay Kazgoz, Mevlut Dogan, Oleg Zatsarinny, Klaus Bartschat, and Don Madison. Theoretical and experimental investigation of $(e, 2e)$ ionization of argon $3p$ in asymmetric kinematics at intermediate energy. *Phys. Rev. A*, 90:012704, Jul 2014.
- [24] A J Murray, N J Bowring, and F H Read. Comparison of argon and helium $(e, 2e)$ differential cross sections at 64.6 eV using symmetric detection energies and angles. *J. Phys. B*, 33(15):2859, 2000.
- [25] Kate L Nixon, Andrew James Murray, and Christian Kaiser. Low energy $(e, 2e)$ studies of the noble gases in the perpendicular plane. *J. Phys. B*, 43(8):085202, 2010.
- [26] Xueguang Ren, Thomas Pflüger, Marvin Weyland, Woon Yoon Baek, Hans Rabus, Joachim Ullrich, and Alexander Dorn. *J. Chem. Phys.*, 141:134314, 2014.
- [27] Xueguang Ren, Elias Jabbour Al Maalouf, Alexander Dorn, and Stephan Denifl. Direct evidence of two interatomic relaxation mechanisms in argon dimers ionized by electron impact. *Nat Commun*, 7:11093, Mar 2016.
- [28] Oleg Zatsarinny and Klaus Bartschat. Nonperturbative treatment of electron-impact ionization of $\text{Ar}(3p)$. *Phys. Rev. A*, 85:032708, Mar 2012.
- [29] Oleg Zatsarinny and Klaus Bartschat. The b-spline r-matrix method for atomic processes: application to atomic structure, electron collisions and photoionization. *J. Phys. B*, 46(11):112001, 2013.
- [30] O Zatsarinny. Bsr: B-spline atomic r-matrix codes. *Comp. Phys. Commun.*, 174:273–356, FEB 15 2006.
- [31] P. G. Burke. *R-Matrix Theory of Atomic Collisions*. Springer-Verlag New York, 2011.

- [32] K Bartschat, E T Hudson, M P Scott, P G Burke, and V M Burke. Electron - atom scattering at low and intermediate energies using a pseudo-state/ r -matrix basis. *J. Phys. B*, 29(1):115, 1996.
- [33] I. Bray, D.V. Fursa, A.S. Kadyrov, A.T. Stelbovics, A.S. Kheifets, and A.M. Mukhamedzhanov. Electron- and photon-impact atomic ionisation. *Phys. Rep.*, 520(3):135 – 174, 2012.
- [34] O. Zatsarinny and K. Bartschat. *Phys. Rev. Lett.*, 107:023203, 2011.
- [35] Igor Bray and Dmitry V. Fursa. Calculation of ionization within the close-coupling formalism. *Physical Review A*, 54:2991–3004, Oct 1996.
- [36] Oleg Zatsarinny and Charlotte Froese Fischer. Atomic structure calculations using mchf and bsr. *Comp. Phys. Commun.*, 180:2041–2065, NOV 2009.

V. THEORETICAL AND EXPERIMENTAL (e,2e) STUDY OF ELECTRON-IMPACT IONIZATION OF LASER-ALIGNED Mg ATOMS

Sadek Amami¹, Andrew Murray,^{r2}Al Stauffer,³Kate Nixon,²Gregory Armstrong,⁴James Colgan,⁴ and Don Madison¹

¹Department of Physics,
Missouri University of Science and Technology,
Rolla, Missouri, USA

²Photon Science Institute, School of Physics and Astronomy,
University of Manchester,
Manchester M13 9PL, United Kingdom

³Department of Physics and Astronomy,
York University,
Toronto, Ontario, Canada M3J 1P3

⁴Theoretical Division, Los Alamos National Laboratory,
Los Alamos, New Mexico 87545, USA

ABSTRACT

We have performed calculations of the fully differential cross sections for electron-impact ionization of magnesium atoms. Three theoretical approximations, the time-dependent close coupling, the three-body distorted wave, and the distorted wave Born approximation, are compared with experiment in this article. Results will be shown for ionization of the 3s ground state of Mg for both asymmetric and symmetric coplanar geometries. Results will also be shown for ionization of the 3p state which has been excited by a linearly polarized laser which produces a charge cloud aligned perpendicular to the laser

beam direction and parallel to the linear polarization. Theoretical and experimental results will be compared for several different alignment angles, both in the scattering plane as well as in the plane perpendicular to the incident beam direction. made within the model.

1. INTRODUCTION

One of the recent significant advances in the field of electron-impact ionization of molecules, or ($e, 2e$), has been the development of the capability to measure ionization of aligned molecules [1, 2, 3, 4, 5] which provides a more sensitive test of theory than measurements which average over all molecular alignments [6, 7, 8, 9, 10]. On the atomic level, the equivalent measurement would be ionization of atoms that have been excited by a linearly polarized laser which produces a charge cloud aligned with the polarization axis of the laser beam. Nixon and Murray [11, 12] have performed such a measurement for laser-aligned Mg, and the purpose of this work is to see how well our theoretical calculations compare with the measurements. Measurements were made for ionization of both the ground 3s state as well as the laser-aligned 3p state, and all measurements were symmetric for final-state energies (i.e., $E_1 = E_2$). For the 3s state, both symmetric and asymmetric angles were examined while for the 3p state only asymmetric angular geometries were measured. For the aligned 3p state, two different measurements were performed—atomic alignment in the perpendicular plane (the plane perpendicular to the beam direction and perpendicular to the scattering plane) [11] and atomic alignment in the scattering plane [12]. In total, nine different angular distributions were measured for nine different alignment directions. However, Stauffer [13] showed that all of these nine different angular distributions (or as many more as you want) can be obtained from the $m = (0,1)$ amplitudes calculated relative to the incident beam direction.

2. THEORETICAL FRAMEWORK

We have used both the perturbative three-body distorted wave (*3DW*) approach and the nonperturbative time-dependent close coupling (*TDCC*) approach to describe the process of interest. Each of them has been described previously. Hence we will only summarize them briefly to the extent necessary for the present discussion, with references where interested readers can find more information.

2.1. TDCC. The *TDCC* calculations presented here have been discussed in detail previously [14]. The *TDCC* method centers around the propagation of a two-electron wave function that accounts for the interaction between the incoming electron and the ionized electron of the target. The interaction of this two-electron wave function with the remaining electrons is included through direct and local exchange potentials. The calculations presented here for electron-impact ionization of ground-state $Mg(3s^2)$ were found to require a large number of coupled channels to converge, and required inclusion of partial waves from $L = 0$ to 12. *TDCC* calculations for two active electrons are also possible for ionization of excited-state $Mg(3s3p)$. However, such calculations only describe the initial state as a $(3s3p)$ configuration, whereas the measurements of interest [11, 12] probe ionization from the $3s3p^1P$ term. Within a three-electron *TDCC* approach [15], one may construct a three-electron wave function that properly accounts for the spin symmetry of the initial $3s3p^1P$ term. However, such calculations are very computationally demanding and are difficult to run to convergence, and so will not be presented here.

2.2. 3DW. The three-body distorted wave (*3DW*) approach has been fully described in previous works [16, 17]. As usual, we evaluate both the direct and exchange amplitudes. For the case of the laser-aligned $3p$ state, the T matrix will depend on the orientation of the initial-state wave function $\Phi_i(\hat{\mathbf{p}})$ where $\hat{\mathbf{p}}$ is a unit vector pointing in the direction of the orientation. The direct T – *matrix* can be written as

$$T_{fi}^{dir}(\hat{\mathbf{p}}) = \langle \Phi_f | W | \Phi_i(\hat{\mathbf{p}}) \rangle. \quad (1)$$

where Φ_i and Φ_f are the initial- and final-state wave functions, respectively, and W is the perturbation. In the 3DW approximation, the initial-state wave function Φ_i is approximated as a product of the initial bound state of the atom $|\Psi_A(\hat{\mathbf{p}})\rangle$ times a distorted wave function χ_i for the incoming electron (the projectile),

$$\Phi_i(\hat{\mathbf{p}}) = \Psi_A(\hat{\mathbf{p}})\chi_i \quad (2)$$

We use numerical Hartree-Fock wave functions for the ground-state 3s orbital and the excited-state 3p orbital. The perturbation (W) is given by

$$W = V - U_i. \quad (3)$$

Here V is the interaction between the incident electron and the atom, and U_i is the initial-state spherically symmetric static approximation for V , which is asymptotically equal to zero.

The final-state wave function Φ_f is approximated as a product of two final-state continuum-electron distorted waves (χ_{scat} and χ_{eject}), and the Coulomb interaction between the outgoing electrons ($C_{ele-ele}$), normally called the postcollision interaction (PCI),

$$\Phi_f = \chi_{scat} \chi_{eject} C_{ele-ele} \quad (4)$$

We use the exact postcollision Coulomb interaction between the two electrons ($C_{ele-ele}$), which is equal to a Gamow factor times a hypergeometric function,

$$C_{ele-ele} = e^{\frac{-\pi\gamma}{2}} \Gamma(1 - i\gamma) {}_1F_1(i\gamma, 1, -i(k_{ab}r_{ab} + \mathbf{k}_{ab} \cdot \mathbf{r}_{ab})), \quad (5)$$

Here ${}_1F_1$ is a confluent hypergeometric function, $\Gamma(1 - i\gamma)$ is the gamma function, $\mathbf{k}_{ab} = \mu \mathbf{v}_{ab}$, $\mu = \frac{1}{2}$ is the reduced mass for two electrons, \mathbf{v}_{ab} is the relative velocity between the two electrons, and γ is the Sommerfeld parameter $\gamma = \frac{1}{v_{ab}}$ which is a measure

of the strength of the Coulomb interaction between the two electrons. We would note that the 3DW approximation contains much more physics than other elementary first-order approximations such as the FBA (first Born approximation) because any “physics” contained in the initial- and final-state wave functions is automatically contained to all orders of perturbation theory. The 3DW has been remarkably successful in predicting low-energy cross sections for electron-molecule scattering recently, and we believe that the primary reason for this is the Coulomb distortion factor of Equation (5) included in the final-state wave function. By including the Coulomb electron-electron repulsion in the final state, we are including this physics to all orders of perturbation theory. The SBA (second Born approximation), on the other hand, would just contain this effect to second order which might not be sufficient. Likewise, the distorted waves contain the interaction of the incoming projectile electron with the nucleus as well as the interaction with a spherically symmetric charge-cloud distribution to all orders, which is not contained at all in the FBA. With these approximations, the 3DW direct T matrix becomes

$$T_{fi}^{dir}(\hat{\mathbf{p}}) = \langle \chi_{scat} \chi_{eject} C_{ele-ele} | V - U_i | \Psi_A(\hat{\mathbf{p}}) \chi_i \rangle \quad (6)$$

We are treating this problem as a three-body problem (one active electron in the target) so Equation (6) is a six-dimensional (6D) integral which we evaluate numerically. The exchange T matrix $T_{fi}^{exe}(\hat{\mathbf{p}})$ is similar to Equation (6) except that the two final-state electrons are interchanged in the final-state wave function Φ_f . Finally, the triple differential cross section (TDCS) for a fixed orientation (\hat{p}) can be written in atomic units as

$$\frac{d^3\sigma}{d\Omega_f d\Omega_e dE_e}(\hat{\mathbf{p}}) = \frac{1}{(2\pi)^5} \frac{k_f k_e}{k_i} (|T_{fi}^{dir}(\hat{\mathbf{p}})|^2 + |T_{fi}^{exc}(\hat{\mathbf{p}})|^2 + |T_{fi}^{dir}(\hat{\mathbf{p}}) - T_{fi}^{exc}(\hat{\mathbf{p}})|^2). \quad (7)$$

Following Stauffer [13], the orientated wave functions $\Psi_A(\hat{\mathbf{p}})$ can be obtained by rotating the wave functions quantized with the z axis parallel to the incident beam direction. We first assume that the m -dependent wave function in the beam direction reference frame

can be written as $R_{nL}(r) Y_{Lm}(\hat{\mathbf{r}})$ where $R_{nL}(r)$ is the radial part and $Y_{Lm}(\hat{\mathbf{r}})$ is the angular part. The charge cloud aligned by the laser beam will be an $m = 0$ state orientated parallel to the linear polarization. Let us start with the second measurement [12]. For this case, the atom is orientated in various directions in the scattering plane. The coordinate system we use has the z axis parallel to the beam direction, the scattering plane is the xz plane, and the y axis is perpendicular to the scattering plane. Consequently, rotating the quantization axis to various directions in the scattering plane can be accomplished by rotating an angle β about the y axis. Using the rotation matrices from Rose [18] [Equation (4.28a), p. 60], the rotated wave function in the scattering plane (SP) can be written as

$$\begin{aligned}\Psi_A(SP) &= \frac{\sin(\beta)}{\sqrt{2}} R_{3p}(r)[-Y_{11}(\hat{\mathbf{r}}) + Y_{1-1}(\hat{\mathbf{r}})] + \cos(\beta) R_{3p}(r) Y_{10}(\hat{\mathbf{r}}) \\ &= R_{3p}(r) \sqrt{\frac{3}{4\pi}} [\sin(\beta) \sin(\theta) \cos(\phi) + \cos(\beta) \cos(\theta)]\end{aligned}\quad (8)$$

where (θ, ϕ) are the spherical angles in the beam direction reference frame. For the first measurement [11], three different orientations were measured-orientated along the x axis, the y axis, and at 45° between the x and y axes. The wave function for the x axis can be determined from equation (8) by setting $\beta = 90^\circ$. For the other two cases, one must use at least two Euler angles. There are different sets of Euler angles that can be used, but the easiest set for the y axis is $(\alpha, \beta, \gamma) = (90, 90, 0)$. For this combination, the rotated wave function is given by

$$\begin{aligned}\Psi_A(y) &= R_{3p}(r) \frac{i}{\sqrt{2}} (Y_{11} + Y_{1-1}) \\ &= R_{3p}(r) \sqrt{\frac{3}{4\pi}} \sin(\theta) \sin(\phi)\end{aligned}\quad (9)$$

Finally, for an orientation at 45° between the x and y axes, the Euler angles are $(\alpha, \beta, \gamma) = (45, 90, 0)$ and the rotated wave function is given by

$$\begin{aligned}\Psi_A(xy) &= R_{3p}(r) \frac{1}{2} [(-Y_{11} + Y_{1-1}) + i(Y_{11} + Y_{1-1})] \\ &= R_{3p}(r) \sqrt{\frac{3}{8\pi}} \sin(\theta) [\cos(\phi) + \sin(\phi)]\end{aligned}\quad (10)$$

Consequently, one way to calculate the results for different orientations is to use equations (8,9,10) to calculate the orientated wave function, and use this orientated wave function in the direct and exchange T matrices. Alternatively, one could simply use T matrices calculated in the initial beam reference frame. For example, the spherical harmonics in Equation (8) are expressed in the coordinate system with the z axis along the beam direction. Consequently, with substitution of the wave function (top line) of Equation (2) into the T matrix, we obtain

$$T_{fi}(SP) = \frac{\sin(\beta)}{\sqrt{2}} [-\Upsilon_1 + \Upsilon_{-1}] + \cos(\beta) \Upsilon_0. \quad (11)$$

where Υ_m is the T matrix for a coordinate system with the z axis parallel to the beam direction. This is Equation (4) of Stauffer [13] for the case $\varepsilon = -\beta$ (to compare with experiment, we will use $-\beta$ in the calculations). It is well known that, for this atomic system, $\Upsilon_1 = -\Upsilon_{-1}$ from symmetry so that

$$T_{fi}(SP) = -\sqrt{2} \sin(\beta) \Upsilon_1 + \cos(\beta) \Upsilon_0. \quad (12)$$

For the x -axis orientation we have Equation (12) with $\beta = 90^\circ$,

$$T_{fi}(x) = -\sqrt{2} \Upsilon_1. \quad (13)$$

For the y -axis, Equation (9) yields

$$T_{fi}(y) = \frac{i}{\sqrt{2}} (\Upsilon_1 + \Upsilon_{-1}) \quad (14)$$

Now, symmetry about the scattering plane ($\Upsilon - 1 = -\Upsilon_1$) reduces this expression to

$$T_{fi}(y) = 0 \quad (15)$$

And finally for the xy orientation, Equation (10) gives us

$$T_{fi}(xy) = \frac{1}{2}[(-1 + i)\Upsilon_1 + (1 + i)\Upsilon_{-1}] = -\Upsilon_1 \quad (16)$$

Consequently, for orientations in the perpendicular plane, we conclude that the cross sections for the y -axis orientation should be zero and the x -axis orientation should have cross sections twice as large as those for the xy orientation, since the cross sections are proportional to the absolute value of the T matrix squared. From Equations (12), (13), (15), and (16), we see that the cross sections for any orientation can be calculated from the Υ_0 and Υ_1 amplitudes as was pointed out by Stauffer [13]. More explicitly, we have both direct and exchange amplitudes so we use equations (12), (13), and (16) for both the direct and exchange T -matrices. Consequently, for the scattering plane (SP), we would have:

$$T_{fi}^{dir}(SP) = -\sqrt{2} \sin(\beta) \Upsilon_1^{dir} + \cos(\beta) \Upsilon_0^{dir} \quad (17)$$

$$T_{fi}^{exc}(SP) = -\sqrt{2} \sin(\beta) \Upsilon_1^{exc} + \cos(\beta) \Upsilon_0^{exc} \quad (18)$$

Then, use equation 7 to calculate cross sections. Typically the exchange amplitude is ignored, which is the case considered by Equation (5) of Stauffer [13]. Since Equation (17) and Equation (18) have the same form of dependence on the orientation angle β , a linear combination of these amplitudes will also have this form. Moreover, a linear combination of the squared moduli of these amplitudes as in Equation (7) will have the same dependence on the orientation angle as given in Equation (5) of [13]. We have verified that we obtain

the same cross sections using the wave function of Equation (8) to calculate the T matrix for the rotated wave function and the amplitudes of Equation. Equation (17) and Equation (18) calculated in the nonrotated reference frame.

3. RESULTS AND DISCUSSION

Triple differential cross sections (*TDCSs*) for ionization of the (*3s*) ground state are presented in Figure 1 for equal final-state energies and asymmetric angles. The figure contains a comparison of *3DW*, distorted wave Born approximation (*DWBA*), and *TDCC* results with the measurements of Nixon and Murray [11]. *DWBA* results are calculated in the same manner as the *3DW* except that the Coulomb interaction factor ($C_{ele-ele}$) in Equation (4) is set equal to unity. Consequently the *3DW* results have the postcollision interaction (*PCI*) contained to all orders of perturbation theory, while the *DWBA* contains this interaction only to first order. Since the experiments are not absolute, all the theories and the experimental data are normalized to unity at the binary peak. It is seen that the *3DW* results are in excellent agreement with the measurements for an initial *3s* state. Both the *DWBA* and *TDCC* predict binary peaks shifted to smaller angles and these calculations display a similar trend over the full range of electron ejection angles.

Figure 2 shows *3DW*, *DWBA*, and *TDCC* results compared with experiment for *Mg(3s)* coplanar symmetric angles and energies. The different panels are for different final-state electron energies starting from 10 eV at the top to 25 eV at the bottom. In general, all three theories are in reasonably good agreement with the experimental data. For most of the cases, it can be seen that the *3DW* exhibits a little better agreement with experimental data than the other two theories. Both the *DWBA* and *TDCC* are becoming in better agreement as the outgoing electrons energy increases from 10 to 25 eV. In Figure 3, we present triple differential cross sections for magnesium atoms laser aligned in a plane perpendicular to the incident electron beam and parallel to the linear polarization. We use a coordinate system for which the incident beam direction is the *z* axis, the scattering plane is

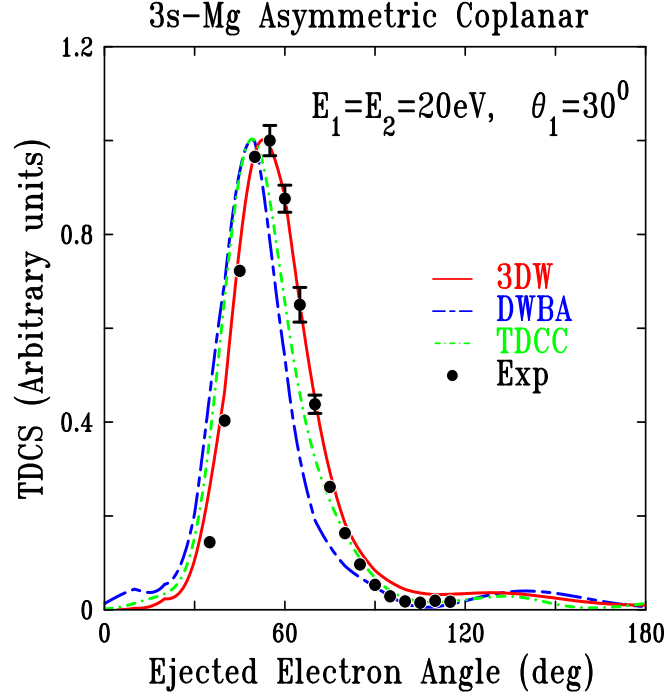


Figure 1. Experimental and theoretical TDCS for electron-impact ionization of the 3s state of Mg. The projectile scattering angle θ_1 is 30° and both outgoing electrons have the same energy ($E_1 = E_2 = 20$ eV). The theoretical calculations are 3DW: solid red; DWBA: dashed blue; and TDCC: dash-dot green. The experimental data are the solid circles. See text for normalization of theories and experiment.

the xz plane, and the xy plane is the plane perpendicular to the incident beam. For all these measurements, the incident projectile electron had an energy of 43.31 eV, the scattered and ejected electrons had equal energies ($E_1 = E_2 = 20$ eV), one of the final-state electrons was detected at a fixed scattering angle of 30° , and the other final-state electron was detected at angles ranging between 35° and 120° . The upper panel corresponds to an alignment parallel to the x axis, the middle panel corresponds to an alignment at 45° between the x and y axes, and the lower panel is for ionization of the $3p$ state that has been laser aligned parallel to the y axis (perpendicular to the incident beam and perpendicular to the scattering plane). We have normalized the experiment and 3DW to unity at the maximum cross section for the x axes (upper panel). We use the same normalization factor for the DWBA as the 3DW. The experimental data for the excited states are relatively absolute (i.e., they

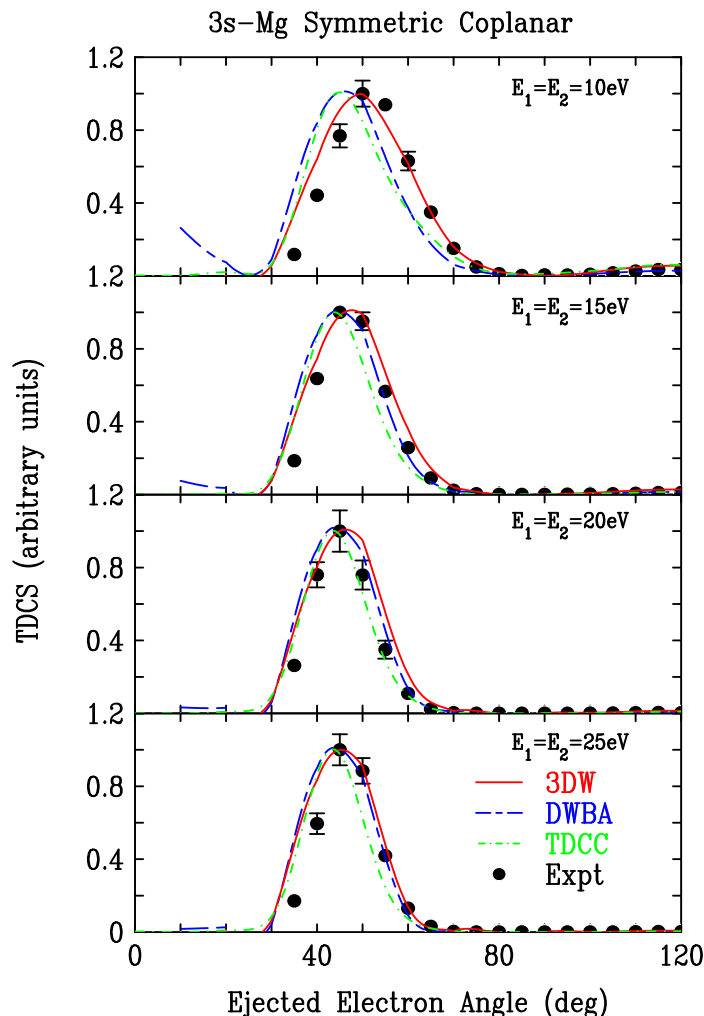


Figure 2. Experimental and theoretical TDCS for electron-impact ionization of the 3s state of Mg for symmetric coplanar geometry. The energies for outgoing electrons are equal and vary for the four panels ranging from 10 to 25 eV. The theoretical calculations are 3DW: solid red; DWBA: dashed blue; and TDCC: dash-dot green. The experimental data are the solid circles. See text for normalization of theories and experiment.

have been internormalized by measuring the cross sections at $\theta_2 = 50^\circ$ for the various laser orientations), so the same normalization is used for Figures 3–5. In the upper panel, it is seen that the 3DW predicts the proper shape of the cross section but the experimental peak is shifted to lower angles. The DWBA has the wrong shape with three peaks instead of one. The fact that the 3DW has the correct shape while the DWBA does not indicates that the Coulomb interaction between the two electrons (PCI) plays a major role in this collision.

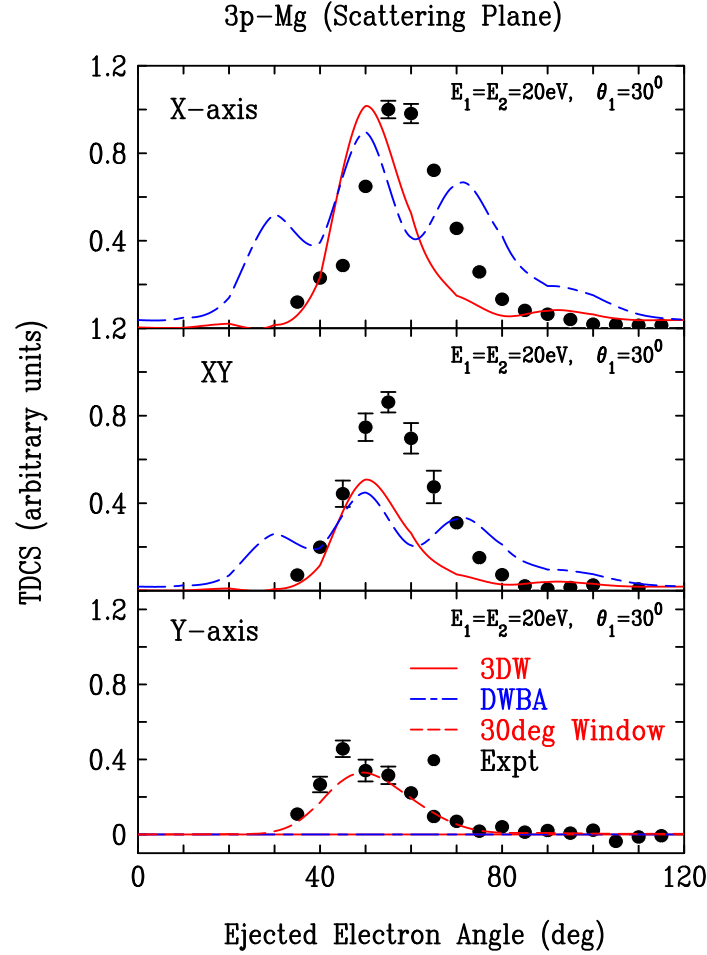


Figure 3. Experimental and theoretical TDCS for electron-impact ionization of the laser-aligned 3p state of Mg. The projectile scattering angle θ_1 is 30° and both outgoing electrons have the same energy ($E_1 = E_2 = 20$ eV). The three panels are for laser alignment parallel to the x axis (see text), laser alignment at 45° between the x and y axes, and laser alignment parallel to the y axis, respectively. In the bottom panel, the 3DW and DWBA results are exactly zero. The theoretical calculations are 3DW: solid red; DWBA: dash-dot blue; and (30° window) dashed red are the 3DW results convoluted over an angular uncertainty of $\pm 30^\circ$. The experimental data are the solid circles. See text for normalization of theories and experiment.

Looking at the middle panel (alignment at 45° between the x and y axes), the DWBA and 3DW results are exactly half the results in the upper panel, as was expected from Equation (13) and (16). However, the results shown in the figure were obtained using the orientated wave functions of Equations (8) and (10). Obviously, the experimental data are not in accord with the symmetry prediction. Experimental results for ionization of a 3p state that

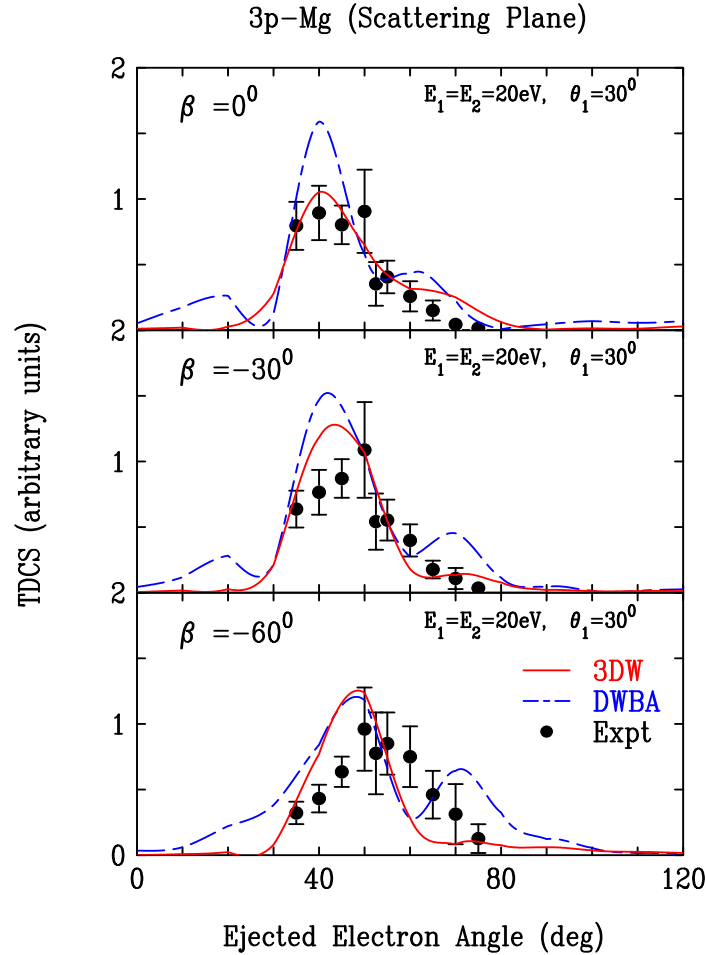


Figure 4. Experimental and theoretical TDCS for electron-impact ionization of the laser-aligned $3p$ state of Mg . The projectile scattering angle is θ_1 is 30° and both outgoing electrons have the same energy ($E_1 = E_2 = 20$ eV). The three panels are for laser alignment in the scattering plane by different orientation angles “beta” relative to the incident beam direction. The theoretical calculations are 3DW: solid red; DWBA: dash-dot blue; the experimental data are the solid circles. See text for normalization of theories and experiment.

has been laser aligned parallel to the y axis are shown in the lower panel in Figure 3. For this case the 3DW and DWBA numerical results were exactly zero using the orientated wave function of Equation (9) for all ejected electron angles in accordance with the prediction of Equation (15). Since the experiment finds significant nonzero results for this orientation, we thought that the problem might be with angular resolution of the experiment. The experimental acceptance angular range is $\pm 3^\circ$ so we convoluted our theoretical results

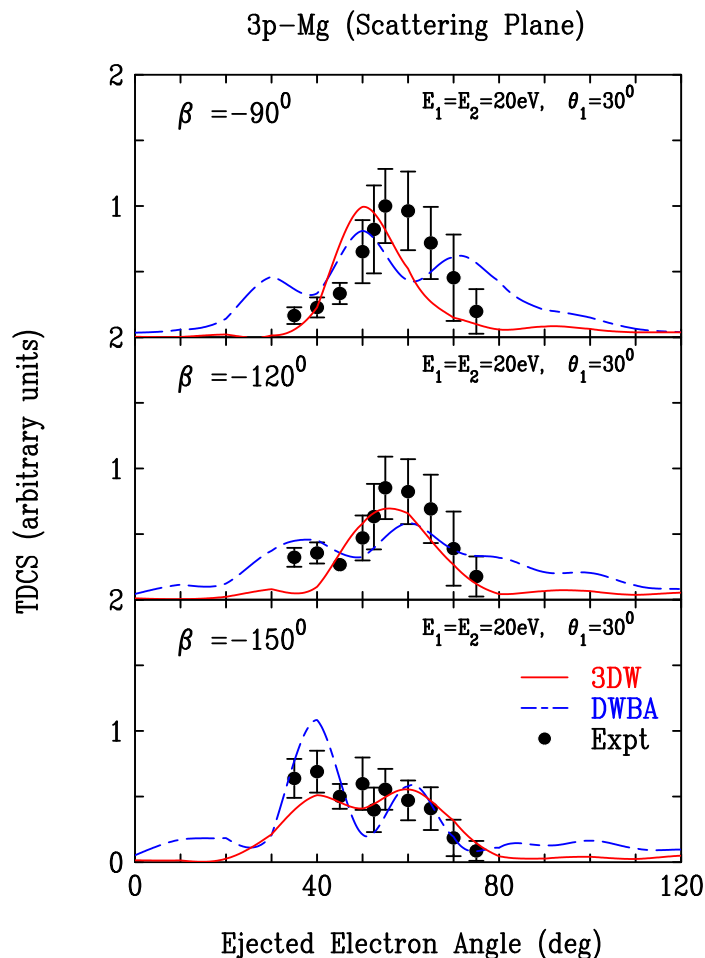


Figure 5. Same as in Figure 4

over this angular range. While we then found a small nonzero cross section, it was still much smaller than experiment. As an interesting exercise, we tried making the acceptance window wider and found that $\pm 30^\circ$ yielded excellent agreement with experiment (dashed red in bottom panel). Obviously this is much larger than the experiment measures, and we show the results for academic interest only. In Figures 4 and 5, we show results for ionization of a $3p$ state that has been laser aligned to different orientation angles β ranging from 0° to -150° in the scattering plane (0° means the incident beam direction, and a negative angle means clockwise rotation). Figure 4 shows results for three different β (0° , -30° , and -60°). The 3DW results are in reasonably good agreement with the experimental data for

most cases. However, the peak in the experimental data shifts a few degrees to the right as the orientation angle (β) increases (see Figure 4). However, overall the 3DW shows much better agreement with experimental data than the DWBA, which has a three-peak structure not seen in the data.

Figure 5 shows the comparison between theory and experiment for the same kinematics as Figure 4 but for higher orientation angles (-90° , -120° , and -150°). Although the upper panel for $\beta = 90^\circ$ corresponds to the x axis results for Figure 3, this is a different data set taken at a different time.

As mentioned earlier, this is the case we used for normalizing both the theory and experiment. Comparing the x -axis results for Figures 3 and 5, it is seen that the experimental data are in agreement with each other, and the comparison with theory looks the same in both cases. In both the middle and the lower panel, the 3DW still predicts most of the experimental data with the location of the experimental peak becoming closer to the data as well. Interestingly, the DWBA showed much better agreement with the experimental data in the middle panel as well as the lower one.

4. ANALYSIS OF THE EXPERIMENTAL DATA

4.1. Effects of Depolarization on the Experimental Data. The large difference found between theory and experiment when the electron charge-cloud alignment is positioned out of the scattering plane requires further consideration. This discrepancy is particularly significant when the state is aligned orthogonal to the plane, since as shown here the calculations predict a zero in the ionization cross section due to symmetry, which the experiments do not find. Indeed as is shown earlier in this paper, for theory to emulate the data under these conditions, the acceptance angles of the electron analyzers would need to be ~ 10 times larger than they are. It is therefore sensible to investigate whether other experimental artifacts may be playing a role in this discrepancy. One difference between experiment and theory is that the calculation assumes the P state is a pure 3^1P_1 state that

is fully aligned orthogonal to the scattering plane by the laser beam. In practice this is not possible, since the laser will have a small elliptically polarized component, with the major axis of this ellipse being orthogonal to the plane. In this case the atoms will be excited with a small state amplitude in the scattering plane that depends upon the degree of ellipticity, due to the electric field component of the light that lies along the minor axis of the ellipse. A second effect that may play a role is that of radiation trapping in the interaction region. Radiation trapping can occur when the incident laser radiation couples to atoms in the ground state [19], as in the experiments described here. In this case, radiation emitted from a laser-excited atom that decays back to the ground state may be reabsorbed by a second atom that is in the ground state. This second excited atom will then spontaneously emit a photon, whose direction and polarization are uncorrelated with the laser field. Further absorption and reemission processes may then occur, so that the radiation is effectively “trapped” inside the interaction region for several decay cycles. The probability of this occurring depends upon the density of atoms in the interaction region, the trapping cycle leading to an overall depolarization of the light emitted from the ensemble. If the trapping process is significant, this would also produce a relative population of excited atoms whose alignment is in the scattering plane. To establish the degree of importance of these processes, measurements were made of the fluorescence emitted from the atomic ensemble using a silicon carbide photodiode that was sensitive to the emitted light at a wavelength of ~ 285 nm. The radiation was collected using a 50-mm-diameter fused silica lens that imaged the interaction region onto the photodiode.

The axis of detection was orthogonal to the incident laser and electron beams, and was in the scattering plane [11, 12]. The normal way to determine the significance of the effects discussed above is to measure the polarization of fluorescence from a pure state (such as the 3^1P_1 state in *Mg* used here), since this should be $\sim 100\%$ for a fully aligned atom with no trapping in the interaction region. This technique was not possible in the current experiments, as efficient linear dichroic polarizers do not exist for radiation at 285 nm. The

polarizer that set the laser polarization was a Barium Borate (BBO) Glan-laser polarizer that does have high efficiency at this wavelength; however, this type of polarizer cannot be used when detecting fluorescence. In the experiments [11, 12] the angle of the incident laser polarization vector was adjusted using a zero-order half-wave plate that was positioned in the beam path after the BBO polarizer, and it is this that could introduce a small ellipticity to the incident laser beam. To establish if the effects of trapping and/or polarization change were significant, the angle of polarization of the incoming laser was varied, and the change in intensity on the photodiode was monitored. For a laser polarization vector orthogonal to the direction of detection, a maximum intensity is expected (since observations are side-on to the excited P state). When the polarization vector points in the direction of detection, a minimum in the fluorescence should then occur (all radiation from a pure state then being emitted in other directions). For a fully aligned P state the minimum intensity I_{\perp} should hence be very close to zero. In this case a fluorescence polarization can be defined, and for a pure P state this is given by

$$P_1^{Fluor} = \frac{I_{\parallel} - I_{\perp}}{I_{\parallel} + I_{\perp}} \sim 1 \quad (19)$$

If $P_1^{Fluor} < 1$ this is evidence of either radiation trapping or that the incoming laser beam is elliptically polarized (it is not possible to distinguish between these different processes from this parameter). Measurements in the experiments using this technique produced a fluorescence polarization $P_1^{Fluor} = 0.95 \pm 0.03$, as shown in Figure 6. Although this is close to unity, it does indicate a small effect may be occurring due to radiation trapping, or due to a slight elliptical polarization of the laser beam. There will also be a small contribution due to the finite acceptance angle of the collecting lens, which also reduces the polarization. In the present discussion the effects of the collecting lens are ignored, allowing an upper bound to be placed on the relative population of excited targets aligned in the scattering plane due to trapping or ellipticity of the laser beam.

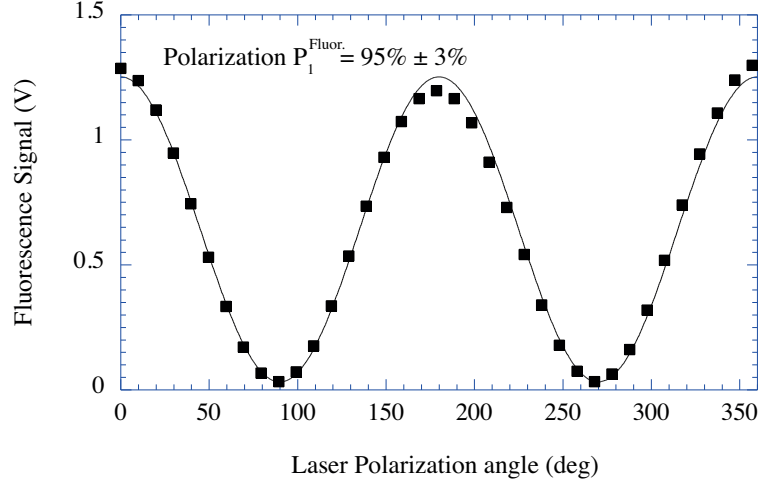


Figure 6. Variation of the measured fluorescence signal as a function of the polarization angle of the laser beam.

4.2. In-Plane Excited-State Population Estimates due to Radiation Trapping.

If the depolarization shown in Figure 6 is all due to radiation trapping, an estimate of the relative population of excited targets in the scattering plane can be made. Due to the random nature of the spontaneous emission process, the trapped radiation can be considered as having equal intensity I^{Tr} in all directions. In this case the fluorescence polarization due to radiation trapping will be given by

$$P_1^{RT} = 0.95 = \frac{(I_{\parallel}^{NT} + I^{Tr}) - I^{Tr}}{(I_{\parallel}^{NT} + I^{Tr}) + I^{Tr}} = \frac{I_{\parallel}^{NT}}{I_{\parallel}^{NT} + 2I^{Tr}} \Rightarrow I_{\parallel}^{NT} = 38I^{Tr} \quad (20)$$

where I_{\parallel}^{NT} is the intensity with no radiation trapping present. Hence $\sim 2.6\%$ of the light is emitted in each orthogonal direction due to radiation trapping. As one of these directions is not observed in the experiment (that is, where the emitting dipoles lie in the scattering plane, and point along the direction of observation), there are then two contributions that can produce excited atoms in the scattering plane, and so at most $\sim 5.2\%$ of the atoms will be aligned in this plane. From these experimental data, radiation trapping can hence only make a small contribution to the measured ionization cross section.

4.3. In-Plane Excited-State Population due to Residual Ellipticity of the Laser Beam Polarization. The second process that can lead to $P_1^{Fluor} < 1$ is due to the incident laser beam being *elliptically* polarized rather than linearly polarized, as noted above. In this case the excited target is once again a pure 3^1P_1 state; however, the transition from the ground 3^1S_0 state will no longer obey the selection rule $\Delta m_j = 0$ for a quantization axis chosen along the direction of the polarization vector. Under these conditions it is sensible to adopt a quantization axis along the laser beam direction [20]. In this configuration linearly polarized radiation excites both $|J, m_j\rangle = |1, \pm 1\rangle$ states with equal amplitude, the normalized wave function then being represented as

$$|\psi\rangle^{3^1P_1} = a_{+1} |1, +1\rangle + a_{-1} |1, -1\rangle = \frac{1}{\sqrt{2}} \left(e^{i\varepsilon} |1, +1\rangle + e^{-i\varepsilon} |1, -1\rangle \right) \quad (21)$$

where ε is a phase angle that defines the direction of polarization. A similar approach can also be formulated to describe an atom excited by elliptically polarized radiation. In this case the substate amplitudes $a_{\pm 1}$ will be unequal in magnitude, and the phase angle ε then defines the direction of the major axis of the charge cloud. It is easiest to adopt a density matrix formalism to describe the resulting P state, since the density matrix in this frame ρ^{Las} can then be rotated into the reference frame of the detector [20]. The relative fluorescence ratio $I_{||}/I_{\perp}$ can then be calculated by an appropriate choice of rotation operators acting on ρ^{Las} . For a fluorescence polarization P_1^{Fluor} as measured above, the density matrix ρ^{Las} for elliptically polarized excitation is then calculated to be

$$\rho_{ij}^{Las} = \frac{1}{2} \begin{bmatrix} 1 \pm \sqrt{1 - (P_1^{Fluor})^2} & 0 & -P_1^{Fluor} \exp(-2i\varepsilon) \\ 0 & 0 & 0 \\ -P_1^{Fluor} \exp(+2i\varepsilon) & 0 & 1 \mp \sqrt{1 - (P_1^{Fluor})^2} \end{bmatrix} \quad (22)$$

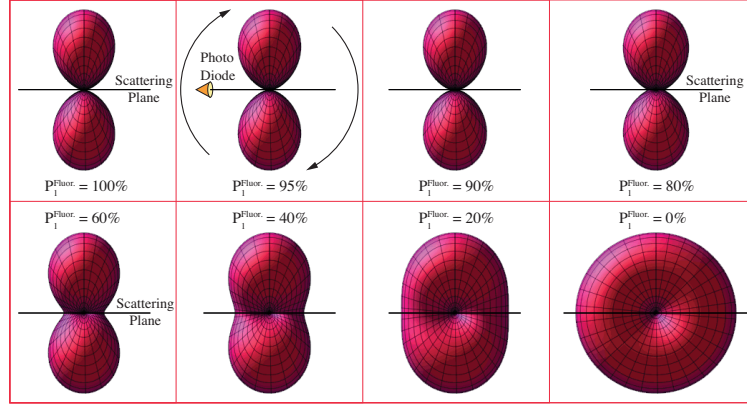


Figure 7. Examples of the angular shape of the pure P-state charge cloud excited by elliptically polarized laser radiation that produces different values of the fluorescence polarization. The arrows show how the state is rotated with respect to the detector so as to measure P_1^{Fluor}

where ε defines the direction of the major axis of the charge cloud with respect to the scattering plane, and the sign of the terms in ρ_{11} and ρ_{1-1} are set by the handedness of the radiation. Under the conditions for a charge cloud that has a major axis orthogonal to the scattering plane, the relative population of atoms in the scattering plane is found to be directly related to I_{\parallel}/I_{\perp} . Hence for $P_1^{Fluor} = 0.95$, the major axis of the charge cloud orthogonal to the scattering plane is ~ 39 times larger than the minor axis that lies in the plane. Figure 7 shows examples of the charge-cloud angular “shape” that would produce different values of P_1^{Fluor} , where the charge cloud is viewed from the direction of the photodiode for vertical alignment of the cloud (i.e., out of the scattering plane). For a fluorescence polarization of 95%, the contribution from the ellipticity of the laser light is hence expected to only make a small change to the measured ionization cross section, since as seen in Figure 7, the in-plane contribution only becomes substantial when the polarization reduces below $\sim 80\%$.

5. CONCLUSION

In conclusion, we have compared experiment and theory for electron-impact ionization of the ground state of Mg as well as ionization of a $3p$ state that has been laser aligned either in the scattering plane or in a plane perpendicular to the incident beam direction. For the ground-state ionization, the experimental results were compared with TDCC (time-dependent close coupling), DWBA (distorted wave Born approximation), and 3DW (three-body distorted wave) approximations. While all three theoretical approaches gave reasonably good agreement with the data, the 3DW predicts the location of the binary peak and width a little better. For ionization of the laser-aligned $3p$ state, the experiment was compared with DWBA and 3DW calculations. The experimental data are relatively absolute, so only one normalization places all the data on an absolute scale. We chose to normalize to the measurement with the alignment parallel to the x axis, since this was the common alignment direction in the two different data sets. For alignment in the scattering plane, the 3DW results were in very good agreement with experiment with the only problem being a small shift in peak location for $(-30^\circ, -60^\circ, \text{ and } -90^\circ)$. For larger and smaller β , the 3DW peak locations are in agreement with experiment. Since all the different orientations can be calculated from the $m = (0, 1)$ amplitudes calculated relative to the z axis being parallel to the incident beam direction, this comparison is an indirect test of the accuracy of the Υ_m amplitudes for $m = (0, 1)$.

For the beam direction along the z axis, we have the well-known symmetry $\Upsilon_{-1} = -\Upsilon_1$. For the case of ionization of the $3p$ state with alignment angles in the perpendicular plane, this symmetry predicts that the cross sections for alignment at 45° between the x and y axes should be half the cross sections for the x -axis alignment, and the cross sections for alignment along the y axis should be zero. Although the theoretical cross sections satisfied these conditions, the experimental data did not. On the other hand, we have learned from the experimental approach and its analysis of the polarization data mentioned above that the effects of both radiation trapping and an elliptically polarized laser beam will not

substantially alter the experimental results. In both cases the relative change is found to be 5% or less. This cannot explain the large discrepancy between theory and experiment that is found when the excited state is aligned orthogonal to the scattering plane. The angular acceptance of the detectors has also been discounted as a significant contributing factor. At the present time it is hence difficult to see where this discrepancy originates, and the results in this paper clearly show that more work is needed to resolve the cause of these differences.

ACKNOWLEDGMENTS

This work was supported, in part, by the United States National Science Foundation under Grant No. PHY-1068237 (S.A. and D.M.). S.A. would also like to thank the Libyan Ministry of Higher Education's Scholarship for funding. A.J.M. and K.L.N. would like to thank Dr. Alisdair McPherson for assistance with the dye laser, which was supplied by the Photon Science Institute at the University Of Manchester. K.L.N. also thanks the European Commission for a Marie Curie International Incoming Fellowship. The Los Alamos National Laboratory is operated by Los Alamos National Security, LLC, for the National Nuclear Security Administration of the US Department of Energy under Contract No. DE-AC5206NA25396.

REFERENCES

- [1] A Senfleben, T Pflüger, X Ren, O Al-Hagan, B Najjari, D Madison, A Dorn, and J Ullrich. Search for interference effects in electron impact ionization of aligned hydrogen molecules. *Journal of Physics B: Atomic, Molecular and Optical Physics*, 43(8):081002, 2010.

- [2] Arne Senftleben, Ola Al-Hagan, Thomas Pflüger, Xueguang Ren, Don Madison, Alexander Dorn, and Joachim Ullrich. Fivefold differential cross sections for ground-state ionization of aligned H_2 by electron impact. *The Journal of Chemical Physics*, 133(4):044302, 2010.
- [3] X Ren, T Pflüger, S Xu, A Senftleben, J Colgan, M S Pindzola, A Dorn, and J Ullrich. Electron impact induced break-up of aligned H_2 : molecular frame (e, 2e) studies. *Journal of Physics: Conference Series*, 388(5):052037, 2012.
- [4] Julian C. A. Lower, Esam Ali, Susan Bellm, Erich Weigold, Allison Harris, C. G. Ning, and Don Madison. Experimental and theoretical cross sections for molecular-frame electron-impact excitation-ionization of D_2 . *Phys. Rev. A*, 88:062705, Dec 2013.
- [5] E. Ali, A. L. Harris, J. Lower, E. Weigold, C. G. Ning, and D. H. Madison. Fully differential cross sections for electron-impact excitation-ionization of aligned D_2 . *Phys. Rev. A*, 89:062713, Jun 2014.
- [6] Junfang Gao, J. L. Peacher, and D. H. Madison. An elementary method for calculating orientation-averaged fully differential electron-impact ionization cross sections for molecules. *The Journal of Chemical Physics*, 123(20):204302, 2005.
- [7] J. Colgan, M. S. Pindzola, F. Robicheaux, C. Kaiser, A. J. Murray, and D. H. Madison. Differential cross sections for the ionization of oriented H_2 molecules by electron impact. *Phys. Rev. Lett.*, 101:233201, Dec 2008.
- [8] E M Staicu Casagrande, A Naja, F Mezdari, A Lahmam-Bennani, P Bolognesi, B Joulakian, O Chuluunbaatar, O Al-Hagan, D H Madison, D V Fursa, and I Bray. (e,2e) ionization of helium and the hydrogen molecule: signature of two-centre interference effects. *Journal of Physics B: Atomic, Molecular and Optical Physics*, 41(2):025204, 2008.

- [9] Kaiser Christian Madison Don Al-Hagan, Ola and Andrew James Murray. Atomic and molecular signatures for charged-particle ionization. *Nature Publishing Group*, 5:59–63, 2009.
- [10] Andrew James Murray. Combining laser and electron interactions – current experiments and future possibilities in excitation and ionization studies. *Journal of Physics: Conference Series*, 212(1):012016, 2010.
- [11] Kate L. Nixon and Andrew James Murray. Differential cross sections for ionization of laser-aligned atoms by electron impact. *Phys. Rev. Lett.*, 106:123201, Mar 2011.
- [12] Kate L. Nixon and Andrew James Murray. Parametrization of electron-impact ionization cross sections from laser-excited and aligned atoms. *Phys. Rev. Lett.*, 112:023202, Jan 2014.
- [13] A. D. Stauffer. Shape of the cross section for electron ionization of laser-excited atoms. *Phys. Rev. A*, 89:032710, Mar 2014.
- [14] G. S. J. Armstrong, J. Colgan, and M. S. Pindzola. Angular distributions for the electron-impact single ionization of sodium and magnesium. *Phys. Rev. A*, 88:042713, Oct 2013.
- [15] J. Colgan and M. S. Pindzola. Angular distributions for the electron-impact single ionization of sodium and magnesium. *Eur. Phys. J. D*, 66:284, Oct 2012.
- [16] Don H. Madison and Ola Al-Hagan. The distorted-wave born approach for calculating electron-impact ionization of molecules. *Journal of Atomic, Molecular, and Optical Physics*, 2010:367180, 2010.

- [17] Sadek Amami, Melike Ulu, Zehra Nur Ozer, Murat Yavuz, Suay Kazgoz, Mevlut Dogan, Oleg Zatsarinny, Klaus Bartschat, and Don Madison. Theoretical and experimental investigation of $(e, 2e)$ ionization of argon $3p$ in asymmetric kinematics at intermediate energy. *Phys. Rev. A*, 90:012704, Jul 2014.
- [18] M. E. Rose. Elementary theory of angular momentum.
- [19] A. J. Murray, W. R. MacGillivray, and M. C. Standage. Radiation trapping in a stepwise-excitation electron-laser coincidence experiment. *Phys. Rev. A*, 44:3162–3168, Sep 1991.
- [20] Andrew James Murray, William MacGillivray, and Martyn Hussey. Theoretical modeling of resonant laser excitation of atoms in a magnetic field. *Phys. Rev. A*, 77:013409, Jan 2008.

VI. THEORETICAL AND EXPERIMENTAL (e,2e) STUDY OF ELECTRON-IMPACT IONIZATION OF LASER-ALIGNED Mg ATOMS

Sadek Amami¹, Andrew Murray,^{r2}Al Stauffer,³Kate Nixon,²Gregory Armstrong,⁴James Colgan,⁴ and Don Madison¹

¹Department of Physics,

Missouri University of Science and Technology,

Rolla, Missouri, USA

²Photon Science Institute, School of Physics and Astronomy,

University of Manchester,

Manchester M13 9PL, United Kingdom

³Department of Physics and Astronomy,

York University,

Toronto, Ontario, Canada M3J 1P3

⁴Theoretical Division, Los Alamos National Laboratory,

Los Alamos, New Mexico 87545, USA

ABSTRACT

We have recently reported a theoretical and experimental study of electron-impact ionization of laser-aligned magnesium. Results were presented for both ionization of the ground state, as well as for laser-aligned atoms in the $3p$ state. For ionization from the $3p$ state, theoretical results were presented using the distorted wave Born (DWBA) and three-body distorted wave (3DW) approximations. Unfortunately, after publication we learned that the theoretical results were incorrect due to one of the arrays in the computer code dimensioned too small. The figures affected by this error are Figures 1–3 in the original paper. The present Figures 1–3 show the corrected results. The DWBA calculation changed

the most. In the original paper, the DWBA had unphysical side lobes for the $3p$ state aligned in the scattering plane (Figures 2 and 3). These side lobes are either reduced or eliminated in the corrected DWBA. However, the main peak magnitudes are now much larger. There is a much smaller correction to the 3DW results. The good news is that overall the 3DW is now in even better agreement with experiment. The fact that both theories predict a zero cross section for alignment of the $3p$ state perpendicular to the scattering plane (the y axis) did not change.

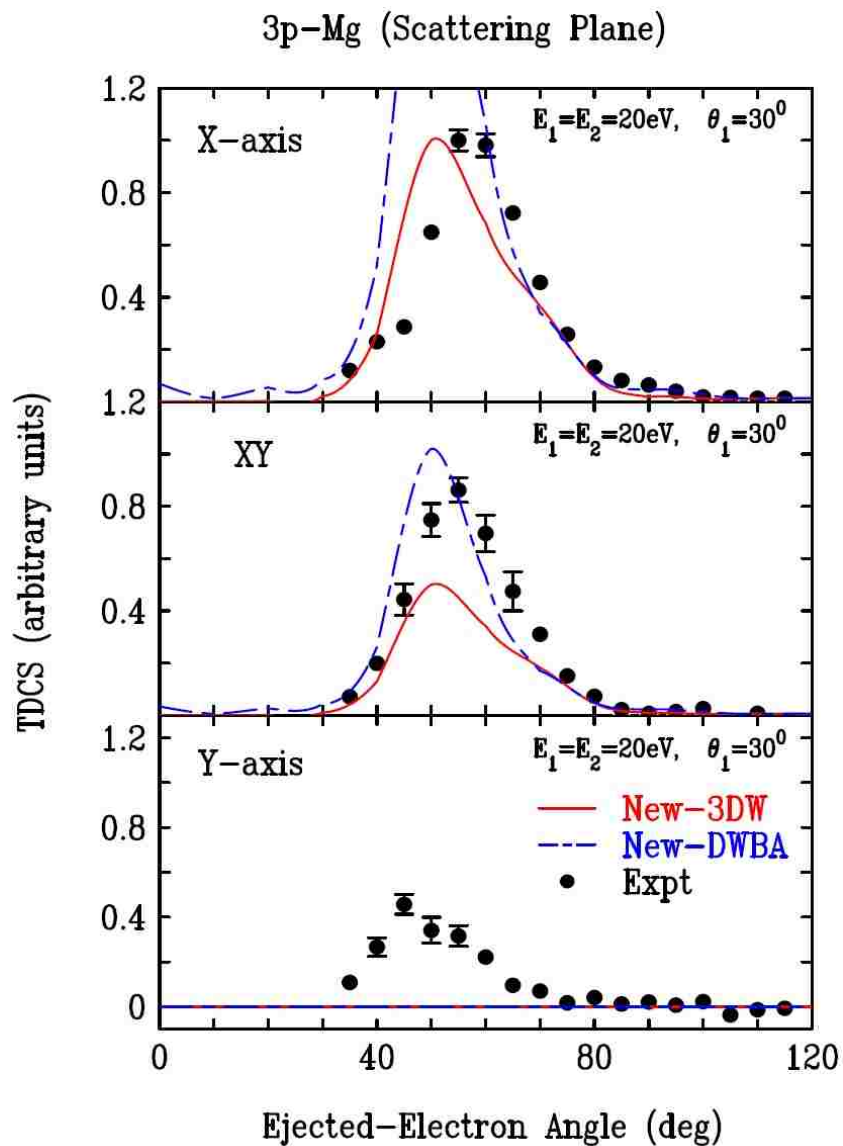


Figure 1. Experimental and theoretical TDCS for electron-impact ionization of the laser-aligned 3p state of Mg. The projectile scattering angle θ_1 is 30° and both outgoing electrons have the same energy ($E_1 = E_2 = 20 \text{ eV}$). The three panels are for laser alignment parallel to the x axis (i.e., in the scattering plane orthogonal to the incident electron beam direction), laser alignment at 45° between the x and y axes, and laser alignment parallel to the y axis (i.e., perpendicular to the scattering plane), respectively. In the bottom panel, the theoretical results are all exactly zero. The theoretical calculations are as follows: new 3DW solid (red); new DWBA dashed (blue).

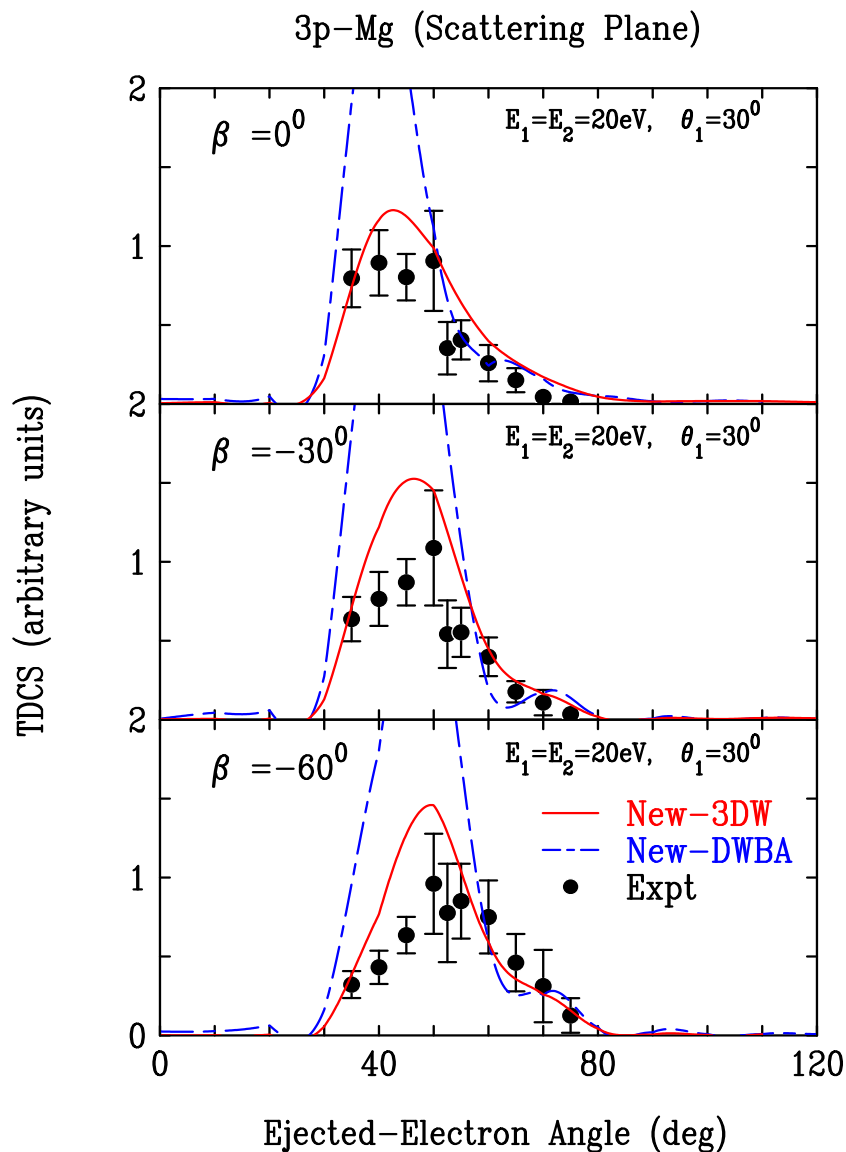


Figure 2. Experimental and theoretical TDCS for electron-impact ionization of the laser-aligned 3p state of Mg. The projectile scattering angle is 30° and both outgoing electrons have the same energy ($E_1 = E_2 = 20 \text{ eV}$). The three panels are for laser alignment in the scattering plane by different orientation angles “beta” relative to the incident electron beam direction. The theoretical calculations are as follows: new 3DW solid (red); and new DWBA dashed (blue).

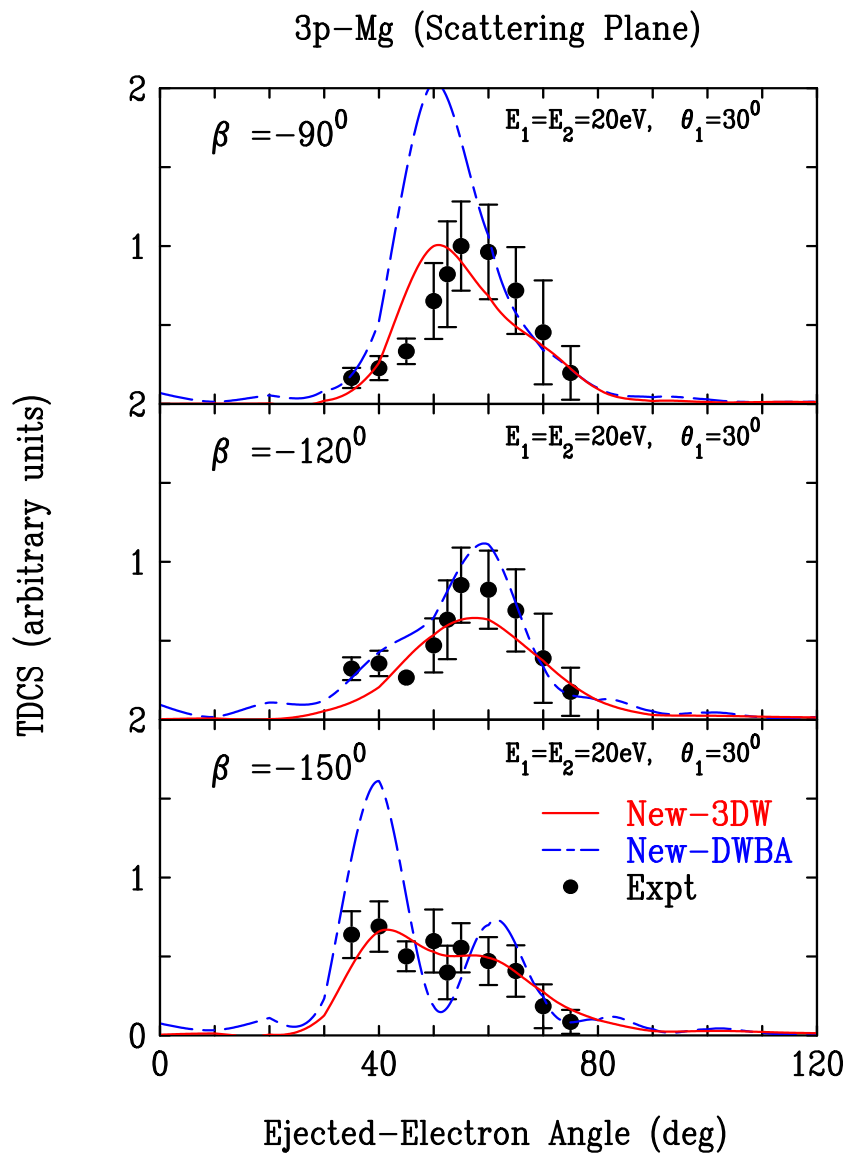


Figure 3. Same as Figure 2 except for larger beta angles.

VII. EVIDENCE FOR UNNATURAL PARITY CONTRIBUTIONS TO ELECTRON-IMPACT IONIZATION OF LASER-ALIGNED ATOMS

G. S. J. Armstrong^{1,2}, J. Colgan², M S Pindzola³, S. Amami⁴, D. H. Madison⁴, J. Pursehouse⁵, K. L. Nixon⁶, and A. J. Murray⁵

¹J. R. Macdonald Laboratory, Department of Physics,
Kansas State University,
Manhattan, KS 66506, USA

²Theoretical Division, Los Alamos National Laboratory,
New Mexico 87545, USA

³Department of Physics,
Auburn University,
Auburn, Alabama 36849, USA

⁴Physics Department,
Missouri University of Science and Technology,
Rolla, MO 65409, USA

⁵Photon Science Institute, School of Physics and Astronomy,
University of Manchester,
Manchester M13 9PL, UK

⁶Departamento de Física,
UFJF, Juiz de Fora,
MG 36036-330, Brazil

ABSTRACT

Recent measurements have examined the electron-impact ionization of excited-state laser-aligned Mg atoms. In this work we show that the ionization cross section arising from the geometry where the aligned atom is perpendicular to the scattering plane directly probes the unnatural parity contributions to the ionization amplitude. The contributions from natural parity partial waves cancel exactly in this geometry. Our calculations resolve the discrepancy between the non-zero measured cross sections in this plane and the zero cross section predicted by distorted-wave approaches. We demonstrate that this is a general feature of ionization from p -state targets by additional studies of ionization from excited Ca and Na atoms.

1. INTRODUCTION

The study of electron-impact single ionization of atomic and molecular targets [often known as $(e,2e)$ studies] has long been a fruitful area of research in atomic collision physics, since it probes the delicate interactions between two outgoing electrons moving in a Coulomb field, i.e. electron-electron correlations [1]. Many fundamental experimental and theoretical studies have been reported for ionization of the simplest atomic systems, H [2, 3, 4, 5, 6, 7] and He [8, 9, 10, 11, 12, 13], and more recently for the simplest molecular system, H₂ [14, 15, 16].

Ionization from *excited* states of atoms has received much less attention due to the difficulty in preparing such targets. Significant advances in such studies were recently reported in experiments where a laser was used to excite Mg atoms into their $3s3p\ ^1P$ state, which then were ionized by an incoming electron beam [17, 18]. Moreover, the laser was used to prepare different alignment angles of the initial p orbital, allowing a probe of the angular distribution dependence on the orientation of the atomic orbital—a first for atomic targets. Recent studies have also examined the angular distribution dependence

of ionization of aligned molecular targets [19]. The experimental studies on Mg [17, 18] were very recently compared to three-body distorted-wave (3DW) calculations [20], and reasonable agreement was found between most of the measured triple differential cross sections and the calculations. However, one striking difference was noted for cross sections measured when the aligned atom was perpendicular to the scattering plane (i.e. the p orbital was aligned along the y direction, see Figure 1); the 3DW calculation predicted an identically zero cross section in this plane, at odds with the measurement that was clearly non-zero. The analysis of this zero cross section was also found to be consistent with other recent theoretical work [21].

In this paper we report close-coupling calculations for the triple differential cross sections from excited Mg atoms, and find that the cross section in the perpendicular geometry arises from the unnatural parity contribution to the ionization amplitude. An unnatural parity state is a state with parity $(-1)^{L+1}$ compared to a natural parity state that has parity $(-1)^L$. Our cross sections in this plane calculated using a time-dependent close-coupling (TDCC) approach are in reasonable agreement with the measured data. We also show that similar non-zero cross sections should be observed in the perpendicular (y) geometry for any atomic p orbital and illustrate this with calculations of the triple differential cross sections from excited-state Na and Ca. For Ca, our calculations are in good agreement with new measurements of these cross sections, which are presented here.

2. THEORY

The time-dependent close-coupling (TDCC) theory as applied to electron-impact ionization has been well described [22, 23]. The extension of the method to treat multi-electron systems, by utilizing an orthogonalization to the filled sub-shells at each time step, was presented recently for calculations for the single ionization of ground-state Mg [24]. The calculations presented here follow this procedure, except that the active electron is now the $3p$ orbital of Mg. The $\text{Mg}^+ [\text{Ne}]3s$ core is the same as used in our previous calculations

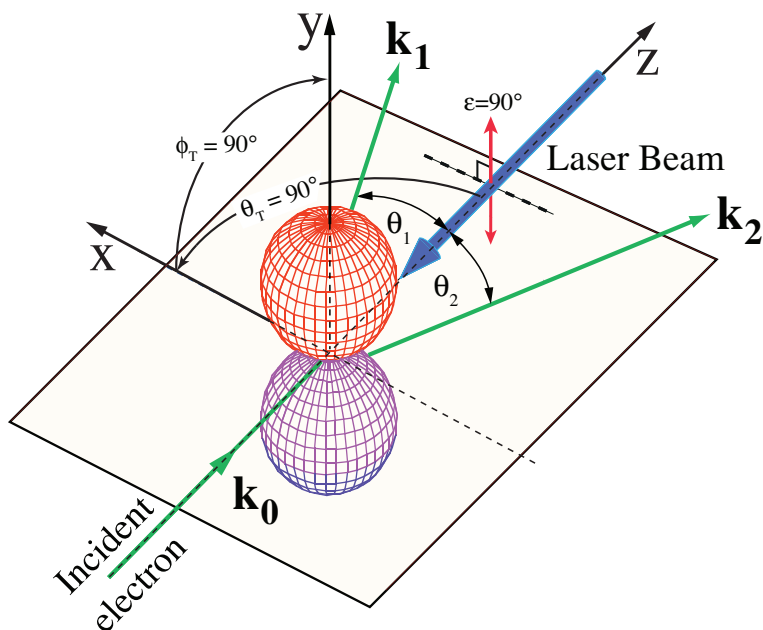


Figure 1. Geometry of the scattering experiments performed on Mg [17] and for the new Ca experiments reported here. The incident electron has momentum \mathbf{k}_0 and the outgoing electrons have momentum vectors \mathbf{k}_1 and \mathbf{k}_2 . The target p -orbital is shown here to be aligned along the y -axis using the laser beam polarization, i.e. perpendicular to the scattering plane (in which the outgoing electrons lie).

from the ground state [24]. We note that this approach is effectively a configuration-average approach to electron-impact ionization, that is, we consider only the $3p$ active orbital as a configuration and do not account for the term splitting of the $3s3p$ Mg configuration into the 1P and 3P terms. This differs somewhat from the measurement [17], since the laser excitation from the ground state in the experiment populates only the $3s3p$ 1P term. It is possible to use a three-electron TDCC approach (in which two bound electrons are active) to create an initial $3s3p$ 1P term and perform calculations of the single ionization of this term. Such calculations are, however, extremely computationally intensive and in this paper we discuss only test calculations made using this approach. The two-electron TDCC approach

centers around the solution of the set of partial differential equations given by

$$i\frac{\partial}{\partial t}P_{l_1l_2}^{LS}(r_1, r_2, t) = [T_{l_1}(r_1) + T_{l_2}(r_2)] P_{l_1l_2}^{LS}(r_1, r_2, t) + \sum_{l'_1l'_2} V_{l_1l_2, l'_1l'_2}^L(r_1, r_2) P_{l'_1l'_2}^{LS}(r_1, r_2, t). \quad (1)$$

These equations are the result of the expansion of the total wavefunction over coupled spherical harmonics, and insertion of this expansion into the time-dependent Schrödinger equation. In Equation (79) $T_l(r)$ represents the one-electron kinetic and potential energy terms, which include direct and local exchange potentials that describe the interaction with the inert core electrons, and $V(r_1, r_2)$ represents the electron-electron interaction potential. The initial $t = 0$ boundary condition is given by

$$P_{l_1l_2}^{LS}(r_1, r_2, t = 0) = \frac{1}{\sqrt{2}} \left[P_{nl_1}(r_1) G_{k_2l_2}(r_2) + (-1)^S G_{k_1l_1}(r_1) P_{nl_2}(r_2) \right] \quad (2)$$

where in the present case $nl \equiv 3p$ and $G_{kl}(r)$ represents the incoming wavepacket [22]. To compare against the measurements of [17, 18], we must also take into account the orientation of the initial $3p$ orbital. We may do this by using a boundary condition of the form [25]

$$P_{l_1l_2}^{LS}(r_1, r_2, t = 0) = \frac{1}{\sqrt{2}} \left[P_{nl_1}(r_1) \mathcal{R}_M G_{k_2l_2}(r_2) + (-1)^S G_{k_1l_1}(r_1) P_{nl_2}(r_2) \mathcal{R}_M \right] \quad (3)$$

where

$$\mathcal{R}_M = \left[-\frac{1}{\sqrt{2}} e^{-i\phi_T} \sin \theta_T \delta_{M,-1} + \cos \theta_T \delta_{M,0} + \frac{1}{\sqrt{2}} e^{i\phi_T} \sin \theta_T \delta_{M,+1} \right], \quad (4)$$

and the angles θ_T, ϕ_T define a given orientation of the initial p orbital with respect to the z -axis, with the z -axis defined along the incident electron beam direction (see Figure 1). Here M is the azimuthal quantum number of the oriented atom, since the wavepacket has

$m = 0$ by definition. Since the \mathcal{R}_M term does not depend on the coupled channels $l_1 l_2$, and since the TDCC Hamiltonian is independent of M , the time propagation of the coupled differential equations is unchanged by the \mathcal{R}_M term in the initial boundary condition. This term will only affect the calculation of the triple differential cross sections, which take the form

$$\begin{aligned} \frac{d^3\sigma}{dE_1 d\Omega_1 d\Omega_2} &= \frac{w_t}{(2l_t + 1)} \frac{\pi}{4k_0^2} \frac{1}{k_1 k_2} \sum_S (2S + 1) \\ &\times \int_0^\infty dk_1 \int_0^\infty dk_2 \delta\left(\alpha - \tan^{-1} \frac{k_2}{k_1}\right) |\mathcal{M}|^2, \end{aligned} \quad (5)$$

where now

$$\begin{aligned} \mathcal{M} &= \sum_L i^L \sum_{M=0,-1,+1} \left[-\frac{1}{\sqrt{2}} e^{-i\phi_T} \sin \theta_T \delta_{M,-1} + \cos \theta_T \delta_{M,0} + \frac{1}{\sqrt{2}} e^{i\phi_T} \sin \theta_T \delta_{M,+1} \right] \\ &\times \sum_{l_1 l_2} (-i)^{l_1+l_2} e^{i(\sigma_{l_1}+\sigma_{l_2})} e^{i(\delta_{l_1}+\delta_{l_2})} \\ &\times P_{l_1 l_2}^{LS}(k_1, k_2, T) \sum_{m_1 m_2} C_{m_1 m_2 M}^{l_1 l_2 L} Y_{l_1 m_1}(\theta_1, \phi_1) Y_{l_2 m_2}(\theta_2, \phi_2). \end{aligned} \quad (6)$$

Note that the M dependence enters into both the first term and in the coupled spherical harmonic in the last line of Equation (84). In Equation (83) w_t and l_t are the occupation number and angular momentum of the initial target orbital, and α is the angle in the hyperspherical plane between the two outgoing momenta vectors \mathbf{k}_1 and \mathbf{k}_2 . In Equation (84) $Y_{lm}(\theta, \phi)$ is a spherical harmonic, $C_{m_1 m_2 m_3}^{l_1 l_2 l_3}$ is a Clebsch-Gordan coefficient, and σ_l and δ_l are Coulomb and distorted-wave phase shifts, respectively. We note here that Equation (83) corrects a typographical error in the denominator of Equation (9) of [24]. The function $P_{l_1 l_2}^{LS}(k_1, k_2, T)$ is formed by projecting the final two-electron radial wavefunction (after propagation to a sufficiently long time T) $P_{l_1 l_2}^{LS}(r_1, r_2, t = T)$ onto the one-electron continuum orbitals.

Our two-electron TDCC calculations used a radial mesh of $(960)^2$ points with variable mesh spacing of between 0.01 and 0.2 a.u. [24]. We found that it was necessary to include partial wave contributions from $L = 0 - 14$ to completely converge our calculations. We also note that, for all partial waves except $L = 0$, we include both ‘odd’ and ‘even’ parity contributions for each partial wave L . These contributions are the result of the increased coupling possibilities afforded by an initial p orbital, and such contributions have been included in previous TDCC calculations from initial p states, such as [26]. As an example, when considering the $L = 1$ partial wave, the natural parity channels that contribute to the $l_1 l_2$ expansion in (1) are ps, sp, pd, dp, df, fd , etc. However, the initial p orbital can also couple to the p channel of the wavepacket to result in an overall symmetry of $L = 1$, with coupled channels pp, dd, ff , etc. This state has even parity. Such ‘opposite’ parity states are usually termed ‘unnatural’ parity contributions in previous work, for example [27]. Studies of unnatural parity states have been conducted in positron scattering systems [28] and in cold atomic gases [29].

3. RESULTS

We first compare our two-electron TDCC calculations to the measurements of Nixon and Murray [17] in Figure 2. We show the triple differential cross section for three orientations of the aligned $3p$ orbital with respect to the scattering plane, for equal energy sharing between the outgoing electrons. The aligned p -state is shown in the perpendicular geometry ($\theta_T = 90^\circ, \phi_T = 90^\circ$) in Figure 1. Since the measurements have an uncertainty of $\pm 5^\circ$ in the scattered and ejected electron angular measurements, we show calculations for both a fixed angle of 30° (as reported in [17]) and of 25° and 35° . We find for $\theta_T = 90^\circ, \phi_T = 0^\circ$ [i.e. the x -axis geometry] that the TDCC calculations are in quite good agreement with the measurement, with the TDCC calculations at the smaller fixed angle in slightly better agreement. For the geometry where the $3p$ orbital is along the y -axis as in Figure 1, we find that the TDCC calculations are in good agreement with experiment as to

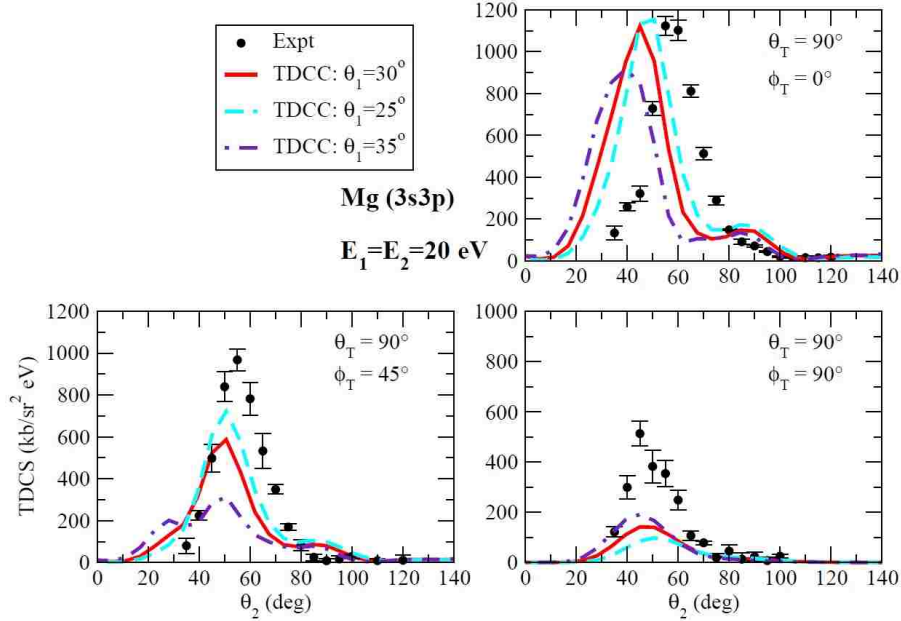


Figure 2. Triple differential cross sections for the electron-impact ionization of excited-state Mg for equal energy-sharing between the outgoing electrons of $E_1 = E_2 = 20$ eV. The measurements of [17] are compared with TDCC calculations for various (θ_T, ϕ_T) orientations of the target $3p$ orbital as indicated. We present TDCC calculations performed at a fixed θ_1 angle of 30° (the fixed angle reported in the measurements of [17]) (solid red lines) and at angles of 25° (dashed blue lines) and 35° (dot-dashed purple lines).

the position of the peak in the triple differential cross section, but are lower in magnitude than the measured values. We note that the relative measurements are normalized to the TDCC calculations for the largest cross section value in the $\theta_T = 90^\circ, \phi_T = 0^\circ$ case, and that this normalization then fixes the relative measurements at other orientations.

We note that the TDCC calculations in the y -axis case ($\theta_T = 90^\circ, \phi_T = 90^\circ$) are clearly not zero, which differs from the identically zero 3DW calculations in this plane that were recently reported [20]. The TDCC cross sections are, however, significantly lower than the measured values. We have investigated the TDCC calculations at this geometry, and find that the usually dominant natural parity contributions to each partial wave (i.e. the coupling of the two outgoing electrons into $^1,3S^e, ^1,3P^o, ^1,3D^e$, etc.) do in fact produce zero contribution to the cross section because the $M = +1$ and $M = -1$ contributions cancel exactly, as found in the distorted-wave calculations reported in [20]. In this geometry the

$M = 0$ contribution is also identically zero. However, the unnatural parity contributions (i.e. ${}^{1,3}P^e$, ${}^{1,3}D^o$, etc.) are such that the $M = +1$ and $M = -1$ contributions do *not* cancel, but instead add (equally), producing a non-zero total cross section in this plane. The non-cancellation for the opposite parity contributions can be traced to a phase factor, $(-1)^{l_1+l_2+L}$, that arises in the Clebsch-Gordan coefficient in the last term in Equation (6). This phase factor produces an extra component of (-1) when comparing the $M = +1$ and $M = -1$ terms, which cancels the additional (-1) factor arising from the spherical harmonic terms for $Y_{lM=+1}$ and $Y_{lM=-1}$ (this latter factor was discussed in detail by Amami et al [20]). For the natural parity terms, the $(-1)^{l_1+l_2+L}$ factor always results in $+1$, so that an overall cancellation of the $M = +1$ and $M = -1$ terms occurs. The 3DW calculations of Amami et al. [20] do not contain the unnatural parity contributions and therefore predict an identically zero cross section in this geometry.

Therefore, we find that the measured cross section in the y -axis geometry *directly* probes the unnatural parity contributions to the triple differential cross sections from ionization of excited-state Mg. Such contributions only occur for non- s state atomic targets. We are unaware of any previous ionization measurements that have probed such states. To further explore the effect of the unnatural parity contributions, in Figure 3 we show TDCC calculations for a fixed angle of 30° (as in Figure 2) and also TDCC calculations where the unnatural parity contributions have been omitted. We find that the unnatural parity terms make no contribution for the x -axis geometry, which is also a consequence of the phase factors that enter the Clebsch-Gordan coefficients in Equation (6). For the case where the alignment is at 45° between the x and y -axes, we find that the unnatural parity contribution is small, but noticeable, and inclusion of these terms moves the TDCC calculations towards the measured cross sections. We also note that omitting the unnatural parity contribution in this case results in a cross section that is exactly one half of the cross section computed for

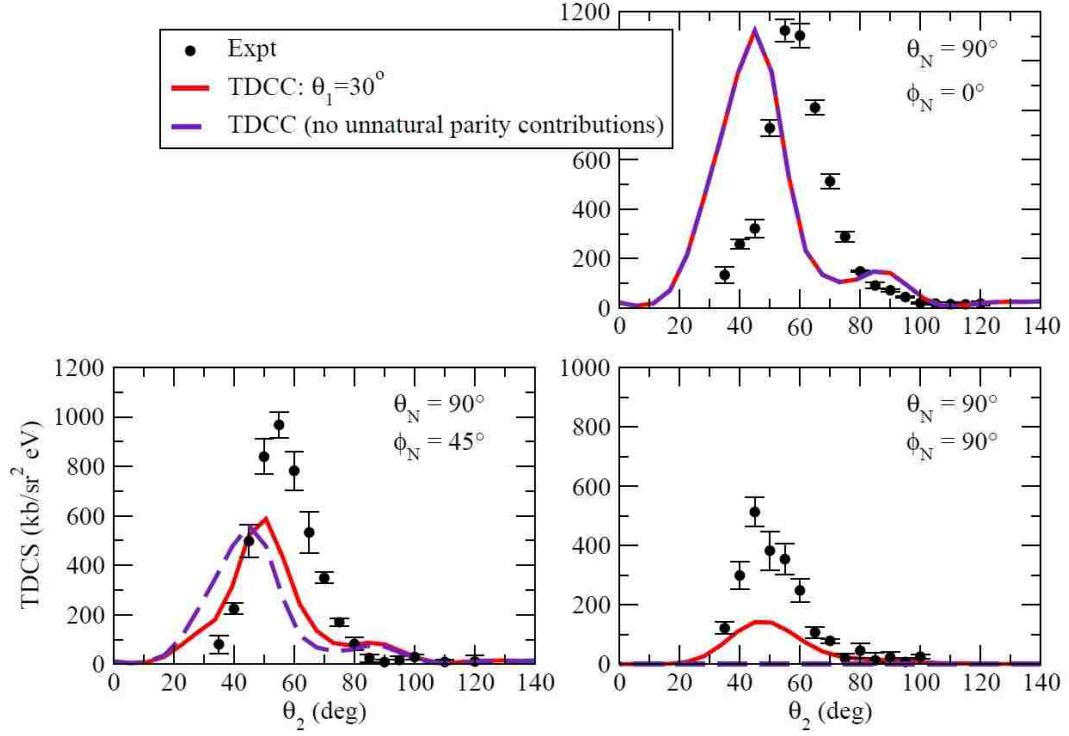


Figure 3. Same as Figure 2, except now we show only the $\theta_1 = 30^\circ$ TDCC calculation. We also present a TDCC calculation (purple dashed lines) in which the unnatural parity contribution is omitted.

the x -axis geometry. This property was noted for the 3DW calculations presented in [20], and we find that this only holds in the TDCC calculations when the unnatural parity terms are omitted.

It is of interest to explore whether or not the non-zero cross section in the perpendicular geometry is also found for other systems. In Figure 4 we present the electron-impact ionization of excited-state Na for the same alignment angles as in Figure 2. Although no measurements are available for excited-state Na, we find that the cross sections from TDCC calculations for Na appear quite similar to those for Mg, and that the y -axis cross section is again non-zero. The TDCC calculation for ionization of the quasi one-electron Na($3p$) target may be considered more ‘robust’ than the corresponding calculation for Mg, since the use of a two-active-electron approximation in the TDCC calculations for ionization of Na($3p$) is well justified. In Figure 4 we also compare with new distorted-wave Born

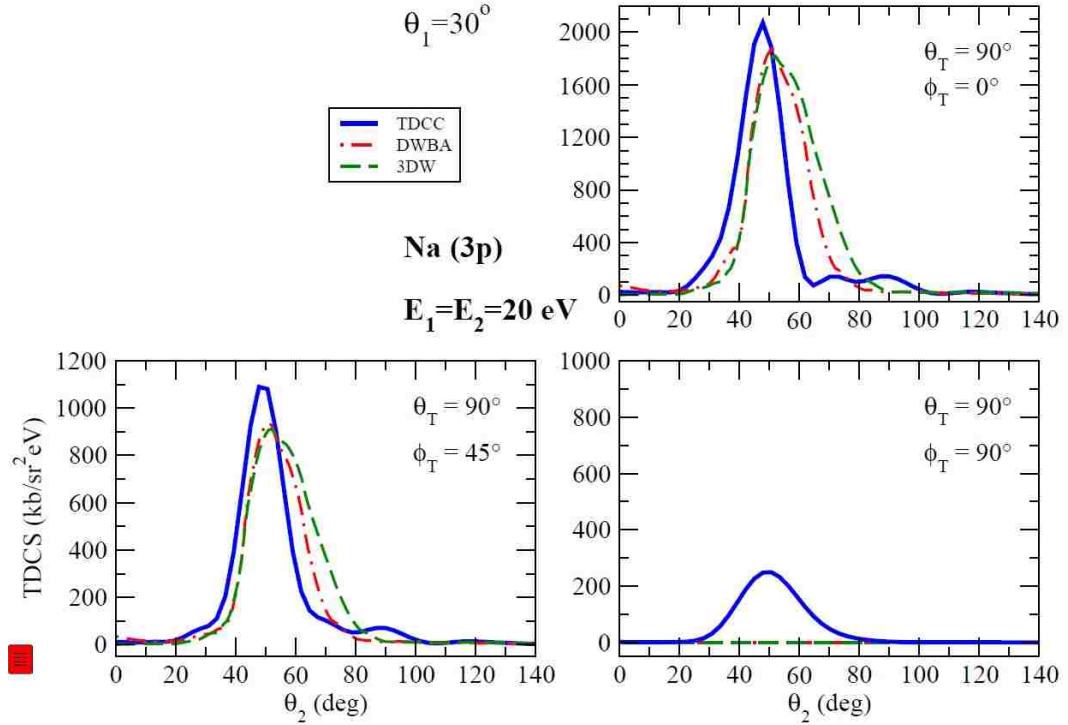


Figure 4. Triple differential cross sections for the electron-impact ionization of excited-state Na for equal energy-sharing between the outgoing electrons of $E_1 = E_2 = 20$ eV. The cross sections are presented for a fixed electron angle of $\theta_1 = 30^\circ$ and at various orientations of the $3p$ orbital as indicated. We compare the TDCC calculations (solid blue lines) with DWBA (dot-dashed red lines) and 3DW calculations (dashed green lines) made in a similar manner to the distorted-wave calculations presented in [20]. In this Figure, the DWBA and 3DW calculations have been normalized to the TDCC calculations.

(DWBA) and three-body distorted-wave (3DW) calculations that were made in a similar manner to those recently made for Mg [20]. The TDCC and distorted-wave calculations are in reasonable agreement for the x-axis geometry ($\theta_T = 90^\circ, \phi_T = 0^\circ$) and the xy geometry ($\theta_T = 90^\circ, \phi_T = 45^\circ$), and we again find that the 3DW calculations predict an identically zero cross section for the y geometry case ($\theta_T = 90^\circ, \phi_T = 90^\circ$).

As a further confirmation of the non-zero cross section in the perpendicular geometry from excited p -state atoms, we have also performed new calculations and measurements of the angular distributions of excited-state Ca in its $4s4p$ state. The TDCC calculations for Ca required finer radial meshes and inclusion of angular momentum states up to $L = 16$

to converge the calculations. New experiments were also performed on Ca using a similar apparatus to the measurements made on excited-state Mg [17, 18]. In Figure 5 we present the TDCS for Ca ($4s4p$) at equal energy sharing between the electrons of 30 eV. The upper panel shows the x -axis geometry cross sections and the lower panel shows the perpendicular geometry (y -axis) cross sections. Because our calculations indicate that the cross section is quite sensitive to the fixed-angle value, we present TDCC calculations averaged over the experimental angular uncertainties, as well as the individual TDCC calculations at each fixed angle. The measurements again find a non-zero cross section in the perpendicular geometry. The TDCC Ca calculations also find a non-zero cross section, although the position of the peak of the cross section is at slightly higher angles compared to the measurement. For the scattering plane cross sections shown in the upper panel, the TDCC calculations at a fixed angle of 45° find a peak that is at significantly lower angles than the measured cross section peak. However, calculations at lower values of the fixed angle appear to move closer to the measured values and also show that the cross section exhibits a strong sensitivity to the fixed-angle value. We note that a calculation at a fixed angle value of 35° (not shown) is reasonably close to the measured cross section, but this is outside the measurement uncertainty of $\pm 5^\circ$ in the fixed angle value. Figure 5 also shows 3DW calculations made for Ca in a similar manner to those made for Na and Mg. The 3DW calculations are in good agreement with the measurement for the x -axis case in the upper panel but again predict a zero cross section for the y -axis case. DWBA calculations (not shown) are very similar to the 3DW calculations presented here.

Finally, we note that a three-electron TDCC method can also be applied to the computation of the single ionization of Mg or Ca, in a similar manner to the calculations used for the electron-impact double ionization of Mg that were recently reported [30]. Such three-electron calculations have an advantage compared to two-electron calculations in that one can construct the initial state to be the $3s3p\ ^1P$ term, which of course is the real initial state of the measurements with which we compare here. However, such three-electron calculations

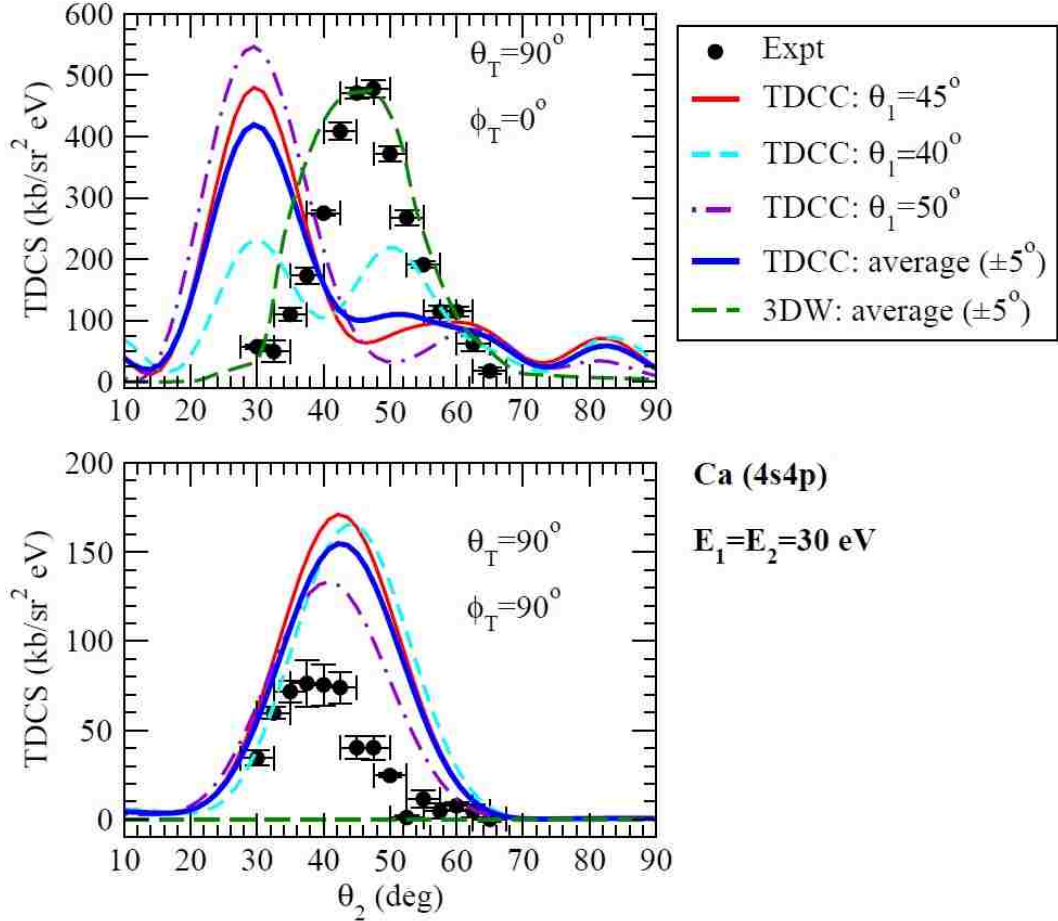


Figure 5. Triple differential cross sections for the electron-impact ionization of excited-state Ca for equal energy-sharing between the outgoing electrons of $E_1 = E_2 = 30$ eV. New measurements are compared with TDCC calculations (solid lines) and 3DW calculations (green dashed line) as described in the text. The measurements were made for a fixed electron angle of 45° . The upper panel shows the cross section for the $4p$ orbital in the scattering plane and the lower panel shows the cross section for the $4p$ orbital perpendicular to the scattering plane. The thick solid blue lines indicates a TDCC calculation averaged over the experimental angular uncertainties, while the thin (solid red, dashed light blue, dot-dashed purple) lines show the individual TDCC calculations at each fixed angle.

are significantly more computationally intensive than the two-electron calculations reported in this manuscript. Complete convergence of the three-electron calculations in terms of all the angular momenta up to $L = 14$ and using a sufficiently large radial mesh is not yet possible given current computational resources. We do find that preliminary calculations using just a few partial waves of our three-electron TDCC approach indicate that the TDCS

in the perpendicular geometry is again not zero and has a peak in the cross section at similar angles to the cross sections presented in Figure 2. This indicates that our configuration-average approach for the ionization of Mg $3s3p$ and Ca $4s4p$ may not be too severe an approximation. In future work we plan to continue our three-electron TDCC investigations and hope that a fully converged calculation is feasible sometime soon.

4. CONCLUSION

In summary, we have presented evidence using TDCC calculations that the measured cross section from ionization of excited-state laser-aligned atoms that are perpendicular to the scattering plane arise solely from unnatural parity contributions to the ionization amplitude. Although the overall agreement between the TDCC calculations and the measured cross sections is only moderately good, our calculations help resolve the discrepancy with the zero cross section predicted by distorted-wave approaches for ionization in this geometry.

ACKNOWLEDGMENTS

We are very grateful for stimulating discussions with A. Stauffer. The Los Alamos National Laboratory is operated by Los Alamos National Security, LLC for the National Nuclear Security Administration of the U.S. Department of Energy under Contract No. DE-AC5206NA25396. This work was supported in parts by grants from the US NSF. Computational work was carried out using LANL Institutional Computing Resources and at NERSC and HLRS. We thank the PSI at the University of Manchester for use of the laser system for these studies. JP thanks the EPSRC for a DTA award. KLN thanks the Royal Society for Newton Alumni Funding for support and CNPq for a BJT scholarship. This work is also supported in part by the Chemical Sciences, Geosciences, and Biosciences Division,

Office of Basic Energy Sciences, Office of Science, U.S. Department of Energy. A portion of this work was done under National Science Foundation grant No. PHY-0757749, and we acknowledge the EPSRC (UK) for supporting the experimental program in the UK.

REFERENCES

- [1] E. Weigold and I. E. McCarthy, *Electron Momentum Spectroscopy* (Kluwer Academic, Dordrecht/Plenum Publishers, New York, 1999).
- [2] T. N. Rescigno, M. Baertschy, W. A. Isaacs, and C. W. McCurdy, *Science* **286**, 2474 (1999).
- [3] M. Baertschy, T. N. Rescigno, W. A. Isaacs, X. Li, and C. W. McCurdy, **63**, 022712 (2001).
- [4] I. Bray, *J. Phys. B* **33**, 581 (2000).
- [5] I. Bray, *Phys. Rev. Lett.* **89**, 273201 (2002).
- [6] I. Bray, K. Bartschat, and A. T. Stelbovics, *Phys. Rev. A* **67**, 060704 (2003).
- [7] J. Colgan and M. S. Pindzola, *Phys. Rev. A* **74**, 012713 (2006).
- [8] I. Bray, D. V. Fursa, J. Röder, and H. Erhardt, *J. Phys. B* **30**, L101 (1997).
- [9] S. Rioual, J. Röder, B. Rouvellou, H. Erhardt, A. Pochat, I. Bray, and D. V. Fursa, *J. Phys. B* **31**, 3117 (1998).
- [10] A. T. Stelbovics, I. Bray, D. V. Fursa, and K. Bartschat, *Phys. Rev. A* **71**, 052716 (2005).
- [11] J. Colgan, M. S. Pindzola, G. Childers, and M. Khakoo, *Phys. Rev. A* **73**, 042710 (2006).

- [12] M. Dürr, C. Dimopoulou, B. Najjari, A. Dorn, and J. Ullrich, *Phys. Rev. Lett.* **96**, 243202 (2006).
- [13] M. Dürr, C. Dimopoulou, A. Dorn, B. Najjari, I. Bray, D. V. Fursa, Z. Chen, D. H. Madison, K. Bartschat, and J. Ullrich, *J. Phys. B* **39**, 4097 (2006).
- [14] O. Al-Hagan, C. Kaiser, D. H. Madison, and A. J. Murray, *Nature Physics* **5**, 59 (2008).
- [15] J. Colgan, M. S. Pindzola, F. Robicheaux, C. Kaiser, A. J. Murray, and D. H. Madison, *Phys. Rev. Lett.* **101**, 233201 (2008).
- [16] J. Colgan, O. Al-Hagan, D. H. Madison, C. Kaiser, A. J. Murray, and M. S. Pindzola, *Phys. Rev. A* **79**, 052704 (2009).
- [17] K. L. Nixon and A. J. Murray, *Phys. Rev. Lett.* **106**, 123201 (2011).
- [18] K. L. Nixon and A. J. Murray, *Phys. Rev. Lett.* **112**, 023202 (2014).
- [19] X. Ren, T. Pflüger, S. Xu, J. Colgan, M. S. Pindzola, J. Ullrich, and A. Dorn, *Phys. Rev. Lett.* **109**, 123202 (2012).
- [20] S. Amami, A. Murray, A. Stauffer, K. L. Nixon, G. S. J. Armstrong, J. Colgan, and D. H. Madison, *Phys. Rev. A* **90**, 062707 (2014); *Phys. Rev. A* **91**, 069906 (2015).
- [21] A. D. Stauffer, *Phys. Rev. A* **89**, 032710 (2014); *Phys. Rev. A* **89**, 049906 (2014)
- [22] M. S. Pindzola, F. Robicheaux, S. D. Loch, J. C. Berengut, T. Topcu, J. Colgan, M. Foster, D. C. Griffin, C. P. Ballance, D. R. Schultz, T. Minami, N. R. Badnell, M. C. Witthoef, D. R. Plante, D. M. Mitnik, J. A. Ludlow, and U. Kleiman, *J. Phys. B* **40**, R39 (2007).
- [23] J. Colgan and M. S. Pindzola, *Euro. Phys. J. D* **66**, 11 (2012).
- [24] G. S. J. Armstrong, J. Colgan, and M. S. Pindzola, *Phys. Rev. A* **88**, 042713 (2013).

- [25] M. E. Rose, Elementary Theory of Angular Momentum (John Wiley & Sons, New York, 1967).
- [26] J. Colgan, M. S. Pindzola, D. M. Mitnik, D. C. Griffin, and I. Bray, Phys. Rev. Lett. **87**, 213201 (2001).
- [27] J. Eiglsperger, B. Piraux, and J. Madroñero, Phys. Rev. A **81**, 042528 (2010).
- [28] M. Umair and S. Jonsell, J. Phys. B **47**, 225001 (2014).
- [29] D. Rakshit, K. M. Daily, and D. Blume, Phys. Rev. A **85**, 033634 (2012).
- [30] M. S. Pindzola, J. A. Ludlow, F. Robicheaux, J. Colgan, and D. C. Griffin, J. Phys. B **42**, 215204 (2009).

VIII. IONIZATION DIFFERENTIAL CROSS SECTION MEASUREMENTS FOR N_2 AT LOW INCIDENT ENERGY IN COPLANAR AND NON-COPLANAR GEOMETRIES

Ahmad Sakaamini¹, Sadek Amami², Andrew James Murray¹, Don Madison²

¹Photon Science Institute, School of Physics and Astronomy,

University of Manchester,

Manchester M13 9PL, UK

²Physics Department,

Missouri University of Science and Technology,

Rolla, MO 65409, USA

ABSTRACT

Ionization triple differential cross sections have been determined experimentally and theoretically for the neutral molecule N_2 over a range of geometries from coplanar to the perpendicular plane. Data were obtained at incident electron energies ~ 10 and ~ 20 eV above the ionization potential of the $3\sigma_g$, $1\pi_u$ and $2\sigma_g$ states, using both equal and non-equal outgoing electron energies. The data were taken with the incident electron beam in the scattering plane ($\psi=0^\circ$), at 45° to this plane and orthogonal to the plane ($\psi=90^\circ$). The set of nine measured differential cross sections at a given energy were then inter-normalized to each other. The data are compared to new calculations using various distorted wave methods, and differences between theory and experiment are discussed.

1. INTRODUCTION

Understanding electron impact ionisation of matter is important in areas ranging from plasma studies, through to detailing ionisation in biology and medicine, to understanding collisions in the Earth's atmosphere and in space. A complete description of the interaction requires quantum calculations to fully detail the collisions that occur. Testing of models is carried out by experiments that measure the probability of ionisation as a function of all parameters that describe the interaction [1][2]. For single ionisation by electron impact where the spins of the electrons are not detected, the interaction is fully characterised by the momentum of the incident electron k_0 as well as that of the scattered and ejected electrons k_1 and k_2 . A triple differential cross section $TDCS(k_0, k_1, k_2)$ is defined, that is directly proportional to the ionisation probability. This probability is determined by measuring the time-correlated signal between scattered and ejected electrons as a function of k_0 , k_1 and k_2 in an (e,2e) experiment.

Following the collision, the scattered and ejected electrons may emerge over 4π steradians, and so it is necessary to define a scattering geometry to allow the data to be compared to theory. In the experiments described here a detection plane is defined by the normal to the plane given by $\hat{n}_D = \hat{k}_1 \times \hat{k}_2$, the incident electron making an angle ψ with respect to this plane as shown in Figure 1. When $\psi = 0^\circ$ the incident electron is in the plane so that $\hat{k}_0 \cdot (\hat{k}_1 \times \hat{k}_2) = 0$. We define the quantization axis (QA) to be in the detection plane along the incident electron direction so that $QA = k_0(\psi = 0^\circ)$. If $\psi = 90^\circ$ the incident electron momentum k_0 is orthogonal to both outgoing electron momenta. For experiments where the outgoing electrons emerge on opposite sides of the plane $\theta_1 = \theta_2 = 90^\circ$. Under these conditions the detection plane is no longer well defined (since $k_1 \times k_2 = 0$) and so the triple differential cross section (TDCS) is independent of the angle ψ . A common point hence exists for all angles ψ when $\theta_1 = \theta_2 = 90^\circ$, so that at any given incident energy the data can be inter-normalized at this point. The (e,2e) spectrometer in Manchester allows ψ to vary from 0° to 90° . The outgoing electrons can be detected from $\theta_{1,2} = 35^\circ$ to 125° when

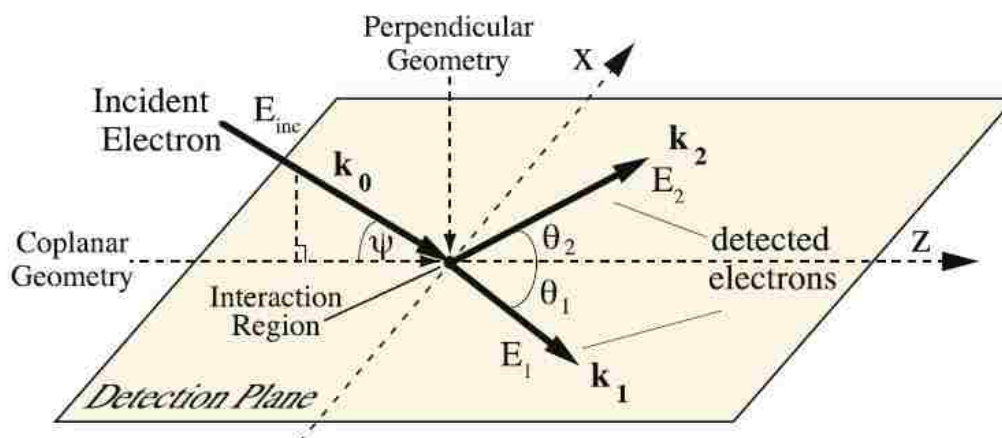


Figure 1. The experimental geometry adopted in this work. For details see text.

$\psi=0^\circ$ to 70° , this range extending to $\theta_{1,2} = 35^\circ$ to 140° when $\psi > 70^\circ$. These constraints are due to the physical size of the electron gun and electron detectors. N_2 is the lightest diatomic molecule apart from H_2 that can easily be studied, since a molecular beam of N_2 can be delivered to the interaction region from a gas needle. H_2 has been extensively investigated both experimentally and theoretically [3–7], leading to considerable progress in understanding the dynamics of the ionizing collision with a molecular target. Models of the interactions include both time-independent studies using distorted wave calculations [3], as well as time-dependent models that use close-coupling techniques [4]. These models have been tested by experiment in both high and low energy regimes, under a wide variety of kinematic conditions [5–7]. Modelling the ionisation of molecules by electron impact is considerably more complex than for atomic targets, since they can have internal energy in rotational and vibrational motion, and their electronic structure is inherently non-spherical due to their distributed nuclei. Almost all (e,2e) experiments carried out so far do not determine the nuclear orientation during the collision, and so the calculations must average over all possible orientations of the target. The energy resolution in most experiments is also insufficient to resolve the rotational and vibrational motion of the target, and so it is necessary to further average over the different states that may contribute. It is possible to determine

individual vibrational contributions from selected targets using energy-selected electron guns, however very few studies have been carried out so far due to the low coincidence yield in these experiments [8].

Several (e,2e) experiments and theoretical calculations have already been carried out from an N_2 target, however these have mostly been in an asymmetric coplanar geometry at medium to high incident energies [9 -16]. By contrast, the work presented here is at low energies in a symmetric configuration. In this regime the cross section is highly sensitive to different collision process including exchange, distortions to the wave-fronts describing the incident, scattered and ejected electrons, target polarisation and post collisional interactions as the electrons leave the interaction region. Calculation of the cross sections in this energy region is hence very challenging, as approximations that are often adopted at higher energies cannot be used.

This paper is divided into five sections. Following this introduction the experimental procedures used to measure the data are briefly described. A description of the theoretical models used to calculate the relevant cross sections is then presented. Section 4 compares the data to results from three different distorted wave models, and differences between these are discussed. Section 5 then summarises these studies so far, and considers the next steps that are required in these investigations.

2. EXPERIMENTAL PROCEDURES

N_2 is a stable diatomic molecule that has 10 valence electrons and 4 core electrons. The valence electrons combine to produce the strong triple bond in the N_2 molecule, the electrons pairing to form the $3\sigma_g^2, 1\pi_u^4$ and $2\sigma_g^2$ bonding orbitals and the $2\sigma_u^2$ anti-bonding orbital. The $2\sigma_g^2$ orbital is the deepest valence state, and has a binding energy more than 20eV higher than that of the $2\sigma_u^2$ orbital. The ground state electronic configuration of N_2 is hence $(2\sigma_g^2 2\sigma_u^2 1\pi_u^2 3\sigma_g^2)^1 \Sigma_g^+$. Ionization can occur from each orbital, leading to N_2^+ ions in different final states. In the work presented here measurements were taken from the three

outer orbitals. This produces the $X^2 \Sigma_g^+ N_2^+$ state for ionization from the $3\sigma_g$ orbital, the $A^2 \Pi_u$ state when electrons are ejected from the $1\pi_u$ orbital, and the $B^2 \Sigma_u^+$ state for ejection of electrons from the $2\sigma_u$ orbital.

An example of the ionization binding energy spectrum produced from different orbitals is shown in Figure 2, taken with the (e,2e) spectrometer in Manchester. The incident electron gun was unselected in energy, and the electron momentum analysers were set to optimise the signal energy resolution while ensuring the best yield for coincidence counting. In this example, the electron analysers each detected electrons with an energy ~ 4.6 eV, and coincidence counts were measured at angles $\theta_1 = \theta_2 = 45^\circ$. The figure shows the results from three different incident electron angles with (a) $\psi = 0^\circ$, (b) $\psi = 45^\circ$ and (c) $\psi = 90^\circ$. The data were obtained by measuring the coincidence yield over a range of incident energies from 23 eV to 29 eV, in steps of 0.125 eV. The data were accumulated for 5000 seconds at each energy, and the results were then normalised to unity at the peak of the $3\sigma_g$ state in a coplanar geometry.

Figure 2 demonstrates that the experimental apparatus can resolve the contribution from each of the orbitals of the molecule, and shows that the cross-section depends on the individual states that are ionized. The spectral scans at each angle ψ were taken under the same operating conditions, and so were used to inter-normalise the results from each of the individual orbitals. The data at different angles ψ were then inter-normalised through the common point at $\theta_1 = \theta_2 = 90^\circ$. Binding energy spectra similar to Figure 2 were taken for each of the data sets that were measured, so that all data at any given energy could be normalised to a common point.

Three sets of coincidence data were taken for outgoing electron energies of (4.6 eV, 4.6 eV), (9.7 eV, 9.7 eV) and (14.5 eV, 4.6 eV), with incident beam angles of $\psi = 0^\circ$, $\psi = 45^\circ$ and $\psi = 90^\circ$. 27 individual angular data sets for the TDCS were hence obtained during this study. The data were accumulated using up to 10 sweeps of the detection plane, with coincidence measurements being taken typically for 5000s at each scattering angle. In all of the

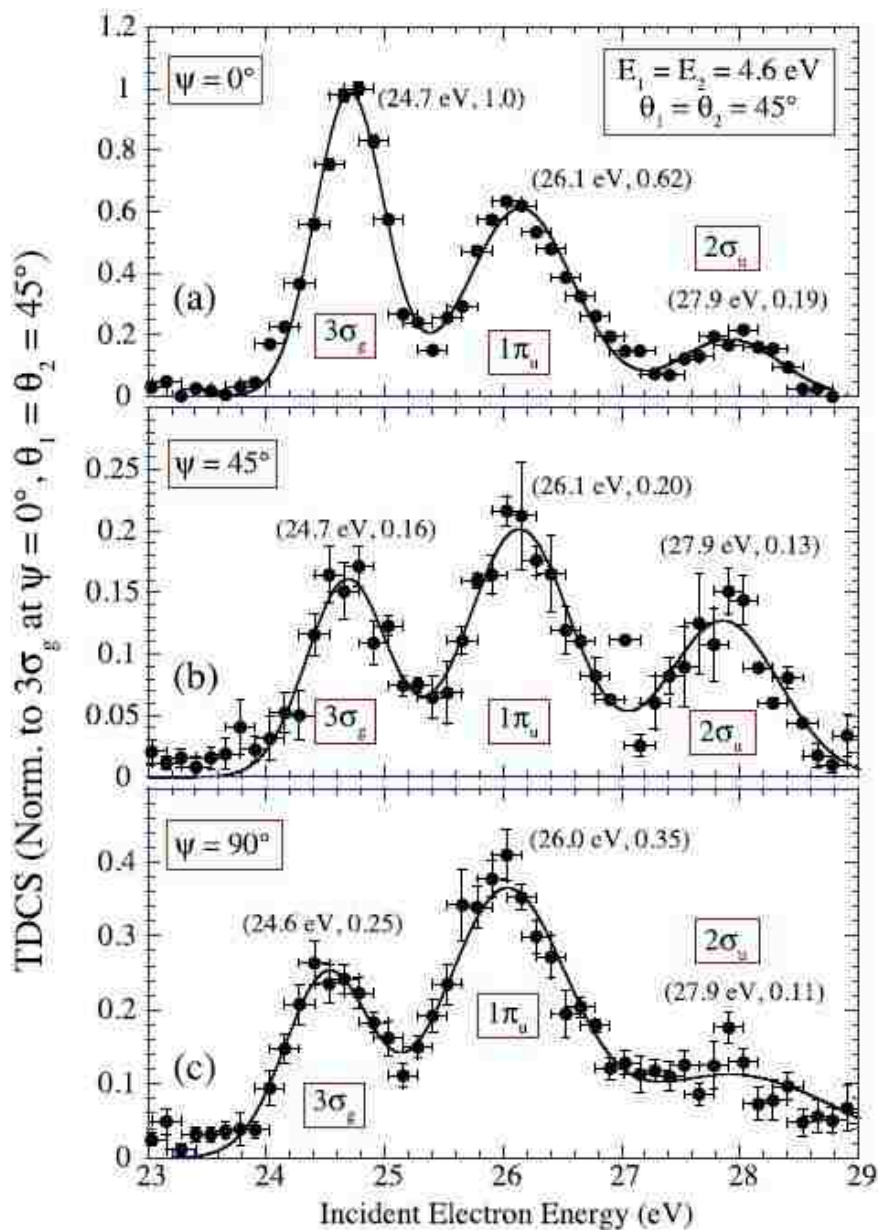


Figure 2. Binding energy spectra for outgoing electron energies of $4.6 \sim \text{eV} \pm 0.5 \text{ eV}$ taken with the electrons detected at a forward angle of 45° to the z -axis. The results are shown for (a) the coplanar geometry, (b) for the incident electron at $\psi = 45^\circ$ to the detection plane, and (c) for the perpendicular geometry ($\psi = 90^\circ$). Gaussians are fitted to the data for each state, so that the relative contributions and their peak energies could be determined. The peak of the $3\sigma_g$ state in a coplanar geometry was set to unity, and all data were then inter-normalised to this peak as discussed in the text.

data sets a symmetric geometry was chosen, so that $\theta_1 = \theta_2 = \theta$. The measurements at each angle θ were then averaged, and their respective uncertainties calculated from the standard error on the mean. In each data set the cross sections were inter-normalised to the peak of the $3\sigma_g$ in a coplanar geometry as discussed above. All experimental TDCS measurements at any given energy were hence placed on a common scale. The energy of the electrons emitted from the electron gun were calibrated against the 19.337 eV elastic resonance in helium [17], whereas the energies of the scattered and ejected electrons detected by the electron energy analysers were determined from inelastic scattering resonances in this target. Helium was chosen for this calibration as its resonances are very well known [18], and since it has no ro-vibrational structure. These energy calibrations were carried out both before and after each set of measurements were made, so as to allow for any variation in the spectrometer operating conditions over time. The typical operating pressure in the vacuum chamber during data accumulation was $\sim 2 \times 10^{-5}$ torr, with a base pressure of 1×10^{-7} torr. The incident electron beam current was set at ~ 200 nA so that the coincidence signal could be easily resolved from the background. The timing window of the time-to-amplitude converter was set to 500 ns, and a delay time of ~ 300 ns was added to the stop signal so that the coincidence peak was positioned close to the centre of the timing spectrum. The spectrometer operated under computer control, the analyser tuning conditions being optimised each time the analysers were moved to a new angle. In this way changes in the operating conditions of the spectrometer as the experiments proceeded could be minimised. Full details of the computer control and optimisation systems used in these experiments can be found in [19].

3. THEORY

We have used three different theoretical models to calculate the TDCS for the N_2 molecule—the molecular three-body distorted wave (M3DW) approximation, the distorted wave Born approximation (DWBA), and the DWBA using the Ward–Macek (WM) approx-

imation for the final state electron–electron interaction, which is normally called the post-collision interaction (PCI). All these approaches have been described in detail previously in several references [2, 3] and [7, 11, 20, 21]. Here we will only give a brief summary of the models to show their differences and similarities. Because the DWBA is a special case of the more general M3DW approximation, we will start our discussion with the M3DW.

3.1. The M3DW Approximation. M3DW

The M3DW direct scattering T -matrix can be written as,

$$T_{dir}^{M3DW} = \langle \Psi_f | W | \Psi_i \rangle \quad (1)$$

Here Ψ_f and Ψ_i are the final- and initial-state wave functions for the system respectively, and W is the perturbation. The initial-state wavefunction Ψ_i is approximated as a product of a distorted wave function $\chi_0^+(\mathbf{r}_1)$ for the incoming electron (the projectile) times the initial Dyson bound state wavefunction $\phi_{Dy}(\mathbf{r}_2)$ for the target N_2 molecule which is averaged over all molecular orientations.

$$\Psi_i = \chi_0^+(\mathbf{r}_1) \phi_{Dy}(\mathbf{r}_2) \quad (2)$$

The final-state wavefunction Ψ_f for the two outgoing electrons, called the scattered and ejected electrons for convenience, is approximated as a product of two final-state continuum electron distorted waves ($\chi_1^-(\mathbf{r}_1)$ and $\chi_2^-(\mathbf{r}_2)$), and the Coulomb interaction between the outgoing electrons ($C_{12}(\mathbf{r}_{12}, \mathbf{k}_{12})$), so that

$$\Psi_f = \chi_1^-(\mathbf{r}_1) \chi_2^-(\mathbf{r}_2) C_{12}(\mathbf{r}_{12}, \mathbf{k}_{12}) \quad (3)$$

where

$$C_{12}(\mathbf{r}_{12}, \mathbf{k}_{12}) = e^{-\pi\gamma/2\Gamma(1-i\gamma)} {}_1F_1(i\gamma, 1, -i[k_{12}r_{12} + \mathbf{k}_{12} \cdot \mathbf{r}_{12}]) \quad (4)$$

Here $\Gamma(1 - i\gamma)$ is a gamma factor, ${}_1F_1$ is a confluent hypergeometric function, r_{12} is the

relative distance between the two electrons, v_{12} is the relative velocity between the two continuum electrons, and $k_{12} = \mu v_{12}$ where k_{12} is the relative momentum, $\mu = \frac{1}{2}$ is the reduced mass for the two electrons in atomic units, and $\gamma = 1/v_{12}$ is the Sommerfeld parameter. When the PCI term is included directly in the final state wavefunction, PCI is included to all orders of perturbation theory. Finally the perturbation W is given by,

$$W = V - U_i \quad (5)$$

where V is the exact initial state interaction between the neutral molecule and the projectile (in this case the incident electron), and U_i is an initial state spherically symmetric approximation for V .

With these approximations, the direct M3DW T -matrix becomes

$$T_{dir}^{M3DW} = \langle \chi_1^-(\mathbf{r}_1) \chi_2^-(\mathbf{r}_2) C_{12}(\mathbf{r}_{12}, \mathbf{k}_{12}) | W | \chi_i^+(\mathbf{r}_1) \phi_{Dy}(\mathbf{r}_2) \rangle \quad (6)$$

The M3DW approximation has been shown to give very good agreement with experiment for ionization of H_2 [7, 22] for energies down to threshold and for N_2 [14, 20, 23, 24] for higher incident energy electrons.

3.2. The DWBA Approximation. In the T -matrix of the standard DWBA approximation, the interaction between the two continuum electrons in the final state C_{12} is omitted in the approximation for the final-state wavefunction. Thus the DWBA T -matrix is

$$T_{dir}^{M3DW} = \langle \chi_1^-(\mathbf{r}_1) \chi_2^-(\mathbf{r}_2) C_{12}(\mathbf{r}_{12}, \mathbf{k}_{12}) | W | \chi_i^+(\mathbf{r}_1) \phi_{Dy}(\mathbf{r}_2) \rangle \quad (7)$$

In the DWBA, PCI is included only to first order.

3.3. DWBA. The DWBA Approximation In this approximation, the Ward-Macek (WM) approximation for PCI has been used [25] for the Coulomb interaction of Equation (4). In the WM approximation, the term $[k_{12}r_{12} + \mathbf{k}_{12} \cdot \mathbf{r}_{12}]$ in the hypergeometric function

is replaced by $2k_{12}r_{12}^{ave}$, where r_{12}^{ave} is the average value of the electron-electron separation.

$$C_{12}^{WM}(r_{ave}, k_{12}) = e^{\frac{-\pi\gamma}{2}} \Gamma(1 - i\gamma) {}_1F_1(i\gamma, 1, -2ik_{12}r_{ave}) \quad (8)$$

Since this factor does not depend on the coordinates being integrated, it can be factored from the integral in the T -matrix and the direct WM T -matrix becomes

$$T_{dir}^{WM} = C_{12}^{WM}(r_{ave}, k_{12}) \langle \chi_1^-(\mathbf{r}_1) \chi_2^-(\mathbf{r}_2) | W | \chi_i^+(\mathbf{r}_1) \phi_{Dy}(\mathbf{r}_2) \rangle \quad (9)$$

or

$$T_{dir}^{WM} = C_{12}^{WM}(r_{ave}, k_{12}) T_{dir}^{DWBA} \quad (10)$$

Finally in all three models, the triple differential cross section (TDCS) in atomic units can be written as,

$$TDCS = \frac{d^5\sigma}{d\Omega_1 d\Omega_2 dE_2} = \frac{1}{(2\pi)^5} \frac{k_1 k_2}{k_i} (|T_{dir}|^2 + |T_{exc}|^2 + |T_{dir} - T_{exc}|^2) \quad (11)$$

Here k_i , k_1 , and k_2 are the magnitudes of the momenta of the initial, the scattered, and the ejected electrons, respectively and T_{exc} is the exchange T -matrix which is calculated similar to T_{dir} except that the two final state electrons are interchanged in the final state wavefunction Ψ_f .

4. COMPARISON OF THEORY TO EXPERIMENT

Figures 3–5 show the complete set of data compared to the three different models described in section 3. Figures 3 and 4 show results when $E_1 = E_2$, whereas Figure 5 shows data when $E_1 \neq E_2$. Figure 3 is for outgoing electron energies of $4.6 \text{ eV} \pm 0.5 \text{ eV}$, Figure 4 shows results when $E_1 = E_2 = 9.7 \text{ eV}$, and Figure 5 shows results for $E_1 = 14.5 \text{ eV}$, $E_2 = 4.6 \text{ eV}$. In all cases $\theta_1 = \theta_2 = \theta$.

Since the experiments did not measure an absolute cross section, the maximum in the data for the $3\sigma_g$ state has been normalised to the peak of the M3DW theory in a coplanar geometry at each energy. All other experimental data in each Figure were then inter-normalised to this peak, as described above. The common point at $\theta_1 = \theta_2 = 90^\circ$ is highlighted with a red circle in each Figure. The calculated theoretical cross sections are all on an absolute scale, and so they could be directly compared to each other. Nine sets of data are shown in each Figure. The first column shows the results from ionizing the $3\sigma_g$ state for (a) $\psi = 0^\circ$, (b) $\psi = 45^\circ$ and (c) $\psi = 90^\circ$. The middle column shows results from the $1\pi_u$ state, whereas the final column shows results from the $2\sigma_u$ state. The M3DW calculation is shown as a solid black curve, the DWBA calculation is shown as a red coarse-dashed curve, and the calculation that includes the WM interaction term for PCI is shown as a blue finely-dashed curve. In all cases when the outgoing electrons have equal energy (as in Figures 3 and 4), PCI between the electrons force the TDCS to be zero at $q = 0^\circ$ and 180° . This can be seen most clearly for both the M3DW and WM models.

Figure 3 shows the results for outgoing electron energies of $4.6 \text{ eV} \pm 0.5 \text{ eV}$ plotted on a logarithmic scale. The coplanar data for the $3\sigma_g$ state indicate that the TDCS is dominated by forward scattering in this geometry, with the peak in the cross section being found at $\theta = 45^\circ$. A minimum occurs at $\theta = 90^\circ$ and the cross section then increases again at higher scattering angles. When the incident electron beam is raised out of the plane, the measured TDCS is no longer dominated by forward scattering. The $3\sigma_g$ data for $\psi = 45^\circ$ indicates that the electrons are preferentially back scattered at this energy, with the cross section being relatively uniform as the scattering angle changes. The TDCS in the perpendicular plane must be symmetric around $q = 90^\circ$, and this is borne out in the data. As for the results at $\psi = 45^\circ$, the measured TDCS shows little structural change under these conditions, and is largely uniform in magnitude over a wide range of scattering angles. The experimental data for the $1\pi_u$ state follows a similar trend to that of the $3\sigma_g$ state, with a maximum in the forward direction for a coplanar geometry, and a slight backscattering dominance when

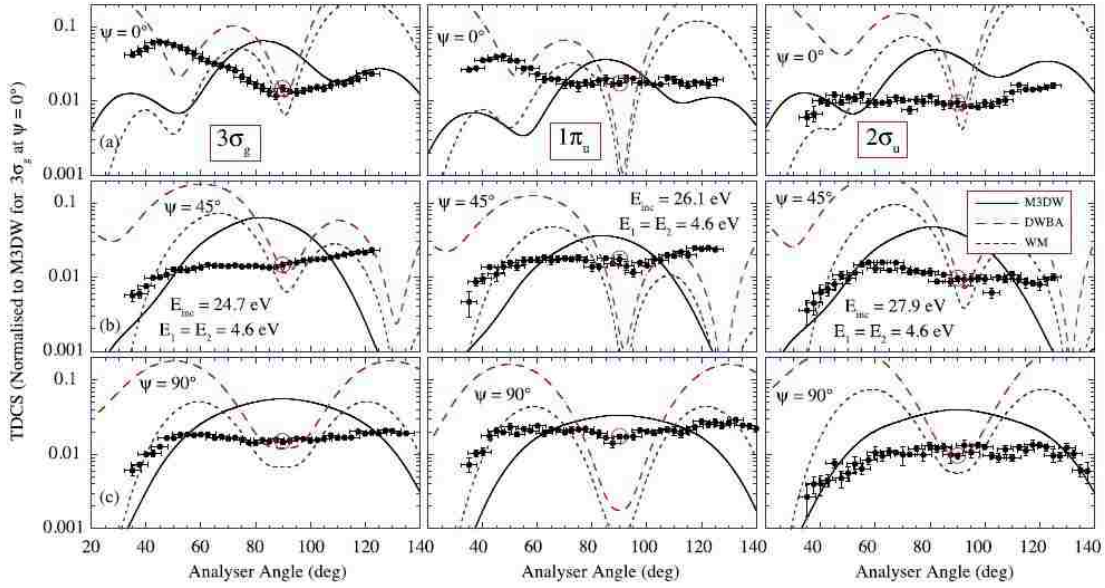


Figure 3. Normalised TDCS data for outgoing electron energies of $4.6 \text{ eV} \pm 0.5 \text{ eV}$ in (a) a coplanar geometry, (b) for the incident electron at 45° to the detection plane, and (c) for the perpendicular geometry. The peak of the experimental data for the $3\sigma_g$ state are set equal to that of the M3DW calculations. The coplanar data for the $1\pi_u$ and $2\sigma_u$ states are then set relative to the $3\sigma_g$ state using the binding energy spectra in Figure 2. The common normalisation point when $\theta_1 = \theta_2 = 90^\circ$ is then used to inter-normalise all data sets which are plotted on a logarithmic scale

$\psi = 45^\circ$. The coplanar forward peak and backscatter peaks are however not as pronounced as for the $3\sigma_g$ state. By contrast, the data from the $2\sigma_u$ state changes little as the incident electron beam direction is changed. In all cases the TDCS measurements for this state are relatively uniform as the scattering angles changed in the experiment, indicating that the scattering dynamics from the $2\sigma_u$ state has no particular preference for either forward or backward scattering. The theoretical calculations at this energy show a very different trend to the experimental data. The DWBA calculation does not include PCI to all orders, and the large difference between this calculation and the data clearly shows the importance of its inclusion. In all cases the DWBA theory over-estimates the cross section, and predicts features that are not seen in the data. Inclusion of the WM interaction significantly improves

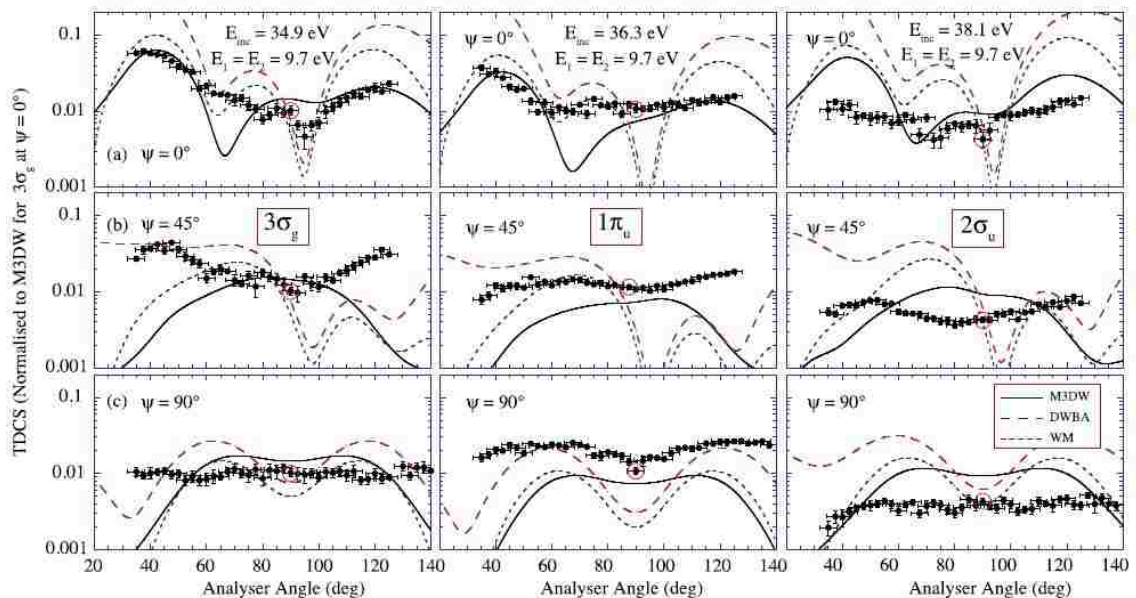


Figure 4. Normalised TDCS data for outgoing electron energies of $9.7 \text{ eV} \pm 0.5 \text{ eV}$ taken in (a) a coplanar geometry, (b) for the incident electron at 45° to the detection plane, and (c) for a perpendicular geometry. The peak of the experimental data for the $3\sigma_g$ state are set to that of the M3DW calculations at this energy. The data are then inter-normalised as described in Figure 3.

the results compared to experiment, however once again this calculation predicts structures that are not observed. The WM theory does however produce peaks that are in the same position as the data in non-coplanar geometries.

The M3DW calculation includes the effects of PCI exactly, and so it would seem that it should provide the most accurate estimate of post-collisional interactions. Somewhat surprisingly this calculation does not improve the results from the WM theory, but rather predicts structures that are in disagreement with the data in all cases. This theory predicts that the TDCS should be dominated by a peak near $\theta = 90^\circ$, as was found for helium at similar energies [26]. It would appear that at these energies the M3DW theory is including PCI too strongly, compared to other scattering processes that lead to ionisation. In earlier works for low energy ionisation of H_2 , we also found that the M3DW overestimated the effects of PCI and that the WM model agreed better with experiment [7]. It is also interesting to note

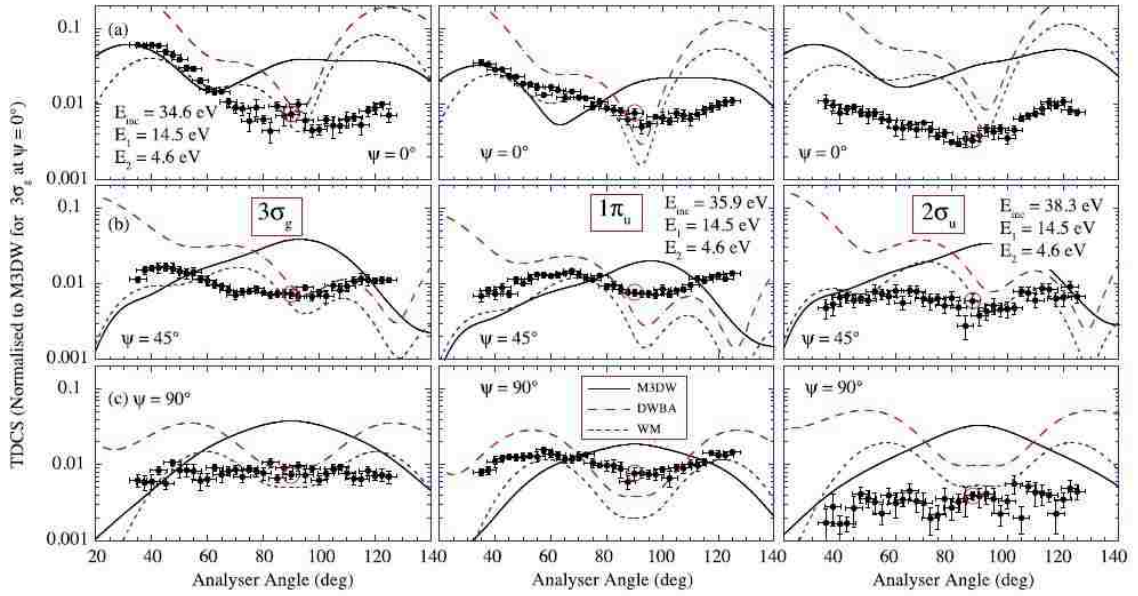


Figure 5. Normalised TDCS data for outgoing electron energies of $4.6 \text{ eV} \pm 0.5 \text{ eV}$ and $14.5 \text{ eV} \pm 0.5 \text{ eV}$ taken in (a) a coplanar geometry, (b) for the incident electron at 45° to the detection plane, and (c) for the perpendicular geometry. The peak of the experimental data for the $3\sigma_g$ state are set to that of the M3DW calculations at this energy. The data are then inter-normalised as described in Figures 3 and 4.

that the M3DW calculation predicts a maximum when $\theta = 90^\circ$ in the perpendicular plane, in contrast to the WM and DWBA theories that predict a minimum. Figure 4 details the results for equal outgoing electron energies of $9.7 \text{ eV} \pm 0.5 \text{ eV}$, and show a much improved comparison between theory and experiment, particularly for the M3DW calculation. Once again for the $3\sigma_g$ and $1\pi_u$ states, forward scattering dominates in a coplanar geometry. The data for $\psi = 45^\circ$ also has more structure than at the lower energy for these states. In the perpendicular plane the data are again broadly featureless as a function of scattering angle, although the data from the $1\pi_u$ state appears to have two broad peaks with a minimum at $\theta = 90^\circ$. The data for the $2\sigma_u$ state again shows very little change with either scattering angle or incident angle at this energy. At this energy the DWBA theory again fails to predict the measured TDCS, however inclusion of the WM approximation for PCI now greatly improves this comparison. The M3DW calculation is the most accurate in the coplanar

geometry, with the calculation closely emulating the data for both the $3\sigma_g$ and $1\pi_u$ states. None of the calculations predict the results for the $2\sigma_u$ state in this geometry. As the incident electron beam is raised out of the scattering plane the calculations more closely emulate the magnitude of the data compared to the lower energy results in Figure 3. The WM calculation more closely emulates the data for both the $3\sigma_g$ and $1\pi_u$ states under these conditions, although none of the calculations predict the data accurately. The calculations for the $2\sigma_u$ state do not agree with the data for any of the incident electron angles.

The final set of results for all three states shown in Figure 5 relax the ‘doubly symmetric’ conditions of the experiment and choose different energies of the outgoing electrons, with $E_1 = 14.5$ eV and $E_2 = 4.6$ eV. The incident electron energies are hence similar to that chosen for the measurements in Figure 4, with the incident energies set by fitting to the data in the binding energy spectrum under these conditions. Once again the data for the $3\sigma_g$ and $1\pi_u$ states in a coplanar geometry are dominated by forward scattering, however the peaks are less pronounced than when the outgoing electron energies are equal. The results when $\psi = 45^\circ$ for these states lie somewhere between those found in Figures 3 and 4, whereas the data in the perpendicular plane is once again broadly featureless as the scattering angle changes. The data for the innermost $2\sigma_u$ state again shows little variation as both q and ψ are varied. The DWBA calculation once more fails to predict the data, whereas the WM calculation now agrees most closely with the results from experiment for the $3\sigma_g$ and $1\pi_u$ states. The M3DW calculation again appears to overestimate the effects of PCI, producing a dominant peak at $\psi = 90^\circ$ in the perpendicular plane that is not seen in the data. Both WM and M3DW calculations predict a higher coplanar cross section in the backward direction than is found in the data. The WM calculation more closely emulates the data under non-coplanar conditions. In all cases the calculations again do not predict the results from the $2\sigma_u$ state. The final set of results shown in Figure 6 are for ionisation from the $3\sigma_g$ state at an incident energy ~ 40 eV above the ionisation potential, to ascertain how each model compares to experiment at this higher energy. No data were taken for the

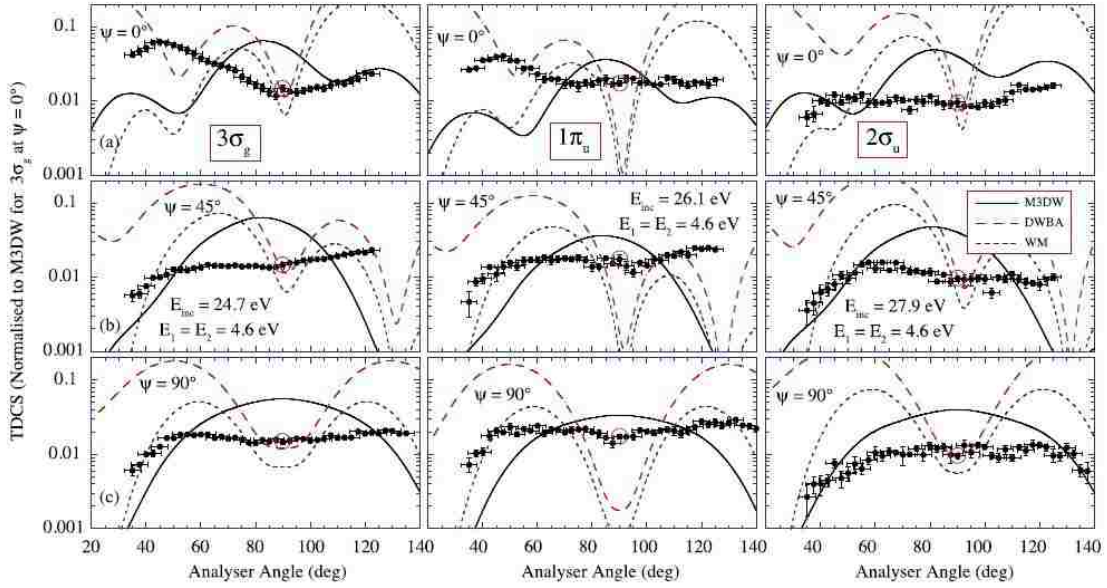


Figure 6. Normalised TDCS data for equal outgoing electron energies of 20 eV \sim 0.5 eV taken in (a) a coplanar geometry, (b) for the incident electron at 45° to the detection plane, and (c) for the perpendicular geometry. The peak of the experimental data for the $3\sigma_g$ state are set to that of the M3DW calculations at this energy. The data are then inter-normalised to the common point.

$1\pi_u$ or $2\sigma_u$ states under these conditions. There is an overall improvement in the coplanar geometry compared to the results at lower energies, particularly in the forward direction where both M3DW and WM models closely emulate the position of the peak in the TDCS. This comparison is less satisfactory at higher scattering angles in this plane. By contrast, the DWBA model agrees most closely with the data for $\psi = 45^\circ$, with both M3DW and WM models underestimating the cross section under these conditions. The agreement for all models is better in the perpendicular plane, although all underestimate the cross section when compared to the data. Overall, it appears that the models are becoming progressively more accurate as the incident energy increases.

5. DISCUSSION AND CONCLUSIONS

The results from these experiments on N_2 show that the ionisation cross-section is very sensitive to both the state from which the ionisation occurs, and the collisional energy of the interaction. The data have been presented over a range of angles from a coplanar geometry through to the perpendicular plane, allowing the data at any given energy to be normalised to a single point. Binding energy spectra were also taken that allowed data from the outermost $3\sigma_g$, $1\pi_u$ and $2\sigma_u$ states to be inter-normalised. These data have been presented for out-going electron energies $E_1 = E_2 = 4.6$ eV, $E_1 = E_2 = 9.7$ eV and $E_1 = 14.5$ eV, $E_2 = 4.6$ eV. Calculations based upon distorted wave methods have also been shown, with three different theories showing the sensitivity of PCI to the scattering process. The importance of post collisional interactions in the model have been demonstrated, with both the WM approximation and a full three-body calculation having been used. It is found that in some cases the full three-body calculation overestimates the effects of PCI, and that the WM approximation proves more accurate. A similar observation was found in earlier low energy ionisation of H_2 . Theory more closely approaches the data as the energy is increased, and so it will be interesting to see if further increases in the energy will improve these comparisons. Additional experiments to test this hypothesis are currently underway.

ACKNOWLEDGMENTS

AS would like to thank the University of Manchester for financial support through their overseas student award. SA and DM would like to acknowledge the support of the US National Science Foundation under Grant No. PHY-1505819 and CN would like to acknowledge the support of the National Natural Science Foundation of China under Grant No. 11174175.

REFERENCES

- [1] E. Weigold and I. E. McCarthy, *Electron Momentum Spectroscopy* (Kluwer Academic, Dordrecht/Plenum Publishers, New York, 1999).
- [2] Madison D H and Al-Hagan O, *J. At. Mol. Opt. Phys.* **2010** 367180 (2010).
- [3] Colgan J, Al-Hagan O, Madison D H, Kaiser C, Murray A J and Pindzola M S *Phys. Rev. A* **79**, 052704 (2009).
- [4] Colgan J, Pindzola M S, Robicheaux F, Kaiser C, Murray A J and Madison D H *Phys. Rev. Lett.* **101**, 233201 (2008).
- [5] Staicu-Casagrande E M et al, *J. At. Mol. Opt. Phys.* **411**, 025204 (2008).
- [6] Ren X et al *Phys. Rev. A* **82** 032712 (2010)
- [7] Al-Hagan O, Murray A J, Kaiser C, Colgan J and Madison D H, *Phys. Rev. A* **81** 030701 (2010)
- [8] Doering J P and Yang J, *Phys. Rev. A* **60** 2176 (1999)
- [9] Toth I and Nagy L, *J. Phys. B: At. Mol. Opt. Phys.* **44** 195205 (2011)
- [10] Naja A, Staicu-Casagrande E M, Lahmam-Bennani A, Nekkab M, Mezdari F, Joulakian B, Chuluunbaatar O and Madison D H, *J. Phys. B: At. Mol. Opt. Phys.* **40** 3775 (2007)
- [11] Gao J, Madison D H and Peacher J L, *Phys. Rev. A* **72** 032721 (2005)
- [12] Lahmam-Bennani A, Staicu-Casagrande E M and Naja A, *J. Phys. B: At. Mol. Opt. Phys.* **42** 235205 (2009)
- [13] Avaldi L, Camilloni R, Fainelli E and Stefani G, *J. Phys. B: At. Mol. Opt. Phys.* **25** 3551 (1992)

- [14] Murray A J, Hussey M J, Gao J and Madison D H, *J. Phys. B: At. Mol. Opt. Phys.* **39** 3945 (2006)
- [15] Murray A J, Hussey M J, Kaiser C, Gao J and Madison D H *J. Electron Spec.* **161** 11 (2007)
- [16] Murray A J *J. Phys. B: At. Mol. Opt. Phys.* **48** 245203 (2015)
- [17] Brunt J N H, King G C and Read F H *J. Phys. B: At. Mol. Opt. Phys.* **10** 1289 (1977)
- [18] Kramida A, Ralchenko Y and Reader J, NIST Atomic Spectra Database (<http://physics.nist.gov/asd>) (2015)
- [19] Murray A J, Turton B C H and Read F H, *Rev. Sci. Instrum.* **63** 3346 (1992)
- [20] Gao J F, Madison D H and Peacher J L, *J. Chem. Phys.* **123** 204314 (2005)
- [21] Nixon K L, Murray A J, Chaluvadi H, Amami S, Madison D H and Ning C, *J. Chem. Phys.* **136** 094302 (2012)
- [22] Al-Hagan O, Kaiser C, Madison D and Murray A, *Nat. Phys.* **5** 59 (2009)
- [23] Gao J, Madison D H and Peacher J L, *Phys. Rev. A* **72** 020701 (2005)
- [24] Hargreaves L R, Colyer C, Stevenson M A, Lohmann B, Al-Hagan O, Madison D H and Ning C G, *Phys. Rev. A* **80** 062704 (2009)
- [25] Ward S J and Macek J H, *Phys. Rev. A* **49** 1049 (1994)
- [26] Murray A J, Read F H and Bowring N J, *J. Phys. B: At. Mol. Opt. Phys.* **30** 387 (1997)

IX. ELECTRON-IMPACT IONIZATION OF H₂O AT LOW PROJECTILE ENERGY: INTERNORMALIZED TRIPLE-DIFFERENTIAL CROSS SECTIONS IN THREE-DIMENSIONAL KINEMATICS

Xueguang Ren,¹ Sadek Amami,² Khokon Hossen,¹ Esam Ali,² ChuanGang Ning,³

James Colgan,⁴ Don Madison,² and Alexander Dorn,¹

¹Max-Planck-Institut für Kernphysik,

69117 Heidelberg, Germany

²Physics Department,

Missouri University of Science and Technology,

Rolla, Missouri 65409, USA

³Department of Physics, State Key Laboratory of Low-Dimensional Quantum Physics,

Tsinghua University,

Beijing 100084, China

⁴Theoretical Division, Los Alamos National Laboratory,

Los Alamos, New Mexico 87545, USA

ABSTRACT

We report a combined experimental and theoretical study on the electron-impact ionization of water (H₂O) at the relatively low incident energy of $E_0 = 81$ eV in which either the $1b_1$ or $3a_1$ orbitals are ionized leading to the stable H₂O⁺ cation. The experimental data were measured using a reaction microscope, which can cover nearly the entire 4π solid angle for the secondary electron emission over a range of ejection energies. We present experimental data for the scattering angles of 6° and 10° for the faster of the two outgoing electrons as function of the detection angle of the secondary electron with energies of 5 eV and 10 eV. The experimental triple-differential cross sections are internormalized across

the measured scattering angles and ejected energies. The experimental data are compared to predictions from two molecular three-body distorted-wave approaches. One applying the orientation-averaged molecular orbital (OAMO) approximation and one using a proper-average (PA) over orientation-dependent cross sections. The PA calculations are in better agreement with the experimental data than the OAMO calculations, for both the angular dependence and the relative magnitude of the observed cross section structures.

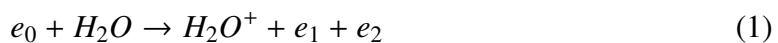
1. INTRODUCTION

Electron-impact ionization dynamics of atoms and molecules have been of great interest from both theoretical and experimental points of view. It plays a crucial role in a variety of scientific and practical applications ranging from radiation chemistry and biology to astrophysics and atmospheric sciences [1, 2]. It has been discovered recently that low-energy electrons can significantly induce DNA strand breaks via the dissociative electron attachment resonances and a superposition of various nonresonant mechanisms related to excitation dissociation and ionization processes [3, 4].

The water molecule (H_2O) is important in this respect, since it is ubiquitous on earth and surrounds all biological matter. Understanding the ionization dynamics requires a detailed knowledge of the interaction probabilities (i.e. the cross sections). A comprehensive way of characterizing the electron-impact ionization dynamics is to detect the two outgoing electrons in coincidence, the so-called (e,2e) studies [5, 6], which determine the momentum vectors of all final-state particles. The quantity measured in the (e, 2e) experiments is the triple-differential cross section (TDCS), i.e., a cross section that is differential in the solid angles of both electrons and the energy of one of them. The energy of the other electron is given by energy conservation [7, 8]. Such kinematically complete experiments serve as a powerful tool to comprehensively test theoretical models that account for the quantum few-body dynamics which are important to aid in the development of theoretical models and to provide the input parameters in Monte Carlo simulation in medical radiation therapy.

In recent years, theory has made tremendous progress in describing the electron-impact ionization dynamics of simple atoms and molecules, see e.g. [9, 10, 11, 12, 13, 14, 15, 16, 17]. Much more challenging, however, is the treatment of more complex targets, like heavy atoms and molecules. Electron-impact ionization dynamics of the water molecule has been previously studied by the Lohmann group in the coplanar asymmetric geometry at $E_0 = 250$ eV using a conventional (e, 2e) spectrometer to examine ionization of the $2a_1$, $1b_2$, $3a_1$ and $1b_1$ states of H_2O [18]. Murray and coworkers performed coplanar symmetric and asymmetric (e, 2e) studies for the $1b_1$ state of H_2O [19] and symmetric coplanar and non-coplanar studies for the $3a_1$ state of H_2O at low impact energies [20]. Several models have been developed to describe the ionization dynamics of H_2O . The agreement between theories and experiments, however, is not as good as results for the ionization of simple targets, see e.g. [18, 19, 20, 21, 22, 23, 24, 25, 26]. Recent calculation of (e, 2e) on CH_4 using the molecular three-body distorted-wave approximation found that the method with proper averages (PA) is in much better agreement with experiment than the orientation-averaged molecular orbitals (OAMO) calculations [27]. On the other hand, experimental techniques were recently developed that allow for simultaneously accessing a large fraction of the entire solid angle and a large range of energies of the continuum electrons in the final state [28, 29], the entire angular acceptance for the slow ejected electron within the scattering plane [30] and, more recently, the measurements of internormalized cross sections [13, 31, 32] which makes the data relatively absolute. Thus, theories can be tested significantly more comprehensively over a large range of the final state phase space.

In the present work, we perform a kinematically complete study of electron-impact ionization of H_2O at low projectile energy ($E_0 = 81$ eV). Ionization of either the $1b_1$ or $3a_1$ orbitals is observed (we do not resolve the individual states) where the residual ion is stable and does not dissociate.



The TDCSs were measured by covering a large part of the full solid angle for the emitted electron. Since the experimental data are internormalized for different kinematical situations, a single common scaling factor is sufficient to fix the absolute value of all the experimental data which then can be compared with the theoretical predictions. The measurements reported here cover two ejected-electron energies ($E_2 = 5.0$ eV and 10.0 eV) and two projectile scattering angles ($\theta_1 = 6^\circ$ and 10.0°). The experimental data are compared with theoretical predictions from two different versions of the molecular three-body distorted-wave approximation (M3DW). While both include the final state post collision interaction (PCI) exactly, they treat the averaging over spatial molecular alignment with different degrees of sophistication [27].

This paper is organized as follows. After a brief description of the experimental apparatus in Section 2, we summarize the essential points of the two theoretical models in Section 3. The results are presented and discussed in Section 4, before we finish with the conclusions in Section 5. Unless specified otherwise, atomic units (a.u.) are used throughout.

2. EXPERIMENTAL METHOD

The experiment was performed using a reaction microscope [28] that was specially built for electron-impact ionization studies. It was recently updated with a pulsed photoemission electron gun [33, 34]. Since details of the experimental setup can be found in [28, 33, 34], only a brief outline will be given here. The well-focused (≈ 1 mm diameter), pulsed electron beam with an energy of $E_0 = 81$ eV is crossed with a continuous supersonic gas jet, which is produced using a $30 \mu\text{m}$ nozzle and two-stage supersonic gas expansion. Here, helium gas with a partial pressure of 1 bar mixed with water vapor with a partial pressure of about 400 mbar was used. The electron beam is generated by illuminating a

tantalum photocathode with a pulsed ultraviolet laser beam ($\lambda = 266$ nm, $\Delta t < 0.5$ ns). The energy and temporal width of the electron pulses are about 0.5 eV (ΔE_0) and 0.5 ns (Δt_0), respectively.

Homogeneous magnetic and electric fields guide electrons and ions from the reaction volume onto two position- and time-sensitive microchannel plate detectors that are equipped with fast multi-hit delay-line readout. The projectile beam axis (defining the longitudinal z -direction) is aligned parallel to the electric and magnetic extraction fields. Therefore, after crossing the target gas jet, the unscattered primary beam reaches the center of the electron detector, where a central bore in the multichannel plates allows it to pass without inducing a signal. The detection solid angle for H_2O^+ ions is 4π . The acceptance angle for detection of electrons up to an energy of 15 eV is also close to 4π , except for the acceptance holes at small forward and backward angles where the electrons end up in the detector bore.

Experimental data are recorded by triple-coincidence detection of two electrons (e_1 and e_2) and the H_2O^+ cation. The three-dimensional momentum vectors and, consequently, kinetic energies and emission angles of final-state electrons and ions are determined from the individually measured time-of-flight and position of particles hitting on the detectors. The electron binding energy ($E_B = E_0 - E_1 - E_2$) resolution of $\Delta E_B \approx 2.5$ eV has been obtained in the present experiment. Since the complete experimentally accessible phase space is measured simultaneously, all relative data are cross-normalized and only a single global factor fixing the absolute scale is required in comparison of theory and experiment [13, 31, 32].

3. THEORETICAL MODELS

We used two theoretical methods to describe the present electron-impact ionization process. Although they have been described previously [35, 36, 37, 38] we summarize the essential ideas and the particular ingredients for the current cases of interest in order to make this paper self-contained. More detailed information can be found in the references given. The direct-scattering amplitude is given by:

$$T_{dir} = \underbrace{\langle \chi_a^-(k_a, r_0) \chi_b^-(k_b, r_1) C_{ab}(r_{01}) }_{\text{Final State}} |W| \underbrace{\phi_{Dy}(r_1, R) \chi_i^+(k_i, r_0) \rangle}_{\text{Initial State}} \quad (2)$$

where k_i, k_a and k_b are the wave vectors for the initial, scattered, and ejected electrons, respectively, $\chi_i^+(k_i, r_0)$ is an initial state continuum distorted wave and the (+) indicates outgoing wave boundary conditions, $\chi_a^-(k_a, r_0), \chi_b^-(k_b, r_1)$ are the scattered and ejected electron distorted waves with incoming wave boundary conditions, and the factor $C_{ab}(r_{01})$ is the final state Coulomb-distortion factor between the two electrons – normally called the postcollision interaction (PCI). The perturbation $W = V_i - U_i$, where V_i is the initial state interaction potential between the incident electron and the neutral molecule, and U_i represents the spherically symmetric interaction between the projectile and the active electron which is used to calculate the initial state distorted wave $\chi_i^+(k_i, r_0)$. Here $\phi_{Dy}(r_1, R)$ is the initial bound-state wave function, which is commonly called the Dyson molecular orbital, for the active electron and it depends both on r_1 and the orientation of the molecule which is designated by R . The triple differential cross section (TDCS) for a given orientation R with respect to the laboratory frame can be obtained from

$$\sigma^{TDCS}(R) = \frac{1}{(2\pi)^5} \frac{k_a k_b}{k_i} \left(|T_{dir}(R)|^2 + |T_{exc}(R)|^2 + |T_{dir}(R) - T_{exc}(R)|^2 \right) \quad (3)$$

where the exchange-scattering T_{exc} is calculated similar to T_{dir} except that the particles 1 and 2 are interchanged in the final state wave function. To take the proper average (PA) over all molecular orientations [37], the TDCS is calculated for each orientation and then averaged over all possible orientations so that

$$\sigma^{PA} = \frac{\int \sigma^{TDCS}(R) d\Omega_R}{\int d\Omega_R}. \quad (4)$$

The only term in the integral for the T-matrix that depends on the orientation is the Dyson wave function. In the OAMO (orientation averaged molecular orbital) approximation [35], we average the wave function over all orientations and then we calculate a single TDCS. This approximation saves a lot of computer time since the PA needs thousands of processors to do a single calculation whereas the OAMO needs less than hundred.

4. RESULTS AND DISCUSSION

Water (H_2O) contains 10 electrons and has five molecular orbitals: $1a_1$, $2a_1$, $1b_2$, $3a_1$ and $1b_1$. The reported valence electron binding energies of water monomer are 32.4 eV, 18.7 eV, 14.8 eV and 12.6 eV corresponding to $(2a_1)^{-1}$, $(1b_2)^{-1}$, $(3a_1)^{-1}$ and $(1b_1)^{-1}$ states, [39] respectively. We study electron-impact ionization of H_2O with the formation of the stable H_2O^+ cation which results from the ionization of either the $1b_1$ or $3a_1$ orbitals. In the present experiment the $1b_1$ and $3a_1$ orbitals are not resolved due to the limited binding energy resolution, thus, the experimental data represent the summed TDCS for the ionization of the $1b_1$ and $3a_1$ orbitals of H_2O . Figure 1 shows the experimental and theoretical TDCS for ionization of H_2O by 81 eV electron-impact as three-dimensional (3D) polar plots for a projectile scattering angle of $\theta_1 = -10^\circ$ as a function of the emission direction of a slow ejected electron with $E_2 = 10$ eV energy. Panel (a) corresponds to the experimental data, while panel (b) shows the calculated result from the OAMO method. The projectile enters from the bottom with momentum k_i and is scattered to the left with

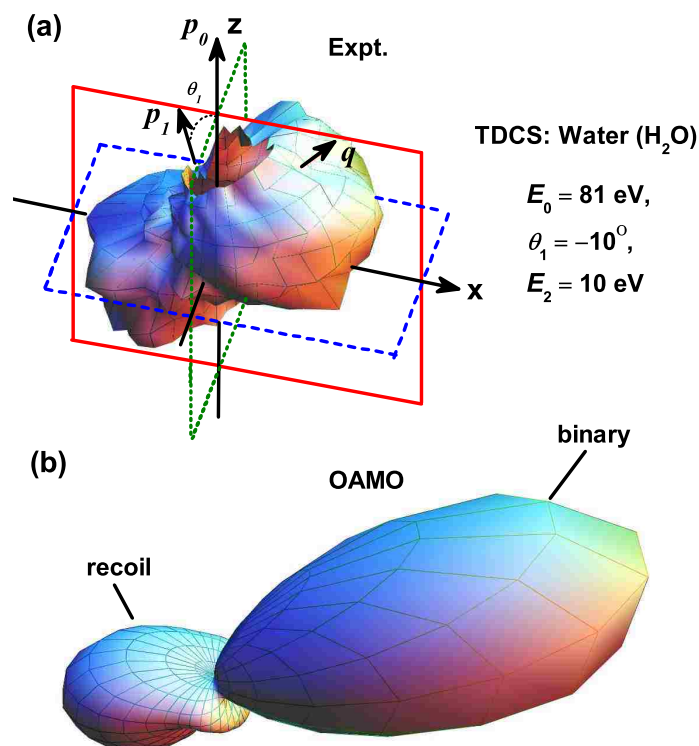


Figure 1. Summed TDCS for experiment (top panel) and OAMO theory (bottom panel) presented as 3D images for electron-impact ($E_0 = 81$ eV) ionization of $1b_1$ and $3a_1$ orbitals of H_2O . The scattering angle is $\theta_1 = -10^\circ$, and the ejected electron energy is $E_2 = 10$ eV.

momentum k_a (hence the minus in the notation for the scattering angle). (Xueguang, We have 2 different definitions of momentum and we would prefer to use k since this is what we have done for a long time.) These two vectors define the scattering (xz) plane, as indicated by the solid frame in panel (a). The momentum transferred to the target $q = k_i - k_a$, is also shown on the figures.

In these 3D-plots, the TDCS for a particular direction is given as the distance from the origin of the plot to the point on the surface, which is intersected by the ejected electron's emission direction. The kinematics chosen displays exemplarily the principal features of the emission pattern: it is governed by the well-known binary and recoil lobes. The binary lobe is oriented roughly along the direction of the momentum transfer q , which would

corresponds to electrons emitted after a single binary collision with the projectile. In the opposite direction the recoil lobe is found, where the outgoing slow electron, initially moving in the binary direction, additionally backscatters in the ionic potential. For ionization from p -orbitals, the binary peak often exhibits a minimum along the momentum transfer direction and there is a small minimum seen in the experimental data. This is the result of the characteristic momentum profile of the p -like $1b_1$ and $3a_1$ orbitals of H_2O that has a node for vanishing momentum [39]. Comparing the experimental data to the theoretical result, we see that the OAMO theory overestimates the size of the binary peak relative to the recoil peak for the case shown. Furthermore, the minimum along the momentum transfer direction indicated in the experimental pattern is not present in the theoretical result. For the PA calculation no full 3D image was obtained since this theory is orders of magnitude computationally much more expensive and so calculations were restricted to major cutting planes which are discussed in the following. However, the PA approach does predict a minimum similar to the experimental data.

For a quantitative comparison between experiment and both the OAMO and PA methods, the cross sections in three orthogonal planes are presented in Figures 2–4. These are cuts through the 3D TDCS image as indicated in Fig. 1(a) by the solid, dashed and dotted frames. The experimental data represent the summed TDCS for the ionization of both the $1b_1$ and $3a_1$ orbitals of H_2O while for theories, both the summed cross sections as well as the separate $1b_1$ and $3a_1$ cross sections are shown in Figures 2–4. The studied kinematical conditions correspond to projectile scattering angles of $\theta_1 = -6^\circ$ and -10° , and to ejected electron energies of $E_2 = 5$ eV and 10 eV, respectively. The scaling factor used to normalize the experimental data to the theories was found by achieving a good visual fit of experiment and the PA calculations for the TDCS in the scattering plane at $\theta_1 = -10^\circ$ and $E_2 = 10$ eV (Fig. 2(h)). This factor was subsequently applied to all other kinematics

and planes, i.e., the experimental data are consistently cross-normalized to each other. The OAMO theoretical results are multiplied by a factor of 10 in order to compare with the results from experiment and PA calculations.

Figure 2 shows the results for detection of the secondary electron in the scattering plane, i.e., the xz -plane of Fig. 1(a). It is obvious that, for the TDCS summed over $1b_1$ and $3a_1$ orbitals, as can already be seen in the 3D plot, the OAMO strongly overestimate the size of the binary peak relative to the recoil peak. While both theories predict a double binary peak for all four cases, the PA calculations have a broader double binary peak with a minimum near the momentum transfer direction which is in better agreement with experiment. For the OAMO results, the second peak is much smaller and shifted to much larger angles. In experiment, the double binary lobes are visible only for $\theta_1 = -6^\circ$ and $E_2 = 5$ eV as well as for $\theta_1 = -10^\circ$ and $E_2 = 10$ eV. While both the OAMO and PA results predict a single peak structure for the recoil lobe, PA predicts a shoulder at the large angle side consistent with the experimental data. Although the cross section close to 180° cannot be accessed experimentally, the available data suggest a very broad recoil peak similar to PA especially for $\theta_1 = -10^\circ$ and $E_2 = 5$ eV. Overall, regarding the relative angular dependence of the TDCSs, The PA is in much better agreement with experiment than the OAMO.

It can be seen in Figure 2 that the two theories differ strongly from each other especially for the separate $1b_1$ calculations. The OAMO TDCS for ionization of the $1b_1$ orbital shows a much stronger binary peak than recoil peak while the PA results exhibit a stronger recoil peak than binary peak consistent with the experimental data. Both the OAMO and PA results have double binary peaks with minimum shifted to larger angles than the momentum transfer direction. However, the OAMO minimum is shifted to much larger angles and the PA minimum is closer to experiment for the cases where experiment sees a double binary peak. On the other side, the predicted patterns for $3a_1$ are rather similar between OAMO and PA with a small binary peak and larger recoil peak.

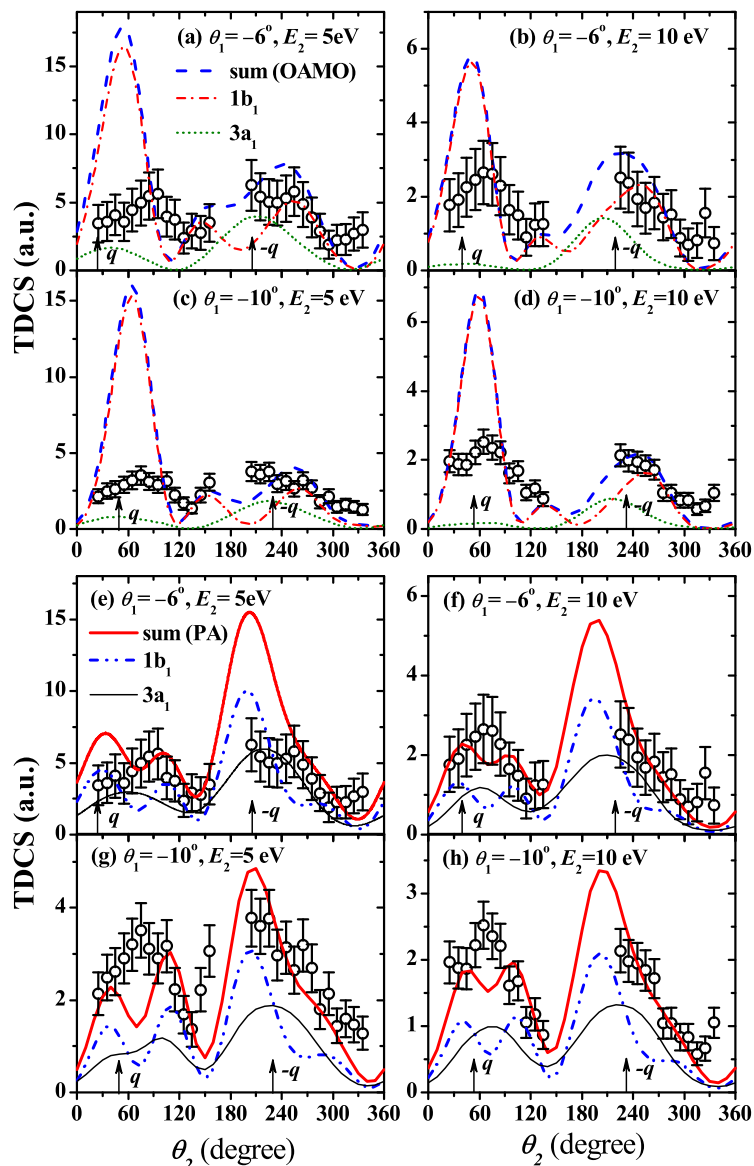


Figure 2. Experimental and theoretical triple-differential cross sections (TDCS) for electron-impact ($E_0 = 81$ eV) ionization of $1b_1$ and $3a_1$ orbitals of H_2O presented as a function of the ejected electron (e_2) emission angle at scattering angles $\theta_1 = -6^\circ$ and $\theta_1 = -10^\circ$ for ejected-electron energies $E_2 = 5$ eV (left column) and $E_2 = 10$ eV (right column). Experimental data (open circles with error bars) are the summed TDCS and theoretical calculations (lines) for the summed and the separate $1b_1$ and $3a_1$ TDCS are obtained by OAMO (top two rows) and PA (bottom two rows) methods. The magnitude of OAMO calculations have been multiplied by a factor of 10. The vertical arrows indicate the momentum transfer direction, q and its opposite, $-q$. The results are for the scattering plane, i.e., the xz -plane of Fig. 1(a).

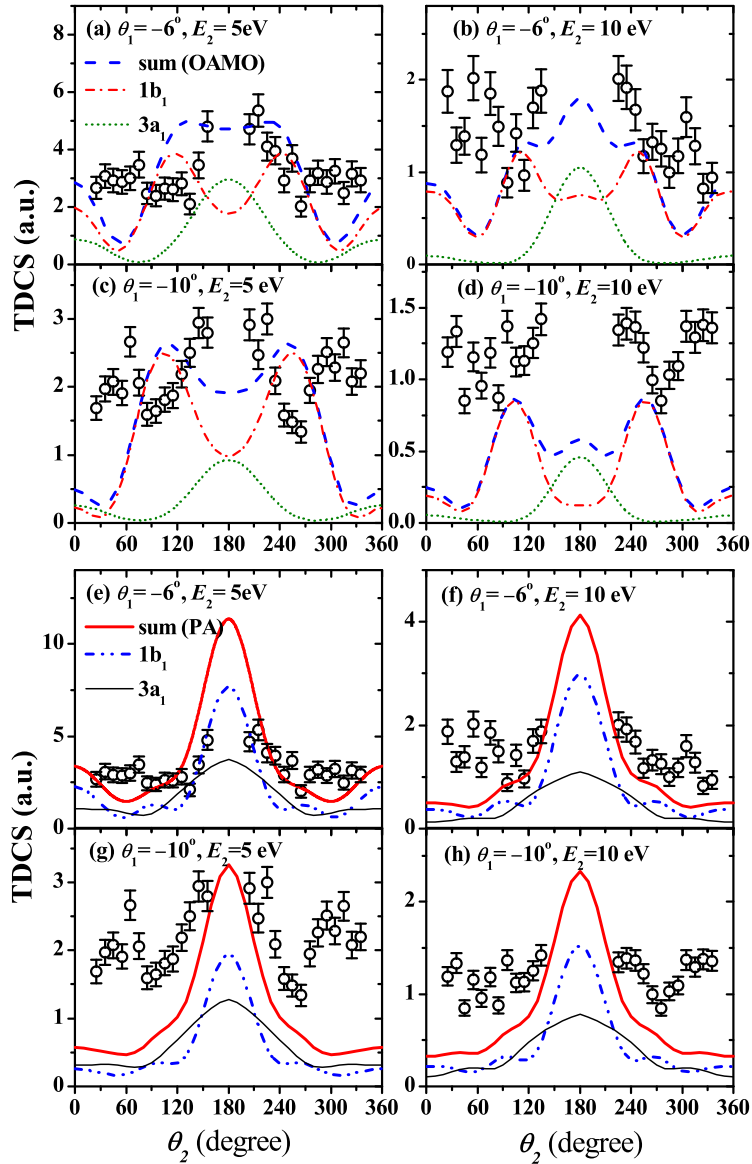


Figure 3. Same as Figure 2 for the “half-perpendicular” plane, i.e., the yz -plane of Fig. 1(a).

Figure 3 shows a comparison between experiment and theory for the yz -plane (half-perpendicular plane). For this plane, symmetry considerations require the cross sections to be symmetric about 180° , which can indeed be seen in both theory and experiment. In experiment, there is an indication of a three-lobe structure for all the cases. It can be seen in the 3D plot of Figure 1(a) that this plane cuts through the binary peak which results two symmetric maxima in the ranges $\theta_2 = 30^\circ - 90^\circ$ and $\theta_2 = 270^\circ - 330^\circ$, respectively.

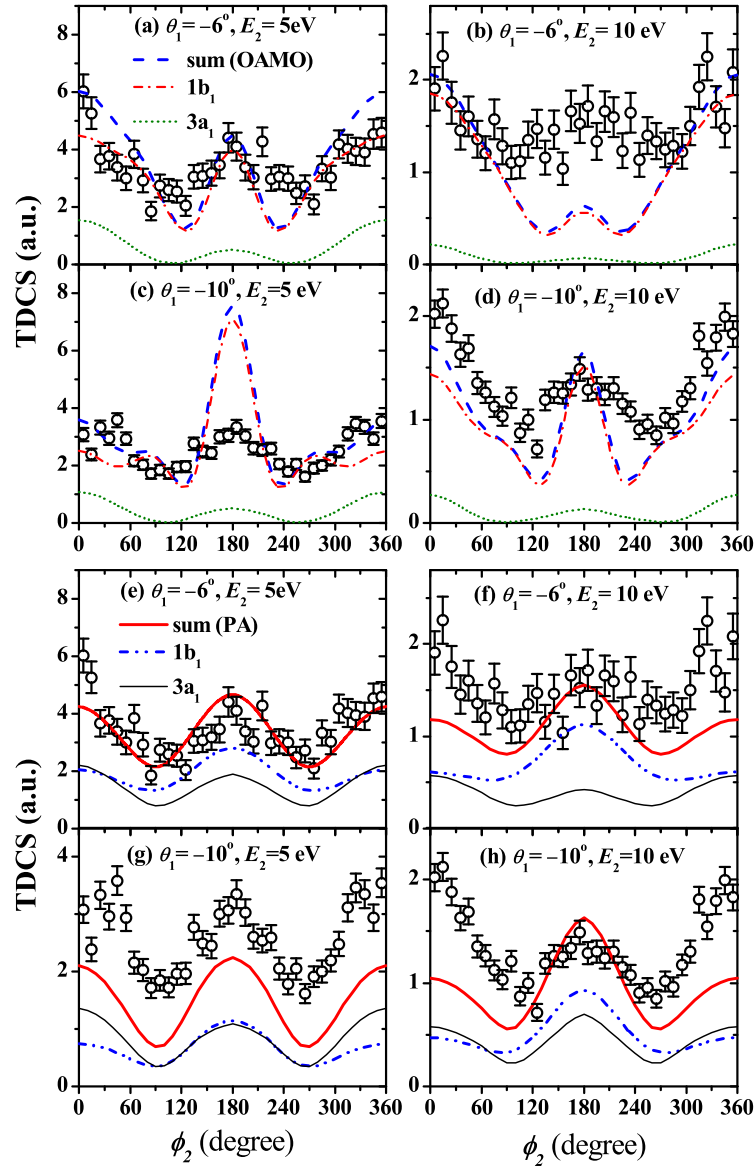


Figure 4. Same as Figure 2 for the “full-perpendicular” plane, i.e., the xy -plane of Fig. 1(a).

In addition, the recoil lobe gives rise to the central maximum at $\theta_2 = 180^\circ$. Concerning the central peaks, the PA is in much better agreement with experiment than the OAMO. Here, the OAMO predicts a minimum or a flat distribution at $\theta_2 = 180^\circ$ except for the case of $\theta_1 = -6^\circ$ for $E_2 = 10 \text{ eV}$. In all panels, the predicted cross sections are significantly smaller than observed experimentally for $\theta_2 \leq 90^\circ$ and, by symmetry, for $\theta_2 \geq 270^\circ$. Both PA and OAMO underestimate the out-of-the scattering plane size of the binary lobes. It

is again interesting to note that significant discrepancies are seen between OAMO and PA in particular for the separate $1b_1$ calculations where the OAMO exhibits a minimum at $\theta_2 = 180^\circ$ with two maximums at about 120° and 240° while the PA predicts a strong maximum at $\theta_2 = 180^\circ$ with two side peaks at about 90° and 270° . The calculations for $3a_1$ are again rather similar between OAMO and PA.

Figure 4 shows the comparison between experiment and theories for the full-perpendicular plane (i.e., the xy -plane). Here, the experimental angular acceptance covers the entire $0^\circ - 360^\circ$ range, but the cross sections are again symmetric with respect to 180° . The binary and recoil peaks are observed in the vicinity of $\phi_2 = 0^\circ$ and 180° , respectively. The two theories in this case agree rather well in shape for the summed and the separate $1b_1$ and $3a_1$ TDCS, and they are in rather good agreement with the experimental data, except that the relative intensity of the recoil peaks are too low for Figure 4(b) and too high for Figure 4(c) in the OAMO curves.

5. CONCLUSIONS

We have reported a comprehensive study of the electron-impact ionization dynamics of H_2O for a projectile energy of 81 eV. Experimentally, the three-dimensional momentum vectors of the final-state particles are determined for a large part of the solid angle for the slow emitted electron. Thus, full three-dimensional representations of the cross sections are accessible. The summed triple-differential cross sections for ionization of $1b_1$ and $3a_1$ orbitals of H_2O obtained experimentally were internormalized across the scattering angles $\theta_1 = -6^\circ$ and -10° and ejected electron energies $E_2 = 5$ eV and 10 eV, thus providing a thorough test for the theoretical models. The experimental data were compared to predictions from the molecular three-body distorted-wave approximation coupled with OAMO and PA methods.

There is overall much better agreement between the PA predictions and the experimental data than the OAMO concerning both the angular dependence of the cross sections and the relative magnitude over the entire range of angle and energy conditions analyzed. Noticeable systematic discrepancies occur in the half-perpendicular plane (Fig. 3), where both OAMO and PA predictions are significantly smaller than that observed experimentally in the angular ranges $\theta_2 \leq 90^\circ$ and, by symmetry, $\theta_2 \geq 270^\circ$. In comparison for ionization of the atomic target Ne, which has the same number of bound electrons as H₂O, the three-body distorted-wave theory reveals an unprecedented degree of agreement with experiment [13, 31]. The two calculations based on the three-body distorted-wave theory differ strongly from each other in both the relative shape and the magnitude of the cross sections. This illustrates the fact that the theoretical treatment of electron-impact ionization of molecule is more complicated and the results are very sensitive to the details of the model employed. The present work indicates that it is more accurate to perform a proper average over orientation-dependent cross sections than to use the orientation-averaged molecular orbital for calculations. The computational cost of the proper average method, however, is much higher than the orientation-averaged molecular orbital approximation. OAMO calculations can be easily performed using less than 100 processors while PA calculations require several thousand processors!

ACKNOWLEDGMENTS

This work was supported, in part, by the United States National Science Foundation under grant No. PHY-1505819 (SA, EA, and DM) and by the National Natural Science Foundation of China under Grant No. 11174175 (CN). Computational work was performed with Institutional Computing resources made available through the Los Alamos National Laboratory. The Los Alamos National Laboratory is operated by Los Alamos National

Security, LLC, for the National Nuclear Security Administration of the US Department of Energy under Contract No. DE-AC5206NA25396. SA and EA would also like to thank the Libyan Ministry of Higher Education's Scholarship for financial support.

REFERENCES

- [1] Elahe Alizadeh, Thomas M. Orlando, and Léon Sanche. Biomolecular damage induced by ionizing radiation: The direct and indirect effects of low-energy electrons on dna. *Annual Review of Physical Chemistry*, 66(1):379–398, 2015.
- [2] Bruce C. Garrett, David A. Dixon, Donald M. Camaioni, Daniel M. Chipman, Mark A. Johnson, Charles D. Jonah, Gregory A. Kimmel, John H. Miller, Thomas N. Rescigno, Peter J. Rossky, Sotiris S. Xantheas, Steven D. Colson, Allan H. Laufer, Douglas Ray, Paul F. Barbara, David M. Bartels, Kurt H. Becker, Kit H. Bowen, Stephen E. Bradforth, Ian Carmichael, James V. Coe, L. Rene Corrales, James P. Cowin, Michel Dupuis, Kenneth B. Eisenthal, James A. Franz, Maciej S. Gutowski, Kenneth D. Jordan, Bruce D. Kay, Jay A. LaVerne, Sergei V. Lymar, Theodore E. Madey, C. William McCurdy, Dan Meisel, Shaul Mukamel, Anders R. Nilsson, Thomas M. Orlando, Nikolay G. Petrik, Simon M. Pimblott, James R. Rustad, Gregory K. Schenter, Sherwin J. Singer, Andrei Tokmakoff, Lai-Sheng Wang, and Timothy S. Zwier. *Chem. Rev.*, 105:355, 2005.
- [3] Michael A. Huels, Badia Boudaiffa, Pierre Cloutier, Darel Hunting, and Leon Sanche. *J. Am. Chem. Soc.*, 125:4467, 2003.
- [4] Simon M. Pimblott and Jay A. LaVerne. Production of low-energy electrons by ionizing radiation. *Radiation Physics and Chemistry*, 76(8–9):1244 – 1247, 2007.
- [5] H. Ehrhardt, M. Schulz, T. Tekaas, and K. Willmann. Ionization of helium: Angular correlation of the scattered and ejected electrons. *Phys. Rev. Lett.*, 22:89–92, Jan 1969.

- [6] U. Amaldi, A. Egidi, R. Marconero, and G. Pizzella. Use of a two channeltron coincidence in a new line of research in atomic physics. *Review of Scientific Instruments*, 40(8):1001–1004, 1969.
- [7] H. Ehrhardt, K. Jung, G. Knoth, and P. Schlemmer. Differential cross sections of direct single electron impact ionization. *Zeitschrift für Physik D Atoms, Molecules and Clusters*, 1(1):3–32, 1986.
- [8] A Lahmam-Bennani. Recent developments and new trends in (e,2e) and (e,3e) studies. *Journal of Physics B: Atomic, Molecular and Optical Physics*, 24(10):2401, 1991.
- [9] T. N. Resigno, M. Baertschy, W.A. Isaacs, and C.W. McCurdy. Collisional breakup in a quantum system of three charged particles. *Science*, 286:2474, 1999.
- [10] I. Bray, D.V. Fursa, A.S. Kadyrov, A.T. Stelbovics, A.S. Kheifets, and A.M. Mukhamedzhanov. Electron- and photon-impact atomic ionisation. *Phys. Rep.*, 520(3):135 – 174, 2012.
- [11] Xueguang Ren, Arne Senftleben, Thomas Pflüger, Klaus Bartschat, Oleg Zatsarinny, Jamal Berakdar, James Colgan, Michael S. Pindzola, Igor Bray, Dmitry V. Fursa, and Alexander Dorn. Propensity for distinguishing two free electrons with equal energies in electron-impact ionization of helium. *Phys. Rev. A*, 92:052707, Nov 2015.
- [12] Oleg Zatsarinny and Klaus Bartschat. Nonperturbative treatment of ionization with excitation of helium by electron impact. *Phys. Rev. Lett.*, 107:023203, Jul 2011.
- [13] Thomas Pflüger, Oleg Zatsarinny, Klaus Bartschat, Arne Senftleben, Xueguang Ren, Joachim Ullrich, and Alexander Dorn. Electron-impact ionization of neon at low projectile energy: An internormalized experiment and theory for a complex target. *Phys. Rev. Lett.*, 110:153202, Apr 2013.

- [14] X. Ren, A. Senftleben, T. Pflüger, A. Dorn, J. Colgan, M. S. Pindzola, O. Al-Hagan, D. H. Madison, I. Bray, D. V. Fursa, and J. Ullrich. Tracing multiple scattering patterns in absolute ($e, 2e$) cross sections for h_2 and he over a 4π solid angle. *Phys. Rev. A*, 82:032712, Sep 2010.
- [15] Ola Al-Hagan, Christian Kaiser, Andrew James Murray, and Don Madison. Atomic and molecular signatures for charged-particle ionization. *Nat Phys*, 5:59–63, Jan 2009.
- [16] X. Ren, T. Pflüger, S. Xu, J. Colgan, M. S. Pindzola, A. Senftleben, J. Ullrich, and A. Dorn. Strong molecular alignment dependence of h_2 electron impact ionization dynamics. *Phys. Rev. Lett.*, 109:123202, Sep 2012.
- [17] Mark C. Zammit, Jeremy S. Savage, Dmitry V. Fursa, and Igor Bray. Complete solution of electronic excitation and ionization in electron-hydrogen molecule scattering. *Phys. Rev. Lett.*, 116:233201, Jun 2016.
- [18] D. S. Milne-Brownlie, S. J. Cavanagh, Birgit Lohmann, C. Champion, P. A. Hervieux, and J. Hanssen. Dynamics in electron-impact ionization of h_2O . *Phys. Rev. A*, 69:032701, Mar 2004.
- [19] Christian Kaiser, Dustin Spieker, Junfang Gao, Martyn Hussey, Andrew Murray, and Don H Madison. Coplanar symmetric and asymmetric electron impact ionization studies from the $1b\ 1$ state of $\text{h}_2\ \text{o}$ at low to intermediate impact energies. *Journal of Physics B: Atomic, Molecular and Optical Physics*, 40(13):2563, 2007.
- [20] Kate L Nixon, Andrew James Murray, Ola Al-Hagan, Don H Madison, and Chuangang Ning. Low-energy symmetric coplanar and symmetric non-coplanar ($e, 2e$) studies from the $3a\ 1$ state of $\text{h}_2\ \text{o}$. *Journal of Physics B: Atomic, Molecular and Optical Physics*, 43(3):035201, 2010.

- [21] C. Champion, C. Dal Cappello, S. Houamer, and A. Mansouri. Single ionization of the water molecule by electron impact: Angular distributions at low incident energy. *Phys. Rev. A*, 73:012717, Jan 2006.
- [22] C. Dal Cappello, Z. Rezkallah, S. Houamer, I. Charpentier, P. A. Hervieux, M. F. Ruiz-Lopez, R. Dey, and A. C. Roy. Second-order born approximation for the ionization of molecules by electron and positron impact. *Phys. Rev. A*, 84:032711, Sep 2011.
- [23] I. Tóth, R. I. Campeanu, and L. Nagy. Triple differential cross sections for the ionization of water by electron and positron impact. *The European Physical Journal D*, 66(1):1–6, 2012.
- [24] Mohammed Sahlaoui, Mammar Bouamoud, Boumediene Lasri, and Mevlüt Dogan. Ionization of a water molecule by electron impact in coplanar symmetric and asymmetric geometries. *Journal of Physics B: Atomic, Molecular and Optical Physics*, 46(11):115206, 2013.
- [25] Chih-Yuan Lin, C. W. McCurdy, and T. N. Rescigno. Complex kohn approach to molecular ionization by high-energy electrons: Application to H_2O . *Phys. Rev. A*, 89:012703, Jan 2014.
- [26] Song Bin Zhang, Xing Yu Li, Jian Guo Wang, Yi Zhi Qu, and Xiangjun Chen. Multi-center distorted-wave method for fast-electron-impact single ionization of molecules. *Phys. Rev. A*, 89:052711, May 2014.
- [27] Hari Chaluvadi, C. G. Ning, and Don Madison. Theoretical triple-differential cross sections of a methane molecule by a proper-average method. *Phys. Rev. A*, 89:062712, Jun 2014.
- [28] J. Ullrich, R. Moshhammer, A. Dorn, R. Dörner, L.Ph.H. Schmidt, and H. Schmidt-Böcking. Recoil-ion and electron momentum spectroscopy: reaction-microscopes. *Reports on Progress in Physics*, 66(9):1463, 2003.

- [29] M Dürr, C Dimopoulou, A Dorn, B Najjari, I Bray, D V Fursa, Zhangjin Chen, D H Madison, K Bartschat, and J Ullrich. Single ionization of helium by 102 eV electron impact: three-dimensional images for electron emission. *J. Phys. B*, 39(20):4097, 2006.
- [30] M. A. Stevenson and B. Lohmann. Fully differential cross-section measurements for electron-impact ionization of argon over the complete in-plane angular range. *Phys. Rev. A*, 77:032708, Mar 2008.
- [31] Xueguang Ren, Sadek Amami, Oleg Zatsarinny, Thomas Pflüger, Marvin Weyland, Woon Yong Baek, Hans Rabus, Klaus Bartschat, Don Madison, and Alexander Dorn. Kinematically complete study of low-energy electron-impact ionization of neon: Internormalized cross sections in three-dimensional kinematics. *Phys. Rev. A*, 91:032707, Mar 2015.
- [32] Xueguang Ren, Sadek Amami, Oleg Zatsarinny, Thomas Pflüger, Marvin Weyland, Alexander Dorn, Don Madison, and Klaus Bartschat. Kinematically complete study of low-energy electron-impact ionization of argon: Internormalized cross sections in three-dimensional kinematics. *Phys. Rev. A*, 93:062704, Jun 2016.
- [33] Xueguang Ren, Thomas Pflüger, Marvin Weyland, Woon Yoon Baek, Hans Rabus, Joachim Ullrich, and Alexander Dorn. An (e, 2e + ion) study of low-energy electron-impact ionization and fragmentation of tetrahydrofuran with high mass and energy resolutions. *The Journal of Chemical Physics*, 141(13):134314, 2014.
- [34] Xueguang Ren, Elias Jabbour Al Maalouf, Alexander Dorn, and Stephan Denifl. Direct evidence of two interatomic relaxation mechanisms in argon dimers ionized by electron impact. *Nat Commun*, 7:11093, Mar 2016.

- [35] Junfang Gao, J. L. Peacher, and D. H. Madison. An elementary method for calculating orientation-averaged fully differential electron-impact ionization cross sections for molecules. *The Journal of Chemical Physics*, 123(20), 2005.
- [36] Don H. Madison and Ola Al-Hagan. The distorted-wave born approach for calculating electron-impact ionization of molecules. *Journal of Atomic, Molecular, and Optical Physics*, 2010:24, 2010.
- [37] Esam Ali, Kate Nixon, Andrew Murray, Chuangang Ning, James Colgan, and Don Madison. Comparison of experimental and theoretical electron-impact-ionization triple-differential cross sections for ethane. *Phys. Rev. A*, 92:042711, Oct 2015.
- [38] Ahmad Sakaamini, Sadek Amami, Andrew James Murray, Chuangang Ning, and Don Madison. Ionisation differential cross section measurements for $n = 2$ at low incident energy in coplanar and non-coplanar geometries. *J. Phys. B*, 49(19):195202, 2016.
- [39] Y. R. Miao, C. G. Ning, and J. K. Deng. Calculation of dyson orbitals using a symmetry-adapted-cluster configuration-interaction method for electron momentum spectroscopy: n_2 and h_2o . *Phys. Rev. A*, 83:062706, Jun 2011.

X. LOW ENERGY (e,2e) MEASUREMENTS OF CH₄ AND NEON IN THE PERPENDICULAR PLANE

Kate L. Nixon,^{1,a)} Andrew James Murray,¹ Hari Chaluvadi,² Sadek Amami,² Don Madison,² and Chuangang Ning³

¹1Photon Science Institute, School of Physics and Astronomy,
University of Manchester,
Oxford Road, Manchester M13 9PL, United Kingdom

²Physics Department, Missouri University of Science and Technology, Rolla, Missouri
65409, USA

³Department of Physics, State Key Laboratory of Low-Dimensional Quantum Physics,
Tsinghua University, Beijing 100084, People's Republic of China

ABSTRACT

Low energy experimental and theoretical triple differential cross sections for the highest occupied molecular orbital of methane ($1t_2$) and for the 2p atomic orbital of neon are presented and compared. These targets are iso-electronic, each containing 10 electrons and the chosen orbital within each target has p-electron character. Observation of the differences and similarities of the cross sections for these two species hence gives insight into the different scattering mechanisms occurring for atomic and molecular targets. The experiments used perpendicular, symmetric kinematics with outgoing electron energies between 1.5 eV and 30 eV for CH₄ and 2.5 eV and 25 eV for neon. The experimental data from these targets are compared with theoretical predictions using a distorted-wave Born approximation. Reasonably good agreement is seen between the experiment and theory for neon while mixed results are observed for CH₄. This is most likely due to approximations of the target orientation made within the model.

1. INTRODUCTION

Electron impact ionization collisions at low energies are important in a number of fundamental areas. These include plasma etching in industry, to the study of natural atmospheric phenomena as well as cancer therapy by radiation treatments. In order to understand the underlying physical process in these areas, a robust understanding of the collision is necessary. Experimental measurements provide data for specific collision parameters from a particular target. By developing comprehensive theoretical models of the collision that are rigorously tested by experiment, accurate predictions for a range of collision parameters from a multitude of targets can then be made. Precise experimental data are hence required to aid in the development of the theoretical models. $(e, 2e)$ experiments control the projectile electron momentum and define the momentum of the electrons resulting from the collision. As such, these kinematically complete experiments provide the most detailed data against which theory can be compared. This field has provided a rich source of information on atomic targets, with good agreement being found between experiment and theory for a range of different atoms. By contrast, the number of molecules that have been investigated is still relatively small, and new models are currently under development. This is due to the more complex nature of molecules compared to atoms. Molecules have spatially distributed nuclei resulting in multiple scattering centers, which means that the wave-functions associated with the electron distribution within the molecule are not spherically symmetric. This reduction in symmetry leads to further complications, since the orientation and alignment of the molecule with respect to the scattering geometry must also be considered. Additionally, the energy levels within molecules are often more closely spaced than in atoms, resulting in neighboring orbitals that may not be resolvable by experiment. Despite these theoretical and experimental challenges, detailed electron impact ionization studies from molecules have been emerging over the past decade.

The molecular target in this current study is methane (CH_4), which is the smallest hydrocarbon and so is a relatively simple molecule. It has five atoms, with ten electrons. The molecule has tetrahedral symmetry and only two valence energy levels. The $1t_2$ level is the highest occupied molecular orbital (HOMO) and is a triply degenerate, p-like orbital. The next highest occupied molecular orbital ($2a_1$) has almost spherical symmetry, and has s-like character. These orbitals are separated in energy by ~ 9 eV, allowing data to be obtained from the individual orbitals without contamination. Recent measurements from CH_4 using scattered electron energies of 500 eV have been reported [12] and corresponding distorted wave Born approximation (DWBA) calculations [22] show good agreement at these higher energies. The data presented here are low energy triple differential cross sections (TDCS) using symmetric energy sharing, where both outgoing electrons leave the collision with equal energy. Perpendicular kinematics were used in which the momentum of the incident projectile electron is orthogonal to the detection plane containing the two outgoing electrons (see Figure 1). In order for both outgoing electrons to leave the collision in this plane, it is necessary for multiple scattering to occur. This geometry hence provides a stringent test of theory. Additionally, marked differences have been observed between atomic helium and molecular H_2 in this plane, in contrast to results taken in a coplanar geometry where the cross sections were similar [1]. Since He and H_2 have the same number of electrons and protons, these results indicate that measurements in the perpendicular plane provide a more sensitive test of the structure of the target than data taken in a coplanar geometry. To further understand the measurements from CH_4 , the resulting TDCS is compared with that from neon. Neon is the iso-electronic atom to CH_4 , both species having 10 electrons. By comparing the atomic and molecular cross sections, similarities in the TDCS may be attributable to a similar electronic structure, while differences may arise due to the molecular nature of the target. A previous study from the NHOMO ($2a_1$) orbital of CH_4 in a coplanar geometry yielded poor statistical accuracy due to very low signal at these energies [16], and so the TDCS for the outermost orbital of the two species are presented here, i.e., the

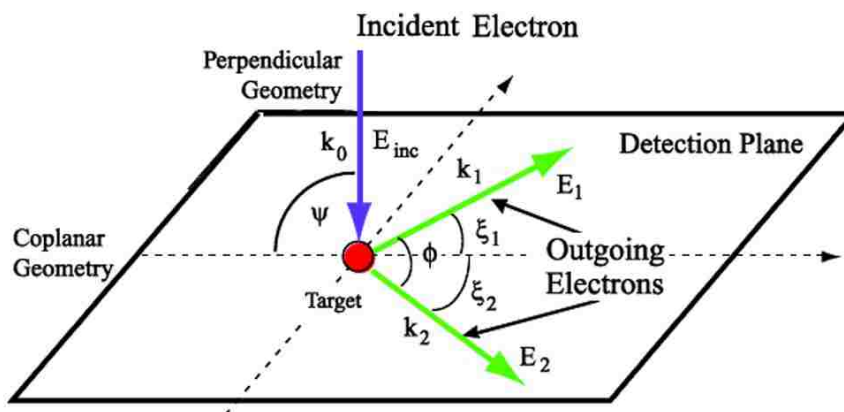


Figure 1. Diagram of the geometry used in this study. A perpendicular geometry ($\psi = 90^\circ$) is defined when the momentum of the incident electron is perpendicular to that of the outgoing electrons, i.e., the detection plane. In the perpendicular geometry only the mutual angle ($\phi = \xi_1 + \xi_2$) is relevant.

$1t_2$ orbital of CH_4 and the corresponding $2p$ orbital of Ne. This paper is structured as follows. Section 2 describes the pertinent details of the apparatus used to collect the data. The theoretical framework used to model the collision is then detailed in Section 3. Results from experimental measurement and theoretical predictions are presented and discussed in Section 4. Section 5 summarizes this study and maps out future work that is needed.

2. EXPERIMENTAL APPARATUS

The fully computer controlled and computer optimized (e,2e) spectrometer at the University of Manchester was used in this work. This apparatus has been described elsewhere [14] so only the salient points are discussed here. The spectrometer consists of an electron gun with an energy resolution of ~ 600 meV, two electron analyzers, a gas jet and a Faraday cup. The electron analyzers are mounted on individual turntables so that they can be independently rotated around the interaction region. The detection plane is defined by these analyzers (see Figure 1). In this study the spectrometer was configured in a perpendicular geometry where the momentum of the incident electron is perpendicular

to the detection plane ($\psi = 90^\circ$). The data are symmetric as the outgoing electrons were detected with equal energies, i.e., $E_1 = E_2$, and the only angle of relevance in this plane is the angle between the analyzers, $\phi = \xi_1 + \xi_2$. High purity CH_4 or neon was admitted into the interaction region through a gas jet. The flow of the target gas was controlled by a needle valve. Typical operating pressures for CH_4 and Ne were 1.2×10^{-5} Torr and 2.2×10^{-5} Torr, respectively. Small incident electron beam currents, typically ~ 120 nA, were used for CH_4 in order to maintain a good signal to background ratio. Higher currents of 300 nA were used for neon. The spectrometer was operated under computer control throughout data collection. The electrostatic lenses in the analyzers were optimized at each new angle to ensure maximum signal. The energy of the incident electron beam was calibrated at the beginning of each new data set by locating the peak in the coincidence binding energy spectrum. The two highest occupied molecular orbitals of CH_4 are well separated by ~ 9 eV. The experimental energy resolution of ~ 1.4 eV easily ensures there is no contamination in the measured data from the neighboring orbital, as is often the case for molecular targets [3, 4, 15]. The data have not been placed on an absolute scale due to the low energies used in this study. Molecular targets may have a dramatic influence on the behavior of the electron beam at these energies [17] and so it is not accurate to assume that the electron beam density remains constant between measurements as the energy is changed or for different target species, as is essential in the formalization methods applied by others at higher energies [10, 11]. Consequently, the data presented here are normalized to unity at the highest data point for each set. Each data set is generated from an average of many sweeps around the detection plane. The error bars on the TDCS represent the standard error derived from this average. The uncertainties on the scattering angle are due to the pencil angle of the incident electron beam, and the acceptance angles of the outgoing electron analyzers. This is estimated to be $\pm 5^\circ$. The experimental data for neon have been published previously [18]. The data are re-presented here so that a direct comparison can be made between the two iso-electronic species.

3. THEORETICAL FRAMEWORK

The molecular 3-body distorted wave (M3DW) approximation [or atomic 3-body distorted wave (3DW) approximation] has been detailed in previous publications [6, 7, 8] so only a brief outline is given here. The TDCS for the M3DW is given by

$$\frac{d^5\sigma}{d\Omega_a d\Omega_b dE_b} = \frac{1}{(2\pi)^5} \frac{k_a k_b}{k_i} |T|^2 \quad (85)$$

where \vec{k}_i , \vec{k}_a , and \vec{k}_b are the wave vectors for the initial, scattered, and ejected electrons. The scattering amplitude is given by

$$T_{dir} = \left\langle \chi_a^-(\vec{k}_a, \mathbf{r}_1) \chi_b^-(\vec{k}_b, \mathbf{r}_2) C_{\text{scat-eject}}(r_{12}) |V - U_i| \phi_{DY}^{OA}(\mathbf{r}_2) \chi_i^+(\vec{k}_i, \mathbf{r}_1) \right\rangle \quad (86)$$

where r_1 and r_2 are the coordinates of the incident and bound electrons, χ_i , χ_a and χ_b are distorted waves representing the incident, scattered, and ejected electrons, respectively, and $\phi_{DY}^{OA}(r_2)$ is the initial bound-state Dyson molecular orbital averaged over all orientations. The molecular wave-functions were calculated using density functional theory along with the standard hybrid B3LYP (Ref. [13]) functional by means of the ADF 2007 (Amsterdam Density Functional) program [9] with the TZ2P (triple-zeta with two polarization functions) Slater type basis sets. For the $1t_2$ state, the average of the absolute value of the Dyson wave-function is taken prior to the collision, since the normal average is zero due to parity of the wave-function.

For the Ne atom, the same matrix element (2) is evaluated except the Dyson orbital is replaced by a Hartree-Fock 2p wave-function. The factor $C_{\text{scat-eject}}(r_{12})$ is the Ward-Macek average Coulomb-distortion factor between the two final state electrons [24] V is the initial state interaction potential between the incident electron and neutral molecule, and U_i is a spherically symmetric distorting potential which is used to calculate the initial-state distorted wave for the incident electron $\chi_i^+(\vec{k}_i, \mathbf{r}_1)$.

The Schrödinger equation for the incoming electron wave-function is given by

$$(T + U_i - \frac{k_i^2}{2})\chi_i^+(\vec{k}_i, r) = 0 \quad (87)$$

where T is the kinetic energy operator and the “+” superscript on $\chi_i^+(\vec{k}_i, r)$ indicates outgoing wave boundary conditions. The initial state distorting potential contains three components $U_i = U_s + U_E + U_{CP}$. U_s is the static potential that contains the nuclear contribution and a spherically symmetric approximation for the interaction between the projectile electron and the target electrons which is obtained from the quantum mechanical charge density of the target. U_E is the exchange potential of Furness-McCarthy (corrected for sign errors) (Ref. [5]) which approximates the effect of the continuum electron exchanging with the passive bound electrons in the molecule. Finally, U_{CP} is the correlation polarization potential of Perdew and Zunger [20], and Padial and Norcross [19].

The final state for the system is approximated as a product of distorted waves for the two continuum electrons multiplied by the average Coulomb-distortion factor. The final state distorted waves are calculated as the initial state, except that the final state spherically symmetric static distorting potential for the molecular ion (or atomic ion) is used for U_s .

4. RESULTS

4.1. Predicted Scattering Signatures using a Classical Mode. A recent investigation by Al-Hagan et al. [1] considers a simple classical picture of the ionization of atoms and molecules in the perpendicular plane that is validated using quantum mechanical calculations. These authors provide an explanation for features observed in the measured cross sections when the experiments do not determine the orientation of a molecular target. Predictions were given for (i) atomic targets, (ii) molecular targets that have a nucleus at the center of mass, and (iii) molecular targets that do not have a nucleus at the center of mass. Experimental and theoretical data from He, H₂, and CO₂ with $E_1 = E_2 = 10 \text{ eV}$ were

used in their study. It was predicted that molecules with no nucleus at the center of mass should produce a minimum contribution to the cross section at angles corresponding to the outgoing electrons emerging back to back, i.e., at $\phi = 180^\circ$. This prediction results from the model averaging over all possible orientations of the molecule prior to the collision (as is adopted in the calculations used in this paper), so that the nuclear charge appears as a thin “shell” of charge with a diameter set by the inter-nuclear distance. In these averaging models, electrons that collide inside the resulting nuclear shell cannot experience any force from the nuclei, and so only a binary collision will occur (no re-collision from the nucleus then being possible). In this case the TDCS in the perpendicular plane should only present peaks at $\phi = 90^\circ, 270^\circ$, as was observed for H₂. The model further suggests that molecular targets that do have a nucleus at the center of mass should then yield a backscattering signature similar to atomic targets, since nuclear re-scattering can then occur. This prediction was confirmed in their data for CO₂, which produced a TDCS similar in structure to that of helium, with peaks at $\phi = 90^\circ, 270^\circ$ (due to binary collisions) and a third peak at 180° (due to re-scattering of one of the electrons from the nucleus). Since CH₄ has a carbon atom at the center of mass of the molecule, this simple classical model predicts that CH₄ should produce a 3-peak TDCS, with significant cross section at $\phi = 180^\circ$.

4.2. 2p Orbital of Neon. The experimental and theoretical TDCS for the valence 2p orbital of neon are shown in Figure 2. The theoretical data have been calculated in the DWBA framework. Two curves are shown that represent different calculations. The first is a basic DWBA calculation (DWBA). The second (3DW) has post-collisional interactions (PCI) included by using the Ward-Macek approximation.¹⁸ The result of an independent theoretical study by Purohit et al. [21] is also shown for an incident electron energy 20 eV above the ionization potential. The structure of the data has been discussed previously. Briefly, a double peak structure is observed at high energies, with a minimum at $\phi = 180^\circ$ in contrast to both the prediction of the simple model described in Sec. 4.1, and the experimental results from helium [18]. As the energy decreases the two peaks

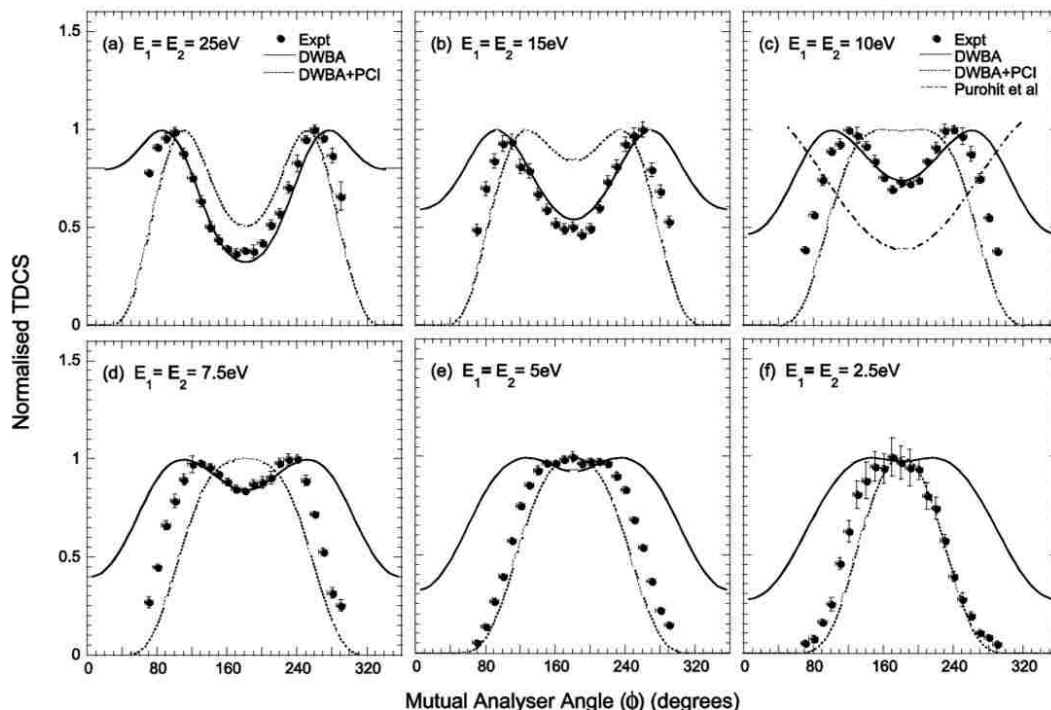


Figure 2. Experimental and theoretical TDCS for the 2p orbital of neon. Incident energies of 5 eV to 50 eV above the ionization potential (IP = 21.6 eV) were used, as indicated on the plots. Two theoretical predictions are shown for all energies; DWBA with no PCI included (solid line) and 3DW (dashed line) where PCI is treated using the Ward-Macek approximation. An additional theoretical curve is shown in (c) following the calculation of Purohit *et al* [21]. The experimental and theoretical data have been independently normalized to unity at the peak of the TDCS for each energy.

move closer together giving a narrower distribution, and the local minimum at $\phi = 180^\circ$ becomes shallower. At the lowest energy studied here ($E_1 = E_2 = 2.5$ eV), a single peak is observed. This peak will include a contribution due to PCI between the two outgoing electrons [23], since at these low energies the longer interaction time between the outgoing electrons results in them asymptotically being driven apart. It is interesting that the simple classical picture³ already appears to fail for this target. The absence of a defined peak at $\phi = 180^\circ$ may be attributable to the proposed nuclear rescattering mechanism having a much smaller probability than for helium, compared with the binary mechanism that gives rise to the peaks on either side. This hypothesis is strengthened by the 3DW model that also predicts a minimum at $\phi = 180^\circ$, in agreement with the data. From a classical viewpoint,

it would be expected that nuclear scattering would be weaker for neon since the classical impact parameters for elastic scattering into the perpendicular plane would be five times larger for neon than helium. Consequently, it appears that the physical effects leading to the shape of the cross section is different for this case. The fact that both the DWBA and 3DW predict a minimum at 180° indicated that the minimum is not related to the electron–electron interaction in the final state. The prediction from the DWBA calculation (i.e., without PCI) shows unphysically high flux when the electrons emerge at the same angle, i.e., at the mutual angles $\phi = 0^\circ$ and $\phi = 360^\circ$. This clearly shows the importance of PCI, as is included in the 3DW prediction. PCI can also be attributed to the narrowing of the TDCS around $\phi = 180^\circ$ as the energy is lowered. This reduction in width is due to the electrons that emerge from the interaction region repelling each other. The correlation between experimental data and the theoretical predictions is interesting. At high energy, the DWBA calculation predicts the depth of the minimum at $\phi = 180^\circ$ with more accuracy than the 3DW calculation, which also predicts too narrow a distribution at these energies. This may indicate that the contribution due to PCI is too strong in the model. Conversely, at the lowest energy the 3DW calculation is far more successful at predicting the width of the distribution. Neither model emulates the success that was found for helium. In addition to the predictions given here, Figure 2(c) also shows the DWBA calculation by Purohit et al. [21] This calculation used a spin averaged static exchange potential, includes PCI via the Gamow factor and employs a polarization potential in the incident channel only. Only one calculation for neon in the perpendicular plane was reported by these authors, at outgoing electron energies $E_1 = E_2 = 10 \text{ eV}$. Their calculation predicts a minimum at $\phi = 180^\circ$, as is observed. By contrast, their predicted cross section increases in both directions towards $\phi = 0^\circ$ and $\phi = 360^\circ$, and their minimum is broader and deeper than is seen in the experimental data.

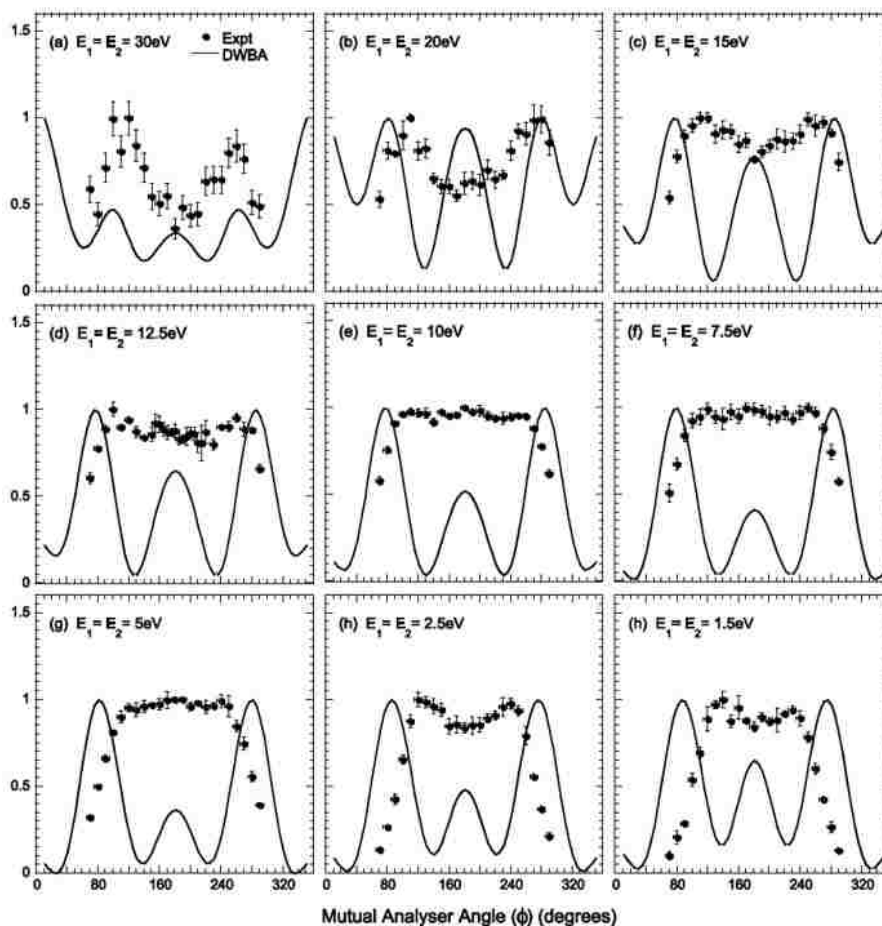


Figure 3. Experimental and theoretical DWBA TDCS for the $1t_2$ HOMO state of CH_4 . Incident energies of 3 eV to 60 eV above the ionization potential ($IP \sim 14$ eV) were used, as indicated on the plots. The experimental and theoretical data have been independently normalized to unity at the peak for each energy.

4.3. $1t_2$ State of Methane. The experimental and theoretical TDCS for the HOMO of CH_4 (the $1t_2$ state), are shown in Figures 3 and 4. Figure 3 compares the data to the DWBA model, whereas Figure 4 shows a comparison with the M3DW model. The HOMO of CH_4 is a triply degenerate state consisting of three p-like orbitals. These orbitals have parity inversion through the center of symmetry, which is also the center of mass in CH_4 . To allow for parity inversion, the present models use the absolute value of the orbital wave-function to generate an averaged wave-function over all orientations of the molecule.

This is used here since the averaging procedure would produce a zero wave-function if parity inversion was included. It has been found that the orientationally averaged molecular wave-function used for this state is of reasonably good quality [16][4] when compared with experimentally measured EMS data [2][24] at high energies. The data show a two-peak structure at the highest energy used here, i.e., $E_1 = E_2 = 30 \text{ eV}$ as shown in Figures 3(a) and 4(a). The peaks are located symmetrically about $\phi = 180^\circ$, at angles of $\phi = 110^\circ$ and $\phi = 260^\circ$. A minimum is observed between the two peaks with a magnitude ~ 0.45 of the peaks. This is similar to that observed for the valence states of neon, argon, and krypton [18]. As the energy of the outgoing electrons is decreased, the two peaks remain approximately in the same position and the local minimum fills in. In Figures 3(d)–(g), the distribution is wide, flat, and almost featureless. Evidence of a faint triple peak structure may be observed. As the energy is lowered further the total angular width of the cross section decreases, and a small two-peak structure is again seen at the two lowest energies. Here, the two peaks are found at $\phi = 120^\circ$ and $\phi = 240^\circ$, and the minimum at $\phi = 180^\circ$ has an intensity ~ 0.85 of the peak height. Both DWBA and M3DW models predict well-resolved triple peak structures at the majority of energies measured. The peak at $\phi = 180^\circ$ seen in the theoretical results emulates the prediction of the classical model described in Al-Hagan et al.³ Initially consider the DWBA prediction as in Figure 3. At high energies the calculation shows unphysical intensity at $\phi = 0^\circ$ and 360° , which is due to the absence of PCI in the model, as seen for neon in Figure 2. The model predicts a triple peak structure at the lower energies, the width of the cross section being overestimated at almost all energies by this calculation. The predictions from the M3DW calculation that includes PCI using the Ward-Macek approximation [18] are shown in Figure 4. In this figure the data are normalized to unity at the two side peaks. The agreement in width of the TDCS between experiment and theory is much more satisfactory for all energies, and the unphysical cross section at $\phi = 0^\circ$ and 360° is now eliminated due to inclusion of PCI. There is, however, a discrepancy in the number of peaks that are predicted, and the large relative magnitude of the TDCS at

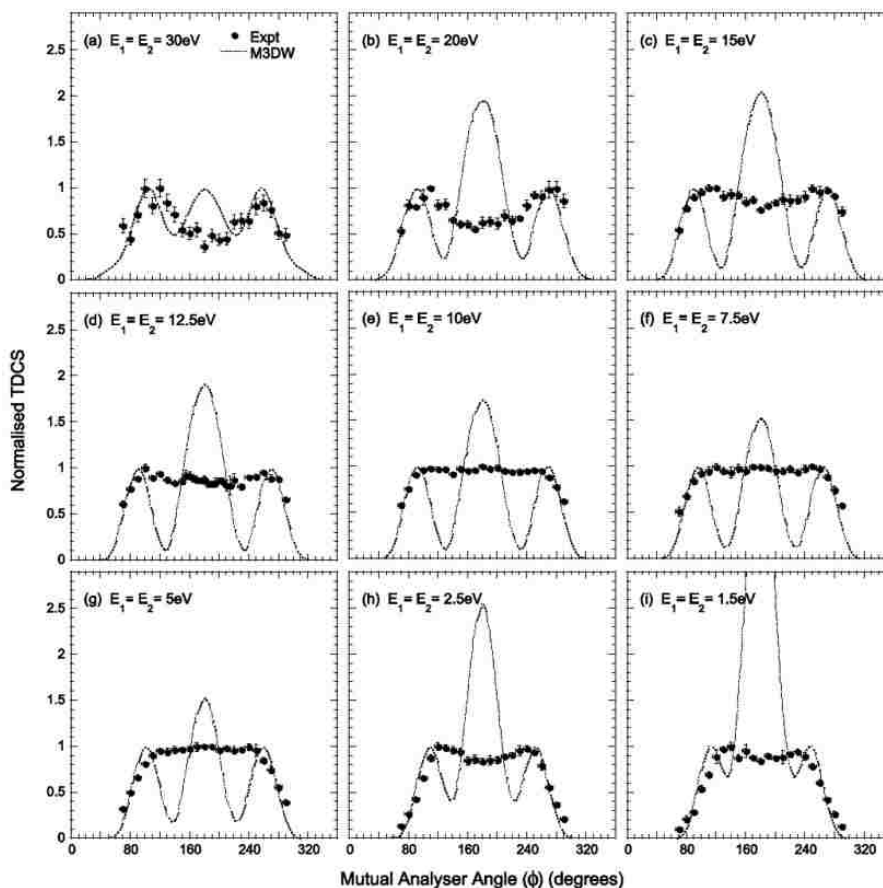


Figure 4. Experimental and theoretical (M3DW) TDCS for the $1t_2$ HOMO state of CH₄. The experimental data have been normalized to unity at the maximum intensity, while the theoretical data are normalized to unity at the side peaks. For details, see text.

$\phi = 180^\circ$ predicted by the model is not observed. Once again, the TDCS generated by this model is in good agreement with that expected from the classical model outlined in Sec. 4.1, with three clearly defined peaks and with a large central peak at $\phi = 180^\circ$ (as observed for helium). The magnitude of the predicted peak at $\phi = 180^\circ$ indicates that rescattering from the carbon nucleus is much stronger than for the iso-electronic neon atom at similar energies. This probably results from the fact that the classical impact parameters for elastic scattering into the perpendicular plane are smaller for the molecule than they are for the atom. A similar discrepancy regarding the number of discrete peaks predicted by theory was noted for H_2O in the perpendicular plane. In these experiments the excess energy

remained constant at 20 eV and the energy sharing between the two outgoing electrons was varied. In the three cases studied for this target, the experimental distribution was relatively flat as is seen here for CH_4 , in contrast to theory that predicted a well-defined triple peak structure.

4.4. Comparison Between the Iso-Electronic Species. The experimental distributions for the two iso-electronic analogues neon and CH_4 , show some similarities in the shape of the cross section. Differences, particularly at intermediate and low energies, are also observed. To summarise; at high energies both targets display a double peak structure. Also, in both cases the local minimum is filled in as the energy is decreased. For neon, the width of the distribution narrows as the energy is lowered, and the angular distribution shows a small flat section at $E_1 = E_2 = 5$ eV where the TDCS transitions between a double peak structure and a single peak. In contrast, the width of the CH_4 distribution remains essentially constant until $E_1 = E_2 = 5$ eV. The TDCS of CH_4 is relatively flat and featureless over the range of outgoing electron energies from 12.5 eV to 5 eV, while the distributions for neon always show a double peak structure until $E_1 = E_2 = 5$ eV. At the lowest energies used here, neon presents a single peak, while CH_4 shows a shallow double peak structure. At these energies the width of the CH_4 distribution starts to reduce.

Comparison with the theoretical results for these two species show large differences. For all but the lowest energy, a minimum is predicted at $\phi = 180^\circ$ for neon. Conversely, a maximum is predicted at $\phi = 180^\circ$ for CH_4 . Indeed, this maximum dominates the predicted TDCS when PCI is included, in contrast to what is observed in the experiment.

5. CONCLUSIONS

In comparing the theoretical predictions for neon to the data, it is seen that neither the DWBA nor the 3DW models provide an accurate description over the entire energy range investigated here. At high energies the DWBA model accurately predicts the depth of the minimum at $\phi = 180^\circ$, but overestimates the width of the distribution. At low

energies inclusion of PCI narrows the width around $\phi = 180^\circ$ so as to be in reasonably good agreement with the data, as is expected. In a similar way, inclusion of PCI for CH_4 narrows the width of the distribution. This produces good agreement with the width of the distribution over all energies, although a large peak at $\phi = 180^\circ$ is predicted that is not observed. Much better agreement between experiment and theory is found for Ne than CH_4 . CH_4 is clearly a more complex target than neon. This additional complexity is reflected in the evolution of the TDCS with energy. The data for neon shows a double peak at high energies that narrows to a single peak as the energy is lowered. The 3DW calculation shows the same transition, except the single peak occurs at a higher energy than experiment. The TDCS for CH_4 also starts with a double peak at high energies. The total angular width of the distribution however remains unchanged until $E_1 = E_2 = 5 \text{ eV}$ at which point the width decreases. The M3DW correctly predicts the width of the peak for all energies. As the energy is lowered however, the experimental minimum at $\phi = 180^\circ$ fills in to yield a broad, flat topped distribution while the M3DW predicts a maximum at $\phi = 180^\circ$ which becomes larger with decreasing energy. The most obvious discrepancy between data and theory is the number of clearly resolved peaks predicted for CH_4 . The peak at $\phi = 180^\circ$ is predicted to be significantly enhanced in the M3DW model in contrast to what is observed. There is perhaps a small triple peak between $E = 12.5 \text{ eV}$ and 7.5 eV in the data, however this is poorly defined. It would be interesting to investigate if the featureless cross section in the data is due to an incoherent summation of cross sections from the different molecular orientations that occur in the experiment, or if it is due to a quantum mechanical effect that is not being reproduced in the theory. To establish this, the model needs to calculate the TDCS for different orientations of the target prior to the collision, and then average the resulting cross sections over all possible orientations of the target. This is a challenging and computationally intensive calculation, however it would provide the most accurate comparison with the data, and would most accurately test the models that are being developed.

In conclusion, it is clear that much has yet to be done to resolve the differences that are seen between theory and experiment at these incident energies. It is important to establish a robust theory for collisions with molecules at these energies since it is here that the cross section for ionization is highest, and so it is in this energy regime where most collisions occur in nature. The contrasts that have been observed between the iso-electronic targets of neon and CH_4 show that conclusions can be made about the nature of the collision for molecular targets. It is clear however that a full calculation that does not include orientation averaging prior to the collision is now required.

ACKNOWLEDGMENTS

This work was supported by the U.S. National Science Foundation (NSF) under Grant. No. PHY-1068237. The author C.N. would like to acknowledge the support of the National Natural Science Foundation of China (NNSFC) under contract No. 10704046. K.L.N. would like to thank the Royal Society for a Newton International Fellowship held at the University of Manchester.

REFERENCES

- [1] Ola Al-Hagan, Christian Kaiser, Don Madison, and Andrew James Murray. Atomic and molecular signatures for charged-particle ionization. *Nat Phys*, 5:59–63, 2009.
- [2] S.A.C. Clark, T.J. Reddish, C.E. Brion, E.R. Davidson, and R.F. Frey. The valence orbital momentum distributions and binding energy spectra of methane by electron momentum spectroscopy: Quantitative comparisons using near hartree-fock limit and correlated wavefunctions. *Chemical Physics*, 143(1):1 – 10, 1990.

- [3] C. J. Colyer, S. M. Bellm, B. Lohmann, G. F. Hanne, O. Al-Hagan, D. H. Madison, and C. G. Ning. Dynamical (e, 2e) studies using tetrahydrofuran as a dna analog. *J Chem Phys*, 133(12):124302, 2010.
- [4] C J Colyer, M A Stevenson, O Al-Hagan, D H Madison, C G Ning, and B Lohmann. Dynamical (e, 2e) studies of formic acid. *Journal of Physics B: Atomic, Molecular and Optical Physics*, 42(23):235207, 2009.
- [5] J B Furness and I E McCarthy. Semiphenomenological optical model for electron scattering on atoms. *J. Phys. B: At. Mol. Phys*, 6(12):2280, 1973.
- [6] J. Gao, D. H. Madison, and J. L. Peacher. Distorted wave born and three-body distorted wave born approximation calculations of the fully differential cross section for electron-impact ionization of nitrogen molecules. *J Chem Phys*, 123(20):204314, 2005.
- [7] J. Gao, J. L. Peacher, and D. H. Madison. An elementary method for calculating orientation-averaged fully differential electron-impact ionization cross sections for molecules. *J Chem Phys*, 123(20):204302, 2005.
- [8] Junfang Gao, D. H. Madison, and J. L. Peacher. Interference effects for low-energy electron-impact ionization of nitrogen molecules. *Physical Review A*, 72(3), 2005.
- [9] C. F. Guerra, J. G. Snijders, G. te Velde, , and E. J. Baerends. Development of the colle-salvetti correlation-energy formula into a functional of the electron density. *Theor. Chem. Acc.*, 99:391, 1998.
- [10] L. R. Hargreaves, M. A. Stevenson, and B. Lohmann. Absolute triple-differential cross sections for intermediate energy electron impact ionization of neon and argon. *Journal of Physics B: Atomic, Molecular and Optical Physics*, 43(20):205202, 2010.

- [11] L. R. Hargreaves, M. A. Stevenson, and B. Lohmann. A simple method for absolute normalization of (e, 2e) cross sections. *Measurement Science and Technology*, 21(5):055112, 2010.
- [12] A. Lahmam-Bennani, A. Naja, E. M. Staicu Casagrande, N. Okumus, C. Dal Cappello, I. Charpentier, and S. Houamer. Dynamics of electron impact ionization of the outer and inner valence (1t₂ and 2a₁) molecular orbitals of ch₄at intermediate and large ion recoil momentum. *Journal of Physics B: Atomic, Molecular and Optical Physics*, 42(16):165201, 2009.
- [13] Chengteh Lee, Weitao Yang, and Robert G. Parr. Development of the colle-salvetti correlation-energy formula into a functional of the electron density. *Physical Review B*, 37(2):785–789, 1988.
- [14] Andrew J. Murray, Brian C. H. Turton, and Frank H. Read. Real-time computer-optimized electron coincidence spectrometer. *Review of Scientific Instruments*, 63(6):3346–3351, 1992.
- [15] A. Naja, E. M. Staicu-Casagrande, A. Lahmam-Bennani, M. Nekkab, F. Mezdari, B. Joulakian, O. Chuluunbaatar, and D. H. Madison. Triply differential (e,2e) cross sections for ionization of the nitrogen molecule at large energy transfer. *Journal of Physics B: Atomic, Molecular and Optical Physics*, 40(18):3775–3783, 2007.
- [16] K. L. Nixon, A. J. Murray, H. Chaluvadi, C. Ning, and D. H. Madison. Low energy (e,2e) studies from ch₄: results from symmetric coplanar experiments and molecular three-body distorted wave theory. *J Chem Phys*, 134(17):174304, 2011.
- [17] Kate L. Nixon, Andrew James Murray, Ola Al-Hagan, Don H. Madison, and Chuan-gang Ning. Low-energy symmetric coplanar and symmetric non-coplanar (e,2e) studies from the 3a₁state of h₂o. *Journal of Physics B: Atomic, Molecular and Optical Physics*, 43(3):035201, 2010.

- [18] Kate L. Nixon, Andrew James Murray, and Christian Kaiser. Low energy (e,2e) studies of the noble gases in the perpendicular plane. *Journal of Physics B: Atomic, Molecular and Optical Physics*, 43(8):085202, 2010.
- [19] N. T. Padial and D. W. Norcross. Parameter-free model of the correlation-polarization potential for electron-molecule collisions. *Physical Review A*, 29(4):1742–1748, 1984.
- [20] J. P. Perdew and Alex Zunger. Self-interaction correction to density-functional approximations for many-electron systems. *Physical Review B*, 23(10):5048–5079, 1981.
- [21] A. Sid. Erratum: Nonlinear inverse bremsstrahlung absorption in laser-fusion plasma corona [phys. plasmas 10, 214 (2003)]. *Physics of Plasmas*, 10(6):2623–2623, 2003.
- [22] I. Tth and L. Nagy. Triple-differential cross-section calculations for the ionization of ch4 by electron impact. *Journal of Physics B: Atomic, Molecular and Optical Physics*, 43(13):135204, 2010.
- [23] Gregory H. Wannier. The threshold law for single ionization of atoms or ions by electrons. *Physical Review*, 90(5):817–825, 1953.
- [24] S. J. Ward and J. H. Macek. Wave functions for continuum states of charged fragments. *Physical Review A*, 49(2):1049–1056, 1994.

XI. DIFFERENTIAL CROSS SECTION MEASUREMENTS FOR IONIZATION OF N_2 IN COPLANAR GEOMETRY

Ahmad Sakaamini¹, Matthew Harvey¹, Sadek Amami², Andrew James Murray¹, Don Madison² and Chuangang Ning¹ ¹Photon Science Institute, School of Physics and Astronomy, University of Manchester, Manchester M13 9PL, UK

²Physics Department, Missouri University of Science and Technology, Rolla, MO 65409, USA

²Dept. of Physics, State Key Laboratory of Low-Dimensional Quantum Physics, Tsinghua University, Beijing 100084, China

ABSTRACT

Triple differential cross section (TDCS) measurements for ionization of N_2 are presented in a coplanar geometry where one of the outgoing electrons was fixed in angle. Data were obtained at incident electron energies 20 eV and 40 eV above the ionization potential (IP) for the $3\sigma_g$ and $1\pi_u$ states, the outgoing electrons carrying equal energies. Six sets of measurements were obtained at each energy, with fixed angles of 45° , 90° and 125° to the incident electron direction. The data are compared to new calculations using distorted wave methods.

1. INTRODUCTION

Ionization of matter by electron impact is a process that occurs throughout the universe. It is therefore important to provide rigorously tested models of these interactions, so that predictions of the probability of ionization can be made. These processes occur in stellar and planetary atmospheres [1, 2], in plasmas and in Tokomaks [3], and they play an important role in the interaction of radiation with living cells that may lead to cancer [4]. In

these latter cases it is the interaction with low and intermediate energy electrons (typically from threshold to ~ 100 eV above the ionization potential) that has particular relevance, since the probability of DNA damage in this regime is highest. As such it is here that there is the greatest possibility of irreversible damage to living cells, that may lead to death.

Quantum mechanical models are essential to describe these interactions at low energies, since both incident electron and target atom (or molecule) must be considered as quantum objects. The models are complicated by the long-range nature of the Coulomb field that governs the forces between the incident electron and the bound electrons and target core. Atomic targets have spherical symmetry, and so the Coulomb field can be described using a spherical basis. By contrast, molecular targets do not possess this symmetry, since the nuclei and bound electrons are distributed throughout the molecule. This reduction in symmetry places considerable demands on computation requirements when solving Schrödinger's equation for the interaction. A further complexity arises since the experiments do not generally measure the alignment of molecular targets, and so the models must also average over all possible target geometries for a valid comparison to experiment [5]. Additional demands in this energy regime are due to the relatively long time that the electrons interact with the target. Time-dependent models have been used to study these processes for the simplest molecule H_2 [6], however the majority of work on more complex targets (such as N_2 as studied here) adopt time-independent approaches [7, 8, 9, 10, 11, 12, 13, 14]. The interaction between the incident electron and target can be modelled using distorted waves [5], and it is also important to include polarization and correlation effects. Following ionization the outgoing electrons interact with each other and with the resulting ion, leading to post-collisional interactions (PCI) that can strongly influence the cross section that is measured in the asymptotic region [15]. Post-collisional interactions are particularly important at low energies, and are strongest when the outgoing electrons share the excess energy equally [16].

Despite these severe demands, models of the dynamics of collisional ionization are proving to be increasingly accurate as more is understood about the processes that are involved. Precise predictions are now possible for many atomic targets, leading to increased confidence that the essential physics of the interactions are being included. The agreement between theory and experiment for molecular targets is however much poorer, and so it is important to provide accurate experimental data for a range of targets to compare to the developing models, and to test the different theoretical approaches that are being formulated.

For single ionization by electron impact where the spins of the electrons are not detected, the collision can be fully characterised by the incident electron momentum k_1 and k_2 that of the scattered and ejected electrons k_0 and k_0 . The most detailed measurements determine a triple differential cross section TDCS (k_0, k_1, k_2) that is directly proportional to the ionization probability. The TDCS is experimentally determined by measuring the time-correlated signal between scattered and ejected electrons as a function of k_0, k_1 , and k_2 in an ($e, 2e$) experiment.

Since the ejected and scattered electrons may emerge from the interaction in any direction, it is necessary to define a scattering geometry to allow theory to be tested by experiment. In the work described in this paper a coplanar geometry is used where the incident, scattered and ejected electrons are detected in the same plane. A further constraint adopted here is that one of the electrons is fixed in angle with respect to k_0 , and the other is detected at different angles around the interaction region so as to obtain the relative ionization probability. The energy of the outgoing electrons is also set to be equal, so that $(|k_1|) = (|k_2|)$ and $E_1 = E_2 = (E_{inc} - IP)/2$.

In practice, the experiment sets k_1 to be fixed while moving k_2 around the plane, and then sets k_2 to be fixed at the equivalent fixed angle while moving k_1 around the plane, as shown in Figure 1. Since the TDCS must be the same for each process, this allows the alignment accuracy of the apparatus to be checked. No difference was found between

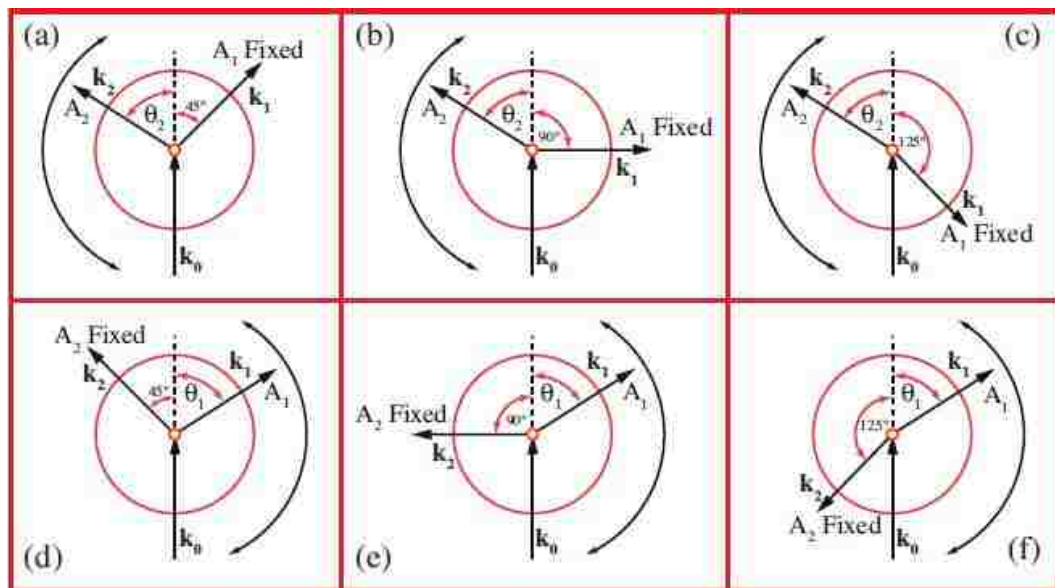


Figure 1. The coplanar geometries in the experiments. (a) and (d) show the geometry when the fixed angle was 45° , (b) and (e) show where the fixed angle was 90° and (c) and (f) show the geometry for a fixed angle of 125° . The TDCS for each of the upper and lower configurations must be the same due to reflection symmetry in the scattering plane.

measurements under these conditions, and so an average of the data was taken over the series of angular runs that were used. Three different fixed angles were chosen, with $\theta_1(\theta_2)^{Fixed} = 45^\circ, 90^\circ$ and 125° as depicted.

In a previous set of experiments carried out in Manchester, TDCS data were obtained for ionization of N_2 in a doubly-symmetric geometry, where both electron detectors were set so that $\theta_1 = \theta_2$ and $E_1 = E_2$. These results were compared to models from the Missouri group of Don Madison and co-workers [17]. The doubly-symmetric geometry is particularly challenging to model, since under these conditions the TDCS is highly sensitive to both initial and final states of the system. In this previous work it was found that the models did not predict the experimental data well for the lowest energy studied ($E_1 = E_2 \sim 5 \text{ eV}$), however as the energy was raised to $E_1 = E_2 = 20 \text{ eV}$ a better agreement was found in

the overall shape of the calculated cross sections. It was suggested at this time that further work was required, including measurements at higher incident energies to establish if the models improved as the interaction time reduced.

The first experiment presented here was hence carried out to ascertain if the models are better at higher energies, and to see how well they predict the TDCS under fixed angle conditions. The same energy-sharing conditions (i.e. $E_1 = E_2$) were adopted so that the new fixed-angle data could be directly linked back to the previous results through their common angles (see below for details). Results from these higher energy experiments on nitrogen are presented in section 4 using a doubly-symmetric geometry with $E_1 = E_2 = 50$ eV. The corresponding comparison with the models demonstrate that at these energies the predictive-power of the theory greatly improves. Following from these experiments, measurements were subsequently carried out using fixed angles as described by Figure 1, at lower energies with $E_1 = E_2 = 10$ eV and 20 eV.

N_2 is a diatomic molecule whose valence electrons combine to produce a strong triple bond, the electrons pairing to form the $3\sigma_g^2$, $1\pi_u^4$ and $2\sigma_g^2$ bonding orbitals and the $2\sigma_u$ anti-bonding orbital.

The ground state electronic configuration of N_2 is hence $(2\sigma_g^2 2\sigma_u^2 1\pi_u^4 3\sigma_g^2) ^1\Sigma_g^+$. Ionization can occur from any orbital, leading to N^+ ions in different final states. In the work presented here ionization was studied from the two outer orbitals, producing the $X^2\Sigma_g^+ N_+^2$ state for electrons ejected from the $3\sigma_g$ orbital, and the $A^2\Pi_u$ state for electrons emerging from the $1\pi_u$ orbital. The spectrometer could resolve these states, since their binding energies are separated by ~ 1.5 eV, and the resolution of the spectrometer under the conditions used in this study was ~ 600 meV. Since the final state of the ion is different in each case, the wave-functions describing the resulting ion states is also different, and so this is expected to influence the measured and calculated TDCS.

To discuss these results, this paper is divided into six sections. Following this introduction the experiment is described briefly in section 2. Section 3 introduces the distorted-wave models used in the calculations, and section 4 compares experimental and theoretical results for coplanar doubly- symmetric ionization from the $3\sigma_g$ orbital 100 eV above the IP. Section 5 shows the results from measurements at fixed angles for both the $3\sigma_g$ and $1\pi_u$ orbitals, and compares these to the calculations. Conclusions are then drawn from these studies in section 6. The

2. THE EXPERIMENTAL APPARATUS

When set to a coplanar geometry, the (e,2e) spectrometer in Manchester can detect outgoing electrons from the interaction region over a range of angles from $\theta_{1,2} = 35^\circ$ to 125° . These angular restrictions arise due to the size of the electron gun and electron detectors. The electron gun adopts a two-stage electrostatic lens, and can deliver electrons with energy from ~ 20 eV to 300 eV, with a beam current of up to $5 \mu A$. The scattered and ejected electron analysers use a triple cylindrical lens to focus electrons emerging from the interaction region onto the entrance aperture of a hemispherical energy selector, the selected electrons being detected by a channel electron multiplier. Details of the spectrometer can be found in previous publications [see e.g. [18, 19, 20]]. A molecular N_2 beam was delivered from a Platinum-Iridium gas needle directed into the interaction region. The spectrometer was evacuated to a base pressure of $\sim 10^{-7}$ torr using a turbo- molecular pump. The vacuum pressure rose to $\sim 2 \times 10^{-5}$ torr when the experiment was running, as monitored using an ion gauge. The electron beam current was typically ~ 200 nA during the experiments, allowing the coincidence signal to be resolved from the background. The spectrometer operated under computer control, with the analyser tuning being optimised each time the analysers were moved to a new angle. In this way any changes in the operating conditions as the experiments proceeded were minimised. A description of the computer control and optimisation systems used in these experiments can be found in [18].

For the experiments in Section 5, a set of coincidence data was taken firstly with analyser 1 fixed in angle as in Figure 1, while analyser 2 swept around the plane. Analyser 2 was then set to the same fixed azimuthal angle, and analyser 1 then swept around the plane. At a given incident energy the data was accumulated for 3000 seconds at each angle, and up to 190 different measurements were produced for a given molecular state. The accumulated data were then averaged for each scattering angle, and the statistical error in the distribution of measurements used to assign an uncertainty.

The incident electron energy was calibrated against the 19.337 eV elastic resonance in helium [21], and the scattered and ejected electron energies were determined from inelastic scattering from this target. Helium was chosen for this purpose, as the inelastic spectrum is well known and can be clearly resolved.

Measurements at the highest energy used in this work (100 eV above the IP for the $3\sigma_g$ state) were taken with each analyser set to select electrons with energy of 50 eV. For this set of data, the analysers were set to the same azimuthal angle ($\theta_1 = \theta_2$). For the fixed-angle measurements shown in section 5, the analysers were adjusted to detect electrons with $(E_1, E_2) = (10 \text{ eV}, 10 \text{ eV})$ and with $(E_1, E_2) = (20 \text{ eV}, 20 \text{ eV})$. The incident electron beam was then scanned in energy to measure a binding energy coincidence spectrum, with the analysers fixed at $\theta_1 = \theta_2 = 45^\circ$. The binding energy spectra then allowed the relative strengths of the signals from each state to be ascertained, so that the data could be inter-normalised. Cross sections measurements were then carried out by adjusting the incident electron beam energy to select either the $3\sigma_g$ or $1\pi_u$ state. Three sets of data were accumulated for each state, by setting $\theta_1^{Fixed}(\theta_2^{Fixed}) = 45^\circ, 90^\circ$ and 125° . Since each set of data contained a common point, this allowed all data at a given energy to be inter-normalised. The experiments did not measure absolute cross sections, and so the data was then scaled to the M3DW calculations as described below.

3. THEORY

A description of the theory was presented in [17] with more detail in [5], so it will not be repeated here. Results are presented for three different distorted wave models – the standard first order distorted wave Born approximation (DWBA), the molecular 3-body distorted wave (M3DW) approximation and the M3DW with the Ward-Macek (WM) approximation for post collisional interactions (PCI) [22].

The important similarities and differences between these three approximations are the following. All three models contain the interaction between the incoming electron and neutral target represented as a spherically symmetric initial state distorting potential. This potential is neutral asymptotically and is a screened nuclear potential for short range. In the spherical approximation, all target nuclei are spread over a thin spherical shell centered on the center-of-mass. For N_2 , this means that we have a charge of +14 on a thin shell with a radius of $1.0371a_0$. For the electronic contribution, we calculate all the molecular wavefunctions using density function theory with a B3LYP/TZ2P basis set on a 3-dimensional numerical grid [5], use these wavefunctions to calculate the electronic charge density on this grid, and then use this density to calculate the spherical symmetric electronic contribution. The final state distorting potential is calculated the same way, except the ionized electron is removed from the charge density such that this potential is asymptotically an ion. The Furness-McCarthy approximation [23] is used to calculate the effect of exchange between the continuum and bound electrons, and the Perdew and Zunger polarization-correlation approximation [24] is used to determine this effect. Both the direct and exchange T-matrices are evaluated for all three approximations.

Finally, we use the orientation averaged molecular orbital approximation to calculate averaging over all molecular orientations. Depending on the symmetry of the state being ionized, this average can be very small or even zero. For states like this, we average over the absolute value of the wavefunction instead of the wavefunction itself. If this average has multiple lobes, we make the first lobe positive, second lobe negative and so forth. For the

$3\sigma_g$ state, we tried both types of averages and the shapes of the resulting cross sections were almost exactly the same, although there was a small magnitude difference. The presented results are for the average over the wavefunction. For the $1\pi_u$ state, we averaged over the absolute value of the wavefunction.

The main difference between the three calculations is the treatment of PCI – the final state post collision interaction between the two electrons that is very important for collisions of this type. In the DWBA, PCI is included only to first order. In the M3DW, PCI is included exactly to all orders of perturbation theory, and in WM, the Ward-Macek approximation is used to approximate PCI. There are two reasons to examine this approximation. First, since it is simply a factor times the DWBA amplitude, it is an easy way to include PCI in a standard DWBA calculation. Second, in some of our early work on molecules, it appeared that the exact PCI overestimated the effects of PCI and the WM approximation gave somewhat better agreement with experiment. In the comparison with experiment below, we show all three approximations that are calculated.

4. COPLANAR DOUBLY-SYMMETRIC EXPERIMENTS 100 EV ABOVE THE $3\sigma_g$ IP

Following from the low energy results detailed in previous work [17], experiments were carried out at higher energies in both a coplanar doubly-symmetric geometry and with the electron gun set to 45° to the detection plane. The motivation for this work was to establish if the comparison between theory and experiment improved as the incident electron energy was increased.

Figure 2 shows the results of these studies plotted on a logarithmic scale for ionization from the $3\sigma_g$ state. The incident electron energy was adjusted to be 100 eV above the ionization potential for this state, and the analysers were selected to have equal energy and equal azimuthal angles throughout data collection ($E_1 = E_2 = 50 \text{ eV}$; $\theta_1 = \theta_2 = \theta$). The electron gun was positioned both in the scattering plane (coplanar geometry) and at an angle

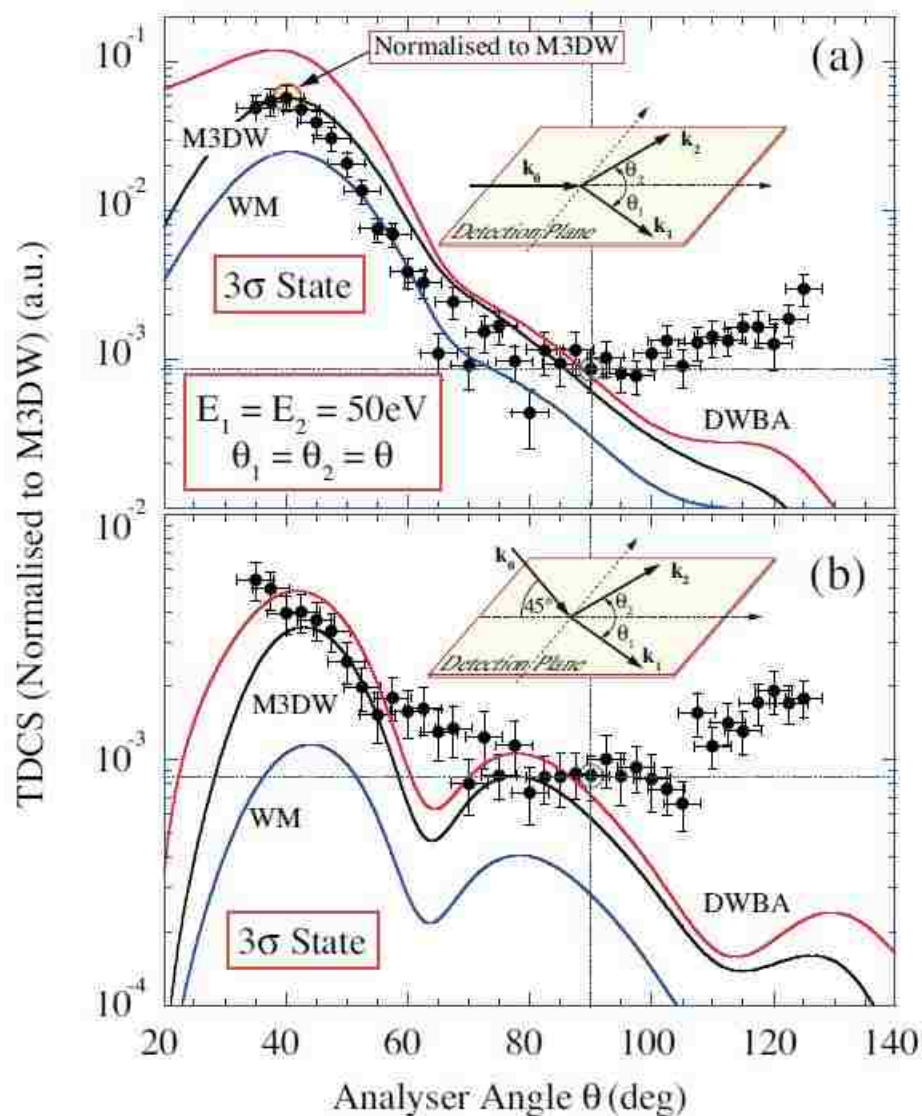


Figure 2. Measurements with incident electron energy 100 eV above the IP for the $3\sigma_g$ state, in both (a) a coplanar doubly-symmetric geometry and (b) for the incident electron beam direction k_0 at an angle of 45° to the detection plane spanned by k_1 and k_2 . A common normalisation point exists between measurements when $\theta_1 = \theta_2 = 90^\circ$. The data are then re-normalised to the M3DW calculation at their peak. DWBA, M3DW and WM theories are shown, together with the M3DW calculation at 45° that has been convoluted with the experimental angular resolution (*dotted curve in (b)*).

of 45° to the detection plane as shown in the inset Figure. The data were normalised to the M3DW calculation at the forward peak in a coplanar geometry, since the experiments

did not measure absolute cross sections. This is the same normalisation technique as was used previously [17], and allows a relative comparison to be made between the data and the different models.

The results from these series of experiments in [17] and as described here show that the ionization cross-section is sensitive to both the state from which ionization occurs, and the collisional energy of the interaction. Comparison of the coplanar data at 100 eV above the IP for the $3\sigma_g$ state (Figure 2(a)) shows considerably better agreement with theory than was found in previous work at lower energies [17], in particular for forward scattering where the M3DW calculation passes closely through the data. In the backscatter direction beyond $\theta = 90^\circ$ however, the calculations predict that the magnitude of the cross section should continue to decrease, in contrast to what is observed.

When the electron gun was raised out of the detection plane (Figure 2(b)), the cross section is seen to decrease as the scattering angle increases from 35° , and shows a plateau region from around 75° to 100° , although the uncertainties and variations in the data are relatively large in this region at these angles. Note that the data in this geometry have been inter-normalised to the coplanar data through the common point $\theta_1 = \theta_2 = 90^\circ$, which is depicted by the dotted lines and as a circle on Figure 2. The cross section is found to increase in the backscatter direction beyond 110° up to 125° . Further measurements were not possible beyond this angle due to the proximity of the analysers to each other. Since the TDCS must be zero at both 0° and 180° under doubly symmetric conditions, the results hence shows evidence of two distinct peaks and a plateau region, with maxima around 35° , 90° and 125° .

The calculations also predict three peaks in the TDCS, however they predict the local minima to be deeper than observed. The predicted forward minima occur at $\sim 60^\circ$, compared to the start of the plateau region at $\sim 75^\circ$ in the data. In the backscatter direction the calculated minima are around 110° , in closer agreement with the measurements. All calculations underestimate the cross section in the backscattering region, whereas in the

forward direction the DWBA model appears to yield the overall best fit to the data. Since electron backscattering requires a strong interaction between the target nuclei and the scattered electrons, the backscatter results imply that the models are underestimating the magnitude of the nuclear force in the interaction. This is probably due to the spherical averaging process that spreads the nuclear charge over a thin spherical shell.

5. COPLANAR MEASUREMENTS WITH FIXED ANGLES

To further test theory, asymmetric coplanar measurements were conducted with one of the electrons detected at a fixed angle, as shown in Figure 1. Prior to measurement of the cross sections, the energy of the detected electrons was set to be either 10 eV or 20 eV, and the energy of the incident electron was adjusted in steps of 0.125 eV so as to obtain a binding energy spectrum from the coincidence signals. These experiments were carried out with $\theta_1 = \theta_2 = 45^\circ$, as this produced a strong signal above the background random counts. The incident energy was hence scanned through ionization from both the $3\sigma_g$ and $1\pi_u$ states. This allowed the ratio of the coincidence count rates to be determined from each state, by fitting a Gaussian to the peaks that were resolved. Figure 3 shows an example of one of the binding energy spectra obtained for outgoing electrons selected to have energy of 10 eV. By taking several binding energy spectra at each energy, the ratio of cross sections from these states was determined to be $(1\pi_u^{45^\circ} : 3\sigma_g^{45^\circ})^{10/10eV} = (49\% \pm 6\%)$. Similar measurements at 20 eV outgoing energy found this ratio to be $(1\pi_u^{45^\circ} : 3\sigma_g^{45^\circ})^{20/20eV} = (23\% \pm 3\%)$. These ratios were then used in the inter-normalisation procedure discussed below.

5.1. Results for Outgoing Electron Energies of 10 eV. Figure 4 shows the results from these studies for outgoing electron energies of 10 eV, at three fixed angles of 45° , 90° and 125° for both $3\sigma_g$ and $1\pi_u$ states. The data are placed on a logarithmic scale to allow comparison to the models, which have all been convoluted with the angular resolution of the experimental apparatus.

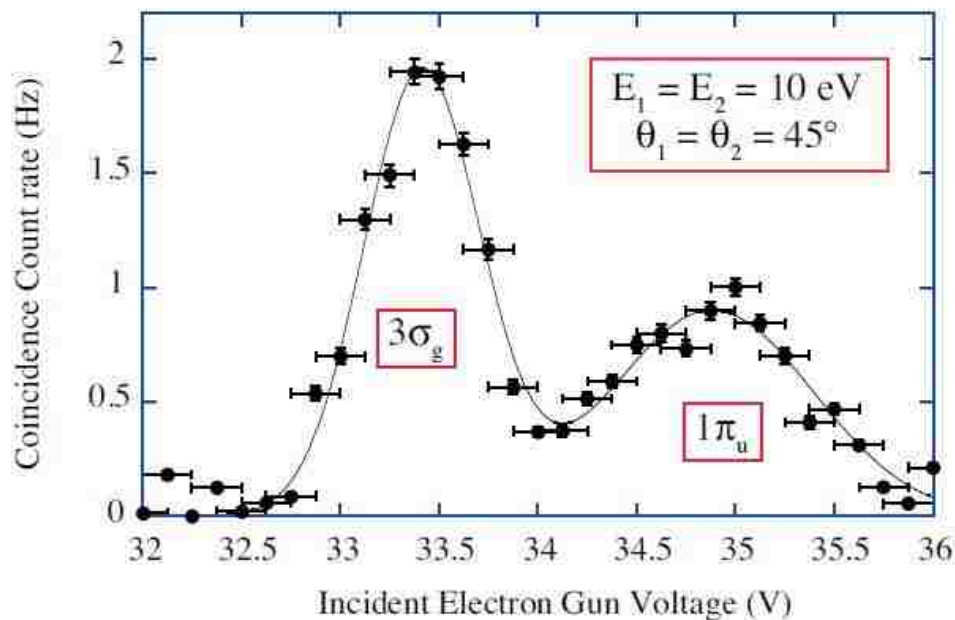


Figure 3. Example of a binding energy spectrum, taken for outgoing electron energies of 10 eV at scattering angles of 45° . The data show that the individual $3\sigma_g$ and $1\pi_u$ states are well resolved, allowing the relative ratios of the TDCS from each state to be determined.

Since the experiments do not measure absolute cross sections, the data are again normalised to the maximum of the M3DW calculation for the $3\sigma_g$ state, as was carried out in [17]. This normalisation point is shown in Figure 4(a). The data for the $3\sigma_g$ state in figures 4(a) to 4(c) were then inter-normalised through their common points, allowing for reflection symmetry in the detection plane as discussed by Figure 1. These points are shown in the Figure. As an example, in Figure 4(b) the left-hand point (blue circle) shows where $TDCS(\theta_1 = 45^\circ, \theta_2 = 90^\circ) \equiv TDCS(\theta_1 = 90^\circ, \theta_2 = 45^\circ)$, whereas the red-circled point shows where $TDCS(\theta_1 = 125^\circ, \theta_2 = 90^\circ) \equiv TDCS(\theta_1 = 90^\circ, \theta_2 = 125^\circ)$.

Figures 4(d)-(f) show results for the $1\pi_u$ state, inter-normalised to the $3\sigma_g$ state through the ratio determined from the binding energy spectra (as in Figure 3). The axes for these set of data are adjusted to be the same as for the $3\sigma_g$ state, allowing direct

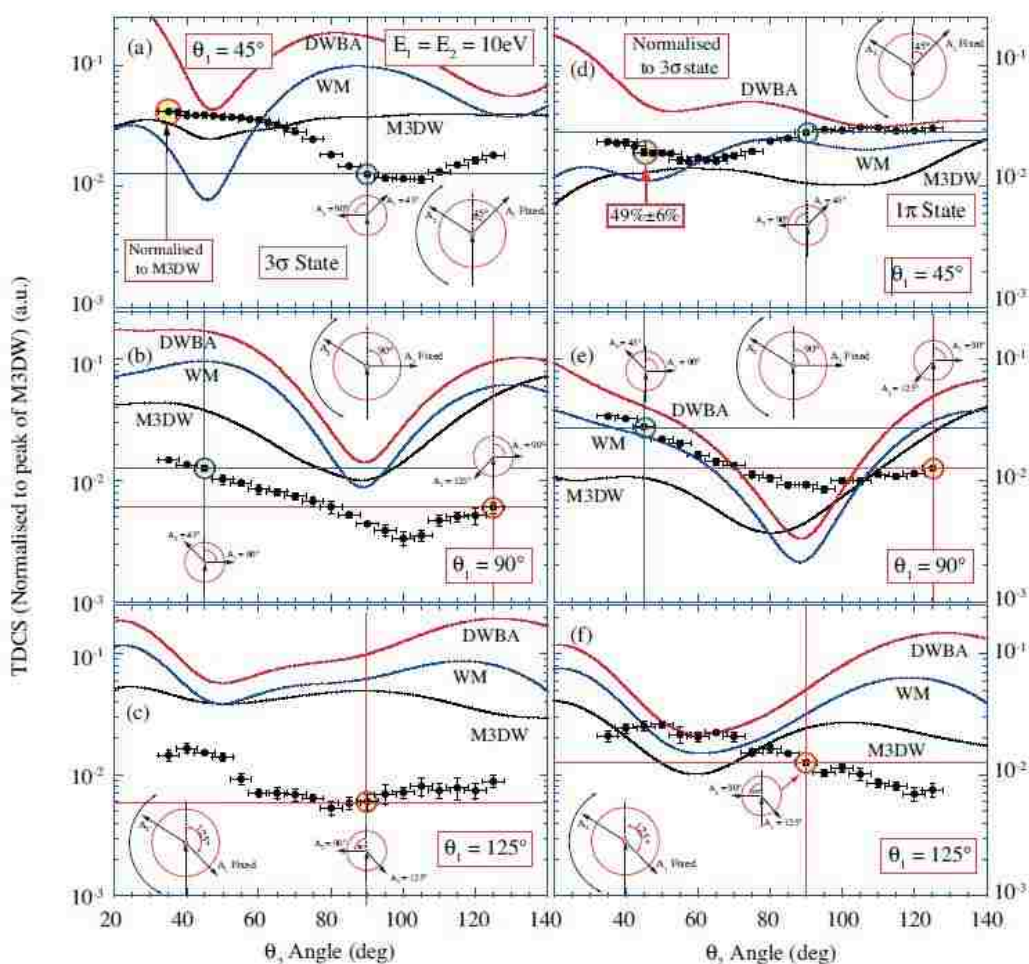


Figure 4. Results for outgoing energies of 10 eV, for the $3\sigma_g$ state (a-c) and the $1\pi_u$ state (d-f). The experimental data are normalised to the peak of the M3DW theoretical calculations in (a), as described in [13]. All other data are then inter-normalised at the angles shown by circles, as described in the text.

comparison of the results. The relative common points are also shown for this state. The inter-normalisation procedure hence allows all six data sets to be re-scaled to the M3DW calculation, as set in Figure 4(a).

The results in Figure 4 show that none of the calculations adequately describe the data at this energy. For the $3\sigma_g$ state at a fixed angle of 45° , all calculations predict minima around 45° in contrast to measurement, and predict maxima around 80° whereas the data finds a minimum in this region. Calculations for the $1\pi_u$ state at this angle (Figure

4(d)) are slightly better as their magnitudes are closer to experiment, however once again the predicted structures do not emulate the data. For a fixed angle of 90° , all calculations predict a broad minimum at $\sim 90^\circ$ for both states. The experiments find a shallow minimum at $\sim 100^\circ$ for the $3\sigma_g$ state and at $\sim 90^\circ$ for the $1\pi_u$ state. The calculations are hence in better agreement here, however for the $3\sigma_g$ state the calculations are broadly an order of magnitude larger than the normalised data. For the fixed scattering angle of 125° , there is little agreement between the calculations and the data for either state, and once again the predicted cross section for the $3\sigma_g$ state is much larger than measured. The models clearly fail to fully include the correct physics of the interaction at these energies, as was also found in [17].

5.2. Results for Outgoing Electron Energies of 20 eV. Figure 5 shows the results at outgoing energies of 20 eV, again for fixed angles of 45° , 90° and 125° . The data are once more placed on a logarithmic axis to allow comparison with Figure 4, and are set to the same scale for both data sets.

The data in Figure 5 are again normalised to each other and to the peak of the M3DW calculations, by consideration of the binding energy spectra at this energy. The common points between data sets are once more shown.

The agreement between experiment and theory improves under these kinematic conditions, however significant differences remain. At a fixed scattering angle of 45° all calculations are closer in magnitude to the data for both states. In this case the M3DW and WM calculations are closer than the DWBA calculation, indicating that post-collisional interactions are playing a significant role here. All calculations again predict broad minima in the forward direction for the $3\sigma_g$ state in contrast to measurement, and predict maxima around 70° which disagrees with observations. For the $1\pi_u$ state (Figure 5(d)), both WM and M3DW calculations align reasonably well with the measurements.

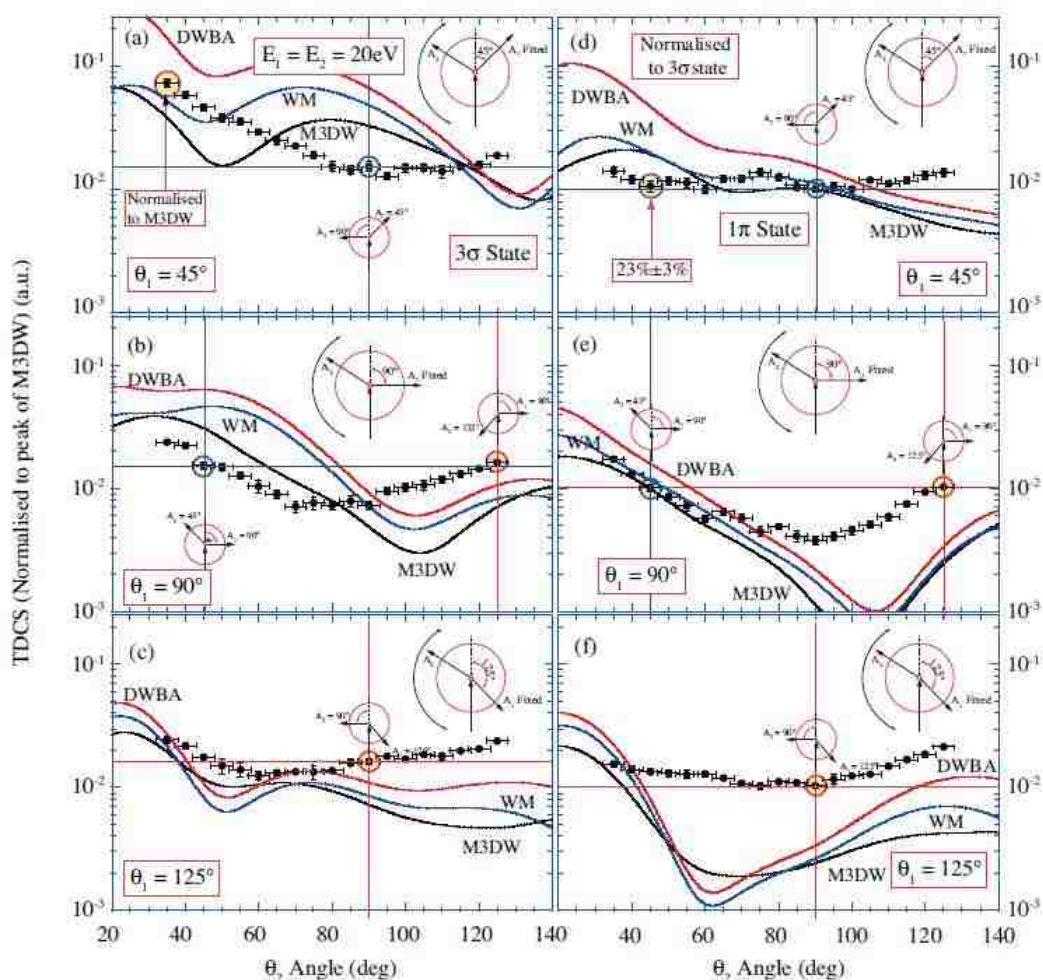


Figure 5. Results with outgoing electron energies of 20 eV for the $3\sigma_g$ and $1\pi_u$ states. The experimental data are normalised to the peak of the M3DW theoretical calculations in (a). All other data are then inter-normalised at the angles shown by dashed lines and circles, as described in the text.

At a fixed angle of 90° for the $3\sigma_g$ state (Figure 5(b)), the M3DW calculation yields the closest fit to the data, however this calculation predicts a minimum at $\sim 105^\circ$ whereas the experiment finds a minimum at $\sim 70^\circ$. By contrast, all three calculations for the $1\pi_u$ state are in closer agreement with the data for forward scattering (Figure 5(e)). The models again predict a minimum at around 105° , whereas the data finds a local minimum at 90° .

For a fixed angle of 125° all theories predict a cross section that is reasonably close to the measurements for the $3\sigma_g$ state (Figure 5(c)), whereas all fail to emulate the data for the $1\pi_u$ state (Figure 5(f)). For the $1\pi_u$ state the predicted cross sections in the forward direction all have deep minima at around 65° , which is not reproduced in the data.

The wide variation found here when comparing theory to experiment makes it difficult to ascertain where improvements can be made to the models. It appears that the calculations from the $1\pi_u$ state overall are in better agreement with the data than for the $3\sigma_g$ state, and so it may be that the $1\pi_u$ target wavefunction used here is better than for the $3\sigma_g$ state. The magnitudes and shapes of the predicted cross sections are however generally in poor agreement with experiment, and indeed do not seem to follow any particular trend as the fixed scattering angle increases. It does appear that the calculations improve as the energy is raised, which is consistent with findings from previous studies [17]. This is perhaps to be expected for these types of calculations, which have proven to be successful particularly at higher energies.

6. DISCUSSION AND CONCLUSIONS

The results from experiments and calculations on N_2 as detailed here show that the ionization cross-section is sensitive to both the state from which the ionization occurs, and the collisional energy of the interaction. Comparison of coplanar experimental data at 100 eV above the IP for the $3\sigma_g$ state shows considerably better agreement with theory than was found in previous work [17], in particular for forward scattering where the M3DW calculation passes closely through the data. In the backscatter direction however, the calculations predict that the magnitude of the cross section should decrease, in contrast to observation. When the electron gun is raised out of the detection plane the calculations again agree with the data in the forward direction, however they all predict a deep minimum at $\sim 60^\circ$ which is not observed. Once again in the backscattering direction the calculations fail to agree with the measurement.

The comparison between theory and experiment at energies 20 eV and 40 eV above the ionization potentials of the $3\sigma_g$ and $1\pi_u$ states is much less satisfactory. Six inter-normalised sets of data were obtained at each energy, allowing a rigorous test of calculation over a range of kinematics. Under certain conditions the calculations emulated the data reasonably well, however in general the magnitude and shape of the predicted cross sections fail to agree with data. No definitive conclusions can be drawn from these results, however it does appear that the calculations for the $1\pi_u$ state more closely agree with the experiment, and that the model improves as the energy is increased.

One possible reason for the poor agreement between theory and experiment found here might be due to the averaging of molecular orbitals approximation that was adopted, as discussed in section 3. Attempts were made in this work to calculate the cross sections using a ‘proper averaging’ approach (i.e. by calculating the TDCS for each orientation of the molecule, then averaging the final results), however these calculations would not converge. Clearly more work is required to ascertain where improvements can be made to the models can be made, so that they can more realistically predict the data.

ACKNOWLEDGMENTS

AS would like to thank the University of Manchester for financial support through their overseas student award. AM and MH would also like to thank the EPSRC for funding this project under award R120272. SA and DM acknowledge the support of the US National Science Foundation under Grant No. PHY-1505819 and CN would like to acknowledge the support of the National Natural Science Foundation of China under Grant No. 11174175.

REFERENCES

- [1] P S Barklem, Y Osorio, D V Fursa, I Bray, O Zatsarinny, K Bartschat and A Jerkstrand
Astron. & Astro. **606** A11 (2017) & references therein

- [2] see e.g. T Rauch, P Quinet, M Knörzer, D Hoyer, K Werner, J W Kruk and M Demleitner *Astron.& Astro.* **606** A105 (2017).
- [3] D C Griffin, M S Pindzola, J A Shaw, N R Badnell, M O'Mullane and H P Summers *J Phys B* **30** 3543 (1997)
- [4] M U Bug, W Y Baek, H Rabus, C Villagrasa, S Meylan and A B Rosenfeld, *Rad. Phys. & Chem.* **130** 459 (2017)
- [5] Madison D H and Al-Hagan O, *J. At. Mol. Opt. Phys.* 2010 367180 (2010).
- [6] Colgan J, Al-Hagan O, Madison D H, Kaiser C, Murray A J and Pindzola M S *Phys. Rev. A* **79**, 052704 (2009)
- [7] Avaldi L, Camilloni R, Fainelli E and Stefani G, *J. Phys. B: At. Mol. Opt. Phys.* **25** 3551 (1992)
- [8] Gao J, Madison D H and Peacher J L, *Phys. Rev. A* **72** 032721 (2005)
- [9] Murray A J, Hussey M J, Gao J and Madison D H, *J. Phys. B: At. Mol. Opt. Phys.* **39** 3945 (2006)
- [10] Naja A, Staicu-Casagrande E M, Lahmam-Bennani A, Nekkab M, Mezdari F, Joulakian B, Chuluunbaatar O and Madison D H, *J. Phys. B: At. Mol. Opt. Phys.* **40** 3775 (2007)
- [11] Murray A J, Hussey M J, Kaiser C, Gao J and Madison D H *J. Electron Spec.* **161** 11 (2007)
- [12] Lahmam-Bennani A, Staicu-Casagrande E M and Naja A, *J. Phys. B: At. Mol. Opt. Phys.* **42** 235205 (2009)
- [13] Toth I and Nagy L, *J. Phys. B: At. Mol. Opt. Phys.* **44** 195205 (2011)
- [14] Murray A J *J. Phys. B: At. Mol. Opt. Phys.* **48** 245203 (2015)

- [15] M Brauner, J S Briggs and H Klar J Phys B **22** 2265 (1989)
- [16] F H Read Electron impact ionization (ed T D Mark and G H Dunn, Vienna: Springer) pp42 (1985)
- [17] A Sakaamini, S Amami, A J Murray, C Ning and D Madison J Phys B. **49** 195202 (2016)
- [18] Murray A J, Turton B C H and Read F H, Rev. Sci.Instrum. 63 3346 (1992)
- [19] Murray A J, Read F H and Bowring N J, J. Phys. B: At. Mol. Opt. Phys. 30 387 (1997)
- [20] M J Hussey and A J Murray J. Phys. B: At. Mol. Opt. Phys. 38 2965 (2005)
- [21] Brunt J N H, King G C and Read F H J. Phys. B: At. Mol. Opt. Phys. 10 1289 (1977)
- [22] Ward S J and Macek J H, Phys. Rev. A 49 1049 (1994)
- [23] J B Furness and I E McCarthy J. Phys. B 6 2280 (1973)
- [24] J P Perdew and A Zunger, Phys. Rev. B 23 (1981).

SECTION

4. SUMMARY AND CONCLUSIONS

Even though there are several theoretical models available for calculating the TDCS for electron-impact ionization numerically, more ($e, 2e$) studies are needed to be able to develop comparable accurate models for atoms and molecules, especially for atoms heavier than the hydrogen atom, such as the noble gases and some other atoms. In this dissertation, I have presented our theoretical distorted wave approach and have compared our results with other approaches for some inert gases atoms such as Ne and Ar and other heavy atoms such as *Mg*, *Na*, and *Ca* as well as some molecules like CH_4 , N_2 , and H_2O in order to examine the accuracy of the prediction of these models and to see how well they describe electron- impact ionization. We have collaborated with different experimental groups which allowed us to test our model for different targets and different types of geometries. We have found that it was very important to include the PCI (Post Collision Interaction) to achieve good agreement between experiment and theory. Several interesting results were found and they will be summarized in the following paragraphs. Starting with heavy atoms, we have examined different kinematics geometries and we have compared the results of the 3DW, WM, and DWBA TDCS for Ne and Ar atoms with experimental data. We compared experimental data and theoretical results for ionization of the Ne 2p- state in the perpendicular plane for symmetric energies between 2.5 eV and 25 eV. Both DWBA and WM approximations gave some discrepancy with the experimental data. In general, however, one can note that WM agreed better with the experimental data than DWBA as the incident electron energy decreased from 25 eV to 2.5 eV. For higher energies, DWBA showed an accurate prediction of the minimum at with an overestimation of the width of the distribution. WM does better for lower energies since PCI becomes more important with decreasing energy and WM

has PCI to all orders of perturbation theory while the DWBA has PCI only to first order. In a second study of Ne (2p) ionization (see Paper I), for an incident energy of 65 eV, Dorn's group in Heidelberg measured a full 3D (3-dimensional) TDCS. We compared the experimental results with four different theoretical models (DWB2-RM, DWBA-WM, 3DW, and BSR). The experimental measurements were made for asymmetric outgoing angles and ejected electron energies ranging between 2 - 8 eV. Detailed comparisons between experiment and theory were made for three planes (scattering, half perpendicular, and full perpendicular). Both DWB2-RM and DWBA approaches provided reasonable agreement with the experimental data for ejected angles ranging between 60° - 300° , where the PCI is not important, while the DWBA-WM approximation, where PCI is included using the Ward-Macek approximation, showed reasonable agreement close to 0° and 360° degrees. This result showed the importance of the PCI effect for low energy electrons being emitted close to each other. On the other hand, the BSR and 3DW models results were in very good agreement with each other and the data. Overall, the agreement provided by both the 3DW and BSR approaches were excellent for this study.

Next we compared DWBA, WM, and 3DW results for electron impact ionization of Ar (3p) for symmetric outgoing angles and equal outgoing electron energies ranging from 15 eV to 100 eV and also for asymmetric scattering angles with equal outgoing electron energies of 92.12 eV. Overall, the results of DWBA approximation for the first case (symmetric outgoing electron angles and energies) showed a failure to predict even the shape of the data. On the other hand, WM showed qualitative agreement as the outgoing electron energies increased from 35 eV to 100 eV, which revealed the importance of the PCI. However, we found that the 3DW agreed much better than WM and DWBA with the data in this energy range. Clearly, this indicates that including PCI exactly in the 3DW was very important. While there was good agreement with the data for energies from 40 eV to 100 eV, there was qualitative agreement for energies from 15 eV to 35 eV. For the asymmetric scattering angles with equal outgoing electrons energies, the 3DW

approximation was in very good agreement with the data at 30° and smaller. We have also extended the comparison of theoretical models with the experimental data for a larger incident electron energy for ionization of Ar (3p) (as seen in Paper III).

For this study the projectile scattering angle was limited to only two angles, 10° and 15° . The 3DW model was compared with the DWB2-RM and BSR models. For both scattering angles, the 3DW approach showed very good agreement with the experimental data. The agreement of the 3DW results and the experimental data improved dramatically as the ejected electron energy increased, and there was an excellent agreement in predicting the shape of the data and the binary peak location as well for the highest energy, with a reasonable agreement for the recoil peak. However, the other theoretical approaches were in good agreement in some places as well. Therefore, it is hard to pick the best one in terms of agreement with the experimental data. We also compared the theoretical models (3DW and BSR) in three-dimensional kinematics for ionization of Ar (3p) at low incident electron energy ($E_0 = 66$ eV) and scattered electron angles of (10° , 15° and 20°) with three different ejected electron energies (2, 5 and 10 eV) (as seen Paper IV). For this study, we compared the available experimental data with only the 3DW and BSR models. Overall, we found that the BSR model gave better agreement with experimental data than the 3DW model. Evidently, there are some additional important physical effects for argon that are not important for neon. One possibility might be the single-configuration description of the initial and final bound states of the target used in the 3DW approach instead of the multi-configuration expansion with term-dependent orbitals that the BSR model used. The strength of the 3DW approach lies in the exact treatment of PCI and this effect provided the qualitative agreement with experimental data that has been obtained for the angular position of the peaks in the scattering plane. On other hand, the binary peak cross-section was too small, especially outside the scattering plane. For the other two planes (half perpendicular

and full perpendicular), the 3DW results was found to be in poor agreement with both the BSR and the experimental data. The results of the study showed that the 3DW approach results are very different for Ne and Ar for almost the same kinematics.

The next thing we studied was triple differential cross sections for electron impact ionization of laser aligned atoms. This type of measurements has been performed for the first time for Mg atoms at the University of Manchester, UK by Murray's group. Papers (V, VI) showed the TDCS for electron impact ionization of the ground state 3s and 3p states. For the ground state Mg (3s), the 3DW, DWBA and TDCC have been compared with the experimental data for equal sharing outgoing electron energies of 20 eV and asymmetric scattering angles. Also, the theoretical models have been tested for different equal sharing outgoing electron energies ranging from 10 eV to 25 eV, and symmetric outgoing electron angles. Overall, we found that the three models gave reasonably good agreement with the data. However, the 3DW model predicted the shape and the location of the binary peak a little better. For the scattering plane, we have only compared the 3DW and DWBA calculations with the experimental data. As mentioned above, this study was the first experiment for aligned atoms, where the atom was excited to an aligned state by a linearly polarized laser (as seen in Papers V, VI). On the scattering plane, for different orientation angles (β) ranging from 0° to 150° , the 3DW approximation results showed very good agreement with the shape and peak location of the data as the orientation angle (β) decreased from ($150^\circ - 40^\circ$). However, there was a small shift in the peak of the experimental data starting from 90° to the smaller angles. On the other hand, DWBA results were in relatively good agreement with data both in shape and peak location, but the cross sections were larger than the 3DW results. However overall, the 3DW results were in much better agreement with experiment than the DWBA results both in and out of the scattering plane. The only significant disagreement with experiment occurred for the alignment being perpendicular to the scattering plane. For this case both the 3DW and DWBA predicted zero cross-sections while experiment found significant non-zero results. The TDCC, on the other hand, predicted a non-zero result

(but much smaller than experiment). The non-zero cross sections predicted by the TDCC resulted from the unnatural parity contributions to the ionization amplitude which is not included in both the 3DW and DWBA approximations. Consequently, it appears that we need to figure out how to include these contributions into the 3DW and DWBA.

Finally, we conclude our ($e, 2e$) study by examining the ionization of some molecules. The theoretical models for molecules (M3DW, DWBA, and WM) have been examined for several molecules such as, N_2 , H_2O and CH_4 . For the N_2 molecule, the triple differential cross-section has been measured and calculated for low incident electron energy ionization of the $3\sigma_g$, $1\pi_u$ and $2\sigma_g$ states for both in and out of the scattering plane and for both symmetrical and asymmetrical kinematic geometries. Outgoing electron energies ($E_1 = E_2$ and $E_1 \neq E_2$) have been investigated. For this experiment, three body distorted wave approximations (M3DW, DWBA, and WM) have been examined. The results of the theoretical approximations showed the relative importance of exact PCI and PCI approximated by WM model. In some cases the M3DW found exact PCI to be overestimated, while WM provided better agreement with the experimental data. For both cases, the theoretical results are in better agreement with the experimental data as the incident energy increases. Consequently, we have made a new study for even higher energies to see if the agreement with experiment continues to improve (see Paper XI). The TDCS were measured and calculated for an incident electron energy at 20 eV and 40 eV above the ionization potential (IP) for two states ($3\sigma_g$ and $1\pi_u$) and for equal outgoing electron energies, and fixed scattered electron angles of (45° , 90° , and 125°). Unfortunately, the results were not as good as expected. On the more positive side, the comparison of the data and the theoretical calculations for 100 eV above the ionization potential (IP) for the state showed a better agreement with experiment than that was found in the previous work (see Paper VIII), especially for the binary peak. We also found reasonable agreement for the magnitude of the recoil peak. In contrast, the TDCS calculated results for the recoil peak ($\psi = 45^\circ$) failed to agree with the experimental data. The only comment that could be made is that

it is hard to draw a good picture for these results, but only we can say that the M3DW improved as the energy increased, and its results for the state were in better agreed with the data than for the state. It is obvious that more investigation should be done to improve the M3DW model. Because of this overall reasonable success for N_2 , one can ask whether or not it will also work for other molecules larger than N_2 . For this matter, the M3DW model has been tested for two more molecules (H_2O and CH_4). For the H_2O case (Paper IX), we have compared the experimental data with two approximations of the M3DW model, the M3DW-OAMO (orientation-averaged molecular orbital) and The M3DW- PA (proper average over orientation) for a projectile energy of 81 eV for the $1b_1$ and $3a_1$ orbital states of water. We were able to compare the full three –dimensional representations of TDCS with the experimental data using only the OAMO approximation due to the much smaller computer time needed for these calculations compared to the PA approximation, which is not feasible due to the cost of the computation. The overall comparison with experiment provided by the OAMO calculations for a scattering angle of 10° and ejected electron energy of 10 eV is that the TDCS was in reasonable qualitative agreement with the experimental data in the binary peak region, but the recoil peak was too small. For a comparison with the PA calculation, we performed our calculations for three perpendicular planes (the scattering plane, half perpendicular, and full perpendicular plane). Overall the comparison between experiment and both approximations indicated that the PA approximation provided a more accurate prediction of the experimental data than the OAMO.

Last but not the least, the low energy theoretical and experimental triple differential cross sections for methane CH_4 for the highest occupied molecular orbital ($1t_2$) HOMO state has been studied using the M3DW and DWBA models for molecules compared with the Ne atom using 3DW and DWBA models for the perpendicular plane, with symmetric kinematics and outgoing electron energies ranging between 1.5 eV and 30 eV. Paper (CH_4 Vs. Ne) showed that the results of the calculations for Ne, in general, were much better than what was found for the case of CH_4 due to the complexity of the CH_4 structure even

though it contains the same number of electrons. It is seen that the M3DW failed even to predict the structure of the data in all cases except the case of the highest energy of 30 eV. All in all, it is clear that the study suggests that more investigation must be done for this molecule using the PA approximation.

REFERENCES

- [1] H. S. W. Massey, E. H. Burhop, and H. Gilbody. collision of electrons with atoms. *Electronic and ionic impact phenomena (Oxford)*, 1, 1969.
- [2] D. H. Madison and O. Al-Hagan. *Journal of Atomic, Molecular, and Optical Physics*, 2010:367180, 2010.
- [3] A. Senftleben, T. Pflueger, X. Ren, O. Al-Hagan, B. Najjari, D. Madison, A. Dorn, and J. Ullrich. *J. Phys. B: At. Mol. Opt. Phys*, 43:081002, 2010.
- [4] A. Senftleben, O. Al-Hagan, T. Pflueger, X. Ren, D. Madison, A. Dorn, and J. Ullrich. *J. Chem. Phys.*, 133:044302.
- [5] X. Ren, T. Pfluger, S. Xu, A. Senftleben, J. Colgan, M. S. Pindzola, A. Dorn, and J. Ullrich. *J. Phys.: Conf. Ser*, 338:052037, 2012.
- [6] X. Ren, S. Amami, O. Zatsarinny, T. Pflüger, M. Weyland, W. Y. Baek, H. Rabus, K. Bartschat, D. Madison, and A. Dorn. *Phys. Rev. A*, 91:032707, Mar 2015.
- [7] J. Colgan, M. S. Pindzola, F. J. Robicheaux, D. C. Griffin, and M. Baertschy. *Phys. Rev. A*, 65:042721, Apr 2002.
- [8] G. S. J. Armstrong, J. Colgan, and M. S. Pindzola. *Phys. Rev. A*, 88:042713, Oct 2013.
- [9] J. Colgan, M. S. Pindzola, F. J. Robicheaux, D. C. Kaiser, A. J. Murray, and D. H. Madison. *Phys. Rev. Lett*, 101:233201, 2008.
- [10] J. Colgan, O. Al-Hagan, D. H. Madison, A. J. Murray, and M. S. Pindzola. *J. Phys. B: At. Mol. Opt. Phys*, 42:171001, 2009.
- [11] K. Bartschat and P. G. Burke. *J. Phys. B: At. Mol. Opt. Phys*, 20:3191–3200, 1987.

- [12] K. Bartschat. *Comput. Phys. Commun.*, 75:219, 1993.
- [13] R. H. G. Reid, K. Bartschat, and A. Raeker. *J. Phys. B: At. Mol. Opt. Phys.*, 31:563, 1998.
- [14] K. Bartschat and P. G. Burke. *J. Phys. B: At. Mol. Opt. Phys.*, 20:3191–3200, 1987.
- [15] X. Ren, T. Pflueger, J. Ullrich, O. Zatsarinny, K. Bartschat, D. H. Madison, A. Dorn, and J. Ullrich. *Phys. Rev. A*, 85:032702, 2012.
- [16] X. Ren, A. Senftleben, T. Pflueger, A. Dorn, K. Bartschat, and J. Ullrich. *Phys. Rev. A*, 83:052714, 2011.
- [17] X. Ren, A. Senftleben, T. Pflueger, J. Ullrich, K. Bartschat, and A. Dorn. *ibid.*, 89:029904(E), 2014.
- [18] M. Ulu, Z. N. Ozer, M. Yavuz, O. Zatsarinny, K. Bartschat, M. Dogan, and A. Crowe. *J. Phys. B: At. Mol. Opt. Phys.*, 46:115204, 2013.
- [19] O. Zatsarinny and K. Bartschat. *Phys. Rev. A*, 85:062709, 2012.
- [20] O. Zatsarinny and K. Bartschat. *Phys. Rev. A*, 85:032708, 2012.
- [21] O. Zatsarinny and K. Bartschat. *J. Phys. B: At. Mol. Opt. Phys.*, 46:112001, 2013.
- [22] X. Ren, T. Pflueger, J. Ullrich, O. Zatsarinny, K. Bartschat, D. H. Madison, A. Dorn, and J. Ullrich. *Phys. Rev. A*, 85:032702, 2012.
- [23] O. Zatsarinny and K. Bartschat. *Phys. Rev. A*, 85:032708, 2012.
- [24] T. Pflueger, O. Zatsarinny, K. Bartschat, A. Senftleben, X. Ren, J. Ullrich, and A. Dorn. *Phys. Rev. Lett.*, 110:153202, 2013.
- [25] K. Bartschat, E. T. Hudson, M. P. Scott, P. G. Burke, and V. M. Burke. *J. Phys. B: At. Mol. Opt. Phys.*, 29(1):115, 1996.

- [26] O. Zatsarinny and K. Bartschat. *Phys. Rev. A*, 85:032708, Mar 2012.
- [27] O. Zatsarinny and K. Bartschat. *Phys. Rev. A*, 85:062709, Jun 2012.
- [28] Oleg Zatsarinny and Klaus Bartschat. *J. Phys. B: At. Mol. Opt. Phys*, 46(11):112001, 2013.
- [29] X. Ren, T. Pflueger, J. Ullrich, O. Zatsarinny, K. Bartschat, D. H. Madison, A. Dorn, and J. Ullrich. *Phys. Rev A*, 85:032702, 2012.
- [30] S. Amami, A. Murray, A. Stauffer, K. Nixon, G. Armstrong, J. Colgan, and D. Madison. *Phys. Rev. A*, 90:062707(E), 2014.
- [31] G. J. Armstrong, J. Colgan, M. Pindzola, S. Amami, D. Madison, J. Pursehouse, K. Nixon, and A. Murray. *Phys. Rev. A*, 92:032706, 2015.
- [32] K. Nixon and A. Murray. *Phys. Rev. Lett.*, 106:123201, 2011.
- [33] S. Amami, A. Murray, A. Stauffer, K. Nixon, G. Armstrong, J. Colgan, and D. Madison. *Phys. Rev. A*, 90:062707, Dec 2014.
- [34] G. S. J. Armstrong, J. Colgan, M. S. Pindzola, S. Amami, D. H. Madison, J. Pursehouse, K. L. Nixon, and A. J. Murray. *Phys. Rev. A*, 92:032706, Sep 2015.
- [35] Y.K. Kim. Theory of electron-atom collisions. *Physics of Ion-Ion and Electron-Ion Collisions. NATO Advanced Study Institutes Series (Series B: Physics)*, 83, 1983.
- [36] Y. Khajuria and D. N. Tripathi. *Phys. Rev. A*, 59:1197–1207, Feb 1999.
- [37] C. J. Joachain. Quantum collision theory, north-holland physics publishing: Amsterdam. 1983.
- [38] P.S. Khare. Introduction to the theory of collisions of electrons with atoms and molecules. 2002.

- [39] C. Champion, J. Hanssen, and P. A. Hervieux. *Phys. Rev. A*, 65:022710, 2002.
- [40] A. M. Duguet, A. Cherid, Lahmam-Bennani, A. Franz, and H. Klar. *J. Phys. B: At. Mol. Opt. Phys*, 20:6145, 1987.
- [41] J Gao, D. H. Madison, and J. L. Peacher. *Phys. Rev. A*, 72:032721, 2005.
- [42] J Gao, J. L. Peacher, and D. H. Madison. *J. Chem. Phys.*, 123:204302–4, 2005.
- [43] D. H. Madison, R. V. Calhoun, and W. N. Shelton. *Phys. Rev. A*, 16:2552, 1977.
- [44] C. T. Whelan and H. R. J. Walters. *J. Phys. B: At. Mol. Opt. Phys*, 23(17):2989, 1990.
- [45] D. H. Madison, K. Bartschat, and J. L. Peacher. *Phys. Rev. A*, 44:1, 304, 1991.
- [46] T. Pflüger, O. Zatsarinny, K. Bartschat, A. Senftleben, X. Ren, J. Ullrich, and A. Dorn. *Phys. Rev. Lett.*, 110:153202, Apr 2013.
- [47] A. Prideaux and D. H. Madison. *Phys. Rev. A*, 67:052710, 2003.
- [48] S. J. Ward and J. H. Macek. *Phys. Rev. A*, 49:1049, 1994.

VITA

Sadek M. F. Amami was born and grew up in Tripoli, Libya. He graduated from Al Fateh University (Recently: University of Tripoli) at Tripoli city in Libya with a Bachelor of Science degree in Physics in 1995-1996. He had served as a high school teacher for several years before he enrolled in the same school for the graduate program in 1998. In the summer semester 2002, he earned a master's degree in Solid State Nuclear Physics from the physics department at University of Tripoli. Then, he continued teaching at the high school until 2005.

In 2005, he started working as a lecturer at the physics department, Faculty of Education, Tripoli University until 2007 when he elected for a scholarship from the Ministry of Higher Education to earn a Ph.D. degree. He earned an M.S. degree in Physics in 2015, and a Ph.D. degree in Physics in December 2017 from Missouri S&T, both in the field of Theoretical and Computational Atomic and Molecular Physics. He has published 12 peer-reviewed articles and presented research results at several national and international conferences. Also, he gave several talks at the professional meeting, GEC (Gaseous Electronics Conference), and participated with posters in many showcases in Missouri University of Science and Technology as well. Also, he has worked as a Graduate Teaching Assistant as well as a Graduate Research Assistant with Dr. Madison since 2011 at Missouri University of Science and Technology.

Finally, he served as a student advisor for two years (2005-2007) in University of Tripoli. In 2008, he served as a representative of the student council at Spring International Language Center in Fayetteville, AR, and as a Vice President of Libyan Association in 2015 at Missouri S&T. Also, he has volunteered as an Arabic language teacher in the Libyan Sunday School in Rolla, MO since 2010.